A STUDY ON THE PERFORMANCE OF PASSIVE AND ACTIVE PNEUMATIC ISOLATION SYSTEMS

Sekar Kalambur

A Research Thesis

in

The Faculty

of

Engineering

Presented in Partial Fulfillment of the Requirements
for the degree of Master of Engineering at
Concordia University
Montreal, Quebec, Canada

September 1979

ABSTRACT

A STUDY ON THE PERFORMANCE OF PASSIVE AND ACTIVE PNEUMATIC ISOLATION SYSTEMS

Sekar Kalambur

In this thesis a study on the performance of a passive and an active pneumatic isolation systems is carried out. For both systems the governing equations that describe the behaviour of the system are formulated and simulated on a digital computer. Input displacement excitations such as sinusoidal, rounded pulse and function of the form $x = x_0 (1-\cos \omega t)$ are considered.

In the case of a sinusoidal input excitation, absolute and relative displacement transmissibility and acceleration transmissibility are plotted in the frequency range of 2.5 to 50 rad/s. For pulse like input excitation, relative displacement and acceleration ratios are plotted for various values of shock severity parameter γ. In addition, the displacement and acceleration time response plots are provided for all input excitations considered.

It is found that for the passive system both absolute displacement and acceleration peak transmissibilities decrease as the orifice area is increased until a critical value. For pulse-like input, the peak acceleration ratio decreases as the severity parameter γ_0 increases. For input excitation of the form $x = x_0 (1-\cos \omega t)$, the output displacement and acceleration for the passive system have the same peak values as that of the input.

In this thesis an active system is synthesized by controlling flow in and out of a cylinder chamber through an electro-pneumatic servo-valve. The control signal (input current) to the servo-valve is generated by manipulating the measured variables such as relative velocity, chamber pressures and output acceleration so that the jerk of the isolated mass is kept at zero.

The simulation results for the active system indicate that the absolute displacement transmissibility is significantly low for lower frequencies up to 40 rad/s and sharply increases for higher frequencies. The relative displacement transmissibility displayed a constant value (0 db) for frequencies up to 40 rad/s and increased sharply for higher frequencies. The results indicate that the acceleration transmissibility has an increasing and decreasing characteristic with three distinct peaks, even so, the peak value of the acceleration transmissibility is less then -26 db. For pulse like input, the acceleration ratio decreased as the severity parameter γ_0 is increased and the relative displacement increased for higher values of $\gamma_0 (\gamma_0 > 3)$. The output displacement and acceleration displayed relatively smaller values compared to the input displacement and acceleration for input of the form $x = x_0 (1-\cos \omega t)$.

An experimental procedure to test the validity of the active systems' performance is outlined. A comparison of the performance between the passive and the active systems shows that superior displacement and acceleration isolation can be achieved by using an active system.

ACKNOWLEDGEMENTS

The author wishes to express his gratitude and deep appreciation to his thesis supervisor, Dr. S. Sankar, for initiating the project and providing continued guidance throughout the investigation.

The plotting subroutines provided by Mr. Albert Carbone, which are used to plot the graphs in this thesis, are very much appreciated. The author also wishes to express his thanks to Mrs. Ilana Crawford and Mrs. Elizabeth Horwood for typing the manuscript.

This work was carried out under FCAC Grant No. 242-110 from the Government of Quebec to whom the author is indebted.

TABLE OF CONTENTS

LIST OF FIGURES

NOMENCLATURE

A	orifice area between the two Chambers (passive system)	m^2
A_1	head side area of the piston	m^2
A_2	rod ride area of the piston	m^2
AR	area ratio A_2/A_1 dimensionless	
A_{s_1}	orifice area created by the movement of the spool in the servo-valve connected to Chamber 1	m^2
A_{s_2}	orifice area created by the movement of the spool in the servo-valve connected to Chamber 2	m^2
A_o	reference area	m^2
a	dimensionless orifice area between the two Chambers (passive system)	
a_s	dimensionless orifice area created by the spool movement in the servo-valve	
a_{s_1}	dimensionless orifice area created by the spool movement in the servo-valve connected to Chamber 1	
a_{s_2}	dimensionless orifice area created by the spool movement in the servo-valve connected to Chamber 2	
c_1	dimensionless constant	
c_2	dimensionless constant	
c_3	dimensionless constant	
c_4	dimensionless constant	
i_c	input current to the serv-valve - dimensionless	
k	mechanical spring stiffness	N/m
k_v	proportional gain of the servo-valve - dimensionless	
k_1	acceleration feedback gain	$\frac{ma\text{-}sec^2}{m}$
k_2	velocity feedback gain	$\frac{ma\text{-}sec}{m}$
k_3	displacement feedback gain	ma/m

k_1^*	dimensionless acceleration feedback gain	
k_2^*	dimensionless velocity feedback gain	
k_3^*	dimensionless displacement feedback gain	
L	reference length	m
M_o	reference mass	kg_m
mg	suspension force	N
$\frac{dM_1}{dt}$	mass flow rate into Chamber 1	kg/s
$\frac{dM_2}{dt}$	mass flow rate into Chamber 2	kg/s
$\frac{dM^*}{d\tau}$	dimensionless mass flow rate	
$\frac{dM_1^*}{d\tau}$	dimensionless mass flow rate into Chamber 1	
$\frac{dM_2^*}{d\tau}$	dimensionless mass flow rate into Chamber 2	
n	polytropic exponent dimensionless	
P_a	atmospheric pressure	N/m^2
p_a	dimensionless atmospheric pressure	
P_s	supply pressure	N/m^2
p_s	dimensionless supply pressure	
P_o	reference pressure	N/m^2
P_1	pressure in Chamber 1	N/m^2
p_1	pressure in Chamber 1 dimensionless	
P_2	pressure in Chamber 2	N/m^2
p_2	pressure in Chamber 2 dimensionless	
R	gas constant	M•N sec/kg °k
s	time	seconds
T_o	reference temperature	k

T_1	temperature in Chamber 1	k
t_1	dimensionless temperature in Chamber 1	
T_2	temperature in Chamber 2	k
t_2	dimensionless temperature in Chamber 2	
t	time	s
V_0	reference volume	m^3
V_1	volume in Chamber 1	m^3
V_2	volume in Chamber 2	m^3
X	input displacement	m
x	input displacement dimensionless	
x_v	displacement of the spool dimensionless	
Y	output displacement	m
y	output displacement dimensionless	
α	reference time	s
β	dimensionless constant	
τ	dimensionless time	
δ	initial compressed length of the mechanical spring	m
δ^*	dimensionless initial compressed length of the mechanical spring	
γ_0	shock severity parameter	
γ	ratio of specific heats	

LIST OF TABLES

CHAPTER 1

CHAPTER 1

INTRODUCTION

1.1 GENERAL

Vibratory forces generated by machines, engines and external disturbances are often unavoidable; however, their effect on a dynamical system can be reduced substantially by properly designed springs and dampers, which are referred to as isolators. In the past, the majority of vibration isolators have employed passive suspension elements which do not require a continuous supply of power for operation, and typically include wheels, linkages, springs and damping elements. While for many applications the performance capability of a passive suspension is adequate, its performance is basically limited since the force generated by the passive system cannot be controlled.

A conventional passive vibration isolator used to isolate the vibration of a mass is usually a combination of linear or non-linear spring and a damper which may have a linear or non-linear damping characteristic. Since, in both cases, mass of the system is generally fixed, the spring rate and the damping coefficients are the only design parameters that could be optimally selected to isolate the mass effectively.

In the case of a linear isolation system, that is, a system having linear spring and damper, the governing equation of the mass is given by a set of linear differential equations. In most cases, given the input excitation, a closed form solution for the differential equation can be obtained and hence the design of such systems are quite simpler and straight forward. But however, the major disadvantage of such systems are

their low frequency performance. Since the spring dominates the low frequency performance, the force transmissibility can never be less than one. One important limitation of passive isolation systems is that the static deflection varies as the inverse square of the natural frequency. For most terrain-induced vibration, the peak input amplitudes occur in the low frequencies, 3 to 5 Hz. A passive isolation system for such applications must have a natural frequency less than or atleast .707 of the excitation frequency. For such low natural frequencies, the static deflection of a linear passive system would be over several meters.

If non-linearities are introduced in the isolator stiffness to limit the dynamic deflections to the desired level, the performance of the system would deteriorate since it would exhibit the vibration isolation characteristics of a stiffer system.

By using a non-linear spring and damper in a passive system, the force generated by the isolator is proportional to the relative velocity and displacement similar to that of a linear spring and damper. So this kind of passive system again faces the problem of low frequency isolation.

To achieve greater system design flexibility and performance, active elements have been applied in isolating systems. In an idealized form, an active suspension element is a controllable force generator powered by an external energy source. Such devices can be programmed to produce forces which are functions of any system variables. By sensing system variables, such as absolute or relative acceleration, velocity or displacement and appropriately combining them, a command signal is generated for the force generator. With such devices, isolation system

performance is limited only by the amount of external power and designer's willingness to expand the complexity.

A fully active vibration isolation system will have good performance compared to a passive system. One main advantage of active isolators is that natural frequencies are substantially lower than those realizable from passive isolators can be provided, with low dynamic deflections particularly under conditions of transient excitations. A wide variety of excitation and response sensors can be employed to provide feedback signals and form a closed-loop active isolation system. For example, command (feedback) signals can be developed which are functions of jerk, accelerations, velocity, displacement, time-integral of displacement, differential pressure or force. The signal processor for controlling the force generator may consist of an active electronic network that performs addition, attenuation, amplification, multiplication, integration and compensation functions.

Types of force generators or actuators that may be used in active isolation systems include mechanical, fluidic, electro-sensitive fluids and electrodynamic force generators. In the case of electrodynamic force generator, either hydraulic or pneumatic fluid may be utilized.

The main disadvantage of active systems are:

i) high cost,

ii) low reliability compared to a passive system,

iii) need of an external power source,

iv) stability of the system.

1.2 REVIEW OF PREVIOUS WORK

To obtain qualitative and quantitative information regarding the vibration isolator, a systematic study of the passive and active vibration isolators are carried out. One of the most important factors in designing an active or a passive vibration isolator is to minimize the force transmitted to the mass from an excitation source. First, conceptual passive suspension design and optimization techniques are reviewed, then the concept and the development of the active suspension are given.

Caton [1] analyzed an isolator embodying a Coulomb-friction element and a return spring. An optimization procedure was carried out for a trade off on the maximum acceleration transmitted to achieve a limit on the maximum relative movement. Cornelius [2] presented a mathematical model of shock mount consisting of a resilient element in parallel with a damper and the response of the shock mount was studied for specified foundation velocity input. The damping force produced by the damper was a linear function of velocity only at low velocities. At higher velocities the damping force was limited to a constant value and was not sensitive to velocity at all. The performance of this shock mount was compared with that of a conventional isolator.

A shock mount having non-linear dual-phase damping which simultaneously minimizes the acceleration and displacement of the mounted mass was considered by Snowdon [3]. The non-linear dashpot considered produced a relatively small damping force when the system passes through abrupt transients. The damper produced relatively larger damping force when the system goes through relatively slow decay of motion than when the system

was subjected to less abrupt transients. The response of the system together with the conventional passive system were given for step like and pulse like inputs.

Another type of dual-phase damper with a mechanical spring arranged in parallel was investigated by Venkatesan [4] to minimize the absolute transmissibility of the mass over the complete frequency range. In this case, the dual-phase damper has the damping ratio that depends on relative displacement; higher damping at low relative displacement and lower damping at higher relative displacement; for intermediate relative displacement there is linear transition between the high and low damping ratios.

An optimum shock isolator which minimizes both the transmitted shock and relative displacement was presented by Mercer [5]. Here the damping force was generated by both Coulomb-friction and by viscous damping. For high frequency and large amplitude input motions the viscous damper was made rigid and the isolator reduced to a spring and Coulomb-friction damper in parallel. For less severe input motions viscous damping was made more dominant than the Coulomb-friction.

A theoretical investigation was carried out by Ruzicka [6] on a single degree of freedom vibration isolation system in which isolator damping force was proportional to the relative velocity across the isolator raised to an orbitary power. Results for parametric variations in damping were also presented for specific values of the relative velocity exponent.

Impact absorber with quadratic damping and a linear spring element in parallel was analyzed by Hundel [7]. Closed form solutions for the

dynamical equations were presented. The results indicate that the system with quadratic damping transmits about 4 percent less force than a linear damper.

Dynamic response of a vibration isolation system with non-rigid foundation was studied by Soliman [8]. Optimization procedures were developed to evaluate the optimium parameters so that the maximum transmitted motion to the mass could be minimized. Design data were published graphically for parameter variations. The effect of fluid and mechanical compliance on the performance of hydraulic shock absorbers was studied by Mayne [9]. It is shown that by using proper compliance, the maximum deceleration levels necessary to stop a given mass from a specified velocity within the shock absorber travel can be achieved.

With the development of high performance feedback control servomechanism a significant development on active suspension has occured since 1950. In the 1950's pneumo-mechanical suspension for automotive type vehicles were developed, as were low frequency load leveling suspensions for several types of vehicles. In the mid 60's interest in active vehicle suspensions increased in order to achieve high speed intercity transport systems. Research and development of advanced rail vehicles which employ active suspensions was initiated because of the greater speed and high level performance requirements.

D.C. Karnopp [10] has compared the active suspensions with practical passive suspensions. Using linear theory and traditional frequency response plots, the author has shown that in the most basic case, a worthwhile, but not crucial, improvement can be gained by the use of active

or semi-active systems, while in a more complex case the best possible passive suspension performance was shown to be very poor compared with the active systems.

In the last two decades, a number of powerful analytical tools have been developed for the design and optimization of suspension systems. Many of the most commonly used methods are summarized by Wolkovitch [11], Karnopp [12] and Hendrik [13].

A number of studies have been done to determine the optimal configurations for generic suspensions. Bender [14], Karnopp and Trikha [15], Hullender [16], Young and Wormly [17] and Hendrik [18] have all used a single degree of freedom generic suspension as shown in Figure 1, to find an optimal linear suspension model which minimized the quadratic performance index:

$$PI = \ddot{y}_2^2 + \rho\, \bar{y}_r^2$$

where

$\ddot{y}_2^2$ = mean square vehicle acceleration

$\bar{y}_r^2$ = mean square relative displacment

ρ = weighting factor

The performance index includes the passenger comfort using the acceleration term and limits the suspension stroke by including the relative displacement term. The optimum suspension can be implemented passively or actively as shown in Figures 2 and 3 respectively.

Crosby and Karnopp descbribe the means by which the desired suspension can be achieved [19,20]. The authors have also given semi-active damping systems which closely approximate optimum suspension

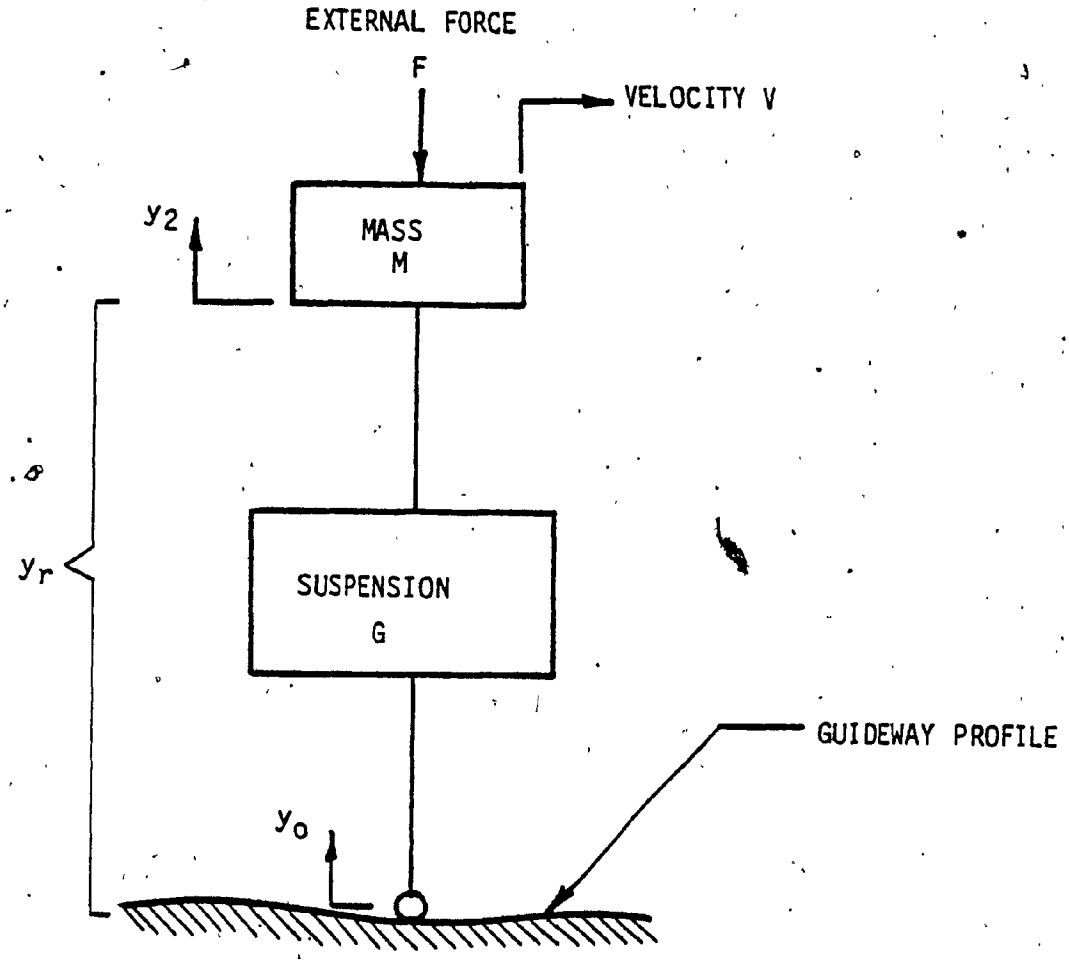

FIGURE 1. One Degree of Freedom Generic Suspension

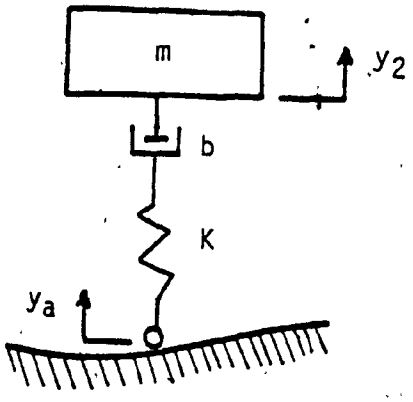

FIGURE 2. Optimal Passive Suspension

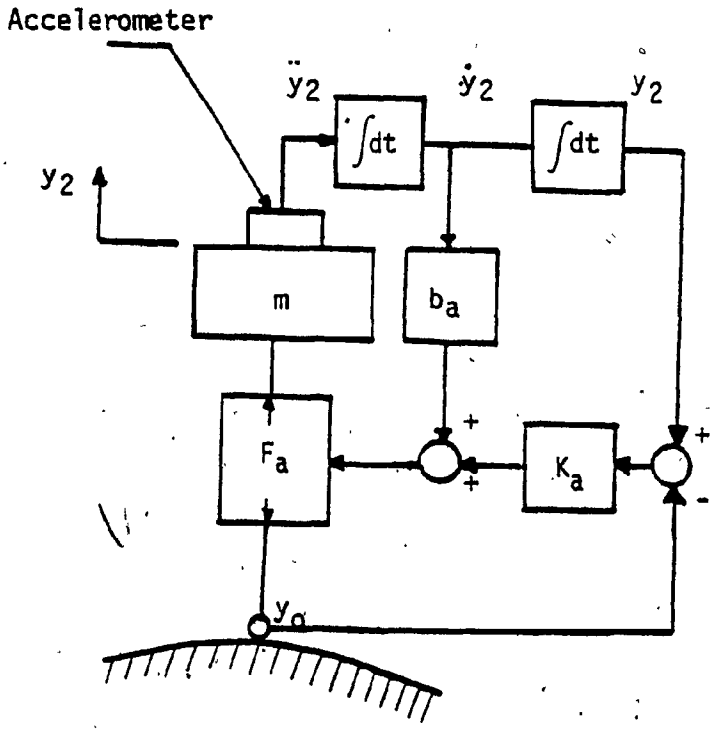

FIGURE 3 Optimal Active Suspension

performance.

To replace the shock absorbers in automobiles, buses and trucks, a hydraulic actuator is used as an active suspension system. This active suspension system was developed by Hanna and Obson [21]. Because of the smoothness of the interstate highways and the development of improved passive suspensions, the widespread use of active suspension in automobiles, buses and trucks was suppressed. But the use of active suspension in passenger and freight trains were the topics of research. Vibration isolation from rail irregularities has been investigated both analytically and experimentally in a scaled model. This isolation system was developed by Obson, Allen and Wilhelm for Westinghouse Research Laboratories [22].

An active suspension system using pneumatic actuators was studied analytically and experimentally by Rinehart, Roach, Bain and Croshaw, [23]. This paper describes analytical and experimental (1/6 scale) studies of different active controllers for a rail transit vehicle. The servo valve in this pneumatic isolator system was controlled individually by both electrical and fluidic signals. Figures 4 and 5 illustrate the conceptual railcar active suspension implementation and the ride quality comparisons reported based upon the 1/6 scale experimental system.

An active, nonlinear pneumatic suspension applicable to passenger railcars is described by Klinger and Calzado [24]. Standard on-off valves are used to modulate the pressure differance between the two chambers. Acceleration, relative displacement, and pressure transducers provide control signal to operate the on-off valve. Simulation results for some typical rail track input profiles indicate improved vibration

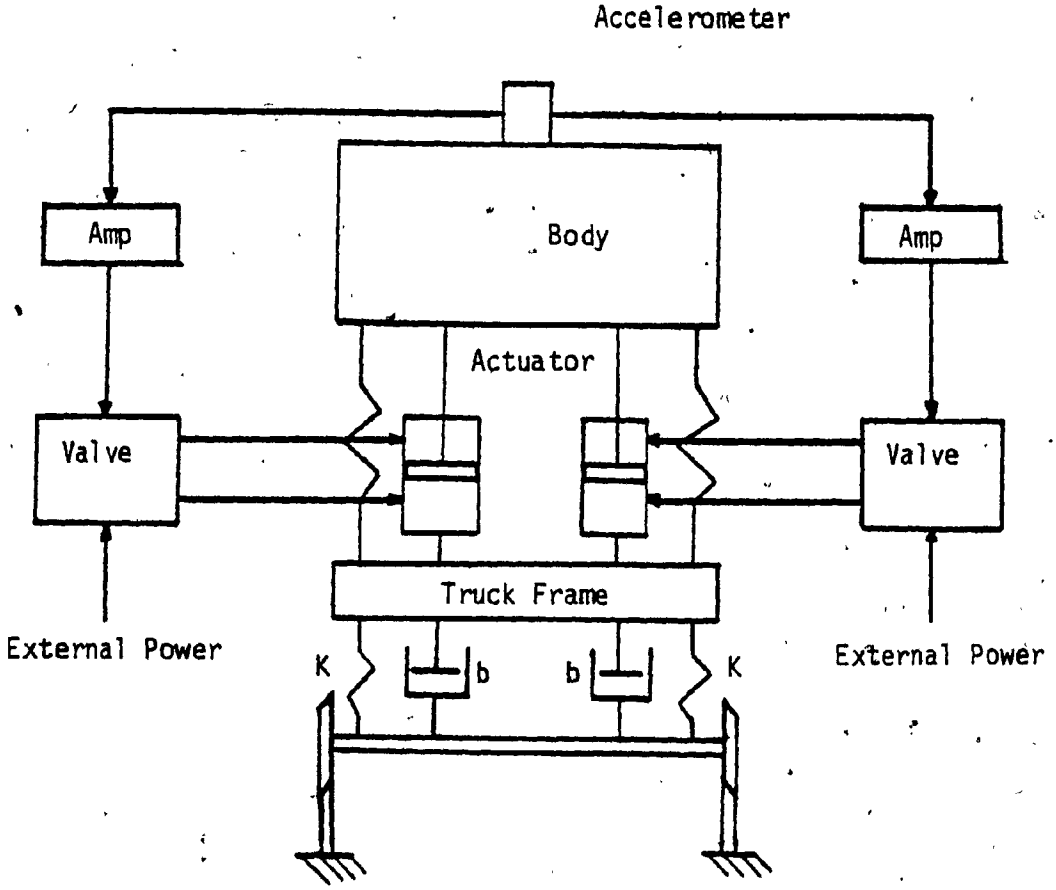

Fig. 4: Conceptual Active Railcar Suspension

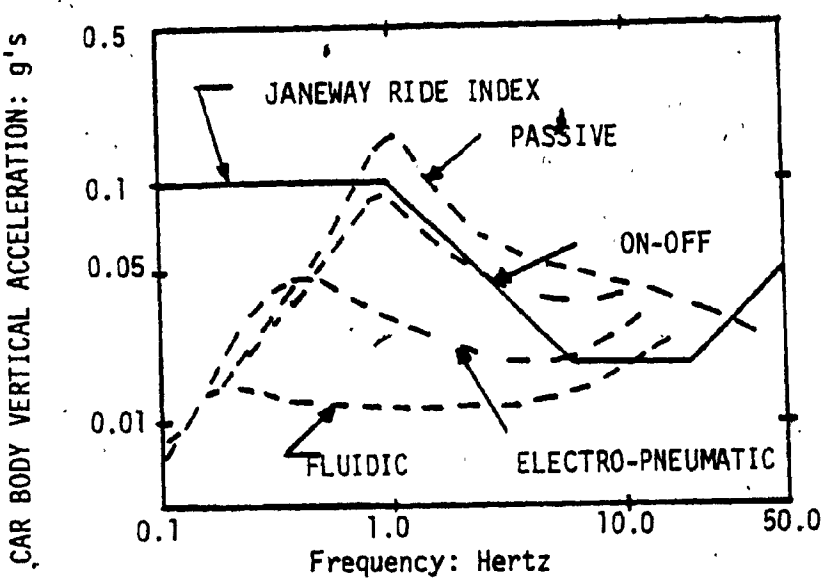

Fig. 5: Scale Model Rail Vehicle Suspension Measured Performance

isolation over the conventional passive system.

1.3 SCOPE OF THE RESEARCH WORK

The first objective of this thesis is to study the performance characteristics of a pneumatic passive isolation system for both vibration and shock excitations. A constant amplitude sinusoidal excitation with frequencies varying from 2.5 rad/s to 50 rad/s is used as the input for investigating isolator vibration characteristics. A rounded pulse with variable shock severity and a periodic pulse of the form $X = X_0(1-\cos\omega t)$ are used as the input source excitation for testing the passive system.

The second objective is to investigate the theoretical feasibility of an electro-pneumatic active suspension system which provides capabilities for low frequency vibration attenuation with zero static deflection. The control policy for the active system is based on controlling the jerk of the mass to zero. Both the performance and stability characteristics of the active isolator for both vibration and shock inputs are investigated. Finally a comparison of the performance of passive and active isolators are presented. The thesis also presents an experimental procedure for setting up the active isolator for testing.

In Chapter 3, the control logic for the active system is formulated. Then the simplified model of the active system equations are analyzed for the stability. The system performance is studied using a digital computer. The computer simulation includes the dynamics of the electro-pneumatic servo valve. The limitations of the active system are outlined.

Chapter 4 describes the experimental procedure to verify the theoretical predictions. Finally, in Chapter 5, a conclusion on the

performance and stability of the active vibration isolator is drawn from the simulation. Recommendations for future research in the area of active vibration isolation systems are also outlined.

CHAPTER '2

CHAPTER 2

PASSIVE PNEUMATIC ISOLATION SYSTEM

2.1 GENERAL

A passive vibration isolator is any combination of spring and damper without any external power. In this study, a passive isolator with mechanical spring and pneumatic damping is used. Since passive systems are simple and easy to understand, a detailed study of the passive system will enable to give a fairly good understanding of an active system.

2.2 FORMULATION OF GOVERNING SYSTEM EQUATIONS

The schematic diagram of a passive pneumatic isolator is shown in Figure 6. Static support of the mass is provided by the pressure in the cylinder chambers and by the mechanical springs. The variable Y is the inertial displacement of the mass and the variable X is the input displacement of the base due to external disturbance. A positive input displacement reduces the volume in chamber 1 and increases the volume in chamber 2 and hence increases the pressure in chamber 1 and reduces the pressure in chamber 2. The difference in pressure in the two chambers, causes the fluid to flow from chamber 1 to chamber 2 through the orifice area, and the mass to have inertial acceleration. The damping in the system is produced by the flow of fluid through the orifice area.

The governing equations of the passive pneumatic isolator system are characterized by:

1. Pressure equations.

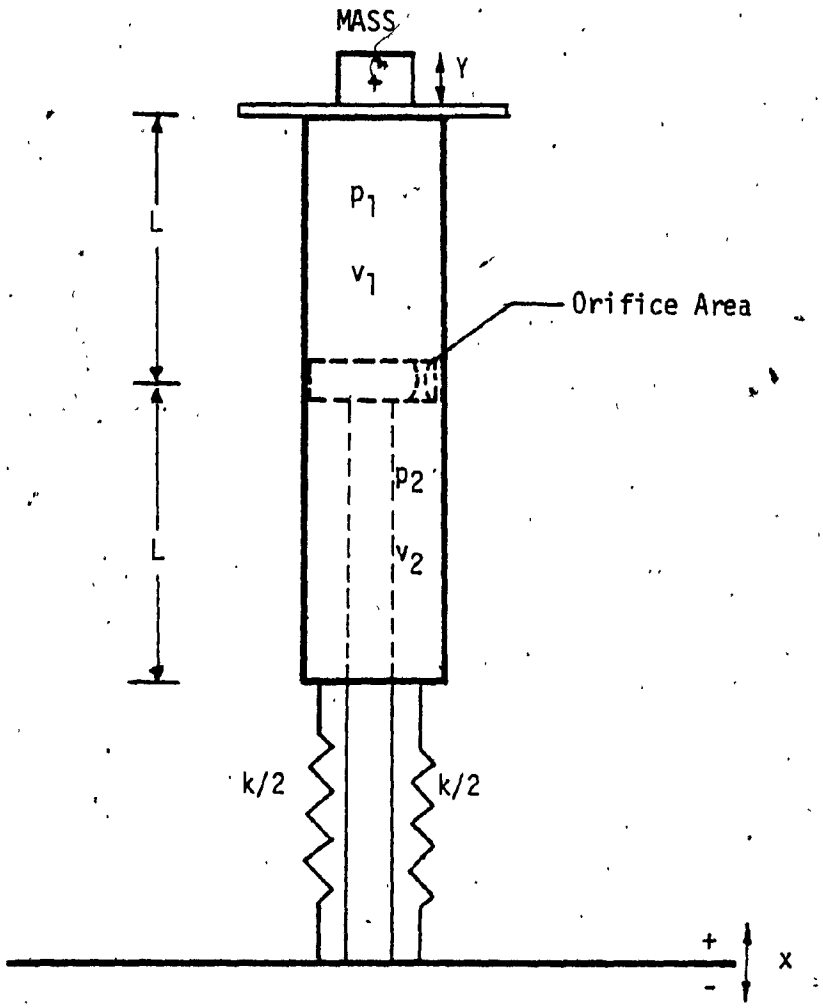

Fig. 6: Schematic Diagram of the Passive Pneumatic Suspension

2. Flow equations.

3. Force balance equation.

Pressure equations relate the rate of change of pressure to the mass flow rate of the fluid and the input velocity. The flow equation describes the relationship between the quantity of flow into and out of the cylinder chambers. Finally, the force balance equation describes the dynamic behavior of the inertial mass.

2.2.1 Pressure Equations

The pressure equation can be derived from the equation of the state

$$PV = MRT \tag{2.1}$$

Differentiating the equation of state (2.1) with respect to time, the rate of change of pressure for the two chambers are given as:

$$\frac{dP_1}{dt} = -\frac{dV_1}{dt}\frac{P_1}{V_1} + \frac{dM_1}{dt}\frac{RT_1}{V_1} + \frac{M_1R}{V_1}\frac{dT_1}{dt} \tag{2.2}$$

and

$$\frac{dP_2}{dt} = -\frac{dV_2}{dt}\frac{P_2}{V_2} + \frac{dM_2}{dt}\frac{RT_2}{V_2} + \frac{M_2R}{V_2}\frac{dT_2}{dt} \tag{2.3}$$

where V_1 and V_2 are the volumes of chambers 1 and 2 respectively. The chamber volumes can be expressed as:

$$V_1 = A_1 (L - X + Y) \tag{2.4}$$

$$V_2 = A_2 (L + X - Y) \tag{2.5}$$

Differentiating equations (2.4) and (2.5) with respect to time, the rate of change of volume in the two chambers can be written as:

$$\frac{dV_1}{dt} = A_1 \left(-\frac{dX}{dt} + \frac{dY}{dt}\right) \tag{2.6}$$

$$\frac{dV_2}{dt} = A_2 \left(\frac{dX}{dt} - \frac{dY}{dt}\right) \tag{2.7}$$

Combining equations (2.2), (2.4) and (2.6) with (2.3), (2.5) and (2.7), the rate of change of pressure in the two chambers can be written as:

$$\frac{dP_1}{dt} = \frac{RT_1}{A_1(L-X+Y)} \frac{dM_1}{dt} + \frac{M_1 R}{A_1(L-X+Y)} \cdot \frac{dT_1}{dt} - \frac{P_1}{(L-X+Y)} \left(-\frac{dX}{dt} + \frac{dY}{dt}\right) \tag{2.8}$$

and

$$\frac{dP_2}{dt} = \frac{R \cdot T_2}{A_2(L+X-Y)} \frac{dM_2}{dt} + \frac{M_2 \cdot R}{A_2(L+X-Y)} \cdot \frac{dT_2}{dt} - \frac{P_2}{(L+X-Y)} \left(\frac{dX}{dt} - \frac{dY}{dt}\right) \tag{2.9}$$

For a polytropic process, the temperatures and pressures can be related as:

$$T_1 = T_0 \left(\frac{P_1}{P_0}\right)^{\frac{n-1}{n}} \tag{2.10}$$

$$T_2 = T_0 \left(\frac{P_2}{P_0}\right)^{\frac{n-1}{n}} \tag{2.11}$$

with temperature assumed to be related to pressures by a polytropic gas constant 'n', equations (2.8) and (2.9) can be further reduced as:

$$\frac{dP_1}{dt} = n\left[\frac{RT_1}{A_1(L-X+Y)} \cdot \frac{dM_1}{dt} - \frac{P_1}{(L-X+Y)} \left(-\frac{dX}{dt} + \frac{dY}{dt}\right)\right] \tag{2.12}$$

and

$$\frac{dP_2}{dt} = n\left[\frac{R \cdot T_2}{A_2(L+X-Y)} \frac{dM_2}{dt} - \frac{P_2}{(L+X-Y)} \left(\frac{dX}{dt} - \frac{dY}{dt}\right)\right] \tag{2.13}$$

The complete derivation of equations (2.12) and (2.13) are given in Appendix A.

2.2.2 Flow Equations

The flow continuity characteristic equation for the pneumatic isolator can be expressed as follows:

The mass flow rate from chamber 1 to 2,

$$\frac{dM_1}{dt} = \frac{dM}{dt} \tag{2.14}$$

and the mass flow rate from chamber 2 to 1,

$$\frac{dM_2}{dt} = -\frac{dM}{dt} \tag{2.15}$$

where $\frac{dM}{dt}$ is the mass flow rate between the chambers and is given by the following expression [25].

For the condition $P_1 > P_2$

$$\frac{dM}{dt} = -K \cdot P_1 \cdot A \cdot N_{12} / T_1^{\frac{1}{2}} \tag{2.16}$$

where the factor K is given by

$$K = \left[\frac{\gamma}{R}\left(\frac{2}{\gamma+1}\right)^{\gamma+1/\gamma-1}\right]^{\frac{1}{2}} \tag{2.17}$$

By assuming a value of $\gamma = 1.4$ for air, the value of K becomes

$$K = 0.04 \quad \frac{kg}{N \cdot S} \quad {}^{\circ}K^{\frac{1}{2}}$$

The factor N_{12} is a function of the ratio of specific heats and pressure ratio, and is given by [25]:

$$N_{12} = \left[\frac{(P_2/P_1)^{2/\gamma} - (P_2/P_1)^{\gamma+1/\gamma}}{\left(\frac{\gamma-1}{2}\right)\left(\frac{2}{\gamma+1}\right)^{\gamma+1/\gamma-1}}\right]^{\frac{1}{2}} \tag{2.18}$$

For the conditions $P_1 < P_2$

$$\frac{dM}{dt} = K \cdot P_2 \cdot A \cdot N_{12}/T_2^{\frac{1}{2}} \tag{2.19}$$

In this case, the factor N_{12} is defined as [25]:

$$N_{12} = \left[\frac{(P_1/P_2)^{2/\gamma} - (P_1/P_2)^{\gamma+1/\gamma}}{(\frac{\gamma-1}{2})\ (\frac{2}{\gamma+1})^{\gamma+1/\gamma-1}}\right]^{\frac{1}{2}} \tag{2.20}$$

Finally, by using the flow continuity equations (2.14) and (2.15), the equations (2.10) and (2.11) can be rewritten as:

$$\frac{dP_1}{dt} = n\left[\frac{RT_1}{A_1(L-X+Y)} \cdot \frac{dM}{dt} - \frac{P_1}{(L-X+Y)}\left(-\frac{dX}{dt} + \frac{dY}{dt}\right)\right] \tag{2.21}$$

$$\frac{dP_2}{dt} = n\left[\frac{RT_2}{A_2(L+X-Y)} \frac{dM}{dt} - \frac{P_2}{(L+X-Y)}\left(\frac{dX}{dt} - \frac{dY}{dt}\right)\right] \tag{2.22}$$

2.2.3 Force Balance Equation

The force balance load equation is given by

$$m \cdot \frac{d^2Y}{dt^2} = P_1 \cdot A_1 - P_2 \cdot A_2 + k(\delta+X-Y) - mg - 14.7 \times 6890\ (A_1-A_2) \tag{2.23}$$

Equations (2.12) to (2.23) completely describe the dynamics of the passive pneumatic isolator system.

2.3 NON-DIMENSIONALIZATION OF EQUATIONS FOR THE PASSIVE SYSTEM

In order to reduce the parametric complexity in simulation and to increase the generality, the governing system equations are non-dimensionalized.

The first step in the non-dimensionalization procedure is to select reference values.

Let,

Reference	Pressure	be	P_o
Reference	Length	be	L
Reference	Area	be	A_1
Reference	Temperature	be	T_o
Reference	Mass	be	$M_o = \frac{P_o V_o}{R T_o}$
Reference	Volume	be	$V_o = A_1 \cdot L \cdot$
Reference	Time	be	α

$$\alpha = \frac{\beta \cdot V_o}{A_1 \cdot K \cdot R \cdot T_o^{\frac{1}{2}}}$$

where β is a non-dimensionalized factor.

Then, $t = \alpha \tau$

where τ is the non-dimensionalized time.

Using these reference values, the equations (2.12) to (2.23) can be non-dimensionalized. Then the non-dimensionalized pressure equations in the two chambers can be written as:

$$\frac{dp_1}{d\tau} = n \left[\frac{dM^*}{d\tau} \cdot \frac{t_1}{(1-x+y)} - \frac{p_1}{(1-x+y)} \left(- \frac{dx}{d\tau} + \frac{dy}{d\tau} \right) \right] \qquad (2.24)$$

and

$$\frac{dp_2}{d\tau} = n \left[- \frac{dM^*}{d\tau} \frac{t_2}{AR(1+x-y)} - \frac{p_2}{(1+x-y)} \left(\frac{dx}{d\tau} - \frac{dy}{d\tau} \right) \right] \qquad (2.25)$$

The non-dimensionalized mass flow equation for $p_1 > p_2$ is given by

$$\frac{dM^*}{d\tau} = - p_1 \cdot a \cdot \beta \cdot N_{12}^{(1)} / t_1^{\frac{1}{2}} \qquad (2.26)$$

where

$$N_{12}^{(1)} = \left[\frac{(p_2/p_1)^{2/\gamma} - (p_2/p_1)^{\gamma+1/\gamma}}{(\frac{\gamma-1}{2})(\frac{2}{\gamma+1})} \right]^{\frac{1}{2}} \qquad (2.27)$$

and for $p_1 < p_2$

$$\frac{dM^*}{d\tau} = p_2 \cdot a \cdot \beta \cdot N_{12}^{(2)} / t_2^{\frac{1}{2}} \tag{2.28}$$

where

$$N_{12}^{(2)} = \left[\frac{(p_1/p_2)^{2/\gamma} - (p_1/p_2)^{\gamma+1/\gamma}}{(\frac{\gamma-1}{2})\ (\frac{2}{\gamma+1})^{(\gamma+1/\gamma-1)}} \right]^{\frac{1}{2}} \tag{2.29}$$

The non-dimensionalized temperature t_1 and t_2 are given by

$$t_1 = (p_1)^{\frac{n-1}{n}} \tag{2.30}$$

$$t_2 = (p_2)^{\frac{n-1}{n}} \tag{2.31}$$

Finally, the non-dimensionalized load equation can be written as

$$\frac{d^2y}{d\tau^2} = c_1 p_1 - c_2 p_2 + c_3 (\delta^* + x - y) - c_4 \tag{2.32}$$

A complete development of these non-dimensionalized equations and the non-dimensionalized constants c_1, c_2, c_3 and c_4 are given in Appendix B.

Equations (2.24) to (2.32) are the non-dimensionalized system of equations which completely describe the dynamics of the system.

2.4 TYPES OF INPUT EXCITATION

The natural frequency of the pneumatic isolation system considered is given by [25]:

$$\omega_n^2 = \frac{n \cdot A_1^2 \cdot P_1}{V_1 \cdot m} + \frac{n\ A_2^2\ P_2}{V_2 \cdot m} + \frac{k}{m}$$

For the selected values of A_1, A_2, k and m, the natural frequency of the

system ω_n is found to be

$$\omega_n \simeq 20.6 \text{ rad/sec.}$$

In calculating ω_n it is assumed that the change in pressure and the volume are negligible.

To study the behaviour of the pneumatic isolation system, three different types of inputs were considered. They are: sinusoidal, rounded pulse and a periodic input of the form $X = X_0 (1-\cos\omega t)$. The amplitudes of excitation for these inputs and the frequency range for sinusoidal input are controlled by the magnitude of the input velocity that the system can take. In this thesis for investigating the performance of the passive system, the maximum velocity is assumed to be 0.23 m/s (9 in/s).

For the sinusoidal input, the frequency was varied from 2.5 rad/sec. to 50 rad/sec. This covers a frequency range of approximately two octaves below and one octave above the natural frequency of 20 rad/sec. The maximum input frequency of 50 rad/sec. limits the input amplitude to be 4.6×10^{-3}m (0.18 in.) so that the maximum input velocity is less than 0.23 m/s (9 in/s).

The second input considered in this thesis is a pulse like input displacement. This input is chosen to be physically realistic in that it describes the translation of the foundation through a finite distance in a finite time with finite acceleration and deceleration. The unidirectional rounded displacement pulse is described by [3]:

$$X(t) = X_{max} (e^2/4) (\gamma_0\omega_n t) e^{-\gamma_0\omega_n t} \quad t \geq 0$$

The parameter γ_0 describes the finite rise times of the steps and

the duration of the pulse in terms of the half-period of natural vibration T/2 of the isolation system. In other words by increasing the parameter γ_0 the shock severity increases. The plot of input displacement, velocity and acceleration for different values of γ_0 are given in Figure 7a, Figure 7b and Figure 7c respectively.

The shock severity parameter γ_0 was varied from γ_0=1 to γ_0=10. The maximum input displacement $X_{max} = 3.8 \times 10^{-3}$m is selected.

Figure 8 shows the third type of input considered in this simulation. This input represents a track profile of a road vehicle encountering a severe grade change, without a transition, at 44.2 m/s (110 mph) [24]. The track profile of Figure 8 is of the form

$$X = 2.5 \times 10^{-2} (1-\cos t) \text{ m}$$

The maximum input displacement for this case becomes 5×10^{-2}m

2.5 SIMULATION OF PASSIVE ISOLATOR

The non-dimensionalized equations presented in section (2.3) describes the behavior of the passive pneumatic isolation system. In order to study the performance of the passive system, the governing differential equations are solved using Runge-Kutta 4th order numerical integration method on a CDC Cyber 172/2 digital computer. Appendix C describes the Runge-Kutta method and the Fortran computer program used for this simulation is listed in Appendix D. Table 2.1 lists the system parameters used in this simulation.

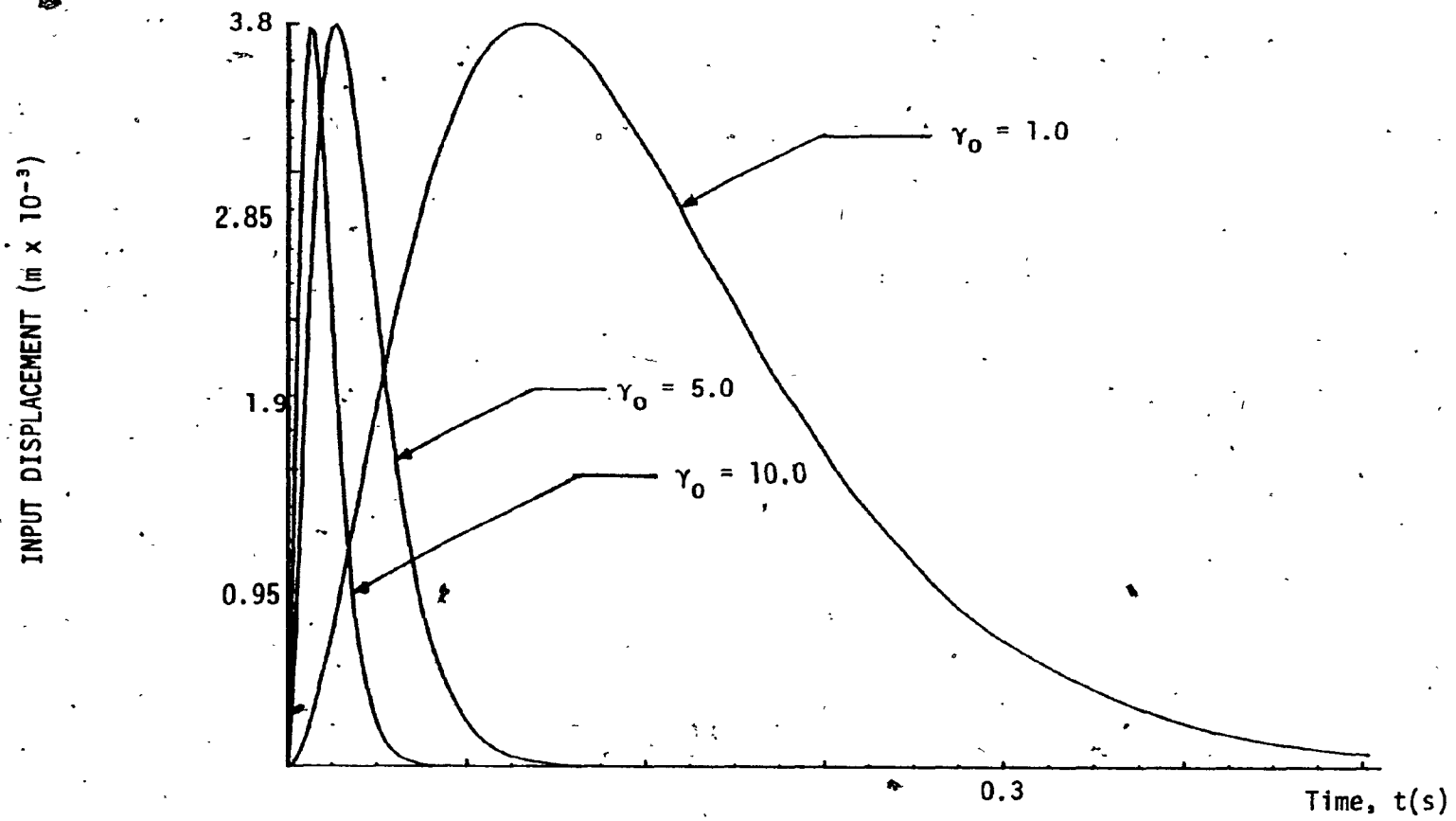

Fig. 7a: Input Displacement for Pulse Like Input

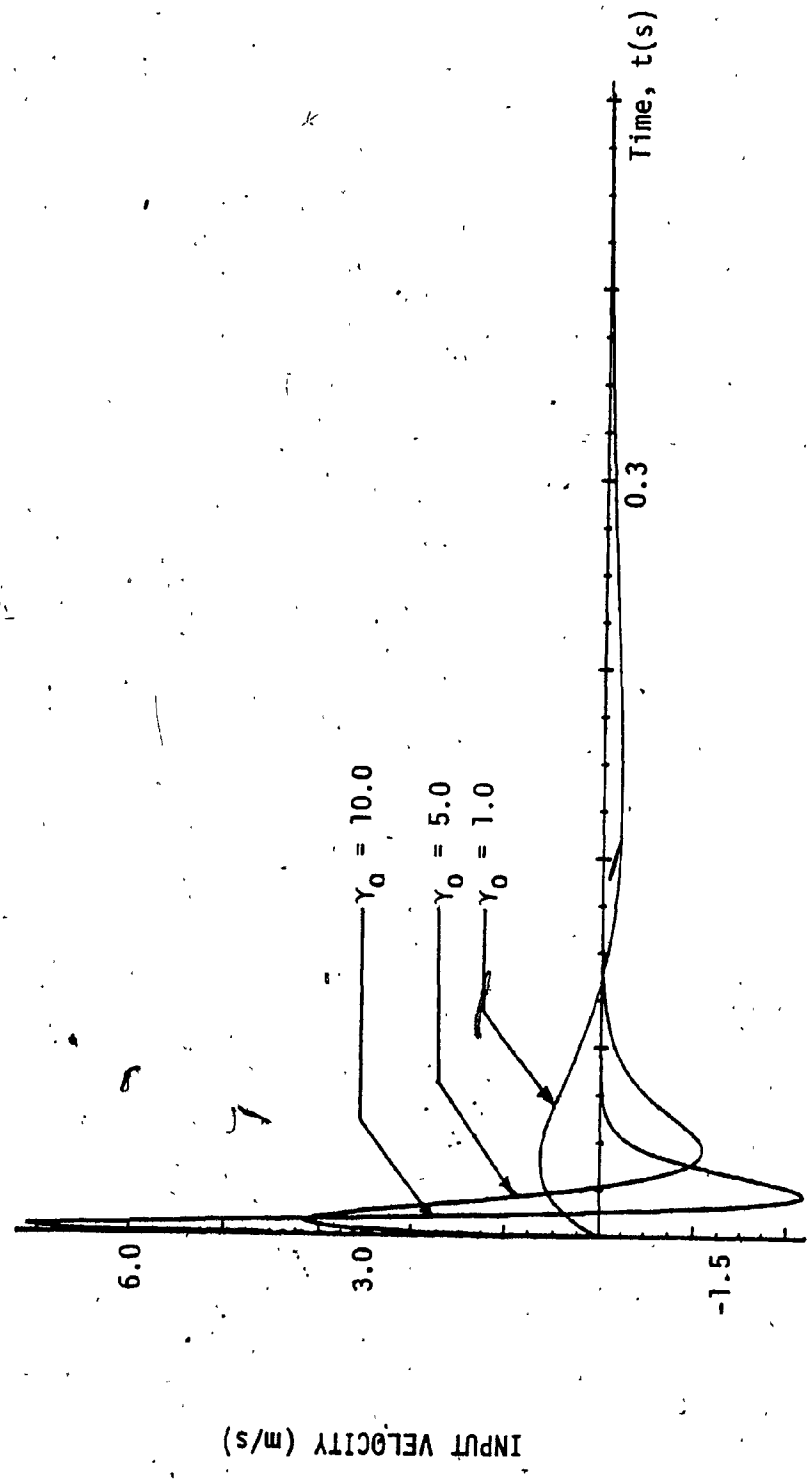

Fig. 7b: Input Velocity for Pulse Like Input

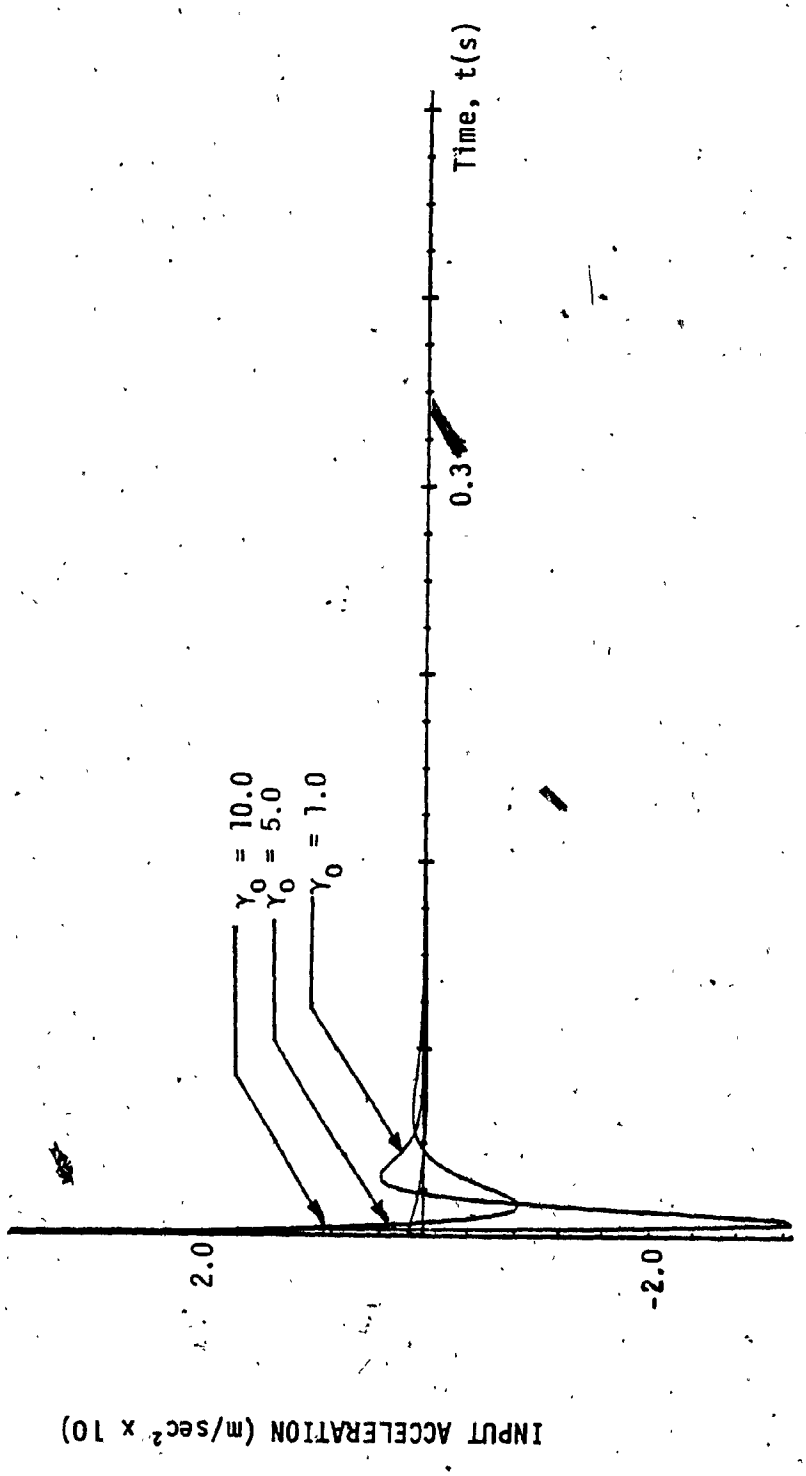

Fig. 7c: Input Acceleration for Pulse Like Input

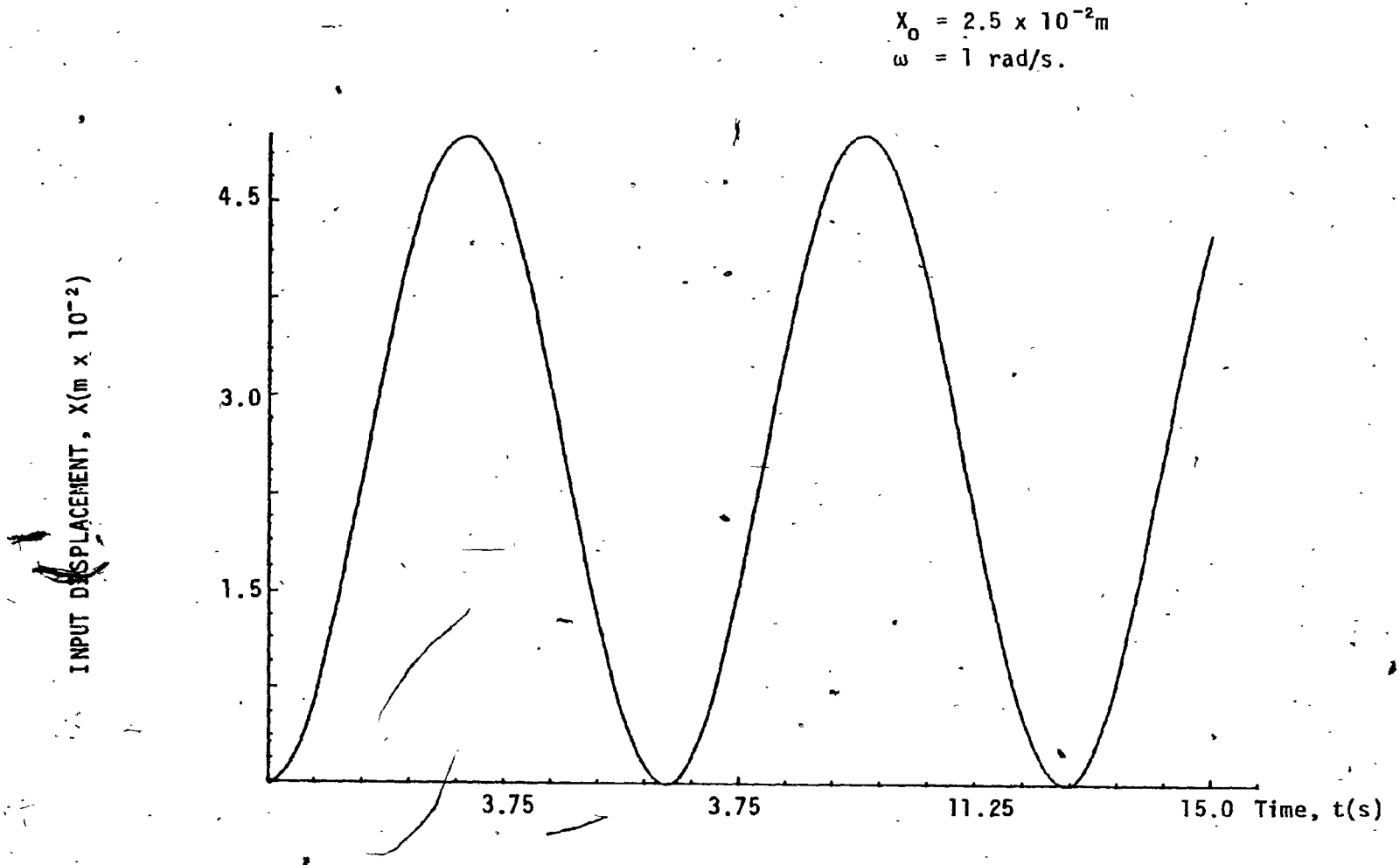

Fig. 8: Input Displacement for Inputs of the Form $X_o(1-\cos\omega t)$

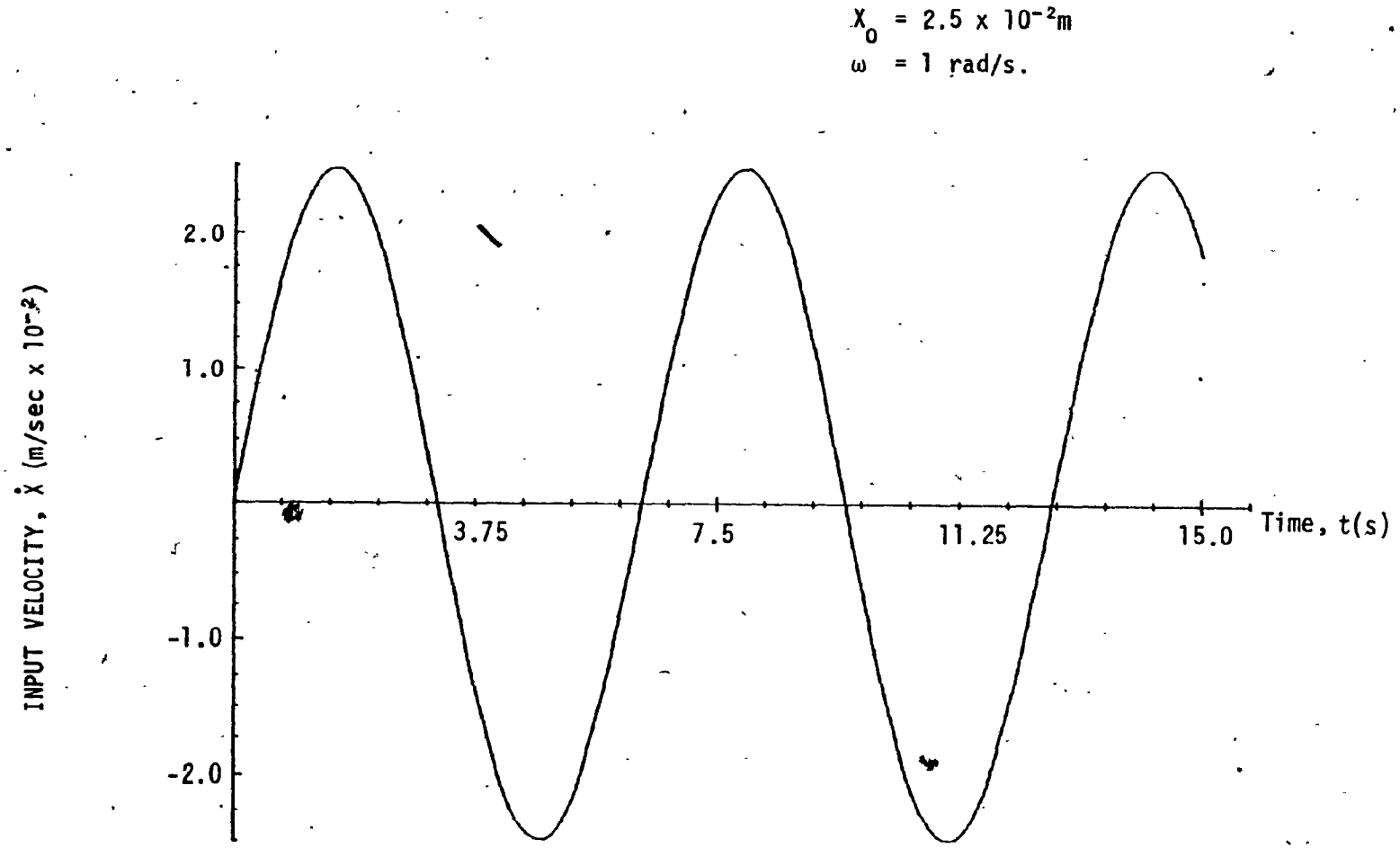

Fig. 8b: Input Velocity for Inputs of the Form $X_0(1-\cos\omega t)$

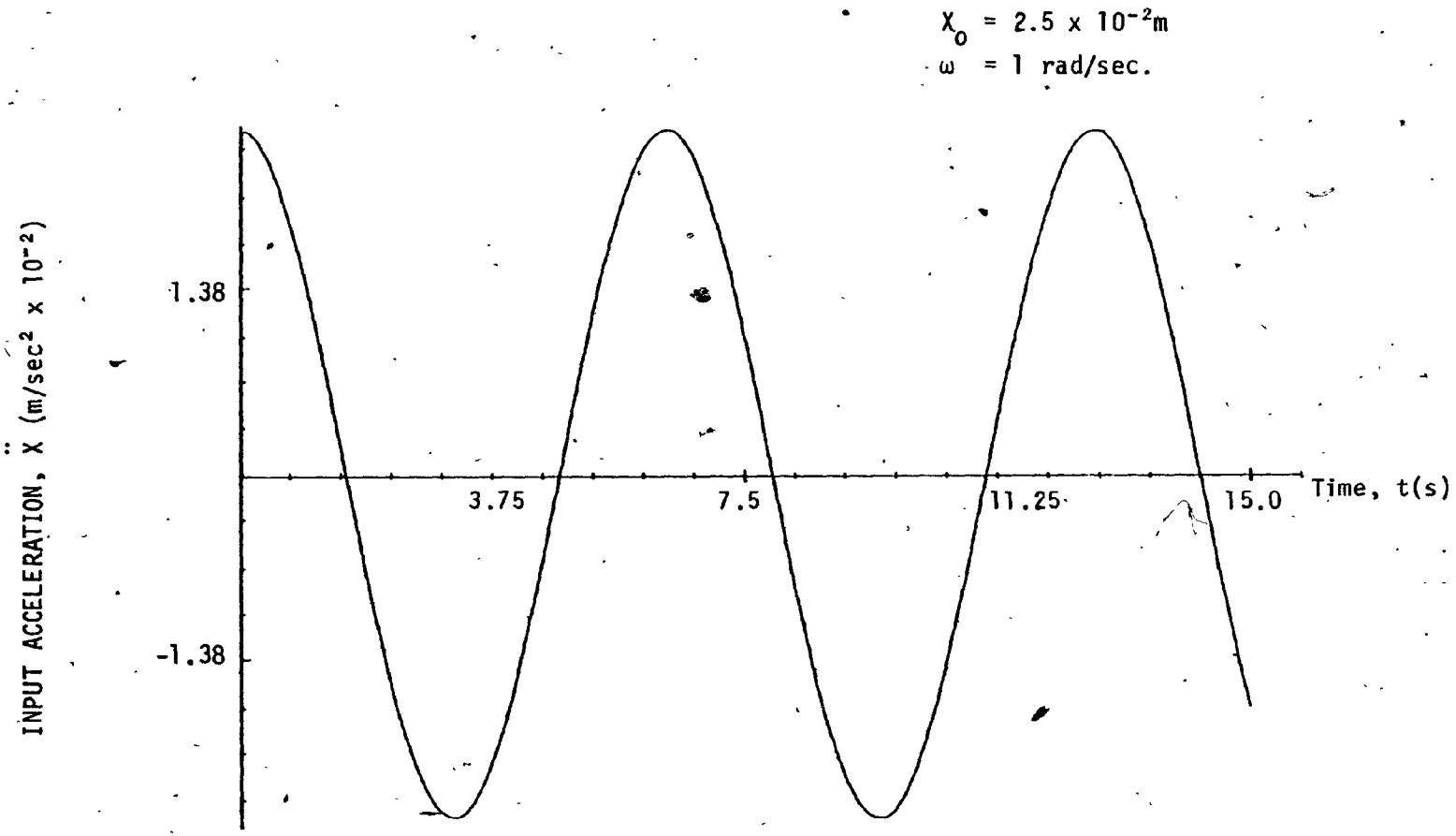

Fig. 8c: Input Acceleration for Inputs of the Form $X_o(1-\cos\omega t)$

TABLE 2.1

VARIABLE	VALUE USED IN THE SIMULATION
A_1	1.14×10^{-3} m^2
A_2	6.41×10^{-4} m^2
k	2.19×10^{3} N/m
K	$0.04 \times \frac{kg}{N \cdot S}\ {}^{\circ}k^{\frac{1}{2}}$
L	7.62×10^{-2} m
mg	4.45×10^{2} N
n	1.4
P_o	5.52×10^{5} N/m^2
T_o	295 °k
V_o	8.6868×10^{-4} m^3
δ	7.62×10^{-2} m

2.5.1 Response to Sinusoidal Input

For the passive system the main source of damping results from the flow of fluid through an orifice area between the two pressure chambers. Since the pressure and the flow equations are non-linear, it is not possible to obtain a closed form relation between the orifice area and the damping ratio.

To evaluate the effect of orifice area on the isolator performance, the size of the orifice area is varied and the sinusoidal response of the isolator evaluated.

The output displacement of the system is plotted against time and the plot is given in Figure 9. For the frequency considered the output displacement follows the input, and is free from any high frequency harmonics. Figure 10 shows the relative displacement between the input and the output. The relative displacement plot clearly shows the presence of initial transient in the output displacement for a period of approximately 0.75 sec and after which the output displacement reaches the steady state.

Figure 11 shows the output acceleration plotted against time. The output acceleration goes through a transient for approximately 0.75 sec and then settles down close to 0.03 m/sec^2. The steady state value of this acceleration is almost equal to the input acceleration. It is important to note that the output acceleration is without high frequency harmonic components. Figure 12 is the force generated by the damper. The steady state force is sinusoidal and the amplitude of oscillation is small.

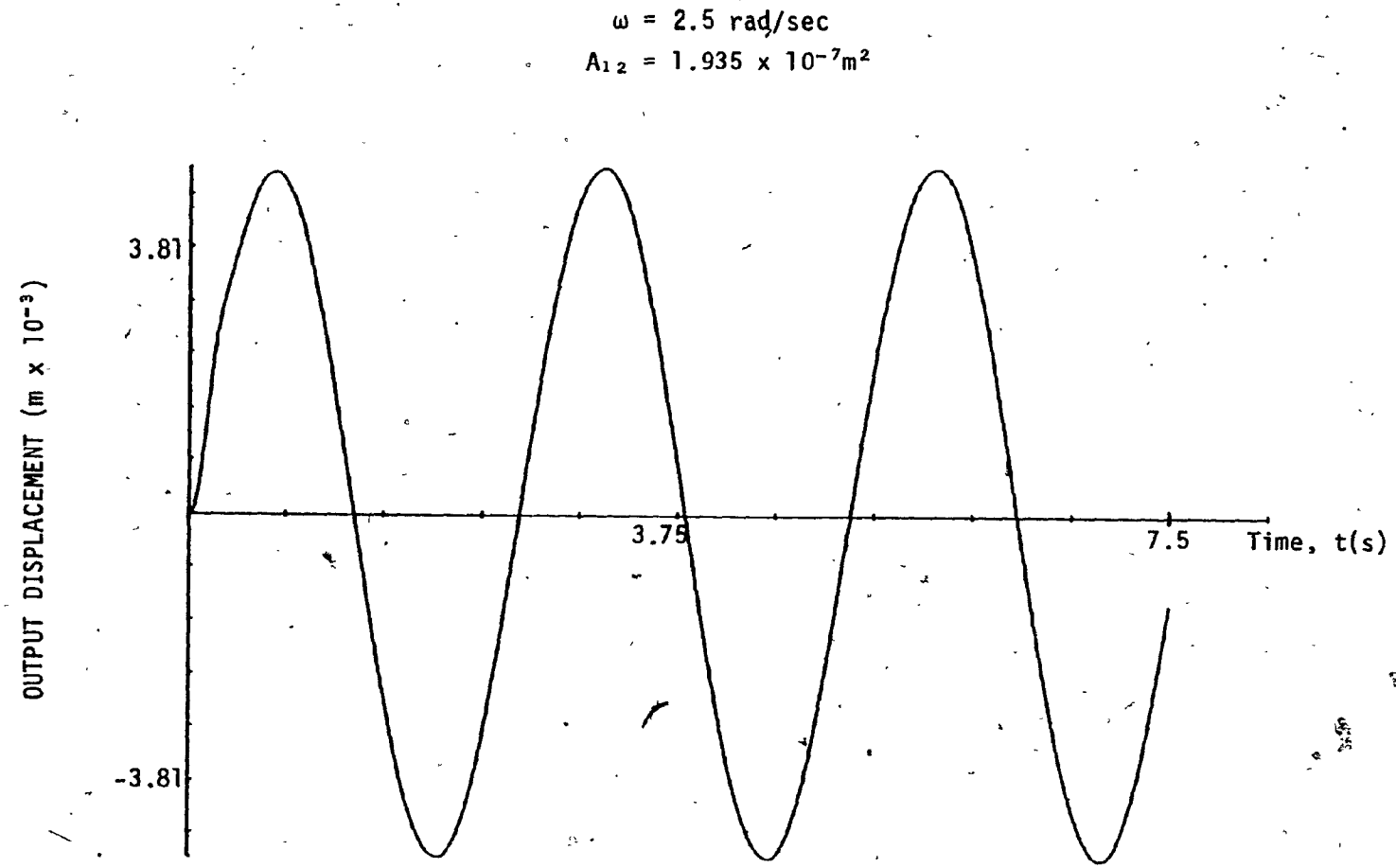

Fig. 9: Displacement Time Response of the Passive Suspension

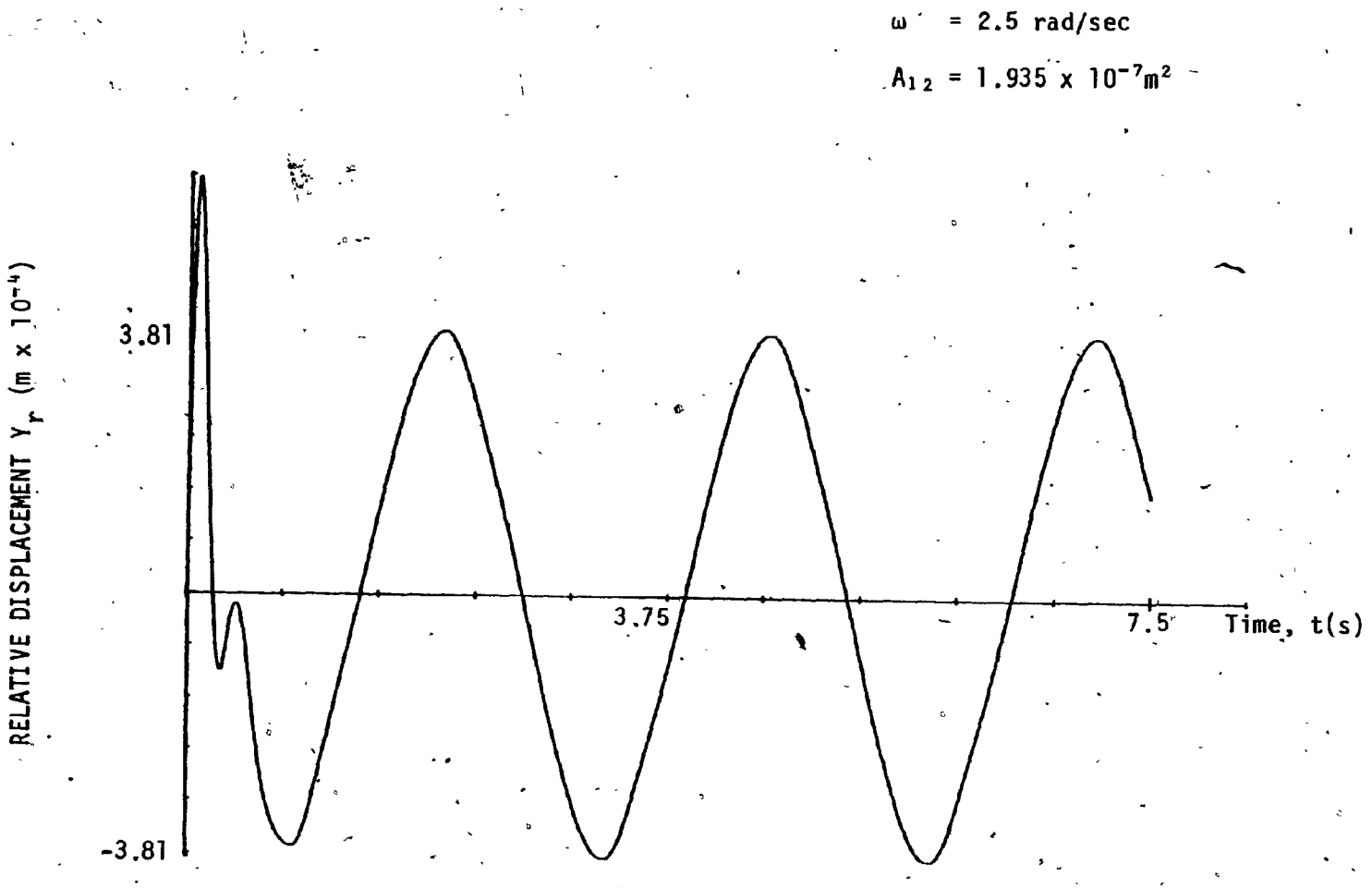

Fig. 10: Relative Displacement Time Response of the Passive Suspension

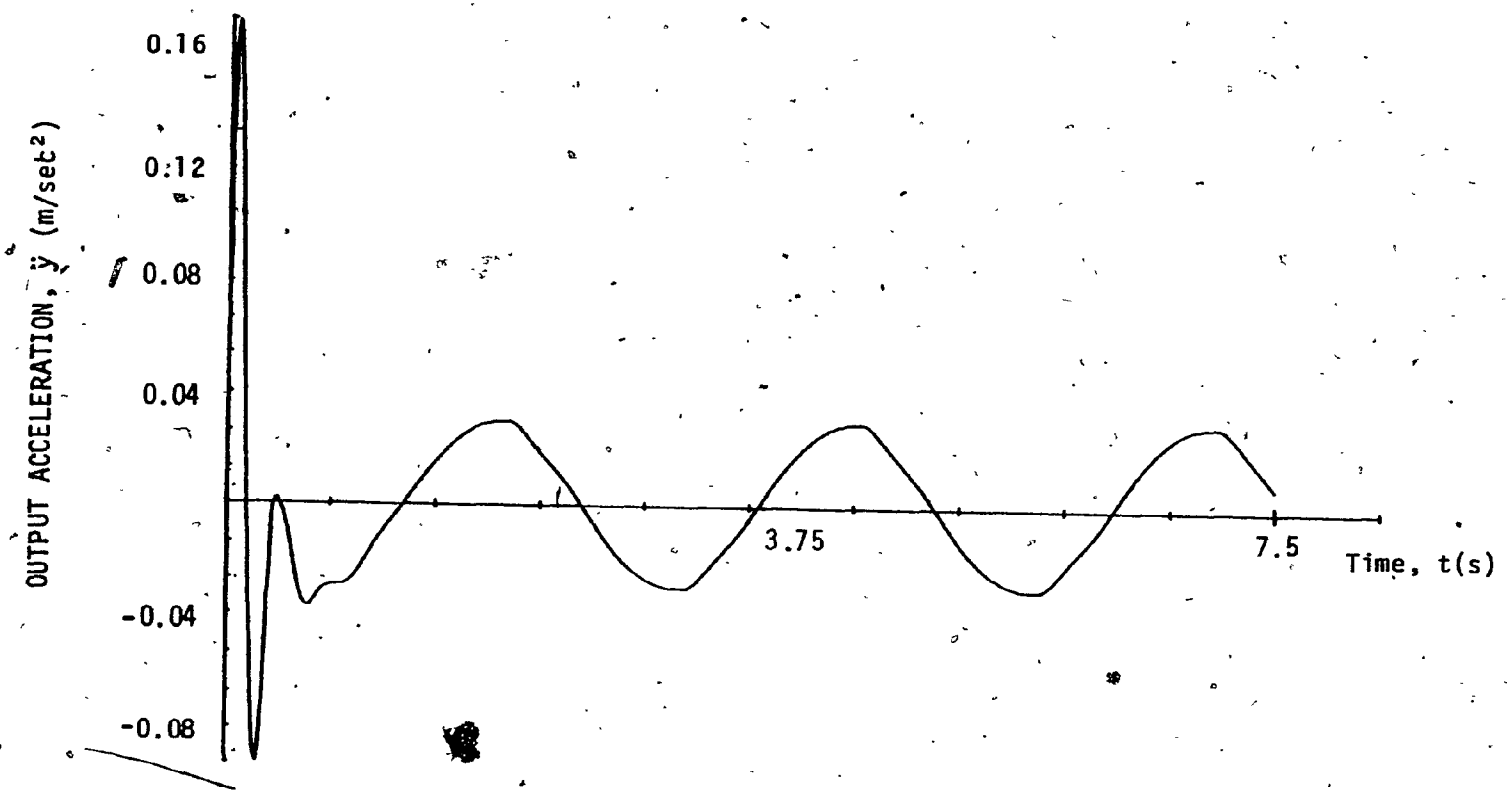

Fig. 11: Acceleration Time Response of the Passive Suspension

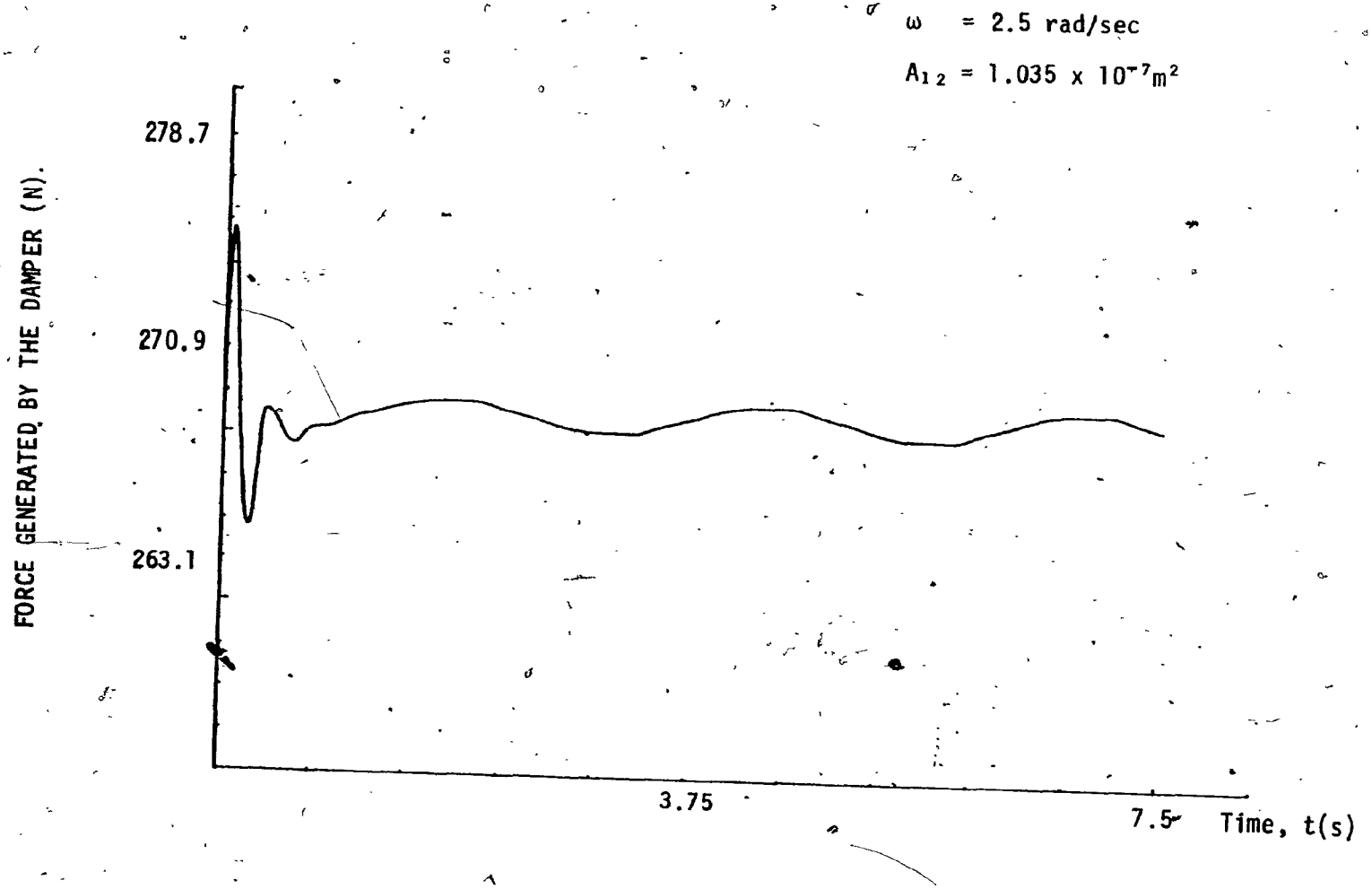

Fig. 12: Force Generated by the Passive Suspension

Figures 13 and 14 show the absolute and relative displacement respectively for an orifice area of $6.45 \times 10^{-7} m^2$. Even though the output displacement has the same frequency as the input, the relative displacement shows that the output displacement does not follow the input closely. From the time plot of the relative displacement, it is evident that there are high frequency fluctuations superposed over a low frequncy component. These high frequency oscillations are due to increasing the orifice area. When the orifice area increases until a critical value, the damping in the system increases and the stiffness decreases which results in lowering the natural frequency, thus introduces high frequency oscillations.

The output acceleration and the force generated by the damper are shown in Figures 15 and 16. Both of them show an oscillatory output. The amplitude of the acceleration decreases with time but as it can be seen from Figure 15 the decay is slow.

In Figure 17 the acceleration transmissibility* of this passive system is given. From the plot it is evident that the steady state peak acceleration reduces as the size of the orifice area is increased. From the absolute acceleration transmissibility curve, the damped natural frequency of the system for orifice areas $6.45 \times 10^{-8} m^2$ and $1.935 \times 10^{-7} m^2$ can be approximated to 20 rad/sec. and for the orifice area of $6.45 \times 10^{-7} m^2$ it is in the vicinity of 10 rad/sec. Figure 17 also shows that higher transmitted acceleration (or force) levels at frequencies below the natural frequency while there is a considerable reduction in the amount of acceleration (or force) transmitted to the mass at higher frequencies

*Ratio of steady state peak output to the peak input plotted against the excitation frequency.

above the natural frequency.

Figures 18 and 19 show the absolute and relative displacement transmissibility plots respectively. There is a considerable variation in the two plots relating to the peak absolute and the relative displacement. At frequencies below the resonance, higher absolute displacement is seen whereas the relative displacement is small. However, at frequencies above the resonance, the absolute displacement decreased montonically in comparison to a constant value for the relative displacement.

One of the major requirements of any vibration isolator is to have minimum (transmitted) acceleration and to have a minimum relative displacement between the vibrating base and the isolated mass. This is one of the hard requirements to achieve and in most of the passive systems including the pneumatic passive isolator presented in this thesis, a compromise is sought between the transmitted acceleration and relative displacement.

By comparing the performance of the four different orifice areas of the system it can be seen that for an effective orifice area of 6.45×10^{-7} m^2 the system performance is good. The mass flow rate between the two pressure chambers is directly proportional to the size of the orifice area. So, when the orifice area is increased even for a small difference in pressure between the two chambers the mass flow rate between the two chambers will be high. This will cause oscillation in the chamber pressures and one of the pressures might go to vacuum pressure. For the passive system considered when the orifice area was increased to 3.225×10^{-6} m^2 the system became unstable.

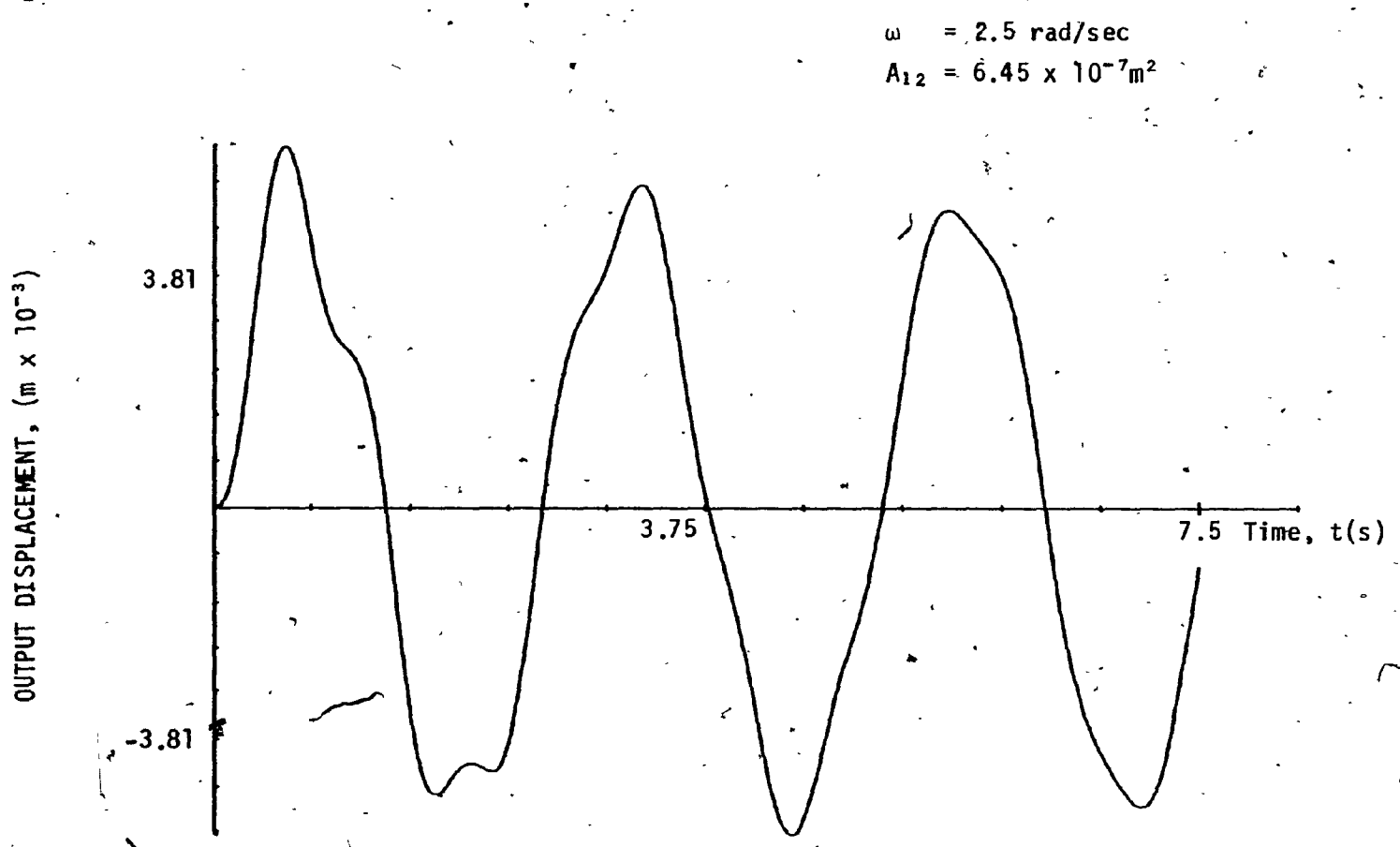

Fig. 13: Displacement Time Response of the Passive Suspension

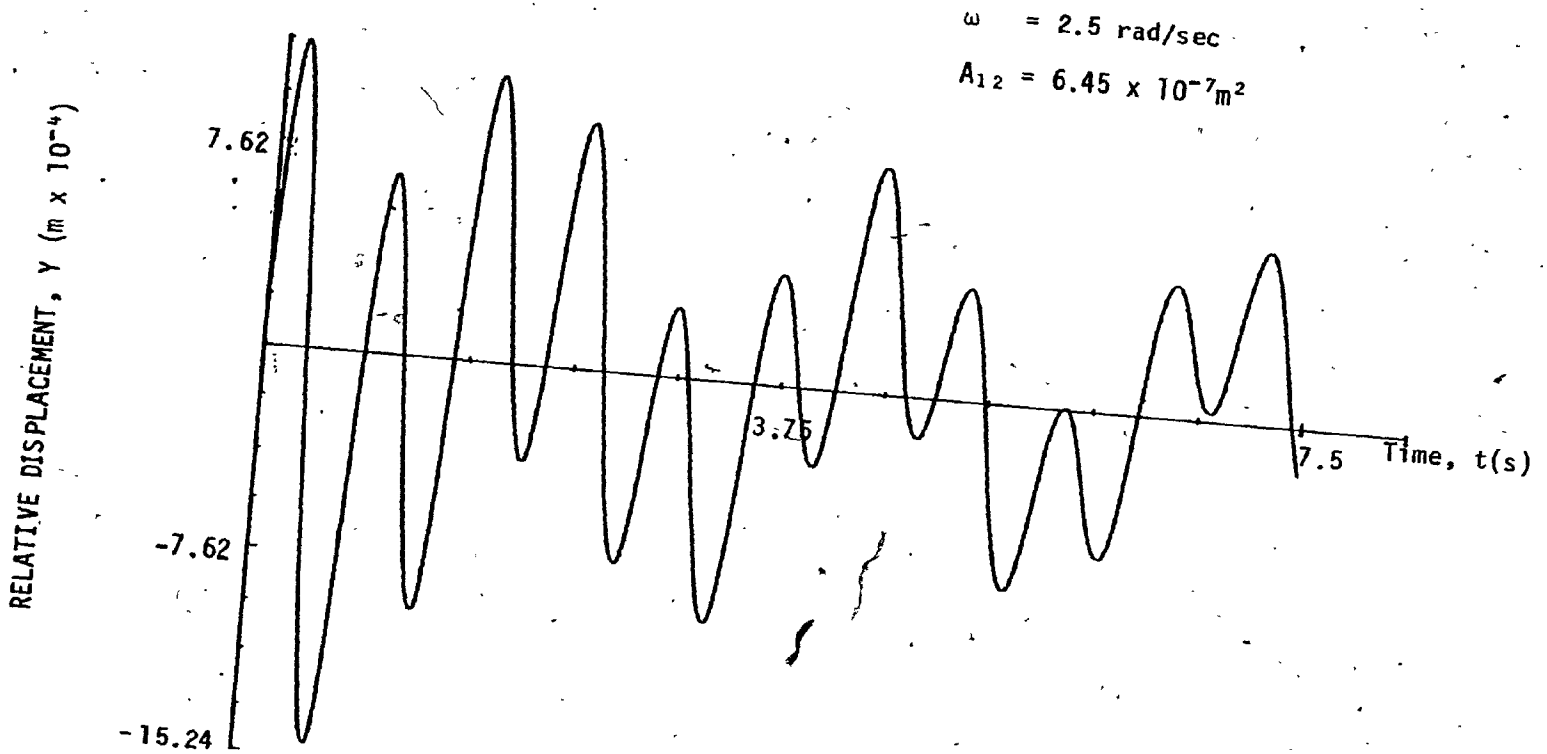

Fig. 14: Relative Displacement Time Response of the Passive Suspension

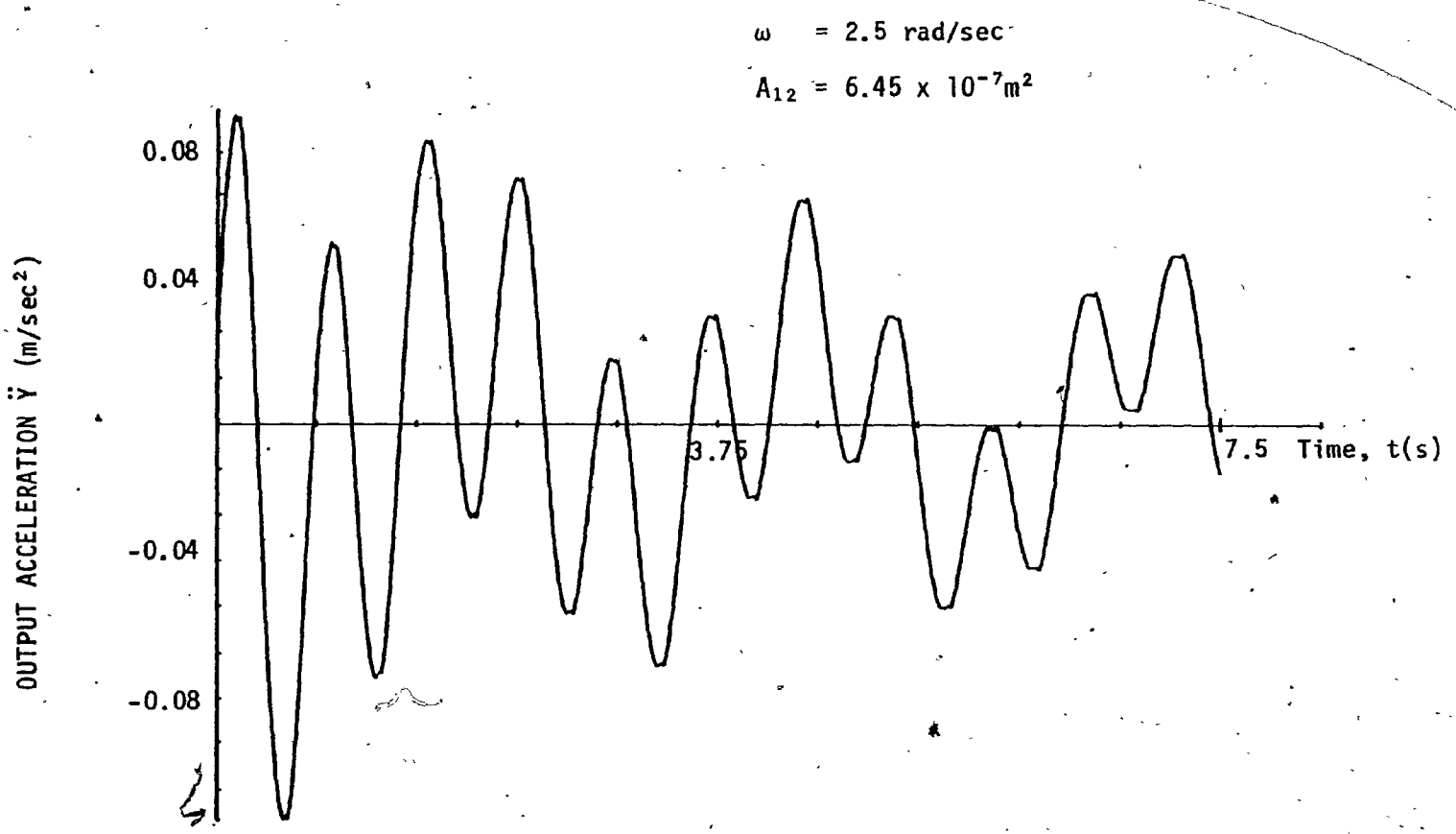

Fig. 15: Acceleration Time Response of the Passive Suspension

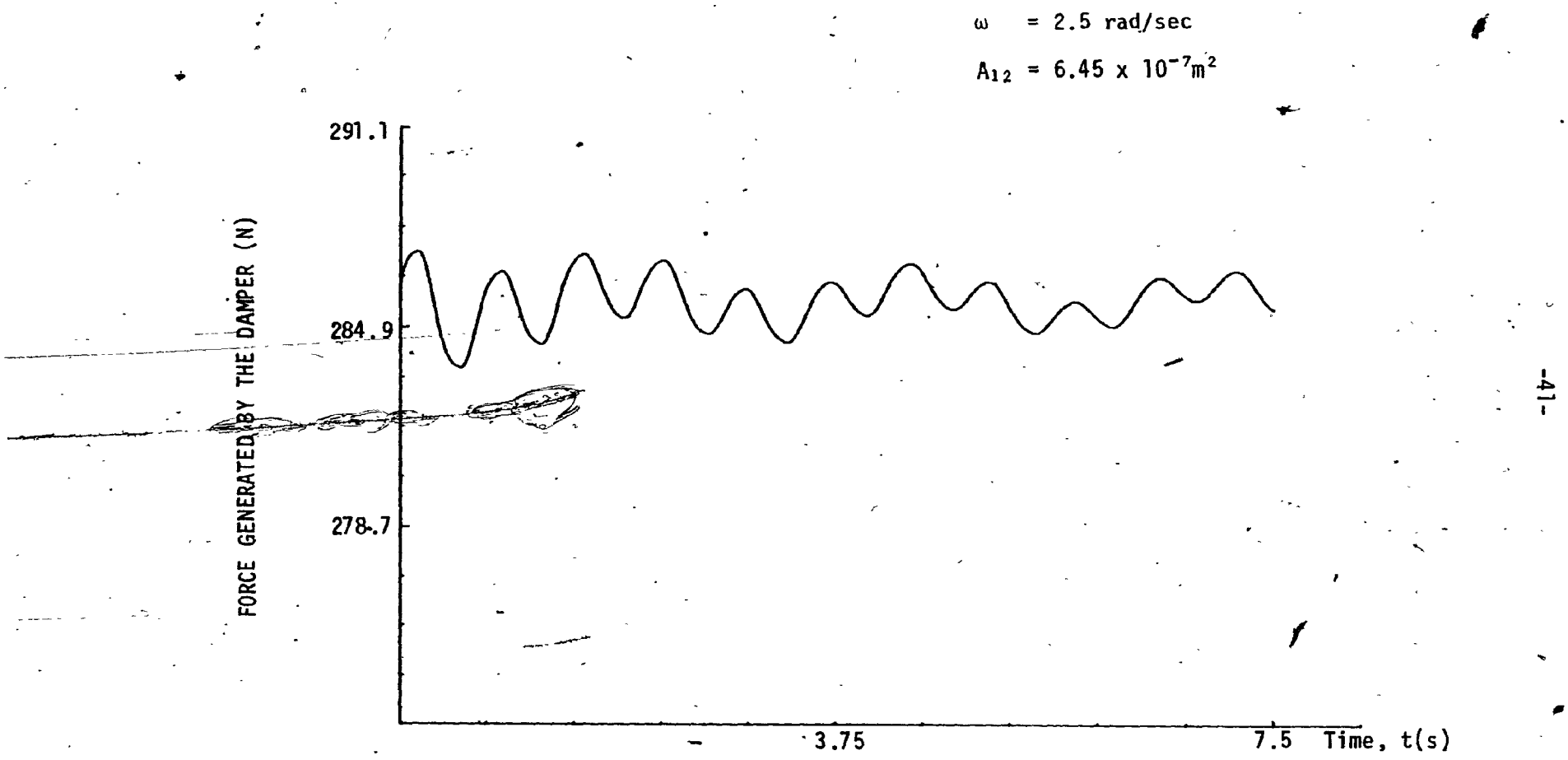

Fig. 16: Force Generated by the Passive Suspension

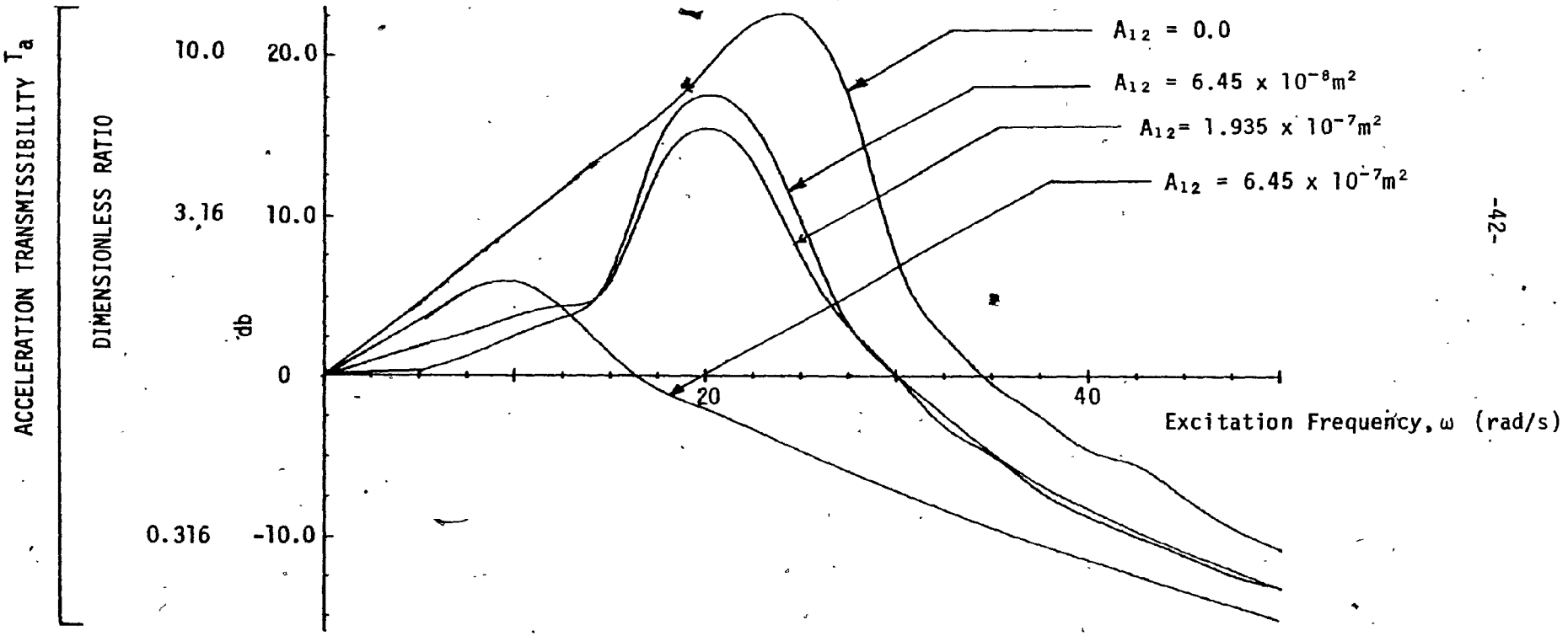

Fig. 17: Absolute Acceleration Transmissibility

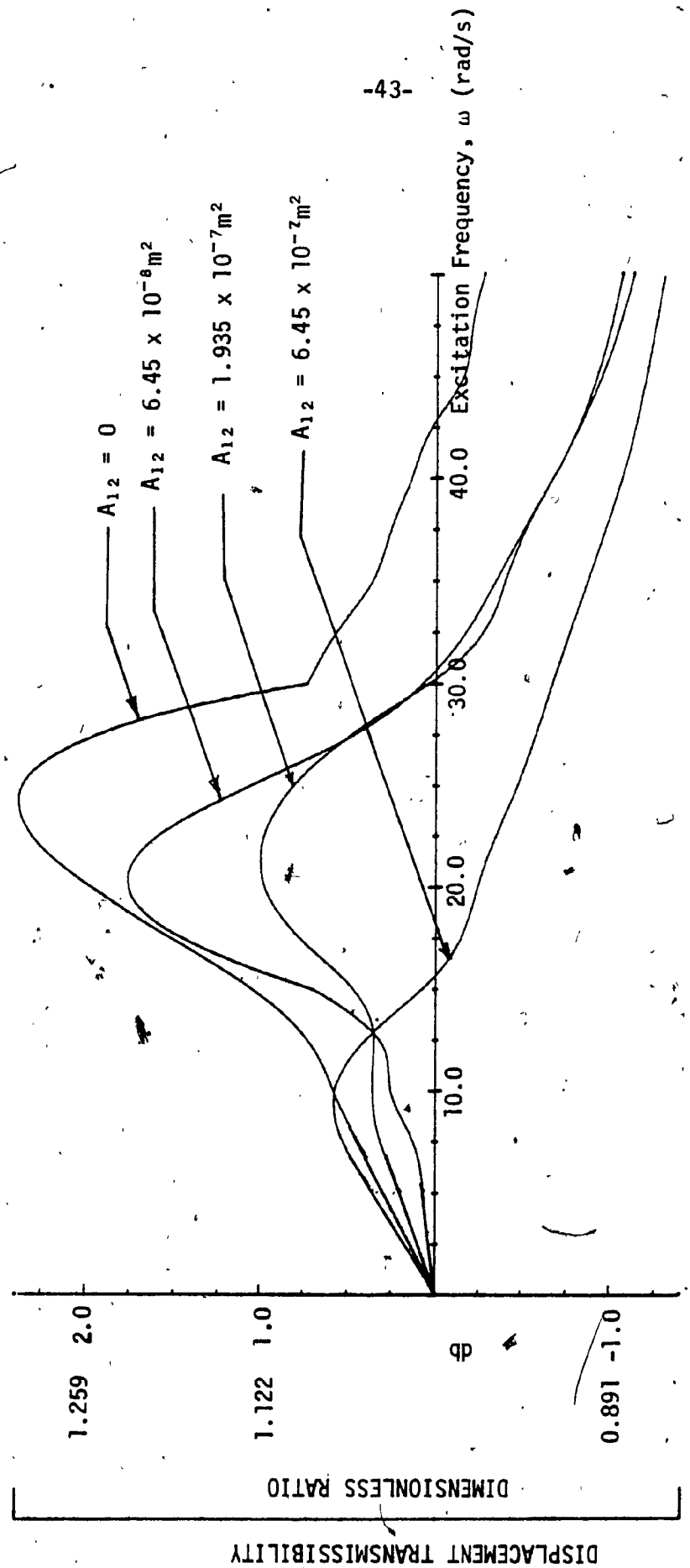

Fig. 18: Absolute Displacement Transmissibility

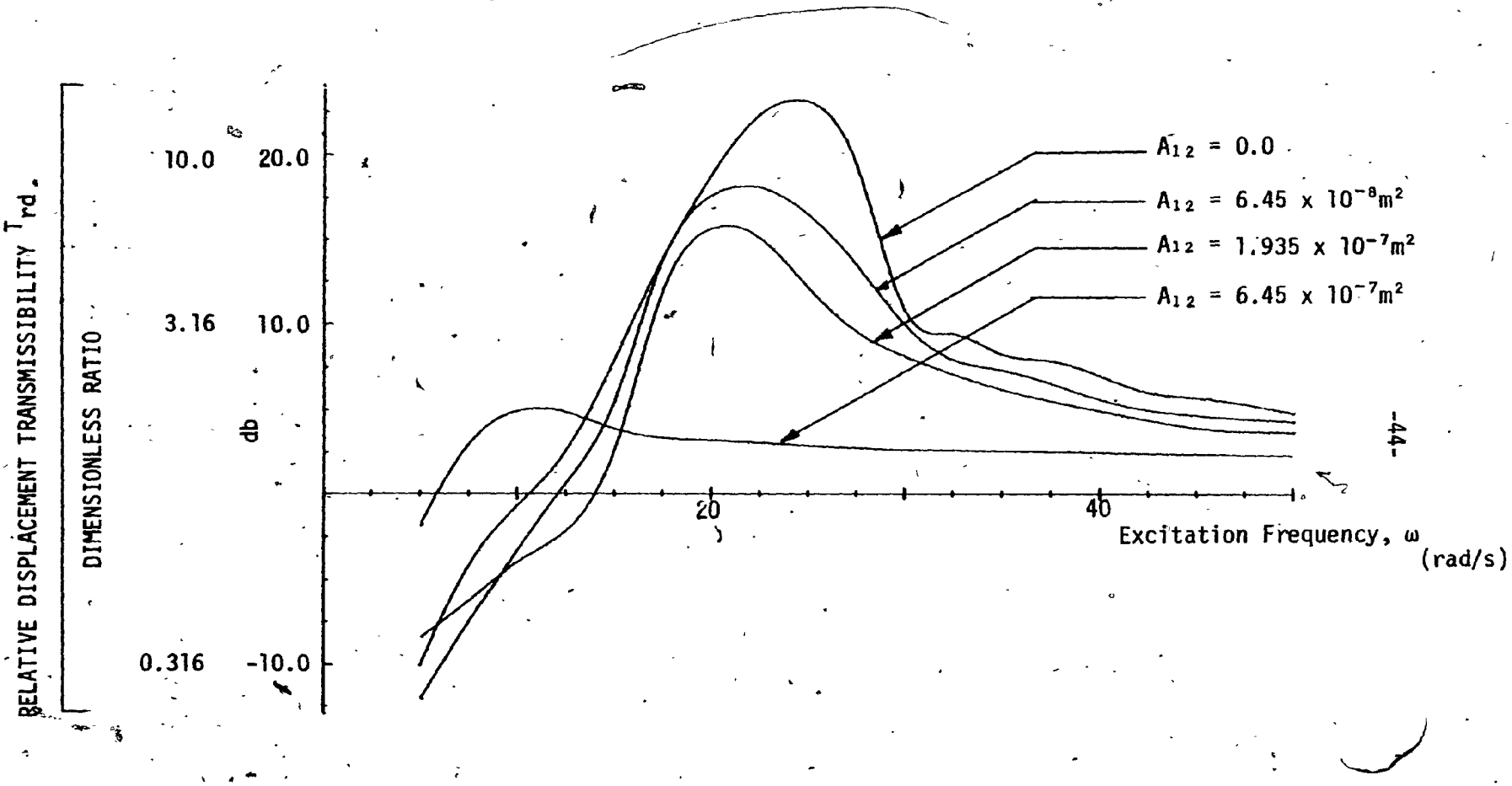

Fig. 19: Relative Displacement Transmissibility

2.5.2 Response to Pulse Like Input Displacement

Figure 7 shows the input displacement velocity, and acceleration of the rounded pulse. As mentioned before the shock severity parameter γ_0 was varied from 1 to 10. The system performance was evaluated for an effective orifice area of 1.935×10^{-7} m^2.

The output displacement for the above mentioned input is given in Figure 20. The maximum output almost has half the amplitude as the input displacement. As it can be seen from Figure 20, the displacement decays exponentially to zero. Figure 21 shows the relative displacement of the system. This has a similar characteristic of that of the output displacement plot. Figure 22 gives the output velocity of the system.

Figure 23 shows the output acceleration of the system. As it can be seen from Figure 23, both the positive and negative peak acceleration takes place within 0.1 sec. eventhough the output acceleration seems to be zero after 1 sec., it still goes through a small amplitude oscillation.

Figures 24 and 25 show the relative displacement and acceleration ratio* plotted against the shock severity parameter γ_0. From these plots it can be seen that as the severity parameter γ_0 increases the transmitted acceleration (or force) to the mass decreases and the relative displacement increases.

2.5.3 Response to Input Excitation of the Form $X = X_0 (1-\cos\omega t)$

For the passive isolation system, an input excitation representing a track profile of the form $X = 0.025 (1-\cos t)$ m is considered.

* Relative displacement and acceleration ratio is defined as the ratio between peak output to the peak input.

Figure 26 is the plot of output displacement. Comparing this plot with the plot 7a of the input displacement it can be seen that the output follows the input very closely. The relative displacement in Figure 27 shows initial transient and reaches steady state after about 7.5 s. It is also seen that the amplitude of the relative displacement is very small.

Figure 28 shows the output velocity of the system plotted against time. The output acceleration of the system given in Figure 29. Similar to the relative displacement response, the acceleration history has an initial transient and is about 2.5 times greater than the input acceleration. During the transient, the system goes through some oscillations and reaches a steady state after about 8 sec. The steady state output acceleration of the mass is about the same magnitude as the input acceleration.

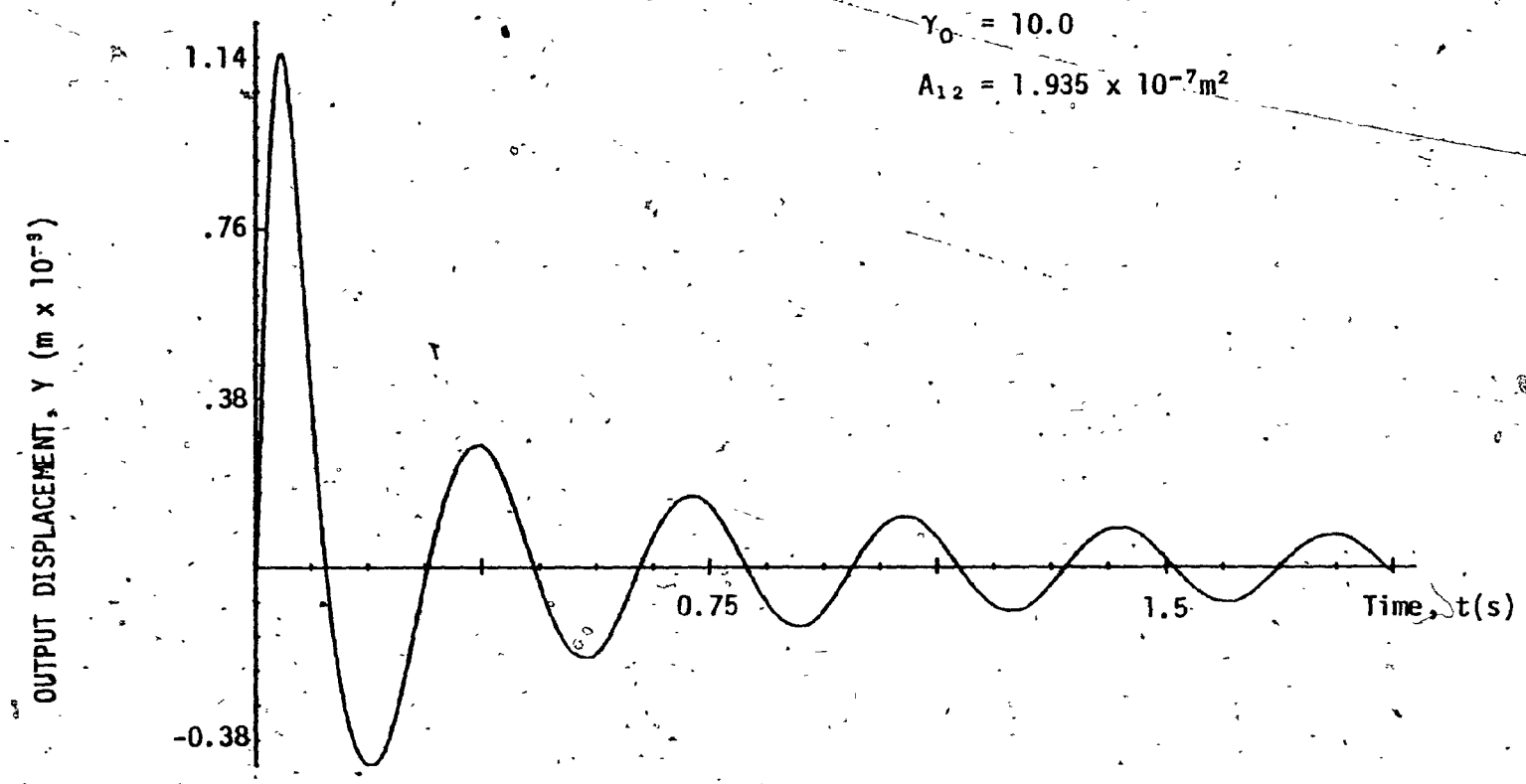

Fig. 20: Displacement Time Response for Rounded Pulse Input

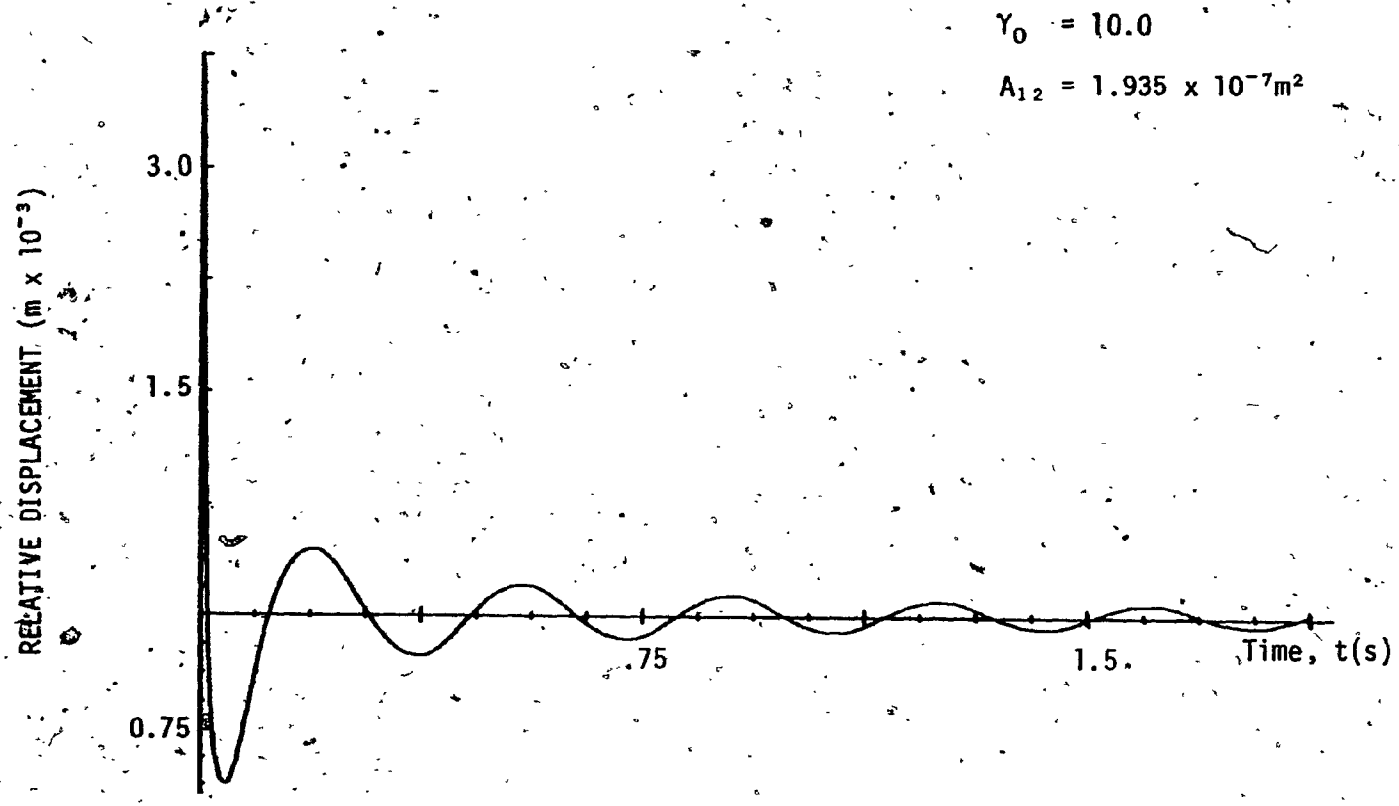

Fig. 21: Relative Displacement Time Response for the Rounded Pulse Input

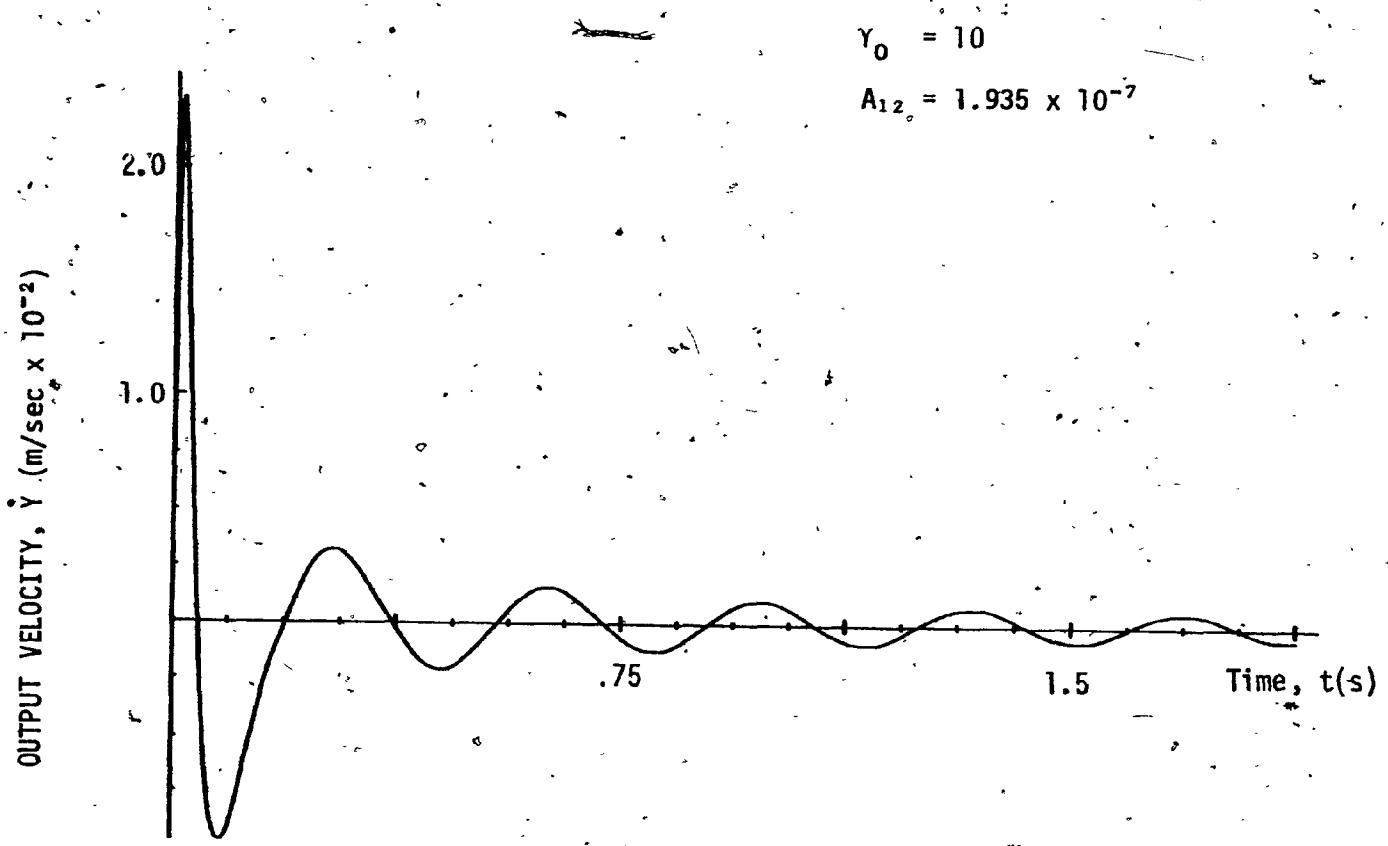

Fig. 22: Velocity Time Response for Rounded Pulse Input

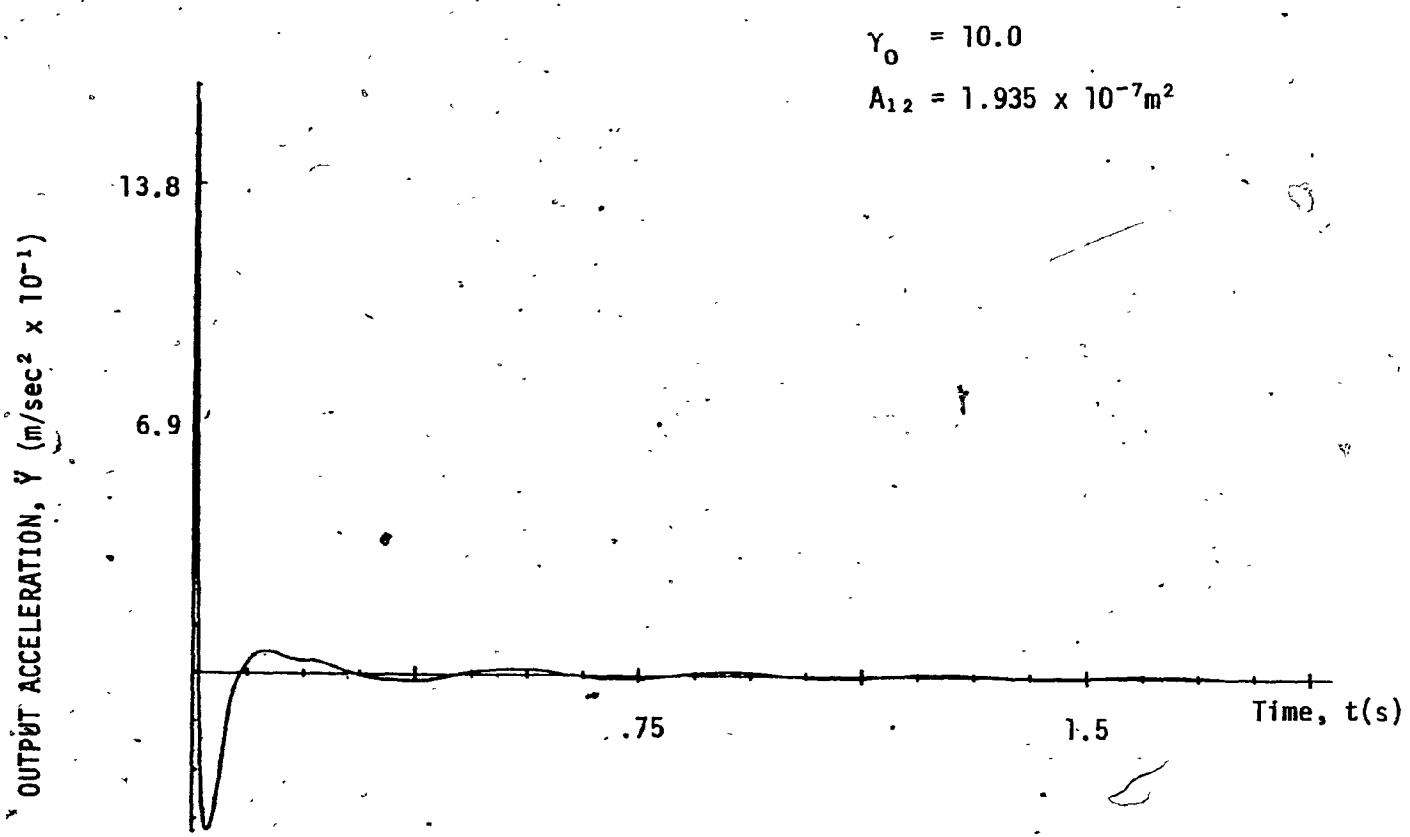

Fig. 23: Acceleration Time Response for Rounded Pulse Input

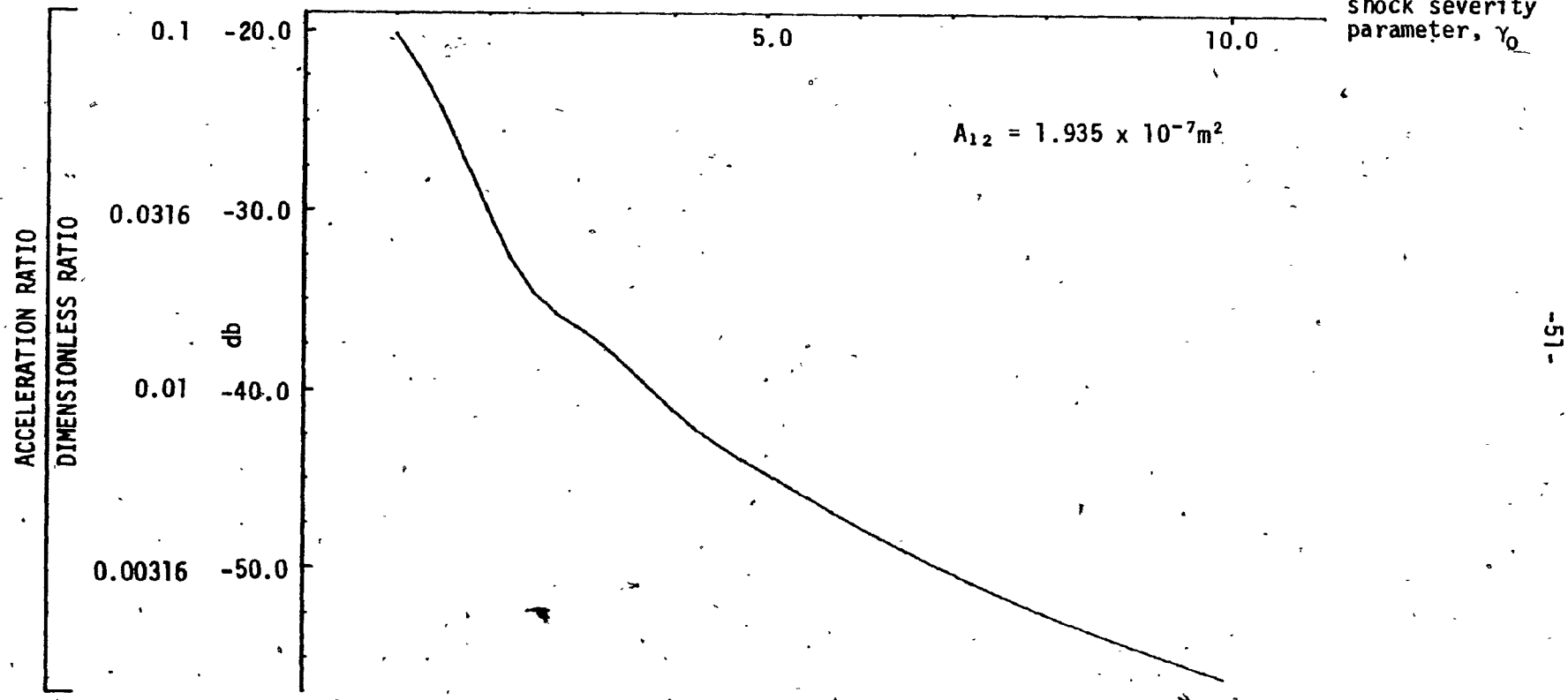

Fig. 24: Acceleration Ratio for Rounded Pulse Input

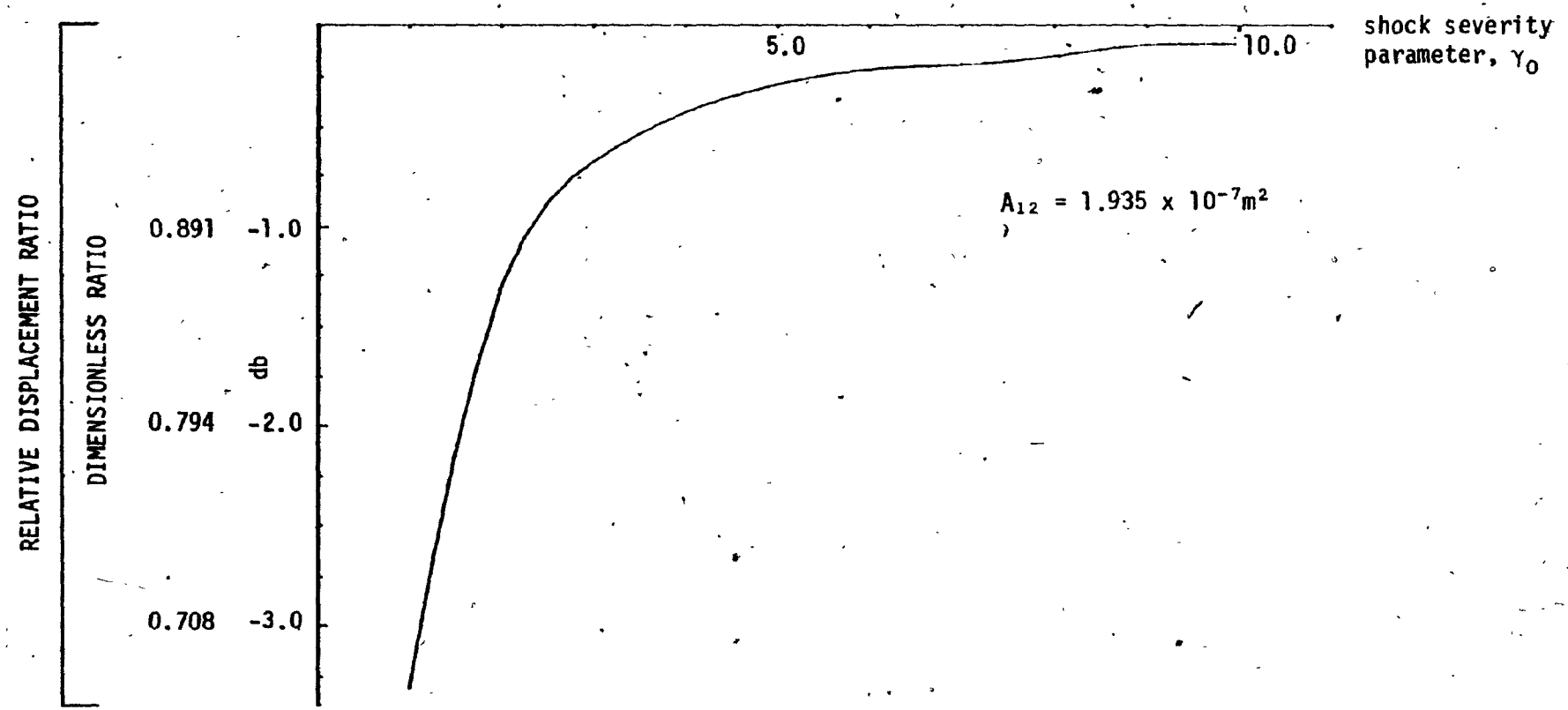

Fig. 25: Relative Displacement Ratio for Rounded Pulse Input

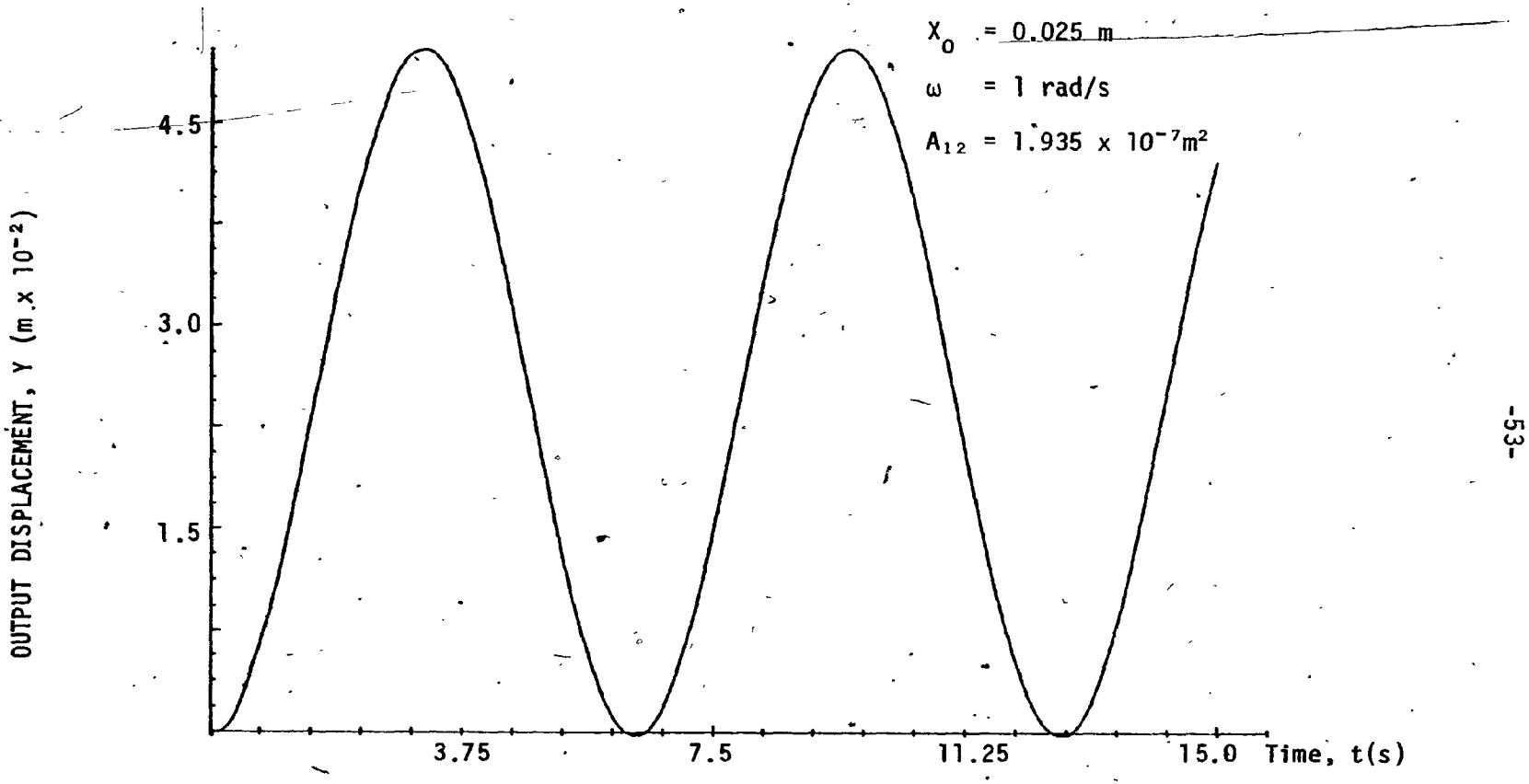

Fig. 26: Response for Input of the Form $X = X_0 (1-\cos\omega t)$

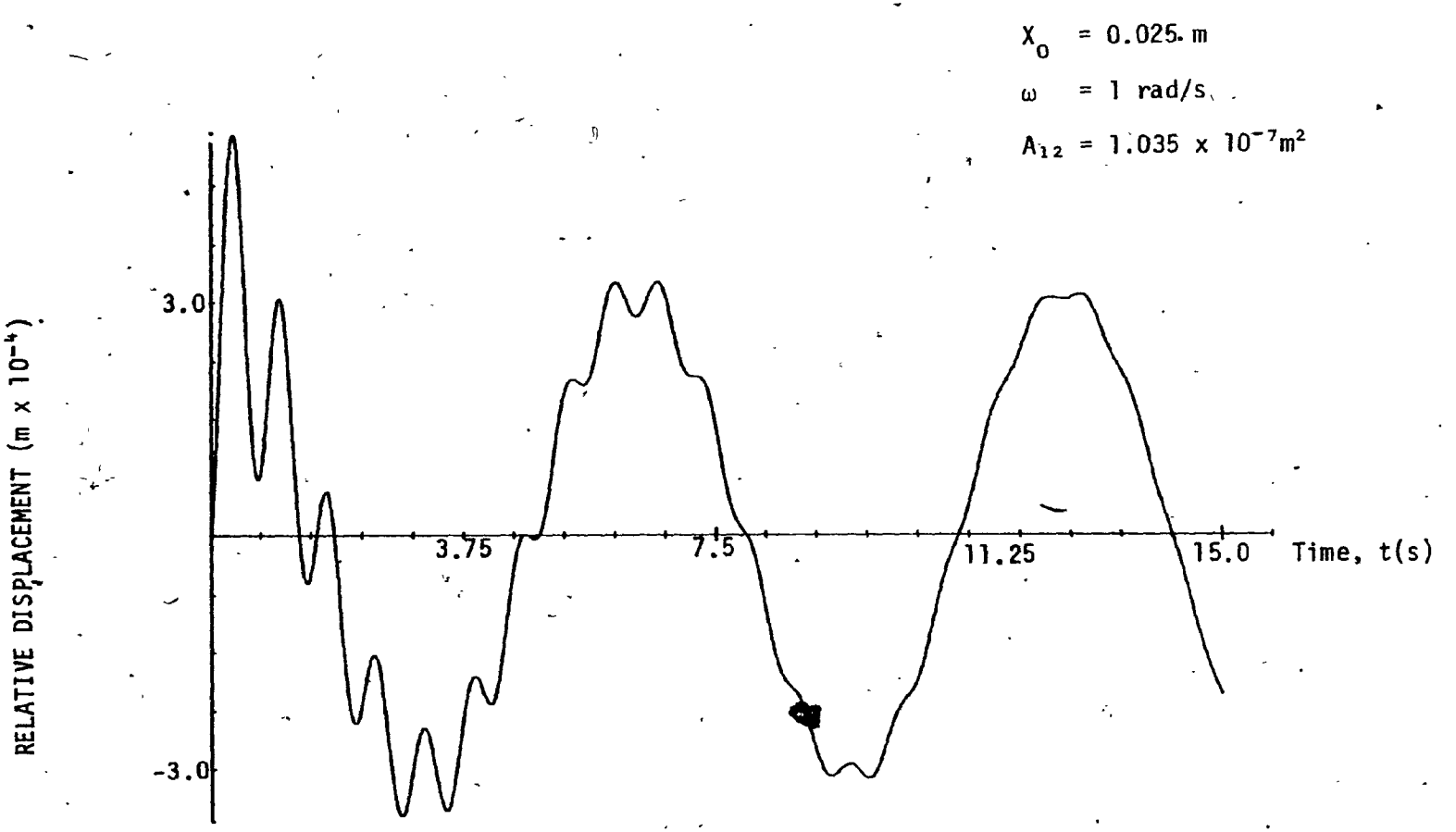

Fig. 27: Time Response for Input of the Form $X = X_o$ (1-cosωt)

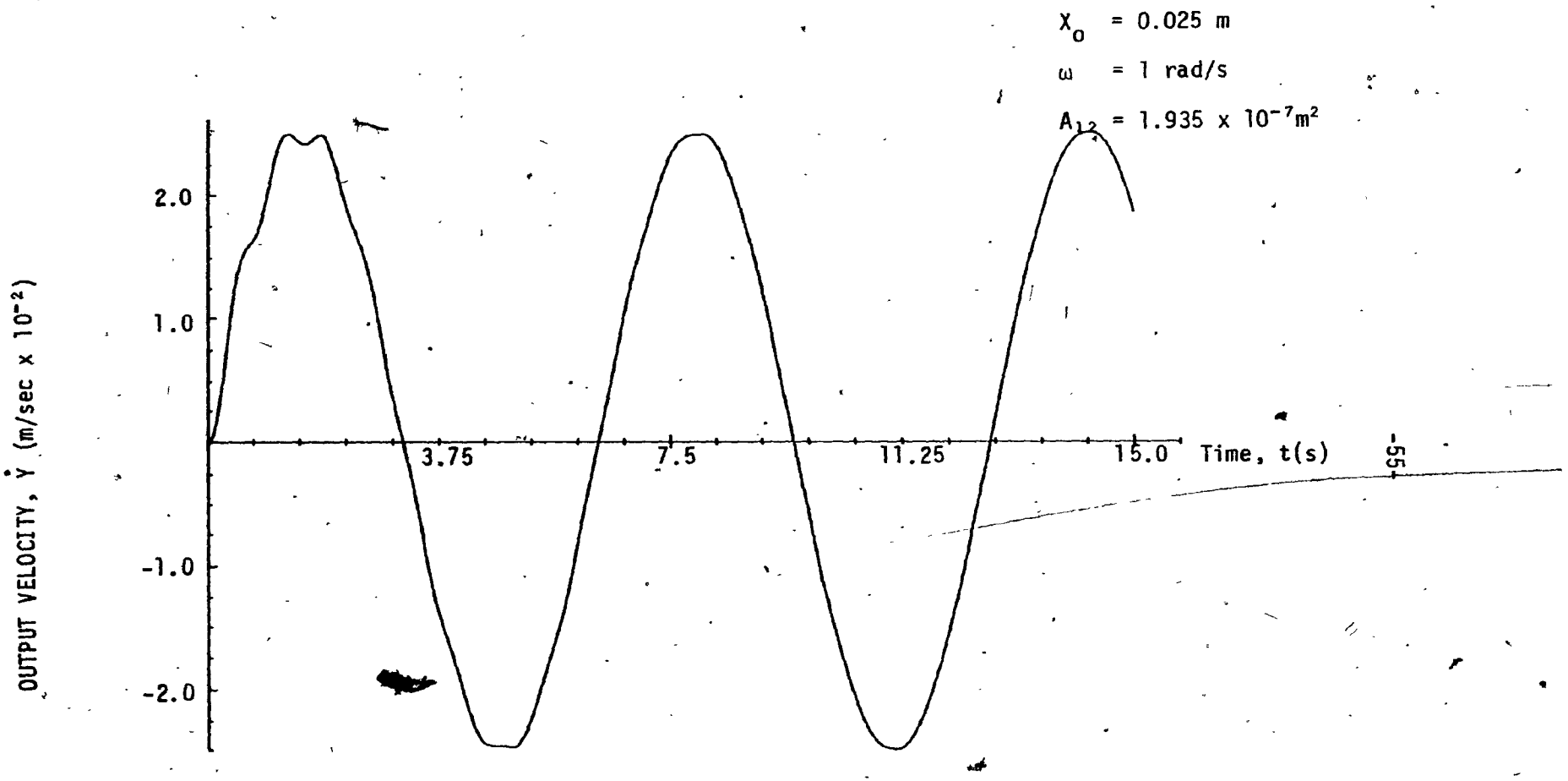

Fig. 28: Time Response for the Input of the Form $X = X_o (1-\cos\omega t)$

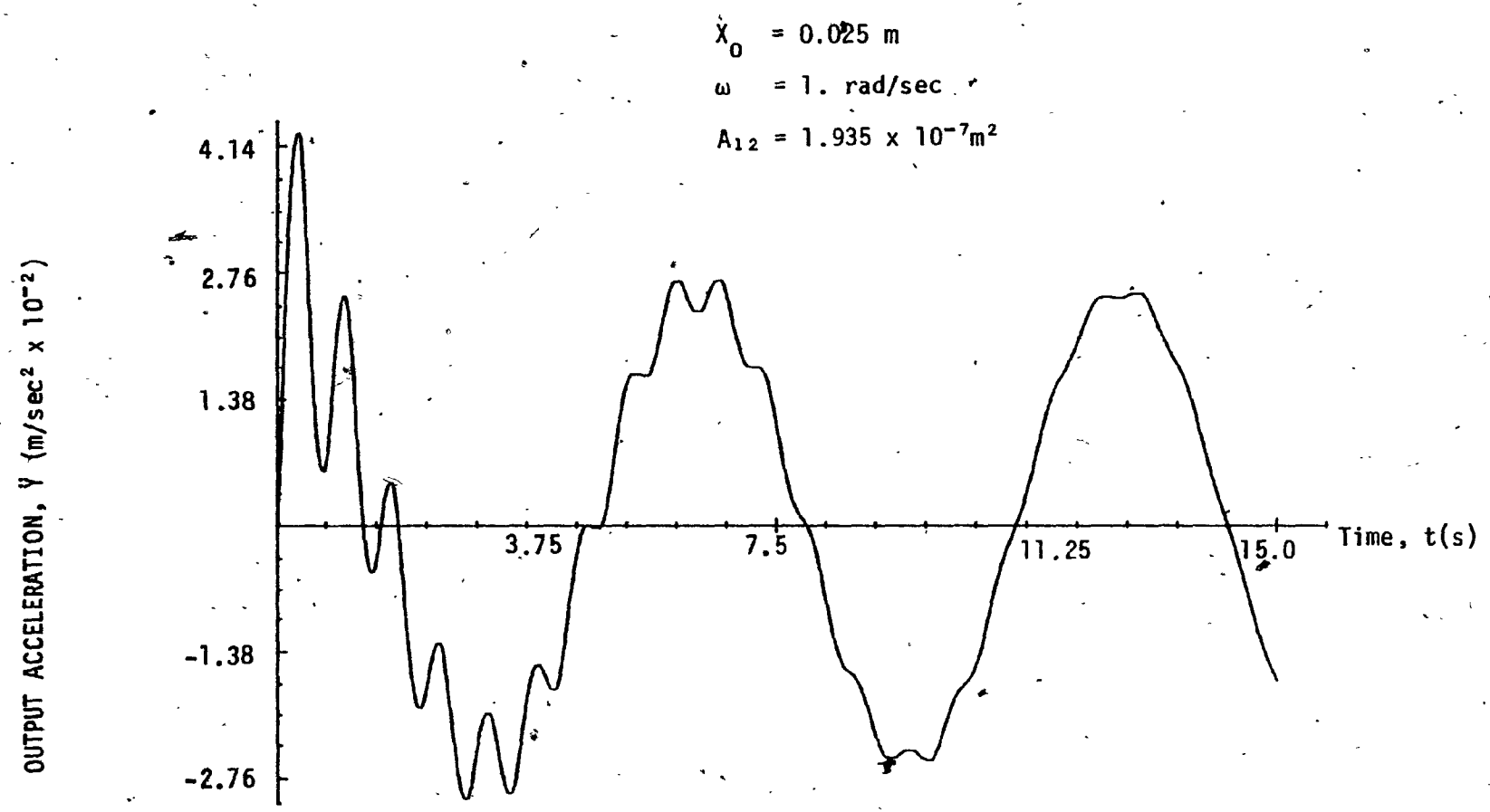

Fig. 29: Time Response for the Input of the Form $X = X_0$ (1-cosωt)

CHAPTER 3

CHAPTER 3

ACTIVE PNEUMATIC VIBRATION ISOLATION SYSTEM

3.1 GENERAL

The performance of the passive system shows that good isolation can be achieved only for input frequencies higher than the natural frequency of the system. But for inputs with low frequency, acceleration transmissibility is high. In order to achieve good isolation over a wide frequency range, an active electro-pneumatic system is considered. The control logic for the active system is developed based on zero jerk for the mass. The governing system equations are derived and a digital simulation procedure is adopted.

3.2 DESCRIPTION OF THE ACTIVE SYSTEM

Two types of active pneumatic vibration isolation system are considered. The schematic of the two active system are shown in Figures 30 and 31. Static support of the mass for both types of active systems are provided by the pressures in the cylinder chambers and by a mechanical spring.

The active isolation system Type 1 (Figure 30) consists of two independent electro-pneumatic servo-valves. These two servo-valves control the flow in and out of the chamber 1 and chamber 2 at every instant of time. When the relative velocity $(\dot{x}-\dot{y})$ is positive, the fluid from chamber 1 is discharged through the servo-valve while the servo-valve connected to the chamber 2 regulates the flow from a pressure source to chamber 1. When the relative velocity $(\dot{x}-\dot{y})$ is negative the flow is discharged from chamber 2 and the chamber 1 is charged from the pressure source.

The active isolation system Type 2 (Figure 31) has only one electro-pneumatic servo-valve. This servo-valve regulates the flow in and out of chamber 1, while the chamber 2 is sealed and hence no flow will go out or come in to chamber 2. Similar to the Type 1 active system, the fluid from chamber 1 is discharged through the servo-valve when the relative velocity is positive. When the relative velocity is negative, the servo-valve regulates the flow from the pressure source to chamber 1.

In both Type 1 and Type 2 active isolation systems, the input current to the servo-valve is provided from the measured values of chamber pressures, the relative velocity, acceleration, velocity and displacement signals.

3.3 GOVERNING EQUATIONS

Similar to passive isolation system the active vibrational isolation system is characterized by

1) pressure equations
2) flow equations
3) force balance equations

3.3.1 Governing Equations for Type 1 Active Isolation System

Pressure Equations

The pressure equations relating the rate of change of pressure in the chambers to the mass flow rate for active isolation system are identical to those for the passive system. Hence rewriting the pressure

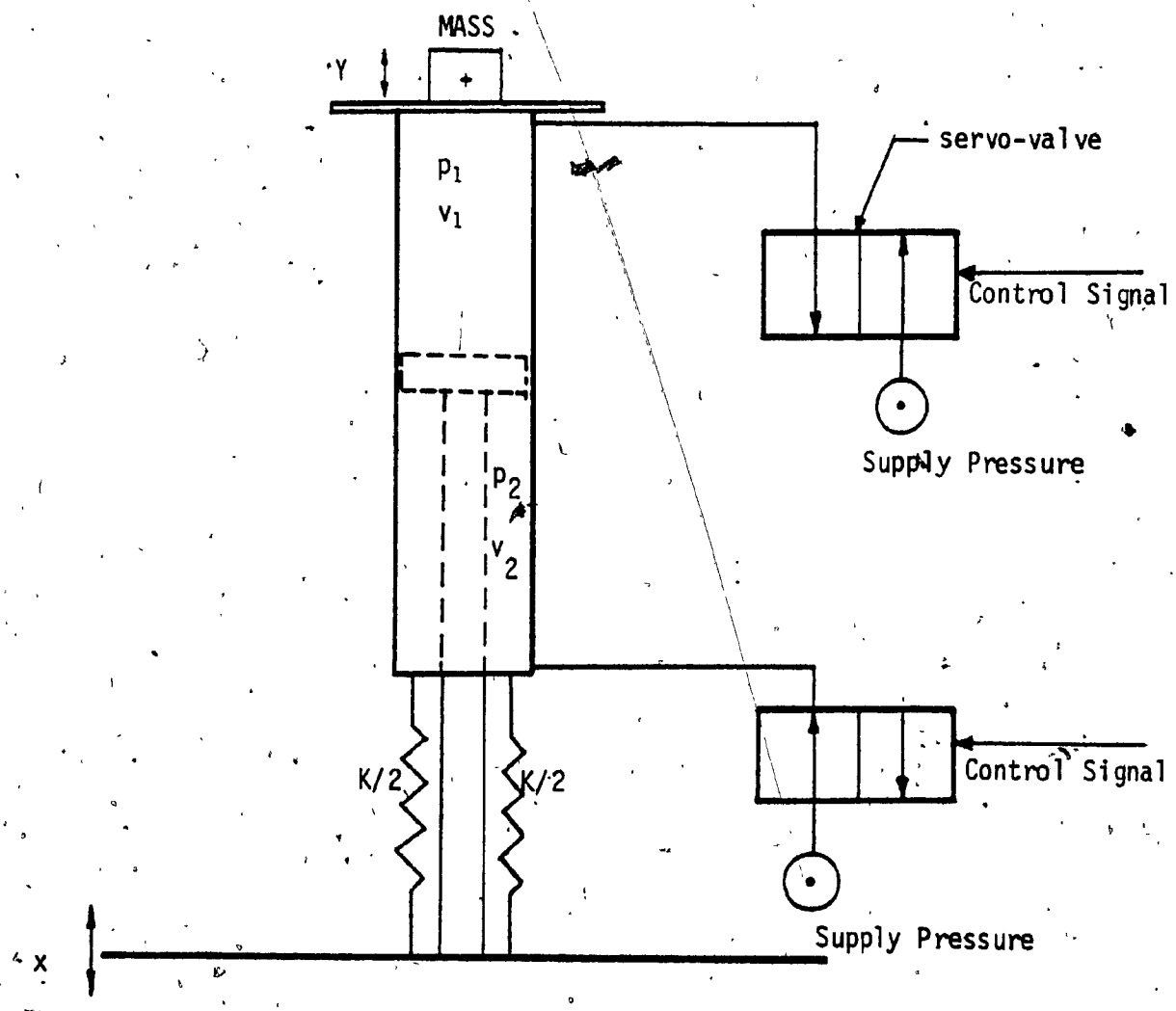

Fig. 30 : Schematic of the Active Suspension Type 1

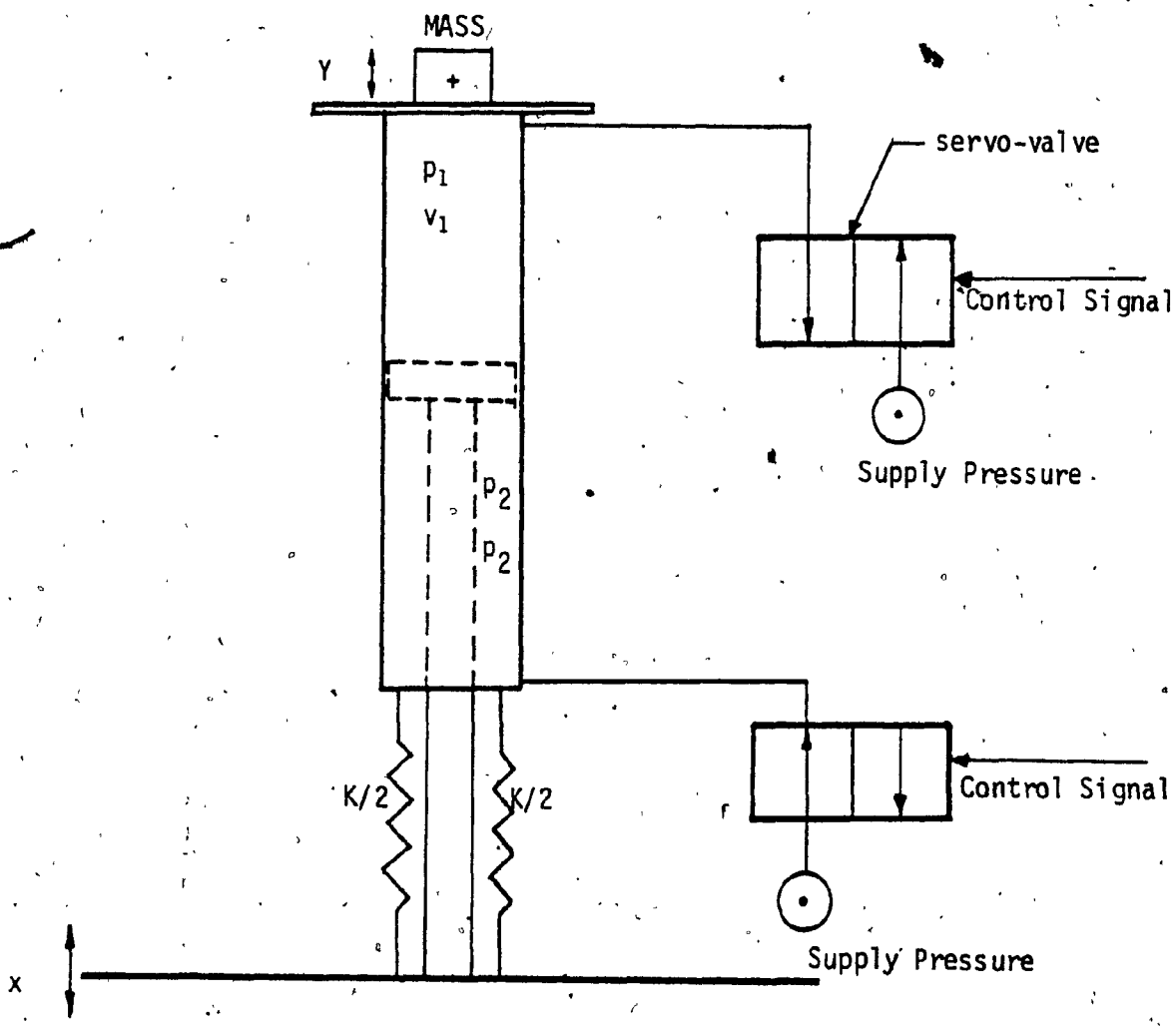

Fig. 31: Schematic of the Active Suspension Type 2

equations (2.10) and (2.11)

$$\frac{dP_1}{dt} = n\left[\frac{R \cdot T_1}{A_1(L-X+Y)}\frac{dM_1}{dt} - \frac{P_1}{(L-X+Y)}\left(-\frac{dX}{dt}+\frac{dY}{dt}\right)\right] \tag{3.1}$$

and

$$\frac{dP_2}{dt} = n\left[\frac{R \cdot T_2}{A_2(L+X-Y)}\frac{dM_2}{dt} - \frac{P_2}{(L+X-Y)}\left(\frac{dY}{dt}-\frac{dX}{dt}\right)\right] \tag{3.2}$$

where the temperatures T_1 and T_2 are given by

$$T_1 = T_o \left(\frac{P_1}{P_o}\right)^{\frac{n-1}{n}} \tag{3.3}$$

$$T_2 = T_o \left(\frac{P_2}{P_o}\right)^{\frac{n-1}{n}} \tag{3.4}$$

Flow Equations

For a positive relative velocity, the fluid is discharged from chamber 1 and the chamber 2 is charged from the pressure source. The mass flow rate going out of chamber 1 can be written from equation (2.16) as

$$\frac{dM_1}{dt} = -\frac{K \cdot P_1 \cdot A_{s1} \cdot N_{e1}}{T_1^{\frac{1}{2}}} \qquad \dot{X}-\dot{Y}>0 \tag{3.5}$$

The mass flow rate into chamber 2 is given by

$$\frac{dM_2}{dt} = \frac{K \cdot P_s \cdot A_{s2} \cdot N_{s1}}{T_2^{\frac{1}{2}}} \qquad \dot{X}-\dot{Y}>0 \tag{3.6}$$

where the factors N_{e1} and N_{s1} are functions of the ratio of specific heats and pressure ratio and are given by

$$N_{e1} = \left[\frac{(P_a/P_1)^{2/\gamma} - (P_a/P_1)^{\frac{\gamma+1}{\gamma}}}{\left(\frac{\gamma-1}{2}\right)\left(\frac{2}{\gamma+1}\right)^{\frac{\gamma+1}{\gamma-1}}} \right]^{\frac{1}{2}}$$

and

$$N_{s1} = \left[\frac{(P_2/P_s)^{2/\gamma} - (P_2/P_s)^{\frac{\gamma+1}{\gamma}}}{\left(\frac{\gamma-1}{2}\right)\left(\frac{2}{\gamma+1}\right)^{\frac{\gamma+1}{\gamma-1}}} \right]^{\frac{1}{2}}$$

where P_a is atmospheric pressure and P_s is the supply pressure.

When the relative velocity is negative, chamber 1 is charged from the pressure source while the fluid is discharged from chamber 2. The mass flow equations for this case can be written similar to equations (3-5) and (3-6) as

$$\frac{dM_1}{dt} = \frac{K \cdot P_s \cdot A_{s1} \cdot N_{s2}}{T_1^{\frac{1}{2}}} \qquad \text{For } \dot{X}-\dot{Y}<0 \qquad (3.7)$$

and

$$\frac{dM_2}{dt} = -\frac{K \cdot P_2 \cdot A_{s2} \cdot N_{e2}}{T_2^{\frac{1}{2}}} \qquad \text{For } \dot{X}-\dot{Y}<0 \qquad (3.8)$$

where N_{s2} and N_{e2} are defined as

$$N_{s2} = \left[\frac{(P_1/P_s)^{2/\gamma} - (P_1/P_s)^{\frac{\gamma+1}{\gamma}}}{\left(\frac{\gamma-1}{2}\right)\left(\frac{2}{\gamma+1}\right)^{\frac{\gamma+1}{\gamma-1}}} \right]^{\frac{1}{2}}$$

and

$$N_{e2} = \left[\frac{(P_a/P_2)^{2/\gamma} - (P_a/P_2)^{\frac{\gamma+1}{\gamma}}}{\left(\frac{\gamma-1}{2}\right)\left(\frac{2}{\gamma+1}\right)^{\frac{\gamma+1}{\gamma-1}}} \right]^{\frac{1}{2}}$$

The Load Equation

The load equation for the active system is exactly the same as that for passive system. So rewriting the load equation (2.22) gives:

$$m \frac{d^2y}{dt^2} = P_1A_1 - P_2A_2 + k(\delta+x-y) - mg - 14.7x6890\ (A_1-A_2) \qquad (3.9)$$

3.3.2 Governing Equations for Type 2 Active Isolation System

For the active isolation system of Type 2, the pressure characteristic and load equations are identical as for the Type 1 active system. However, the flow equation for Type 2 system is different from the Type 1 system because of the difference in the behaviour of charging or discharging the pressure chambers.

Flow Equation for Type 2 System

Type 2 active isolation system has exactly the same flow conditions as type 1 system except that the flow in and out of chamber 2 is zero. Hence, the flow equations for type 2 system can be written as:

For $(\dot{x}-\dot{y})>0$

$$\frac{dM_1}{dt} = -\frac{K \cdot P_1 \cdot A_{S1} \cdot N_{e1}}{T_1^{\frac{1}{2}}} \tag{3.10}$$

and

$$\frac{dM_2}{dt} = 0 \tag{3.11}$$

For $(\dot{x}-\dot{y})<0$

$$\frac{dM_1}{dt} = \frac{K \cdot P_S \cdot A_{S1} \cdot N_{S2}}{T_1^{\frac{1}{2}}} \tag{3.12}$$

and

$$\frac{dM_2}{dt} = 0 \tag{3.13}$$

The orifice areas A_{S1} and A_{S2} in type 1 and the orifice area A_{S1} in type 2 are all time functions. The equations of these orifice areas for each instant of time are derived in Section 3.4.

3.3.3 Non-Dimensionalized Equations for the Active System

Using the non-dimensionalization procedure described in Section (2.3), the governing equations (3.1)-(3.13) of the active system are non-dimensionalized. The non-dimensionalized equations for the active system type 1 are as follows:

For Type 1 Active System

Pressure Equations

The rate of change of pressure in chamber 1 is given by:

$$\frac{dp_1}{d\tau} = n\left[\frac{dm_1^*}{d\tau} \cdot \frac{t_1}{(1-x+y)} - \frac{p_1}{(1-x+y)}\left(-\frac{dx}{d\tau} + \frac{dy}{d\tau}\right)\right] \tag{3.14}$$

and for chamber 2 it is given as:

$$\frac{dp_2}{d\tau} = n\left[\frac{dm_2^*}{d\tau} \cdot \frac{t_2}{AR(1+x-y)} - \frac{p_2}{(1+x-y)}\left(\frac{dx}{d\tau} - \frac{dy}{d\tau}\right)\right] \tag{3.15}$$

where the non-dimensionalized temperatures are given by:

$$t_1 = (p_1)^{\frac{n-1}{n}} \tag{3.16}$$

and

$$t_2 = (p_2)^{\frac{n-1}{n}} \tag{3.17}$$

Flow Equations

$$\frac{dm_1^*}{d\tau} = -\frac{a_{s1} \cdot \beta \cdot p_1}{t_1^{\frac{1}{2}}} N_{e1} \tag{3.18}$$

and For $\dot{x}-\dot{y}>0$

$$\frac{dm_2^*}{d\tau} = \frac{p_s \cdot a_{s2} \cdot \beta}{t_2^{\frac{1}{2}}} N_{s1} \tag{3.19}$$

$$\frac{dm_1^*}{d\tau} = \frac{a_{s1} \cdot \beta \cdot p_s}{t_1^{\frac{1}{2}}} N_{s2} \tag{3.20}$$

and For $\dot{x}-\dot{y}<0$

$$\frac{dm_2^*}{d\tau} = -\frac{a_{s2} \cdot p_2 \cdot \beta}{t_2^{\frac{1}{2}}} N_{e2} \tag{3.21}$$

Load Equation

The non-dimensionalized load equation can be written as:

$$\frac{d^2y}{d\tau^2} = c_1 p_1 - c_2 p_2 + c_3(\delta^*+x-y) - c_4 \tag{3.22}$$

For Type 2 Active System

The non-dimensionalized equations for the active system of type 2 can similarly be written as:

Pressure Equations

$$\frac{dp_1}{d\tau} = n\left[\frac{dm_1^*}{d\tau}\frac{t_1}{(1-x+y)} - \frac{p_1}{(1-x+y)}\left(-\frac{dx}{d\tau} + \frac{dy}{d\tau}\right)\right] \tag{3.23}$$

and

$$\frac{dp_2}{d\tau} = n\left[-\frac{p_2}{(1+x-y)}\left(\frac{dx}{dy} - \frac{dy}{d\tau}\right)\right] \tag{3.24}$$

where the non-dimensionalized temperature t_1 is given by:

$$t_1 = (p_1)^{\frac{n-1}{n}} \tag{3.25}$$

Flow Equations

$$\frac{dm_1^*}{d\tau} = -\frac{a_{s_1} \cdot \beta \cdot p_1}{t_1^{\frac{1}{2}}} N_{e1} \tag{3.26}$$

and For $\dot{x}-\dot{y}>0$

$$\frac{dm_2^*}{d\tau} = 0 \tag{3.27}$$

$$\frac{dm_1^*}{d\tau} = \frac{a_{s_1} \cdot \beta \cdot p_s}{t_1^{\frac{1}{2}}} N_{s2} \tag{3.28}$$

and For $\dot{x}-\dot{y}<0$

$$\frac{dm_2^*}{d\tau} = 0 \tag{3.29}$$

Load Equation

$$\frac{d^2y}{d\tau^2} = c_1p_1 - c_2p_2 + c_3(\delta^*+x-y) - c_4 \tag{3.30}$$

3.4 DEVELOPMENT OF THE CONTROL LOGIC

The control logic for the active system is derived from the equations given in Section (3.3). It is primarily derived from the fact that the acceleration of the mass should be minimized. From the load equation (3.30) it is clear that the acceleration of the mass can be effectively controlled by changing the pressures in chamber 1 and chamber 2. This implies that the mass flow rate in and out of chamber 1 and chamber 2 should be controlled in such a way that any desired pressure can be attained in the two chambers to reduce the acceleration of the mass. Equations relating the orifice area and the pressures are derived as follows.

Differentiating the load equation and letting the jerk of the mass to be zero, equation (3.30) becomes:

$$\dot{p}_1 = \frac{c_2}{c_1}\dot{p}_2 - \frac{c_3}{c_1}(\dot{x}-\dot{y}) \qquad (3.31)$$

where a "dot" represents differentiation with respect to the non-dimensionalized time τ.

3.4.1 Control Logic 1

Two control logics are derived based on two different values of $\dot{p}_2$. In the first case the flow in and out of chamber 2 is controlled in such a way that the rate of change of pressure in chamber 2 is zero. The pressure in chamber 1 is controlled in such a way that the jerk of the mass is zero. For these criteria, the equations relating the orifice area and the pressures are derived as follows:

Since $\dot{p}_2 = 0$, equation (3.31) reduces to:

$$\dot{p}_1 = -\frac{c_3}{c_1}(\dot{x}-\dot{y}) \tag{3.32}$$

Solving equations (3.32) and (3.14) for $\dot{m}_1$*

$$\dot{m}_1^* = -\frac{(1-x+y)}{n \cdot t_1}\left[\left(\frac{c_3}{c_1}\right)+\frac{n \cdot p_1}{(1-x+y)}\right](\dot{x}-\dot{y}) \tag{3.33}$$

and substituting $\dot{p}_2 = 0$ in equation (3.15) $\dot{m}_2$* becomes:

$$\dot{m}_2^* = \frac{p_2 \cdot AR}{t_2}(\dot{x}-\dot{y}) \tag{3.34}$$

By comparing equations (3.18) and (3.33), and (3.19) and (3.34), the orifice areas a_{s1} and a_{s2} for $\dot{x}-\dot{y}>0$ are given by:

$$a_{s1} = \frac{(1-x+y)}{p_1 \cdot \beta \cdot N_{e1} \cdot n \cdot t_1^{\frac{1}{2}}}\left[\left(\frac{c_3}{c_1}\right) + \frac{n \cdot p_1}{(1-x+y)}\right](\dot{x}-\dot{y}) \tag{3.35}$$

$$a_{s2} = \frac{p_2 \cdot AR}{p_s \cdot \beta \cdot N_{s1} \cdot t_2^{\frac{1}{2}}}(\dot{x}-\dot{y}) \tag{3.36}$$

Similarly by solving equations (3.20) and (3.33), and (3.21) and (3.34), the orifice areas a_{s1} and a_{s2} for $\dot{x}-\dot{y}<0$ can be written as:

$$a_{s1} = \frac{(1-x+y)}{p_s \cdot \beta \cdot N_{s2} \cdot n \cdot t_1^{\frac{1}{2}}}\left[\left(\frac{c_3}{c_1}\right) + \frac{np_1}{(1-x+y)}\right](\dot{y}-\dot{x}) \tag{3.37}$$

and

$$a_{s2} = \frac{AR}{\beta \cdot N_{s2} \cdot t_2^{\frac{1}{2}}}(\dot{y}-\dot{x}) \tag{3.38}$$

Equations (3.35), (3.36) and (3.37), (3.38) give the value of orifice areas at any instant of time to maintain a zero output jerk for

both positive and negative relative velocities.

3.4.2 Control Logic 2

Control logic 2 is derived for the Active isolation system of Type 2. In this case, the chamber 2 is sealed so that the pressure in chamber 2 will vary according to the relative velocities as:

$$\dot{p}_2 = n\left[- \frac{p_2}{(1+x-y)}(\dot{x}-\dot{y}) \right] \tag{3.39}$$

Substituting equation (3.39) in (3.31), the rate of change of pressure in chamber 1 becomes:

$$\dot{p}_1 = - \frac{nc_2}{c_1} \frac{p_2}{(1+x-y)}(\dot{x}-\dot{y}) - \frac{c_3}{c_1}(\dot{x}-\dot{y}) \tag{3.40}$$

Solving equation (3.40) and (3.23) for $\dot{m}_1$*

$$\dot{m}_1^* = - \frac{(1-x+y)}{t_1}\left[\frac{p_1}{(1-x+y)} + \frac{c_2}{c_1}\frac{p_2}{(1+x-y)} + \frac{c_3}{c_1}\frac{1}{n}\right](\dot{x}-\dot{y}) \tag{3.41}$$

Now by comparing equations (3.41) and (3.26), and (3.41) and (3.28) the orifice area a_{s1} for both positive and negative relative velocities are given as

For $\dot{x}-\dot{y}>0$

$$a_{s1} = \frac{(1-x+y)}{p_1 \cdot \beta \cdot N_{e_1} \cdot t^2}\left[\frac{p_1}{(1-x+y)} + \frac{c_2}{c_1}\frac{p_2}{(1+x-y)} + \frac{c_3}{c_1}\frac{1}{n}\right](\dot{x}-\dot{y}) \tag{3.42}$$

and for $\dot{x}-\dot{y}<0$

$$a_{s1} = \frac{1-x+y}{p_s \cdot \beta \cdot N_{s1}\, t^2}\left[\frac{p_1}{(1-x+y)} + \frac{c_2}{c_1}\frac{p_2}{(1+x-y)} + \frac{c_3}{c_1}\frac{1}{n}\right](\dot{y}-\dot{x}) \tag{3.43}$$

3.4.3 Simplified Version of Control Logic

From the development of control logics 1 and 2, it can be noted that the orifice area is a function of relative displacement, relative velocity and the pressures in the cylinder chambers. If the orifice area is controlled as given in the control logics for maintaining zero jerk for the mass, then measurements have to be made for both relative displacement and velocity, and pressures p_1 and p_2. In order to reduce the complexity of the orifice area expression and also to reduce the cost of implementing such control, it is assumed that the relative displacement $(x-y)$ is small compared to unity. Also, the temperature change during the operation of the active system is assumed to be negligible and the flow into and out of cylinder chambers are assumed to be sonic. Based on these assumptions, the following expressions can be written:

$$\left.\begin{aligned} 1 \pm (x-y) &\simeq 1 \\ t_1^{\frac{1}{2}} \simeq t_2^{\frac{1}{2}} &\simeq 1 \\ N_{e_1} \simeq N_{e_2} &\simeq 1 \\ N_{s_1} \simeq N_{s_2} &\simeq 1 \end{aligned}\right\}$$

With the above assumptions and using an average value of 1.2 for the polytropic exponent "n", the expressions for the orifice area based on the control logic 1 can be written from equation (3.35), (3.36), (3.37) and (3.38) can be written as:

$$a_{s_1} = \frac{1}{p_1 \beta}\left[\frac{1}{1.2}\cdot\frac{c_3}{c_1} + p_1\right](\dot{x}-\dot{y}) \qquad (3.44)$$

$$\dot{x}-\dot{y}>0$$

$$a_{s_2} = (p_2/p_s)(AR/B)(\dot{x}-\dot{y}) \tag{3.45}$$

$$a_{s_1} = \frac{1}{p_s\beta}\left[\frac{1}{1.2}\left(\frac{c_3}{c_1}\right) + p_1\right](\dot{y}-\dot{x}) \qquad \dot{x}-\dot{y}<0 \tag{3.46}$$

$$a_{s_2} = (AR/\beta)(\dot{y}-\dot{x}) \tag{3.47}$$

Using the same assumptions, the orifice area for the control logic 2 is given as:

$$a_{s1} = \frac{1}{p_1\beta}\left[\frac{1}{1.2}\left(\frac{c_3}{c_1}\right) + \left(\frac{c_2}{c_1}\right)p_2 + p_1\right](\dot{x}-\dot{y}) \qquad \dot{x}-\dot{y}>0 \tag{3.48}$$

and

$$a_{s_2} = \frac{1}{p_s\beta}\left[\frac{1}{1.2}\left(\frac{c_3}{c_1}\right) + \left(\frac{c_2}{c_1}\right)p_2 + p_1\right](\dot{y}-\dot{x}) \qquad \dot{x}-\dot{y}<0 \tag{3.49}$$

Equations (3.44) to (3.49) give the expressions for the orifice area required at any instant of time to have a zero jerk at the mass. Comparing the two types of control logic it can be seen that the control logic 2 is less complex and needs fewer hardware. Since the control logic 2 corresponds to an active isolation system of type 2 characteristics, only simulation and stability analysis of this system are presented in this thesis.

3.5 STABILITY ANALYSIS OF ACTIVE ISOLATION SYSTEM WITH CONTROL LOGIC

In order to understand the behaviour of the active system and to estimate the stability of the system, the system equation for the type 2 active system given in section (3.4) is solved.

From the development of control logic presented in section (3.4) the mass flow rate, $\dot{m}_1^*$ required at every instant of time to provide

zero jerk to the mass is given in equation (3.41). If it is assumed that this flow rate $\dot{m}_1^*$ can be obtained at every instant of time as given by the equation (3.41), then the displacement time response of the mass can be derived as follows:

Using this expression for $\dot{m}_1^*$ and substituting in equation (3.23), the rate of change of pressure in chamber 1 can be rewritten as

$$\dot{p}_1 = n\left[-\frac{c_2}{c_1}\left(\frac{p_2}{1+x-y}\right)(\dot{x}-\dot{y}) - \frac{c_3}{c_1}\frac{1}{n}(\dot{x}-\dot{y})\right] \tag{3.50}$$

The equation relating the rate of change of pressure in chamber 2 remains as given by equation (3.24) and is given as:

$$\dot{p}_2 = -n\left[\frac{p_2}{1+x-y}(\dot{x}-\dot{y})\right] \tag{3.51}$$

where "dot" represents differentiation with respect to the non-dimensionalized time τ.

Combining equations (3.40) and (3.51), the rate of change of pressure can further be simplified as:

$$c_1\dot{p}_1 = c_2\dot{p}_2 - c_3(\dot{x}-\dot{y}) \tag{3.52}$$

Using the initial conditions

$$p_1(0) = 1;\ p_2(0) = 1;\ x(0) = 0;\ y(0)$$

and taking Laplace transform of equation (3.52), the pressure equation can be modified as:

$$c_1p_1(s) - c_2p_2(s) = c_3\left[y(s)-x(s)\right] + \frac{1}{s}(c_1-c_2) \tag{3.53}$$

Now taking the Laplace transform on both sides of equation (3.30) with initial conditions

$$\dot{y}(0) = 0;\ y(0) = 0;\ x(0) = 0$$

the load equation can be modified as:

$$s^2y(s) = c_1p_1(s) - c_2\ p_2(s) + \frac{c_3\delta^*}{s} + c_3[x(s)-y(s)] - c_4/s \tag{3.54}$$

Combining equations (3.53) and (3.54) the output displacement of the system can be written as:

$$y(s) = \frac{1}{s}\ [c_1 - c_2 + c_3\delta^* - c_4] \tag{3.55}$$

By taking the inverse Laplace transform of equation (3.55), the time response of the output displacement of the mass can be obtained as:

$$y(\tau) = \frac{\tau^2}{2}\ [c_1 - c_2 + c_3\delta^* - c_4] \tag{3.56}$$

Then, the nondimensionalized output velocity and acceleration time response are given by:

$$\dot{y}(\tau) = \tau[c_1 - c_2 + c_3\delta^* - c_4] \tag{3.57}$$

and

$$\ddot{y}(\tau) = [c_1 - c_2 + c_3\delta^* - c_4] \tag{3.58}$$

From equation (3.58) it can be seen that the output acceleration time response of the mass is a constant and is independent of time. Now if we consider the non-dimensionalized load expression given in equation (3.30) and substituting the initial conditions; $\dot{y}(0)=0$, $p_1(0)=1$, $p_2(0)=1$, $x(0)=0$ and $y(0)=0$, then it is seen that the constant in right hand side of the equation (3.58) is zero. That is, ideally, the output acceleration of the mass will be zero when the orifice area is controlled as given by the control logic. If $\ddot{y}(\tau)$ is zero, then the output velocity and displacement of the mass will also be zero for all instants of time.

However, it should be noted that this ideal situation can never be achieved in practice and the output acceleration $\ddot{y}(\gamma)$ will be a constant with a very small value. For this condition, both the output velocity and displacement time response will be a time function and hence for increasing time they will become unbounded, resulting in an unstable system behaviour.

In order to have a stable system performance, it is possible to include some feedback signals such as output acceleration, velocity and displacement. These feedback signals can be used to control the mass flow rate into and out of the cylinder chambers. Then the equation (3.41) for the mass flow rate $\dot{m}_1$ can be modified as:

$$\dot{m}_1^* = -\frac{(1-x+y)}{t_1}\left[\left(\frac{p_1}{1-x+y}+\frac{c_2}{c_1}\cdot\frac{p_2}{1+x-y}+\frac{c_3}{c_1}\cdot\frac{1}{n}\right)(\dot{x}-\dot{y}) - k_1^*\ddot{y} - k_2^*\dot{y} - k_3^* y\right] \tag{3.59}$$

where k_1^*, k_2^* and k_3^* represent the feedback gains for the acceleration, velocity and displacement feedback loops.

Now, if the modified equation (3.59) for $\dot{m}_1^*$ is used in the derivation of the equations for the orifice area in control logic 2, then the equations (3.48) and (3.49) become altered as:

For $(\dot{x}-\dot{y})>0$

$$a_{s1} = \frac{1}{p_1\cdot\beta}\left[\left(p_1+\frac{c_2}{c_1}\cdot p_1+\frac{c_3}{c_1}\cdot\frac{1}{1.2}\right)(\dot{x}-\dot{y}) - k_1^*\ddot{y} - k_2^*\dot{y} - k_3^* y\right] \tag{3.60}$$

For $(\dot{x}-\dot{y})<0$

$$a_{s1} = \frac{1}{p_s\cdot\beta}\left[\left(p_1+\frac{c_2}{c_1}\cdot p_1+\frac{c_3}{c_1}\cdot\frac{1}{1.2}\right)(\dot{y}-\dot{x}) - k_1^*\ddot{y} - k_2^*\dot{y} - k_3^* y\right] \tag{3.61}$$

The time response of the mass using the mass flow equation

(3.59) can be derived as follows:

Combining equations (3.61) and (3.23) the rate of change of pressure in chamber 1 can be written as:

$$\dot{p}_1 = n\left[-\frac{c_2}{c_1}\left(\frac{p_2}{1+x-y}\right)(\dot{x}-\dot{y})-\left(\frac{c_3}{c_1}\right)\frac{1}{n}(\dot{x}-\dot{y}) - k_1^*\ddot{y} - k_2^*\dot{y} - k_3^*y\right] \quad (3.62)$$

The rate of change of pressure in chamber 2 is given by equation (3.51). Now combining equation (3.62) and (3.51), the rate of change of pressure can be simplified as:

$$c_1\dot{p}_1 = c_2\dot{p}_2 - c_3(\dot{x}-\dot{y}) - k_1^*\ddot{y} - k_2^*\dot{y} - k_3^*y \quad (3.63)$$

Using the initial conditions

$p_1(0) = 1$; $p_2(0) = 1$; $x(0) = 0$; $y(0) = 0$

and taking Laplace transform of equation (3.63) the pressure equation can be modified as:

$$c_1p_1(s)-c_2p_2(s) = c_3\,y(s)-x(s) + \frac{1}{s}(c_1-c_2)-c_1k_1^*sy(s) - c_1k^*y(s)\frac{c_1k^*_3}{s}\,y(s) \quad (3.64)$$

Combining equations (3.64) and (3.54) the output displacement of the active system can be written as:

$$y(s) = \frac{c_1-c_2+c_3\delta^*-c_4}{s^3+c_1k_1^*s^2+c_1k^*_2s+k^*_3c_1} \quad (3.65)$$

So it is evident from equation 3.54 that even if there is any delay in providing the mass flow rate $\dot{m}_1^*$ the system with the feedback signals can be made stable by selecting proper feedback gains k_1^*, k_2^*

and k_3^*.

3.6 CONTROL INPUT USING ELECTRO-PNEUMATIC SERVO-VALVE

To achieve a continuous change in the orifice area so that the mass flow rate in and out of cylinder chambers can be controlled according to the equation (3.59), an electro-pneumatic servo-valve is used. An electro-pneumatic servo-valve provides an output flow of air proportional to an electrical input current. The valves use a force motor and a main stage spool valve to provide air flow for actuator operation. Since in this servo-valve, the input required to move the spool to provide the required mass flow rate to the cylinder is in the form of input current, it can be assumed that the displacement of the valve-spool is directly proportional to the input current. Therefore

$$x_v = K_v\, i_c \tag{3.66}$$

where K_v is the proportional gain of the servo-valve.

If Ag is the area gradient of the spool, then the non-dimensionalized area due to the spool movement can be written as

$$a_s = \frac{L \cdot Ag}{A_0}\, x_v \tag{3.67}$$

Combining equation (3.66) and (3.67), the orifice area in terms of the input current to the servo-valve can be written as:

$$a_s = \frac{L \cdot Ag}{A_0}\, K_v\, i_c \tag{3.68}$$

Now comparing equation (3.68) with (3.60) and (3.61), the control signal i_c for the servo-valve can be obtained for both positive and nega-

tive relative velocities as:

For $\dot{x}-\dot{y}>0$

$$i_c = -\frac{A_0}{K_v \cdot L \cdot A_g \cdot \beta}\left[\left(\frac{c_2}{c_1}\frac{p_2}{p_1} + \frac{c_3}{c_1}\frac{1}{1\cdot 2\cdot p_1} + 1\right)(\dot{x}-\dot{y}) - k_1\ddot{y} - k_2\dot{y} - k_3 y\right] \qquad (3.69)$$

and for $\dot{x}-\dot{y}<0$

$$i_c = \frac{A_0}{K_v \cdot L \cdot A_g \cdot \beta}\left[\left(\frac{c_2}{c_1}\frac{p_2}{p_1} + \frac{c_3}{c_1}\frac{1}{1\cdot 2\cdot p_1} + 1\right)(\dot{y}-\dot{x}) - k_1\ddot{y} - k_2\dot{y} - k_3 y\right] \qquad (3.70)$$

Equations (3.69) and (3.70) give the value of input current at any instant of time to maintain a zero output jerk for the positive and negative relative displacement.

By measuring the cylinder chamber pressures, output acceleration, velocity and displacement, and the relative velocity of the active system and using electrical network in accordance with equations (3.64) and (3.65), the control current i_c to the servo-valve can be generated. A diagram of this configuration is shown in Figure 32. This control current will provide an output displacement x_v at the valve. Since a servo-valve is characterized with a finite time response, the output displacement x_v cannot be assumed to be proportional to the input current i_c. However, x_v and i_c are related through the dynamic transfer function of the valve. In order to obtain such a relationship, the electro-pneumatic servo-valve can be modelled as a first order system with the following characteristic equation:

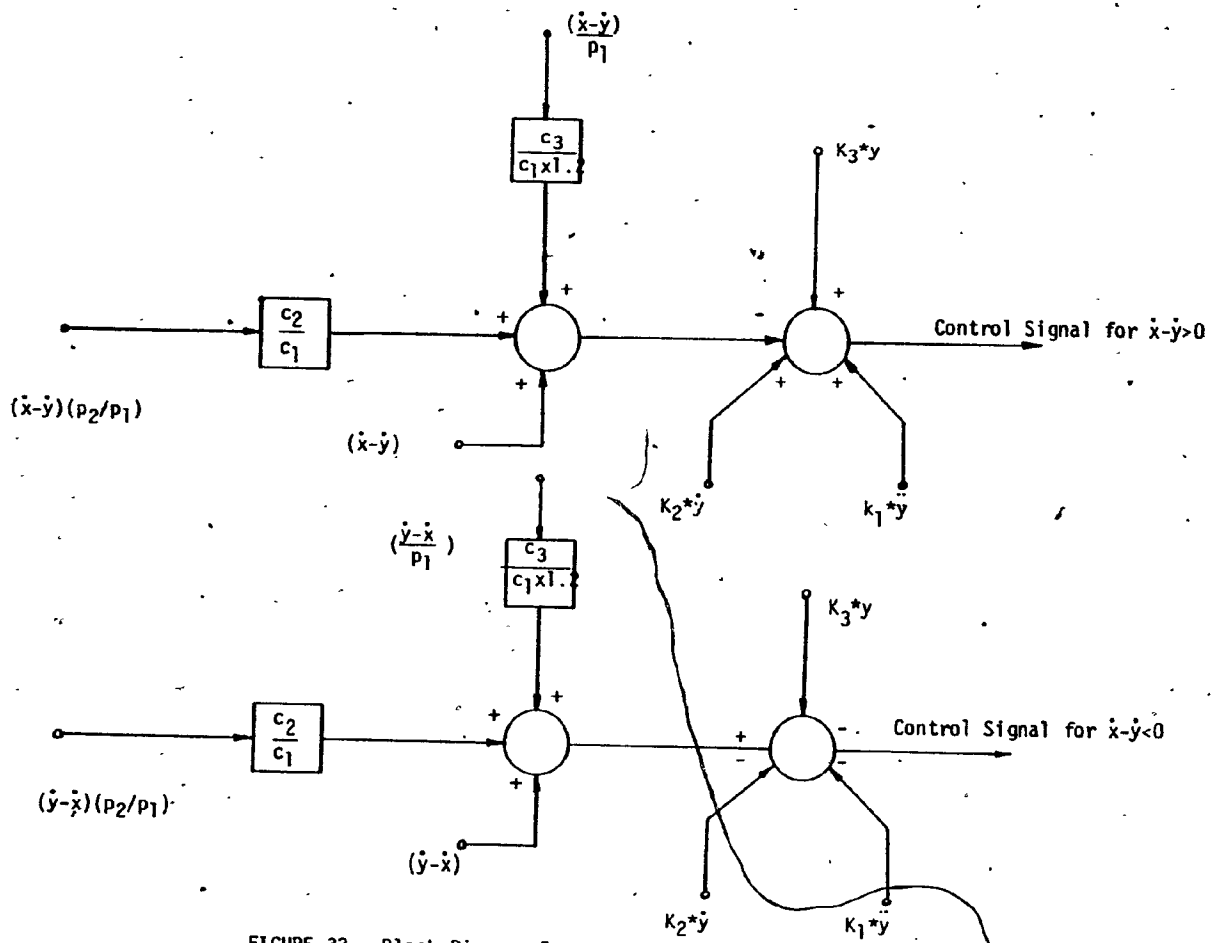

FIGURE 32. Block Diagram Representation of the Control Signal

$$\dot{x}_v = (i_c - x_v) \cdot \frac{\alpha}{\tau_v} \tag{3.71}$$

where τ_v is the time constant of the servo-valve and α is the reference time as defined earlier.

The non-dimensionalized orifice area of the servo-valve can be related to the valve displacement x_v through the area gradient Ag as:

$$a_{s_1} = \frac{L \cdot Ag}{A_o} \quad x_v \tag{3.72}$$

3.7 SUMMARY OF EQUATIONS FOR TYPE 2 ACTIVE ISOLATION SYSTEMS

Summarizing the equations for the active vibrational isolation system type 2, the pressure equations in the two chambers are given as:

$$\frac{dp_1}{d\tau} = n \left[\frac{dm_1^*}{d\tau} \quad \frac{t_1}{(1-x+y)} - \frac{p_1}{(1-x+y)} \left(- \frac{dx}{d\tau} + \frac{dy}{d\tau} \right) \right] \tag{3.73}$$

$$\frac{dp_2}{d\tau} = n \left[- \frac{p_2}{(1+x-y)} \left(\frac{dx}{d\tau} - \frac{dy}{d\tau} \right) \right] \tag{3.74}$$

where the non-dimensionalized temperature t_1 is given by:

$$t_1 = (p_1)^{\frac{n-1}{n}} \tag{3.75}$$

Equations for Servo-Valve

The input current to the servo-valve is given by:

$$i_c = - \frac{A_o}{K_v \cdot L \cdot Ag \cdot \beta} \left[\left(\frac{c_2}{c_1} \quad \frac{p_2}{p_1} + \frac{c_3}{c_1} \quad \frac{1}{1 \cdot 2 \cdot p_1} + 1 \right) (\dot{x}-\dot{y}) - k_1 \cdot \ddot{y} - k_2 \cdot \dot{y} - k_3 \cdot y \right] \quad (\dot{x}-\dot{y}) > 0 \tag{3.76}$$

and

$$i_c = \frac{A_o}{K_v \cdot L \cdot Ag \cdot \beta} \left[\left(\frac{c_2}{c_1} \quad \frac{p_2}{p_3} + \frac{c_3}{c_1} \quad \frac{1}{1 \cdot 2 \cdot p_s} + 1 \right) (\dot{y}-\dot{x}) - k_1 \cdot \ddot{y} - k_2 \cdot \dot{y} - k_3 \cdot y \right] \quad (\dot{x}-\dot{y}) < 0 \tag{3.77}$$

The dynamics of the servo-valve:

$$\dot{x}_v = [(i_c - x_v) \cdot \alpha] \ \tau_v \qquad (3.78)$$

and

$$a_{s_1} = \frac{L \cdot Ag}{A_o} \cdot x_v \qquad (3.79)$$

Flow Equations

$$\frac{dm_1^*}{d\tau} = - \frac{a_{s_1} \cdot \beta \cdot p_1 N_{e1}}{t_1^{\frac{1}{2}}} \qquad (\dot{x}-\dot{y})>0 \qquad (3.80)$$

and

$$\frac{dm_1^*}{d\tau} = \frac{a_{s_1} \cdot \beta \cdot p_s N_{s1}}{t_i^{\frac{1}{2}}} \qquad (\dot{x}-\dot{y})<0 \qquad (3.81)$$

Load Equation

$$\frac{d^2x}{d\tau^2} = c_1 p_1 - c_2 p_2 + c_3(\delta^* + x-y) - c_4 \qquad (3.82)$$

3.8 SIMULATION OF TYPE 2 ACTIVE ISOLATION SYSTEM

The input excitation considered for the active system is similar to that of passive system. The three inputs considered are sinusoidal, rounded-pulse and an input displacement of the form $x = x_o(1-\cos \omega t)$. The description of the inputs and their amplitude and frequencies are as given in Section (2.5).

The non-dimensionalized equations of the active system type 2 which describe the behaviour of the system are simulated using the Runge-Kutta 4th order numerical integration method on a CDC Cyber 172/2 digital computer. The Fortran computer program used for the simulation is given in Appendix E. Table 3.1 shows the system parameters used in

TABLE 3.1

VARIABLE	VALUE USED IN THE SIMULATION
A_1	1.14×10^{-3} m^2
A_2	6.41×10^{-4} m^2
k	2.19×10^{3} N/m
K	0.04 $\frac{kg}{N \cdot S}$ $^{\circ}k^{\frac{1}{2}}$
L	7.62×10^{-2} m
mg	4.45×10^{2} N
n	1.4
P_o	5.52×10^{5} N/m^2
P_s	8.3×10^{5} N/m^2
T_o	295 °k
V_o	8.6868×10^{-4} m^3
δ	7.62×10^{-2} m
Ag	2.54×10^{-4} m
τ_v	0.1 sec

TABLE 3.1 CONT'D

VARIABLE	VALUES USED IN THE SIMULATION
k_1	0.73 $\frac{ma\text{-}sec^2}{m}$
k_2	0.98 $\frac{ma\text{-}sec}{m}$
k_3	2.63 ma/m

the simulation of the active systems.

3.8.1 Response to Sinusoidal Input for Type 2 Active System

Figure 33 shows the output displacement of the active system for a input frequency of 2.5 rad/sec. As it can be seen from Figure 33, the output displacement does not have any high frequency component and does not seem to have a steady state value with continuous variation in amplitude and frequency. In order to see if the output displacement reaches a steady state the simulation was carried for 50 sec. The output displacement showed a similar characteristic to the one shown in Figure 33. It is important to note that the peak output displacement is about 15 times less than that of the peak input displacement. Figure 34 shows the relative displacement plotted against time. Since the output displacement is very small compared to the input the relative displacement is very close to the input displacement.

The output velocity of the active system is plotted against time and the plot is given in Figure 35. It is clear from Figure 35 that the velocity of the system goes through a transient for a period of 4 sec. This time response of the system is similar to that of output displacement with two frequency components. Figure 36 gives the output acceleration of the system. The output acceleration also goes through the initial transient for about 5.25 sec. During this transient period, the output acceleration has a magnitude comparable to the input acceleration. But in the steady state, the output acceleration or the force transmitted to the mass is about 8 times less than the input acceleration. Even in the

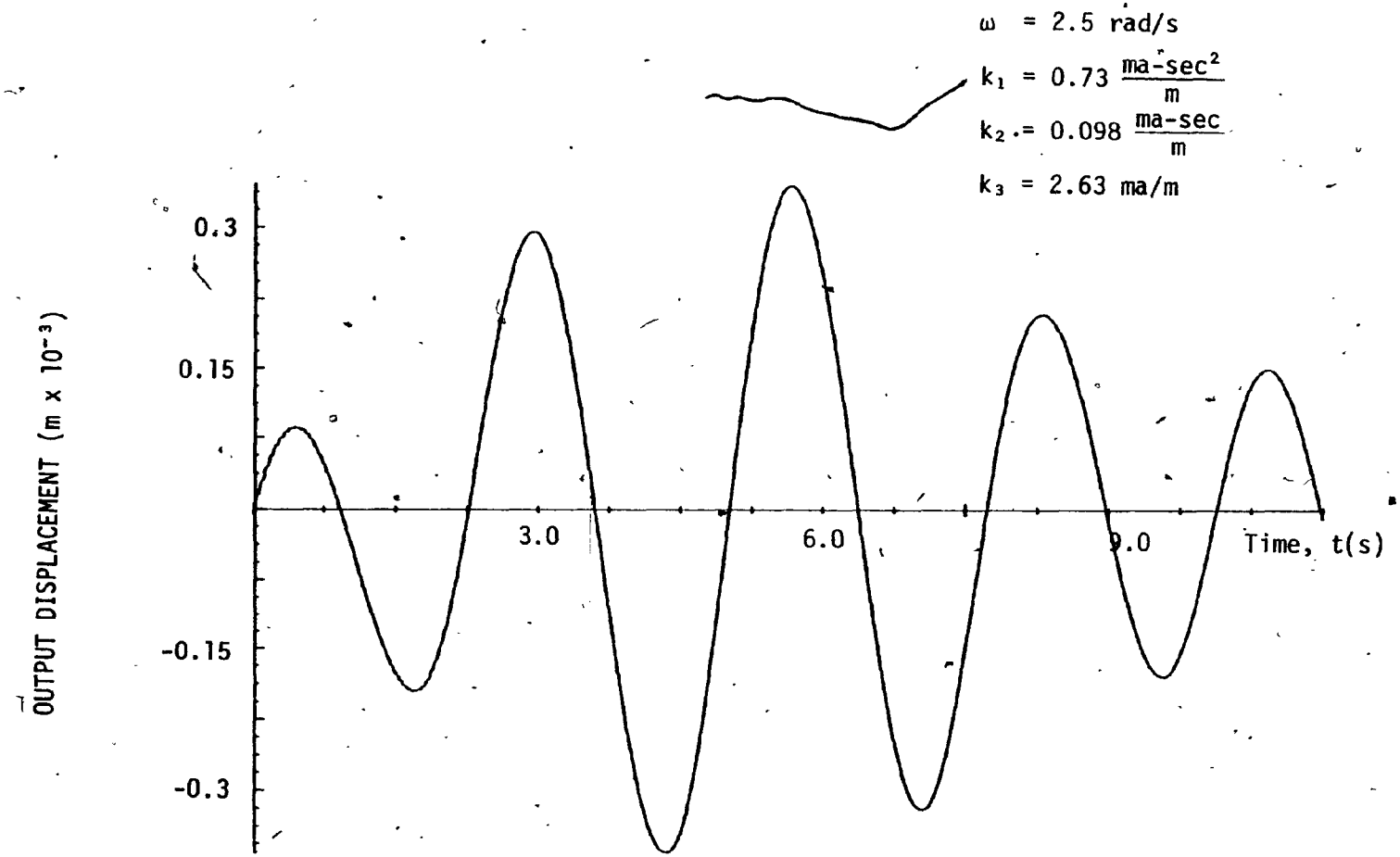

Fig. 33: Displacement Time Response of the Active System at 2.5 rad/s

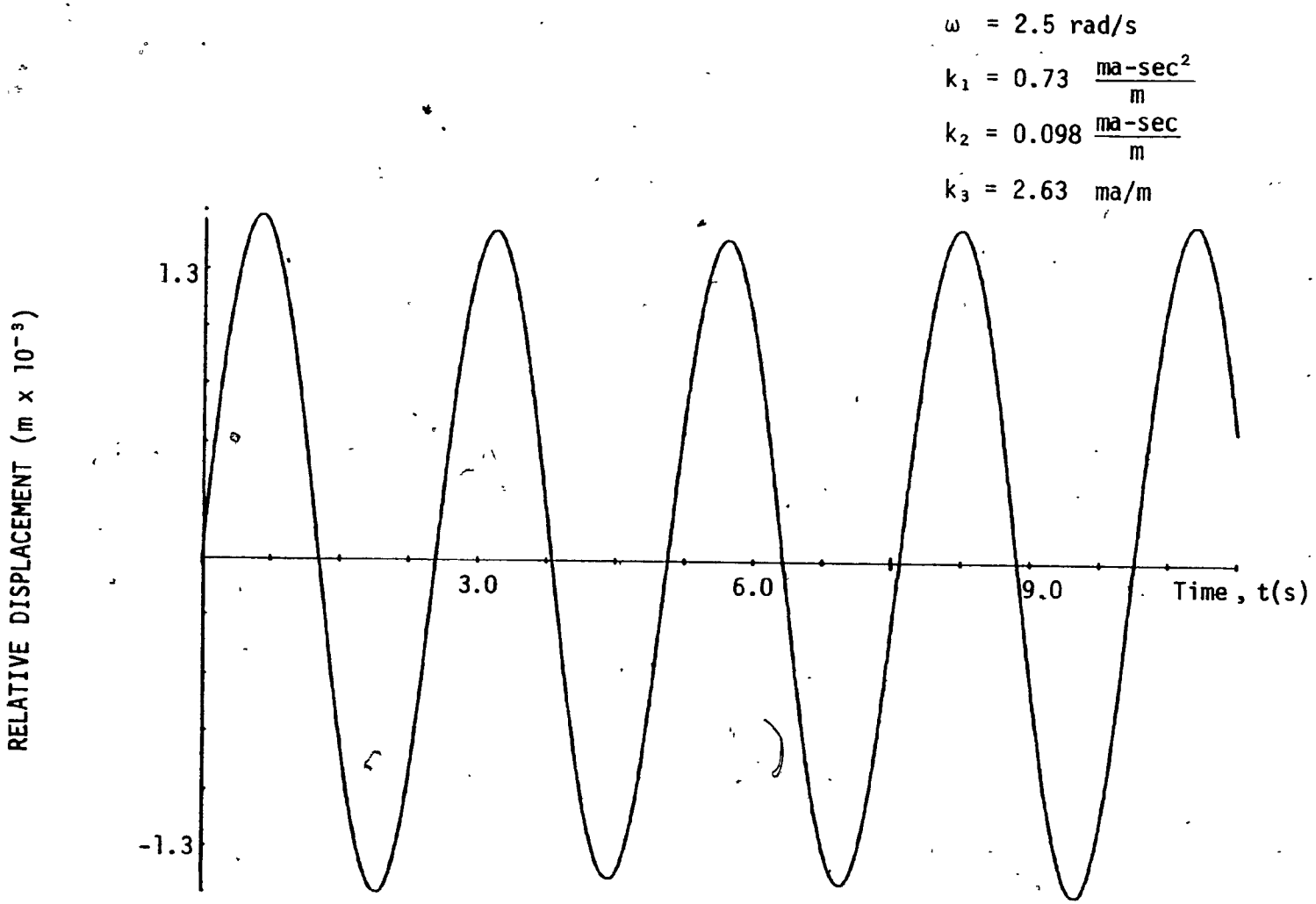

Fig. 34: Relative Displacement Time Response of the Active System at 2.5 rad/s.

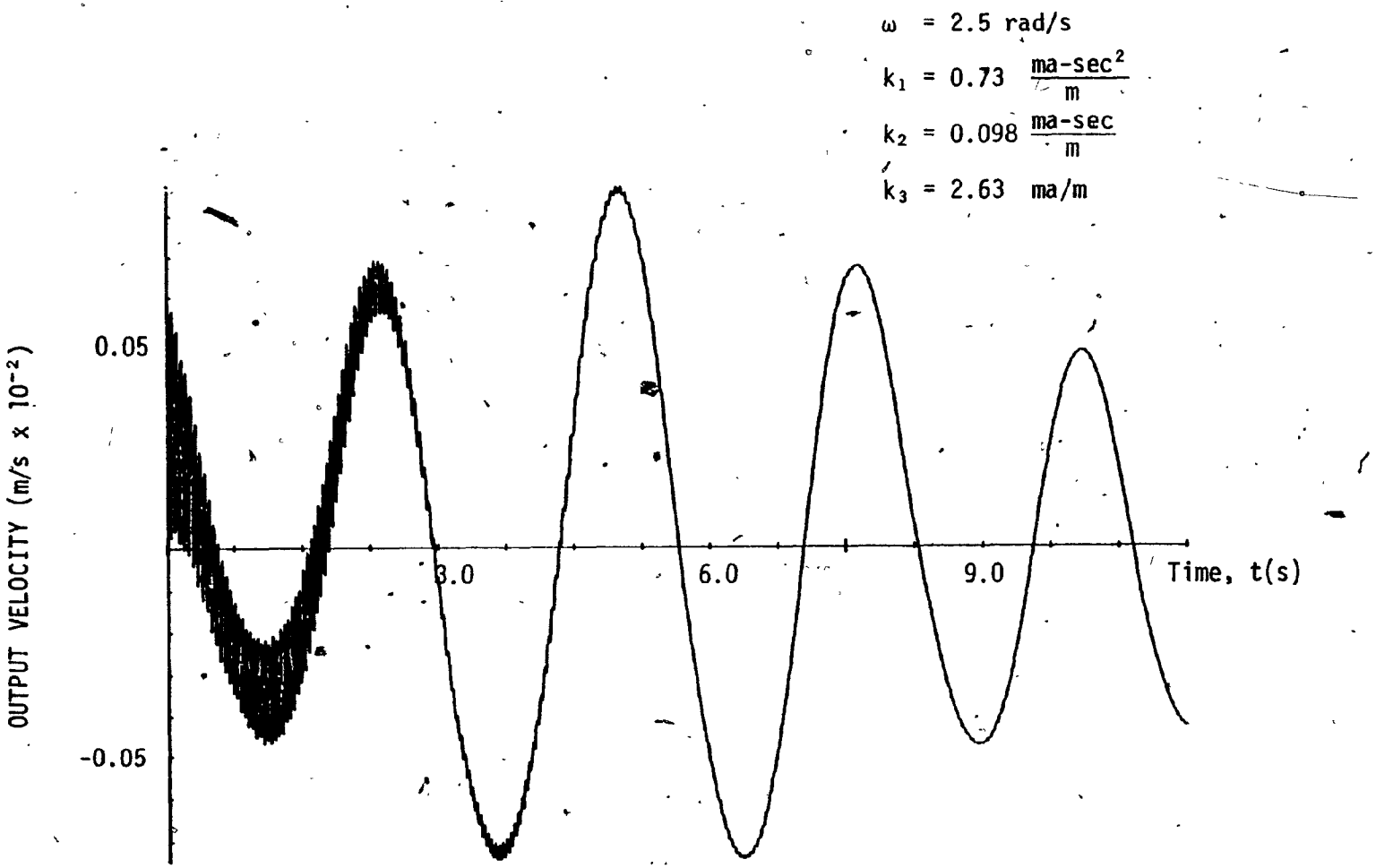

Fig. 35: Velocity Time Response of the Active System at 2.5 rad/s.

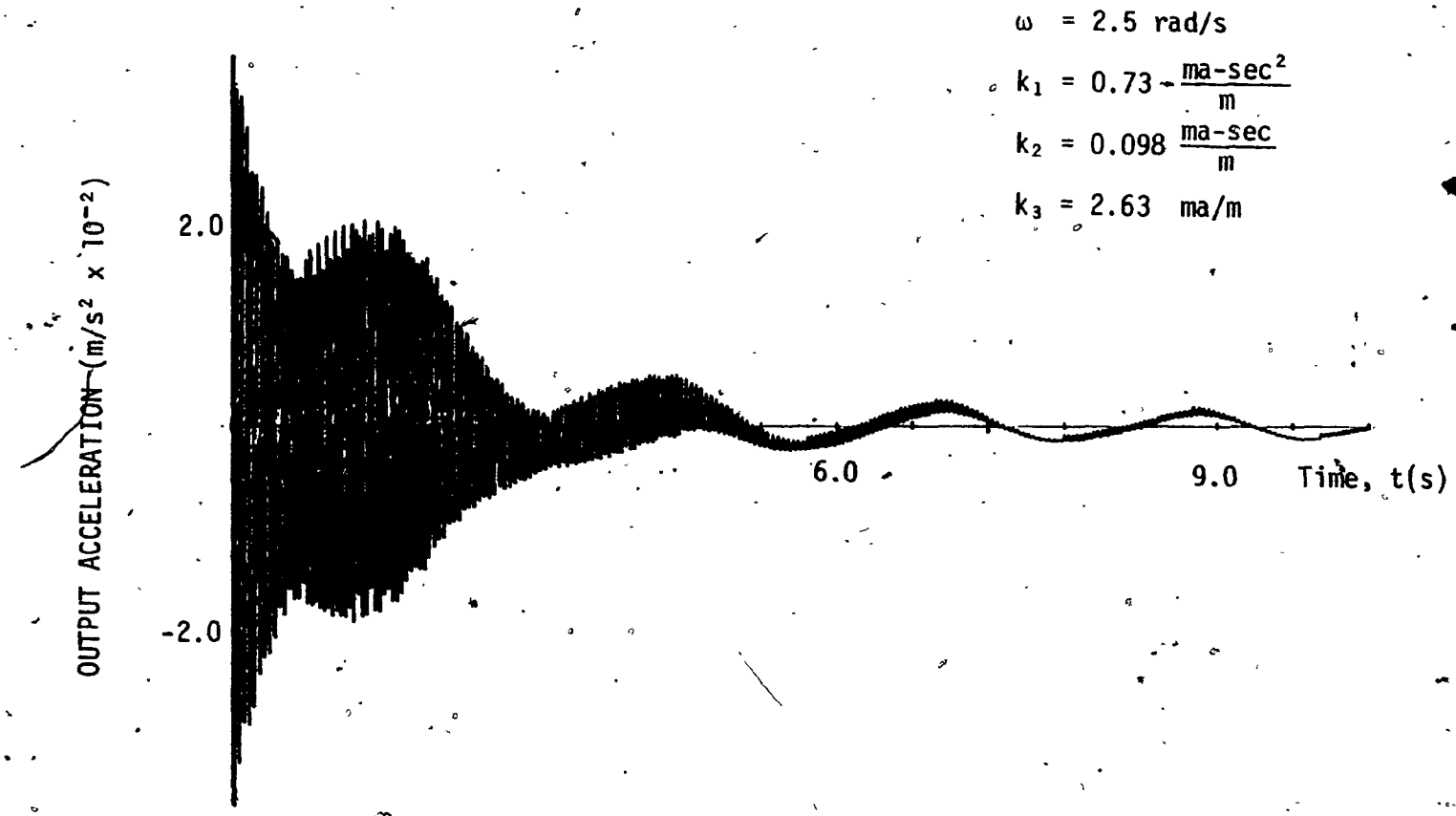

Fig. 36: Acceleration Time Response of the Active System at 2.5 rad/s.

steady state, the output acceleration has some high frequency noise. These high frequency fluctuations can be eliminated by selecting a lag-lead network function instead of a proportional gain for the feedback signals.

The mass flow rate and the force generated by this active damper are plotted in Figure 37 and Figure 38 respectively. Both the mass flow rate and the force generated by the damper are sinusoidal with an initial oscillatory transient.

The power needed by the active system is shown in Figure 39. The system requires power only when the chamber 1 is charged from the pressure source. When the pressure from chamber 1 is discharged, the only power required by the system is the power required to operate the servo-valve. The power demand goes through a high oscillation during the transient and settles down after 5.5 sec.

Figure 40 shows the pressure in chamber 1 plotted against time. The chamber pressure goes through a transient for about 0.75 sec. It is important to note that in the steady state the chamber pressure oscillates about the initial pressure of 5.52×10^5 N/m^2 in the cylinder chamber.

Figure 41 shows the output displacement of the active system for an excitation frequency of 20 rad/sec. As it can be seen from Figure 41, the amplitude of the output displacement decreases as the time increases. This plot clearly shows that the output displacement contains more than one frequency. The peak output displacement is about 15 times less than the peak input displacement. Since the output displacement is very small

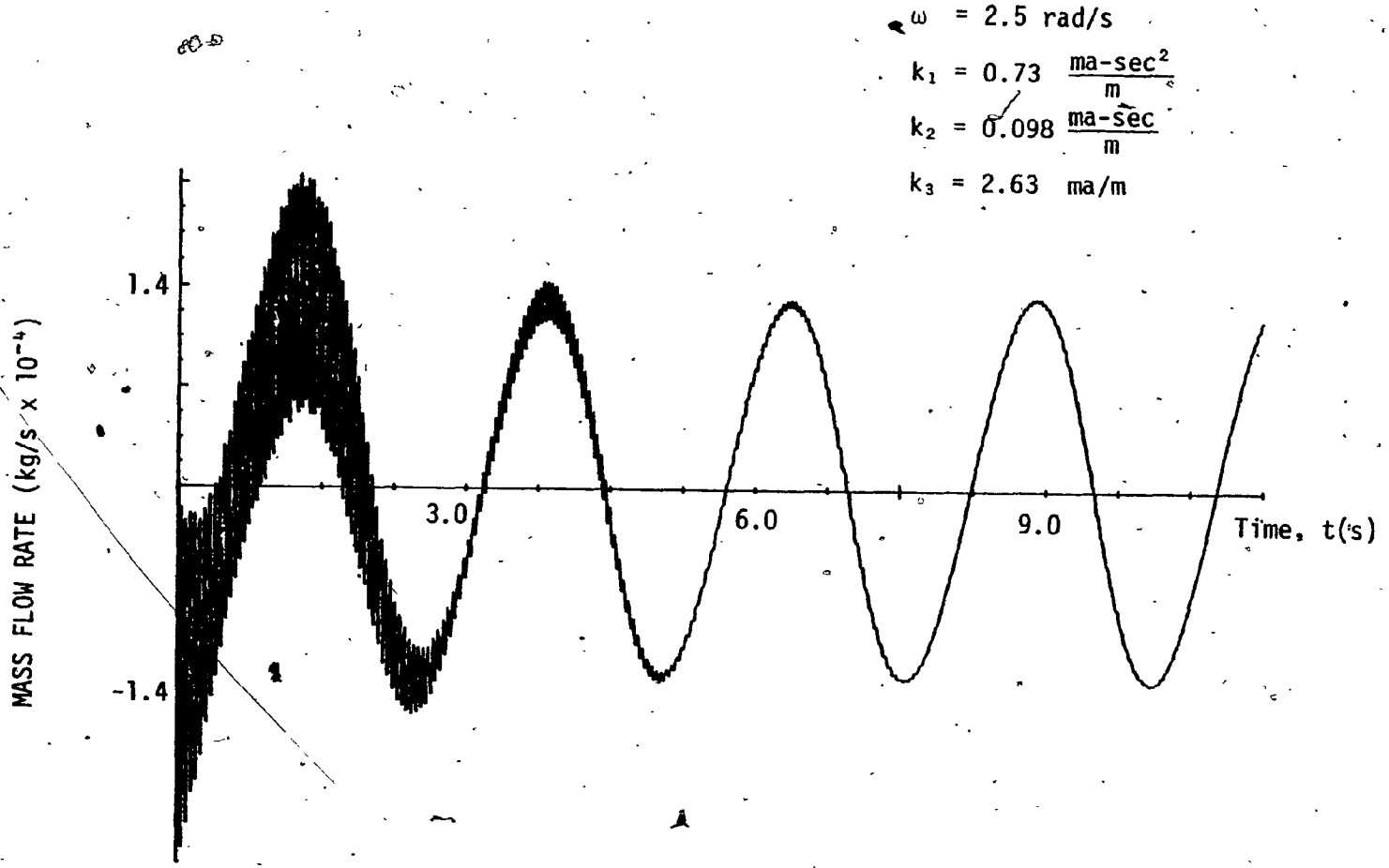

Fig. 37: Time Response of the Mass Flow Rate at 2.5 rad/s.

ω = 2.5 rad/s

k_1 = 0.73 $\frac{\text{ma-sec}^2}{\text{m}}$

k_2 = 0.098 $\frac{\text{ma-sec}}{\text{m}}$

k_3 = 2.63 ma/m

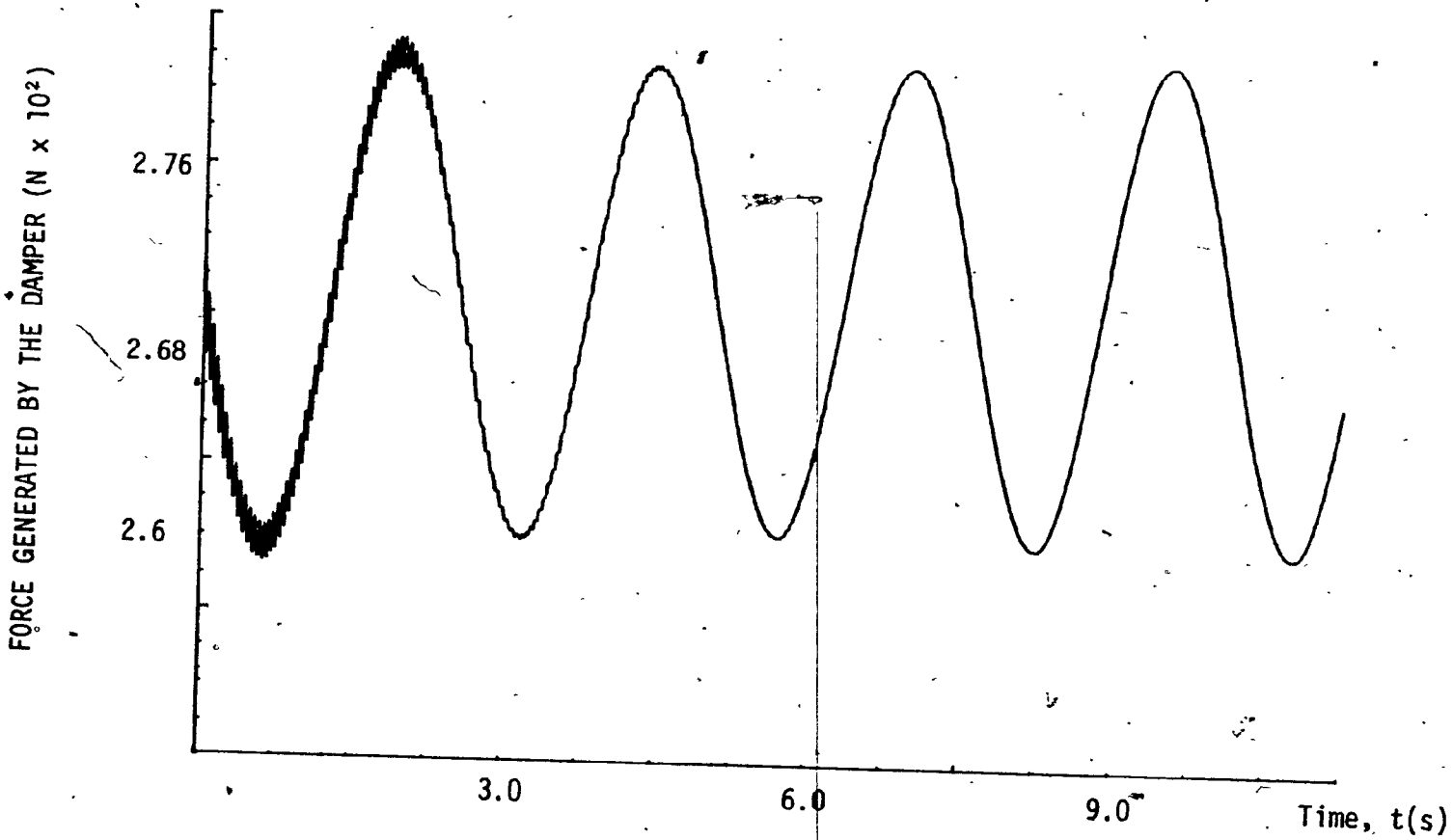

Fig. 38: Force Generated by the Aetive System at 2.5 rad/s.

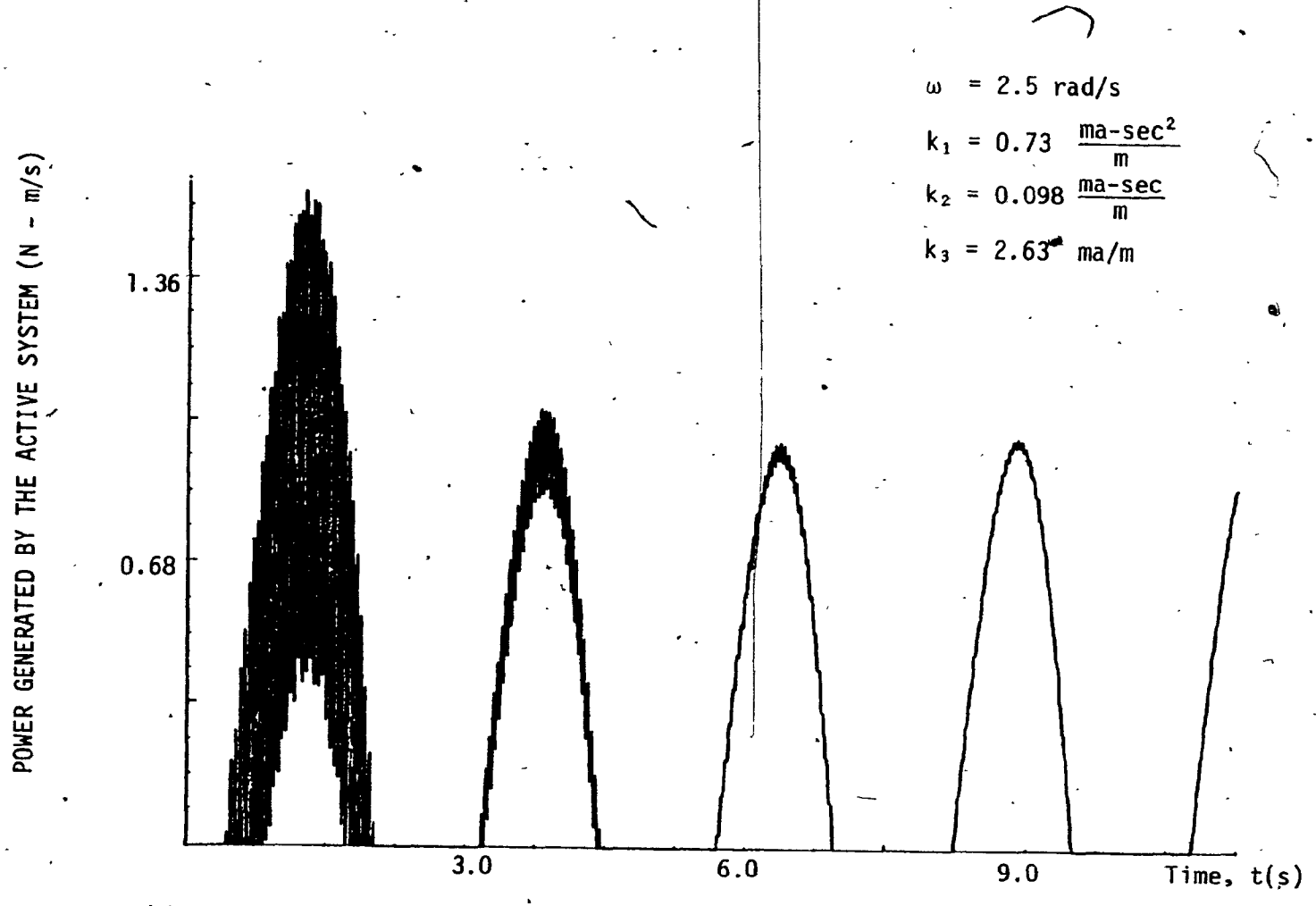

Fig. 39: Power Required by the Active System at 2.5 rad/s.

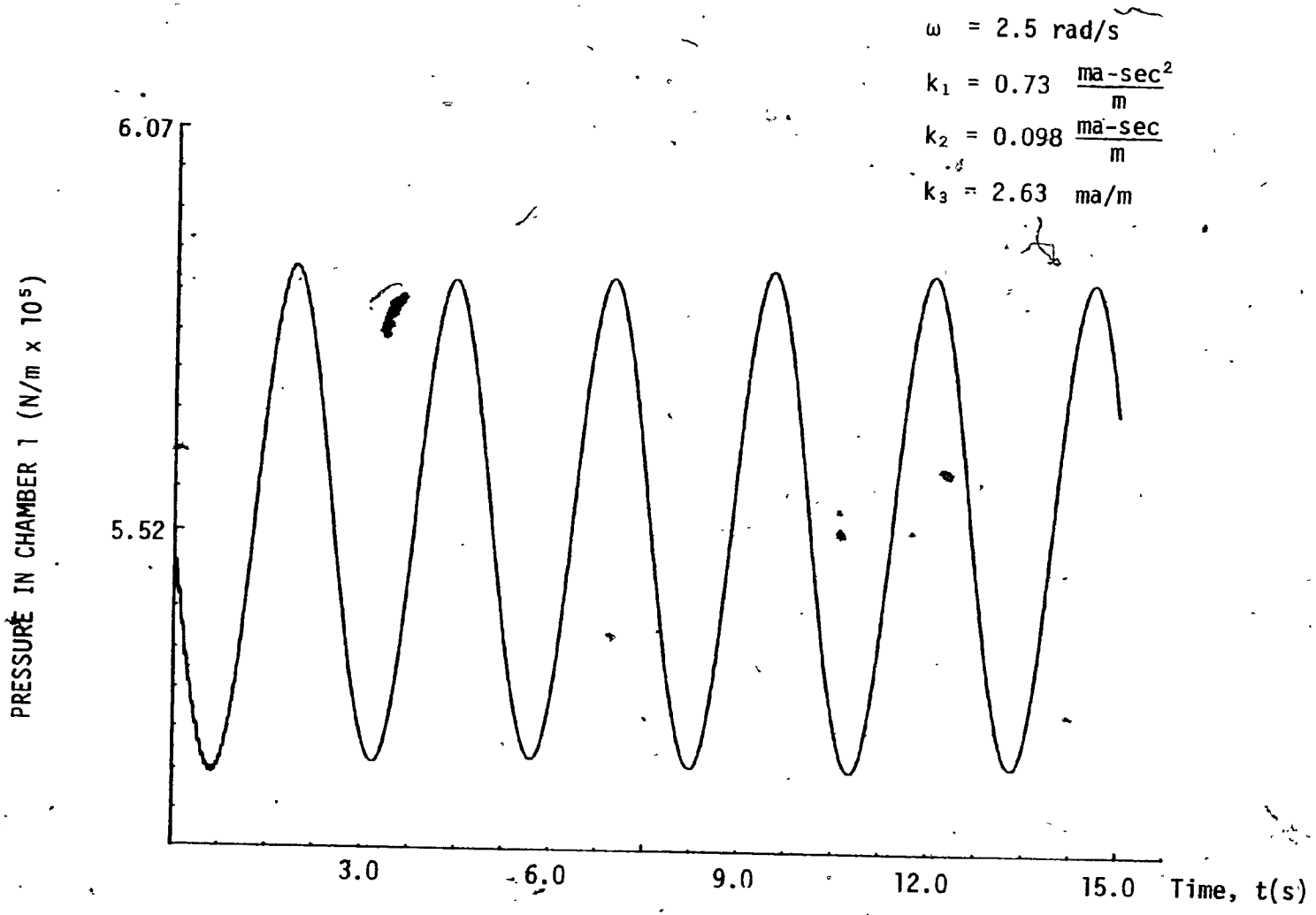

Fig. 40: Pressure Time Response of the Active System at 2.5 rad/s.

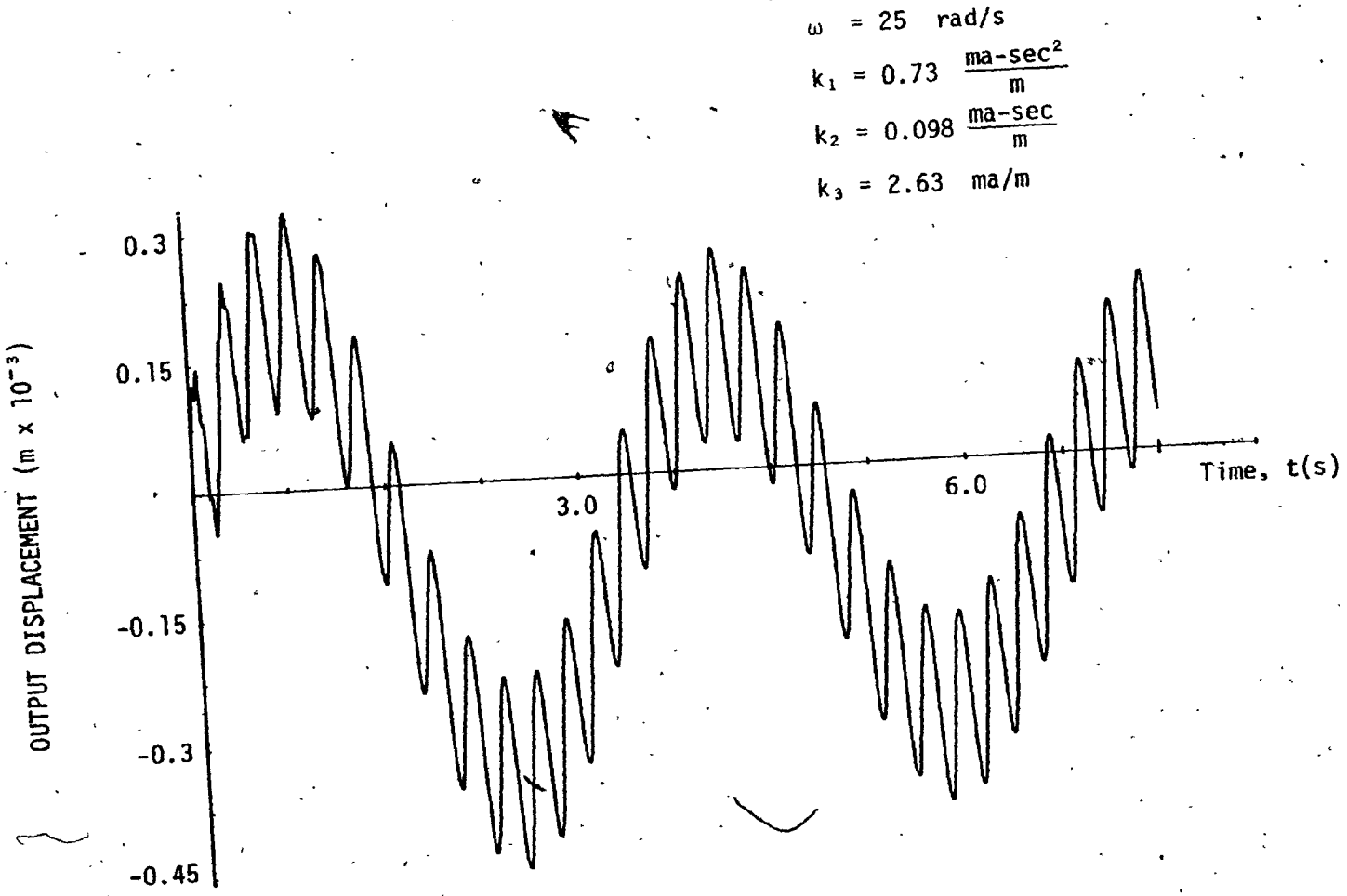

Fig. 41: Displacement Time Response of the Active System at 25 rad/s

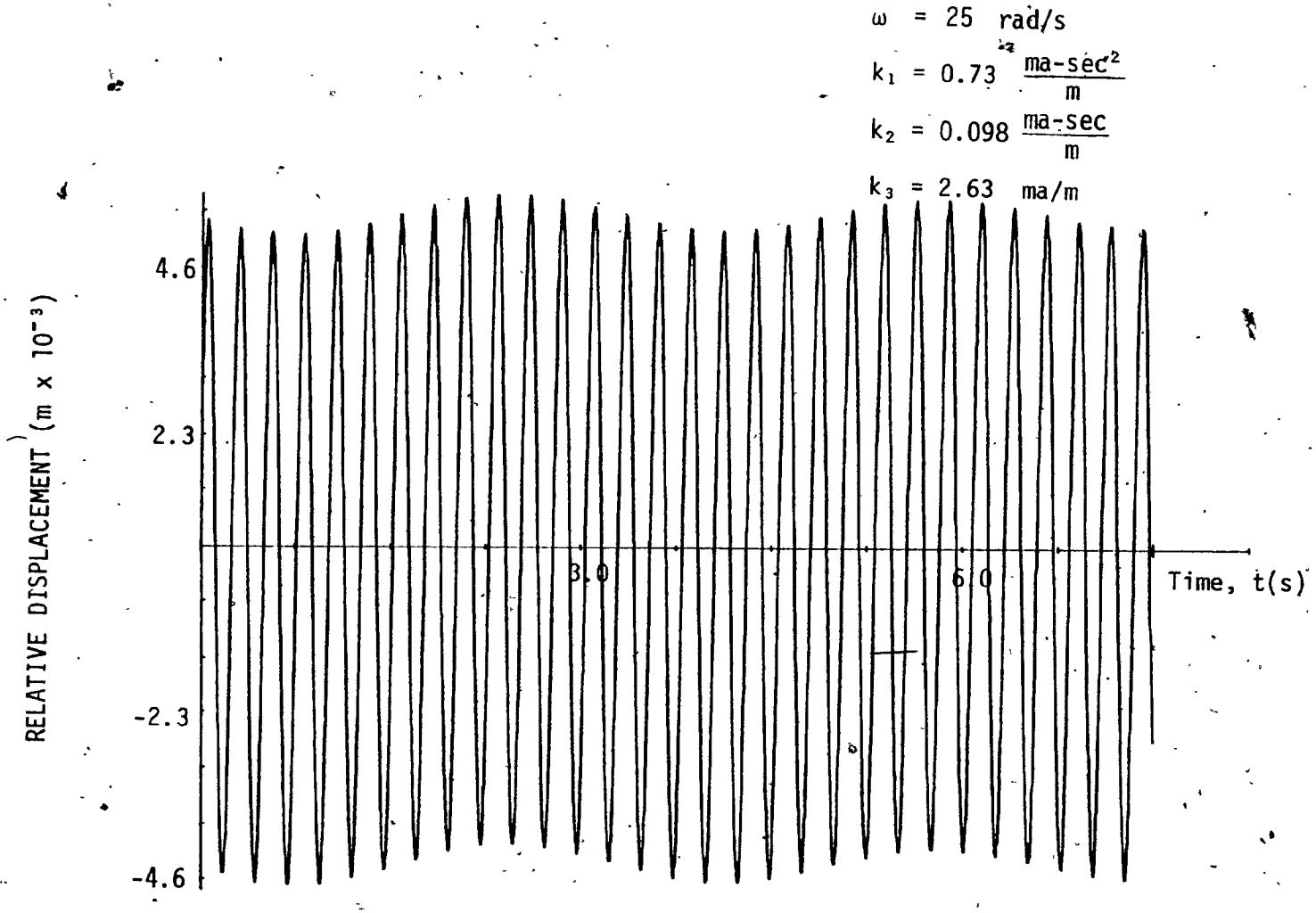

Fig. 42: Relative Displacement Time Response of the Active System at 25 rad/s

compared to the input, the relative displacement is very much the same as the input displacement. The relative displacement is plotted against time and the plot is shown in Figure 42.

The output velocity is shown in Figure 43. The output velocity goes through transient for about 2 sec. and settles down to a value of 3×10^{-3} m/sec. The output velocity also shows that it contains more than one frequency. The output acceleration of the active system is shown in Figure 44. The output acceleration also has initial transient for about 2.5 sec. and settles to a value of 0.1 m/sec.^{2} The maximum force transmitted to the mass is about 9 times less than the input. In the steady state, the acceleration (or the force) transmitted to the mass is about 27 times less than the input acceleration. The output acceleration is almost sinusoidal with no significant high frequency component.

The mass flow rate and the force generated by the active damper are shown in Figures 45 and 46 respectively. Both the mass flow rate and the force generated by the damper goes through transient for about 2.5 sec. and then settles down. By comparing this mass flow rate at 25 rad/sec. with 2.5 rad/sec. we can see that for an excitation frequency of 25 rad/sec. the mass flow rate is about 10 times greater. The reason for greater mass flow rate is due to the larger relative velocity which increases the size of the orifice area controlled by the servo-valve. The force generated by the damper is almost the same for the above two frequencies.

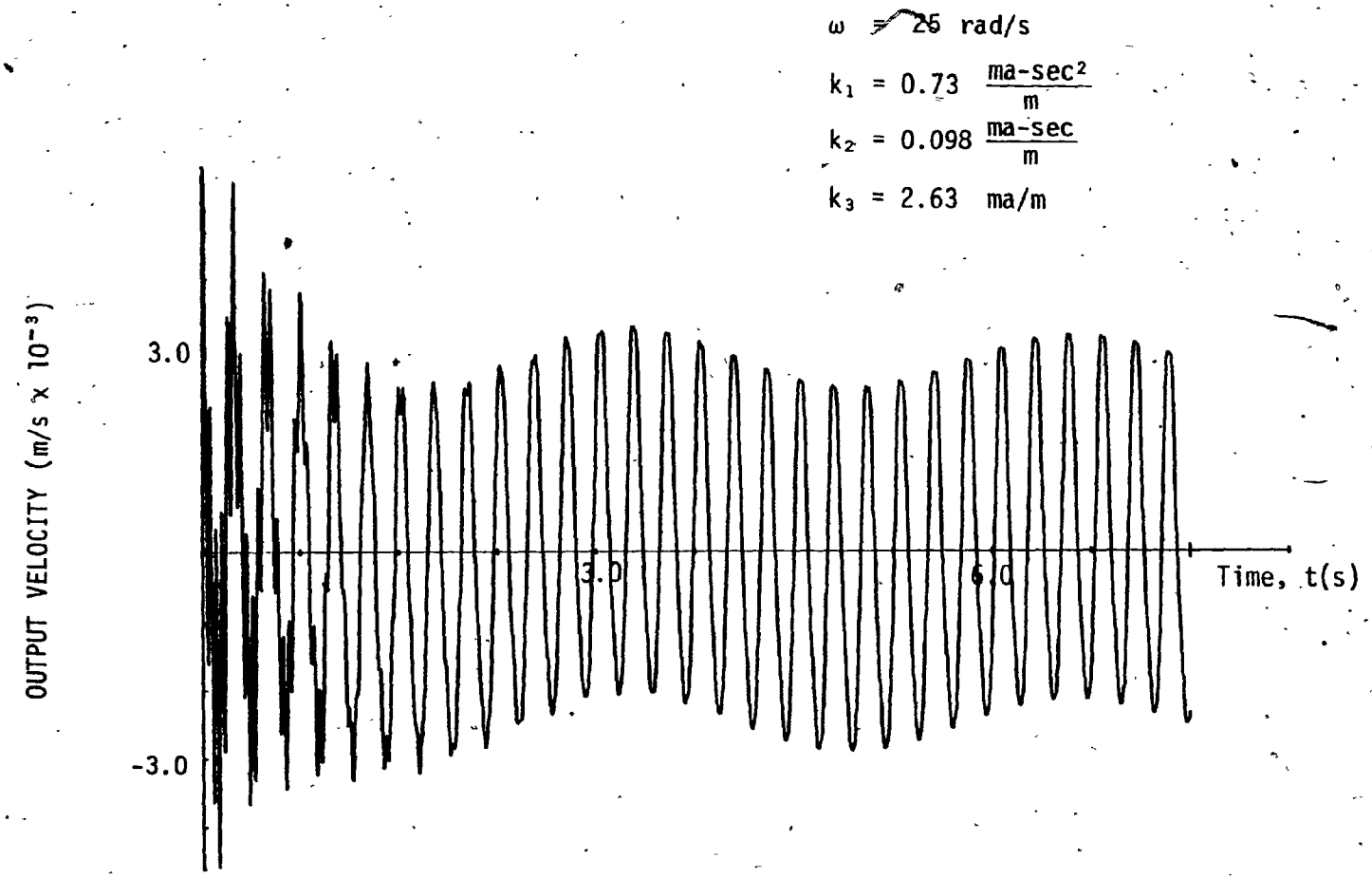

Fig. 43: Velocity Time Response of the Active System at 25 rad/s

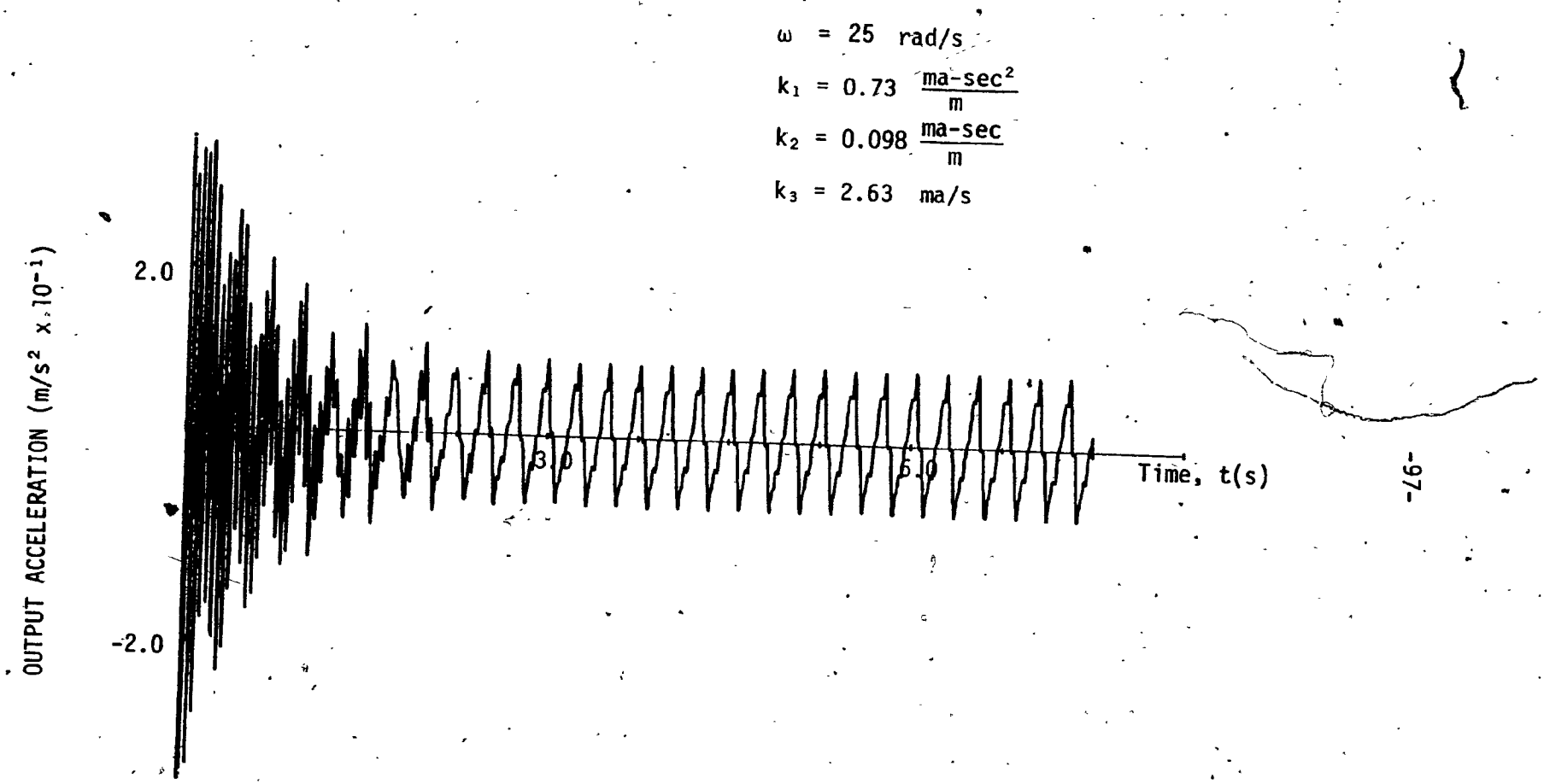

Fig. 44: Acceleration Time Response of the Active System at 25 rad/s

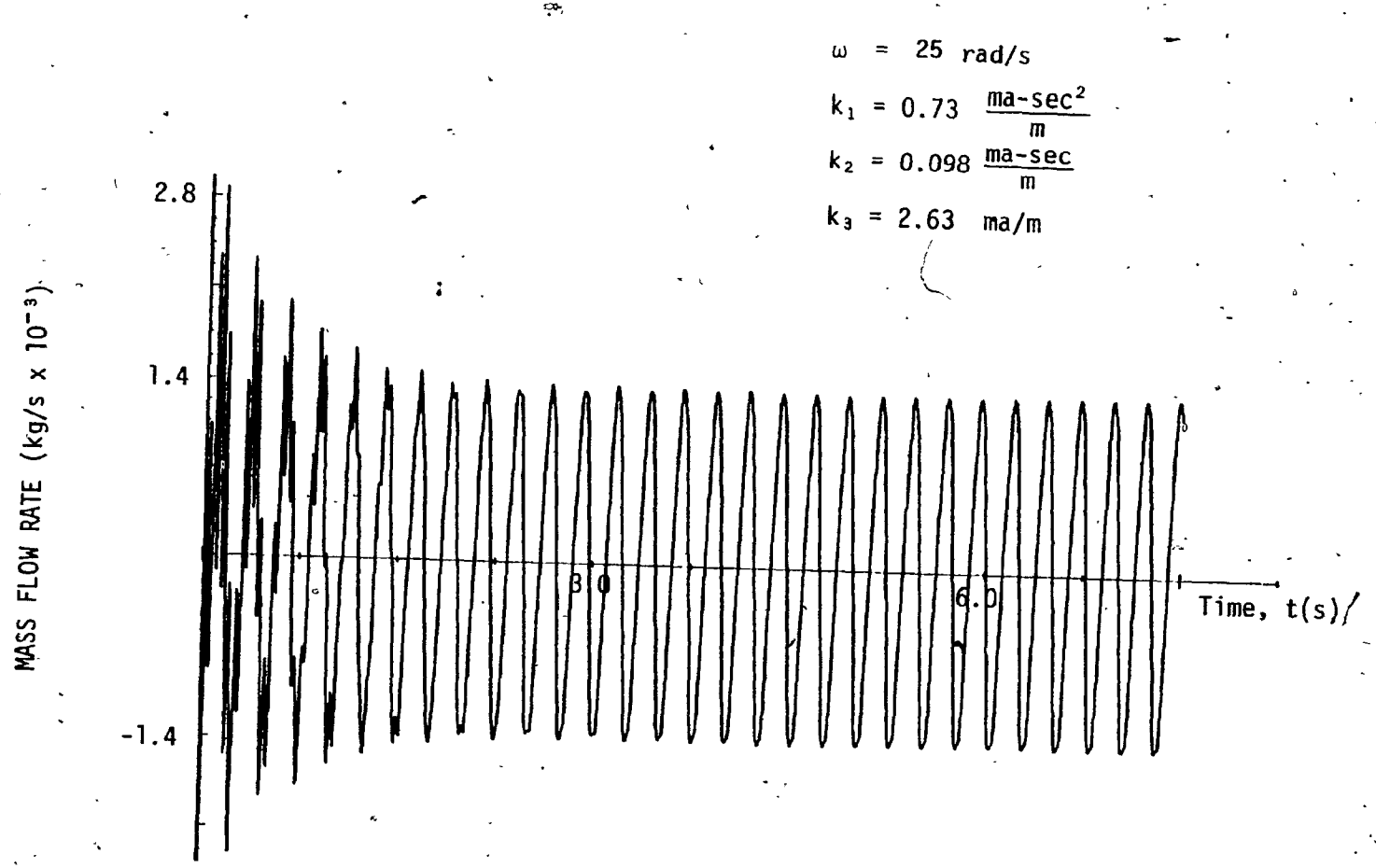

Fig. 45: Time Response of the Mass Flow Rate at 25 rad/s

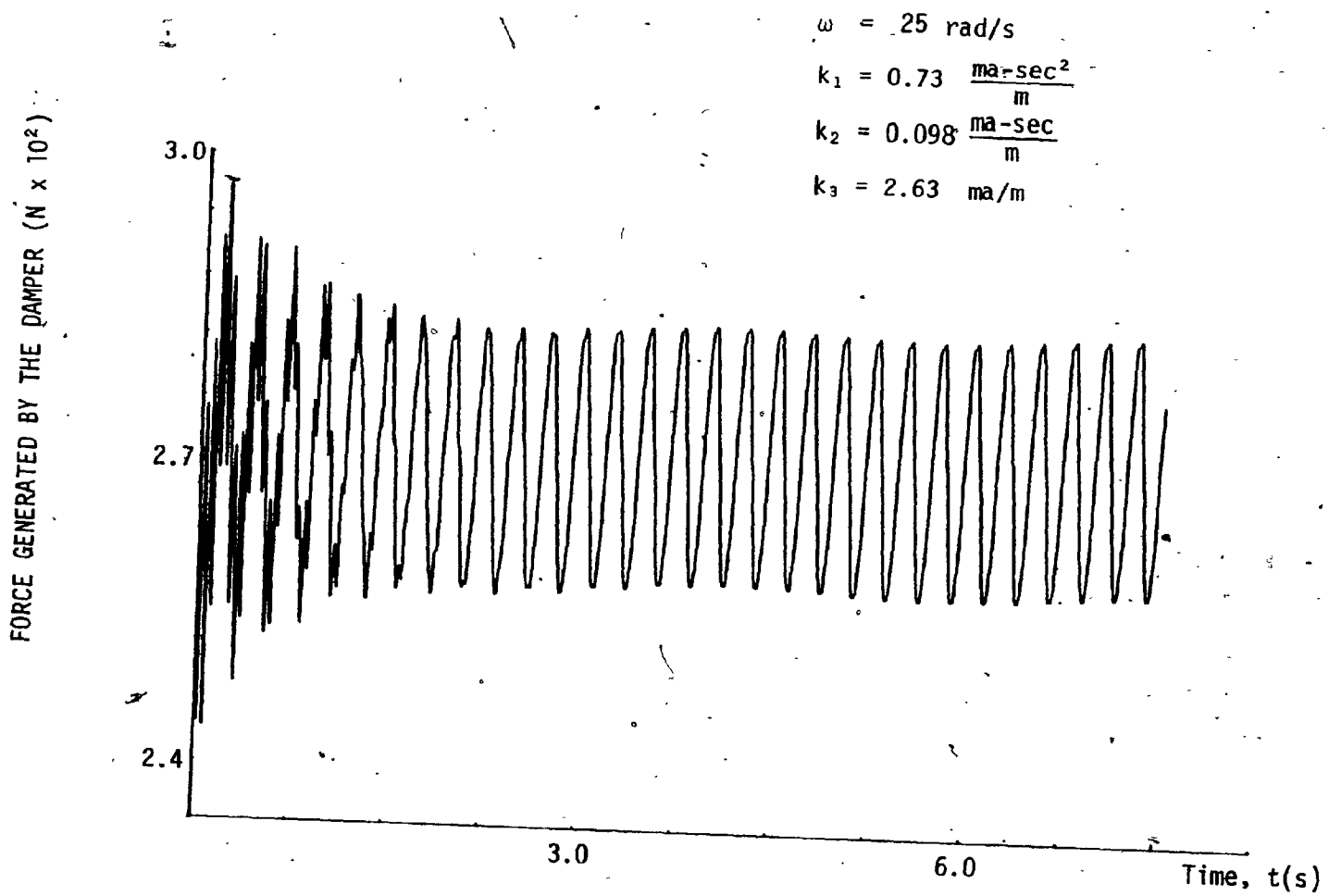

Fig. 46: Force Generated by the Active System at 25 rad/s

The power required by the active system for 25 rad/sec. is shown in Figure 47. As it can be seen from Figures 39 and 47, the power required by the active system increases as the input excitation frequency increases.

Figure 48 shows the pressure in chamber 1 for the excitation frequency of 25 rad/sec. The pressure in chamber 1 has a transient for 0.75 sec. In the steady state, the pressure oscillates evenly around the initial pressure of 5.52×10^5 N/m^2. This ensures that the system will come to rest when the inputs are zero.

Figure 49 shows the absolute displacement transmissibility for the active system. As it can be seen from Figure 49, the displacement transmissibility has very low value for low frequencies and as the frequency increases up to 35 rad/s, the absolute displacement also increases. In the frequency range 30 to 42 rad/s, increasing the excitation frequency decreases the transmissibility. However, for input frequencies greater than 42 rad/s, the transmissibility increases sharply with the frequency. It should be noted that the absolute displacement transmissibility even at 30 rad/s is less than -10 db (0.317).

The relative displacement transmissibility is shown in Figure 50. The relative displacement transmissibility is very similar to that of the absolute displacement transmissibility plot. Since the output displacement is small, the relative displacement transmissibility is around unity until 42 rad/s. For frequency higher than 42 rad/s, the relative displacement transmissibility increases and has a value of

ω = 25 rad/s

k_1 = 0.73 $\frac{\text{ma-sec}^2}{\text{m}}$

k_2 = 0.098 $\frac{\text{ma-sec}}{\text{m}}$

k_3 = 2.63 ma/m

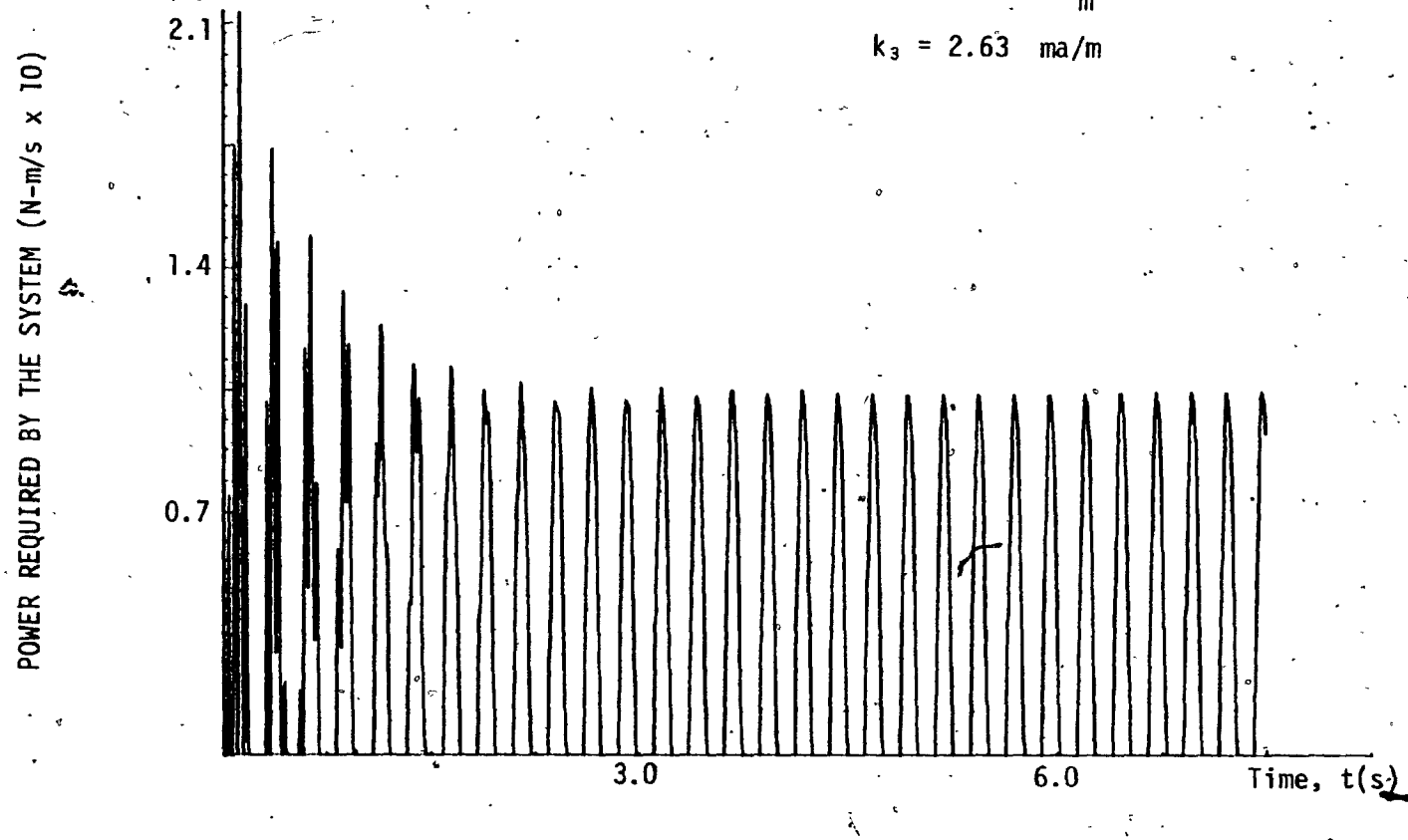

Fig. 47: Power Required by the Active System at 25 rad/s

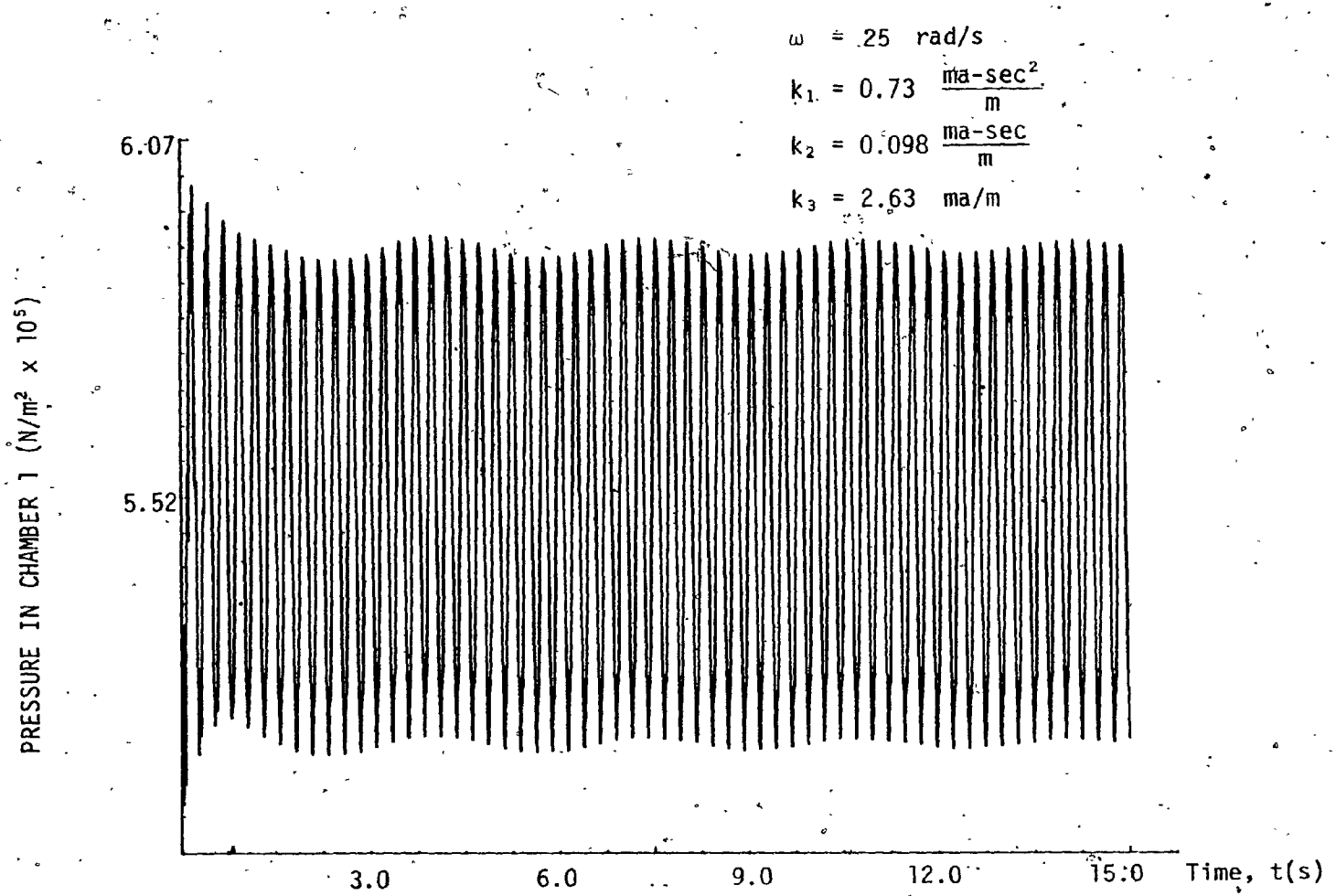

Fig. 48: Pressure Time Response of the Active System at 25 rad/s

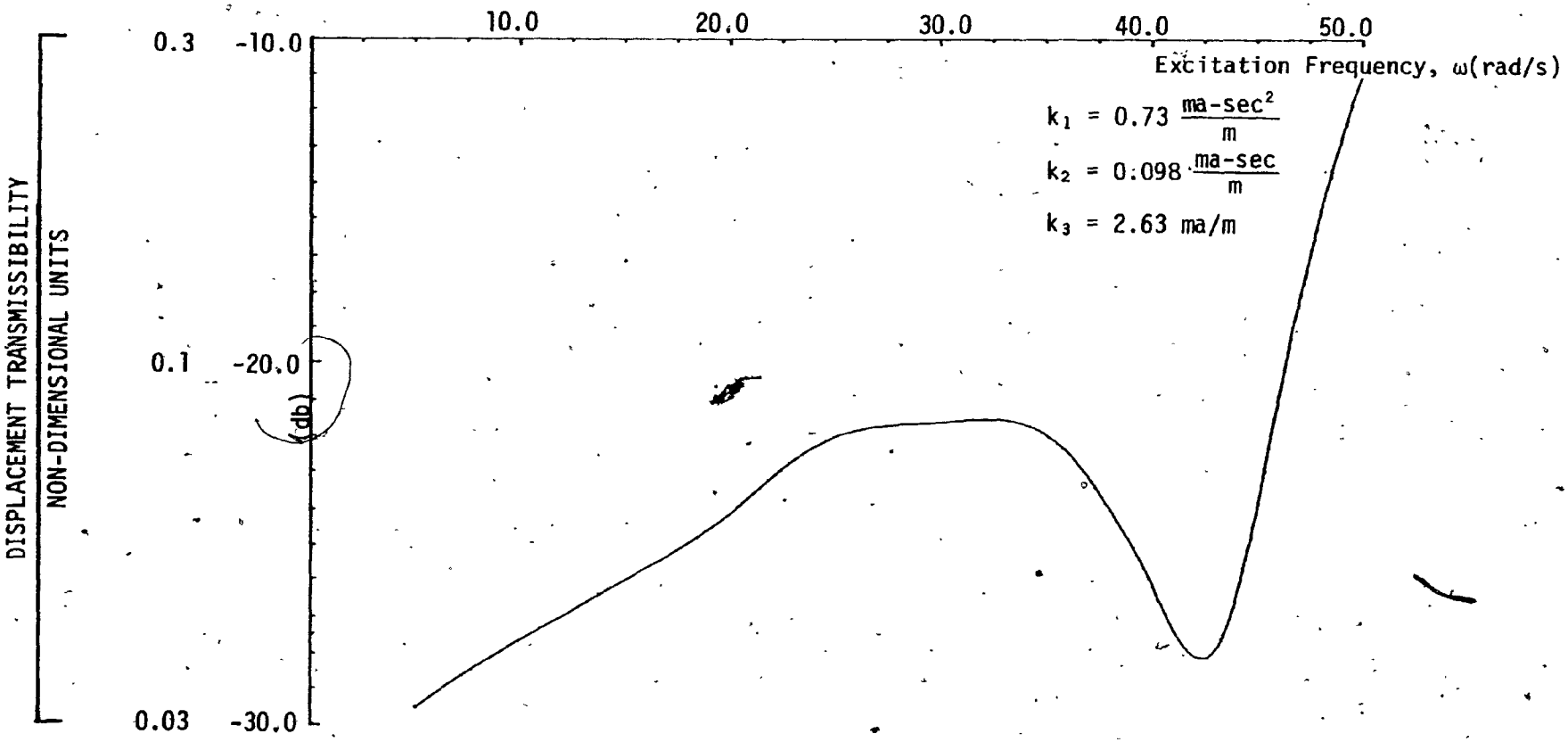

Fig. 49: Displacement Transmissibility Plot for Type 2 Active System

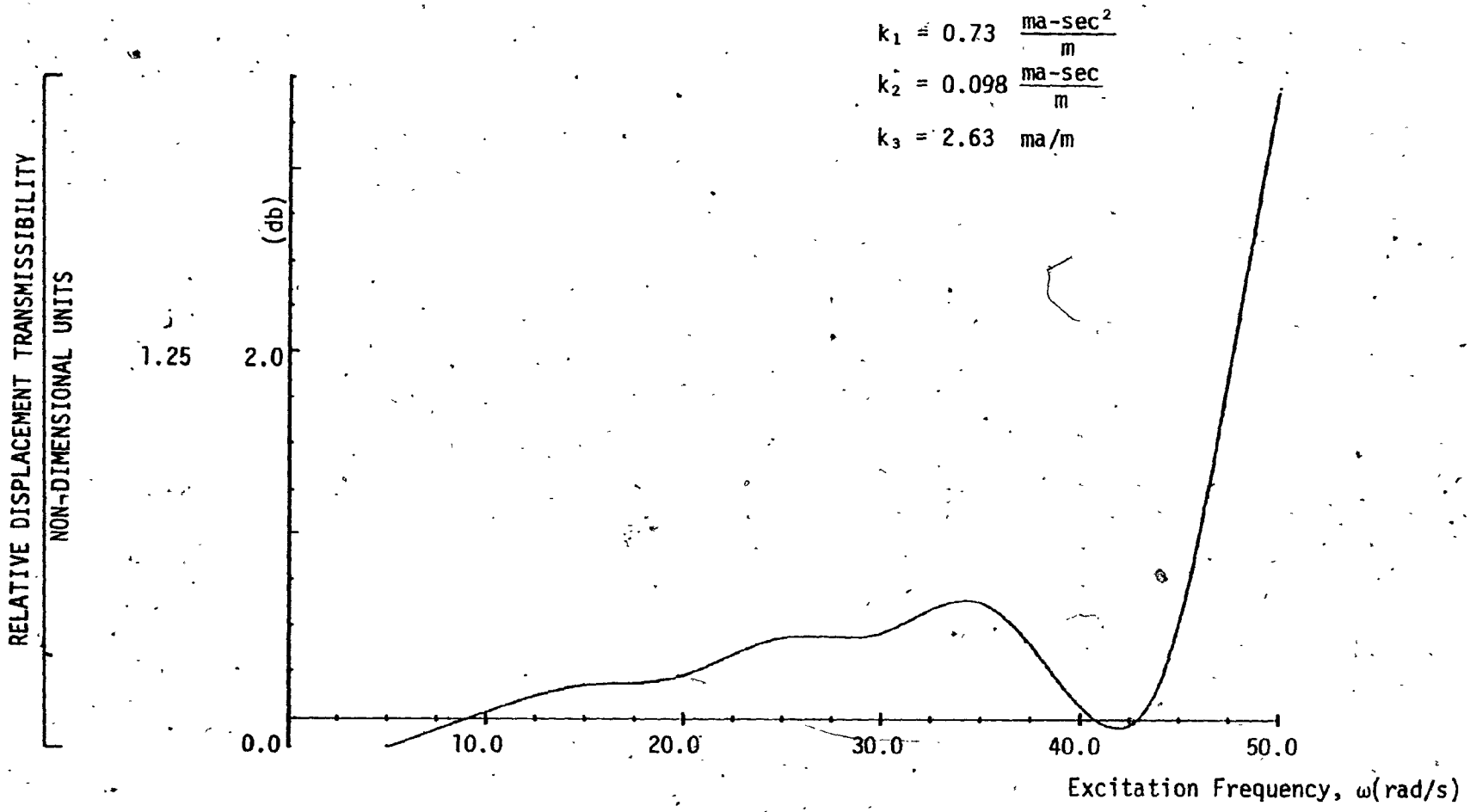

Fig. 50: Transmissibility Plot for Type 2 Active System

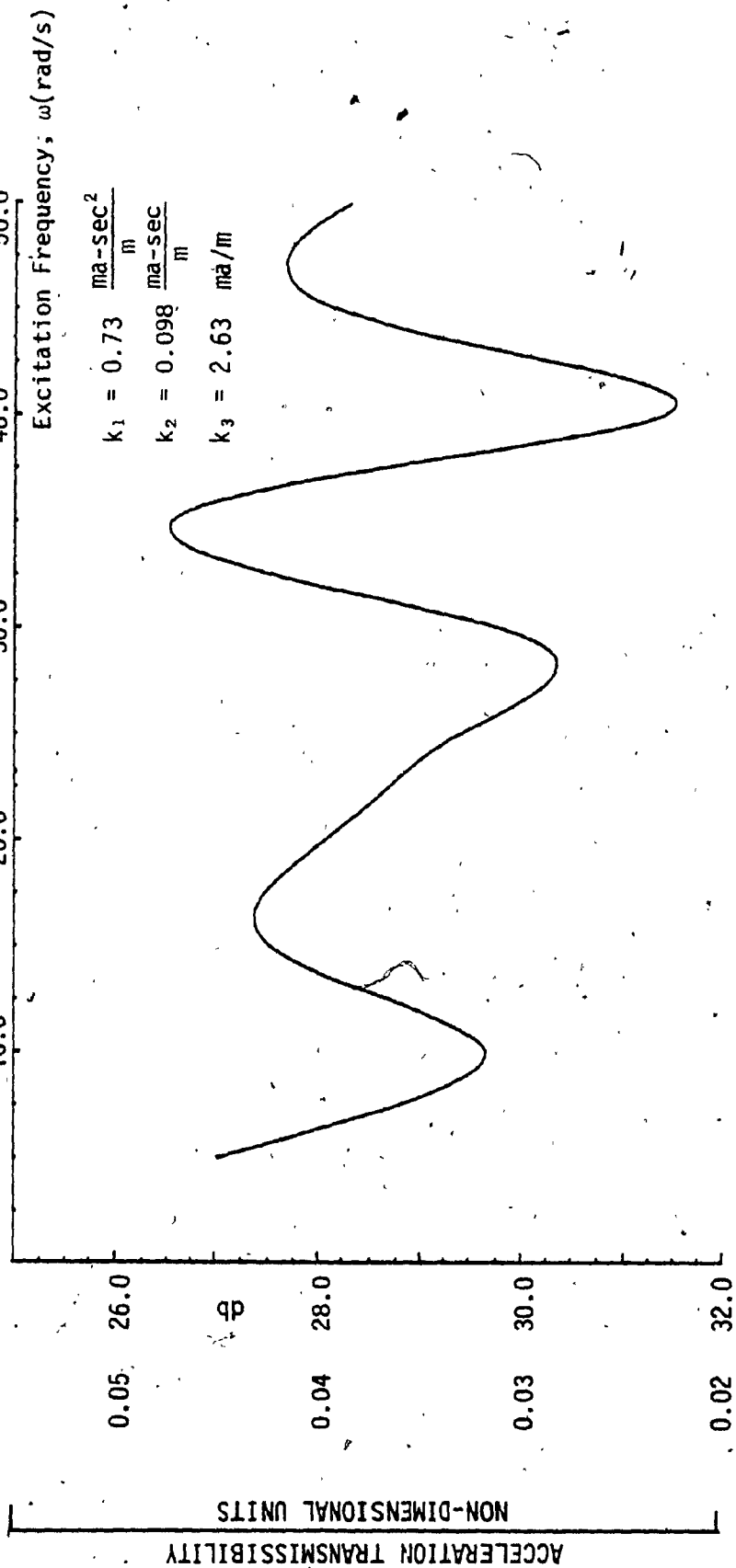

Fig. 51: Transmissibility Plot for Type 2 Active System

3.5 db at 50 rad/s.

The acceleration (force) transmissibility is plotted in Figure 51. The acceleration transmissibility has three peaks at approximately 18 rad/s, 35 rad/s and 48 rad/s. The peak transmissibility is observed to be less than -26 db(0.05) and shows good isolation characteristics of the active system.

3.8.2 Response to Sinusoidal Input for Type 1 Active System

The active system of type 1 is simulated using the Runge-Kutta 4th order method on a CDC Cyber 172/2 digital computer. The Fortran computer program used for the simulation is given in Appendix F.

The output displacement of the active system Type 1 is shown in Figure 52 for an input excitation frequency of 25 rad/sec The output displacement does not have equal amplitude about the time axis and is very similar to the response of Type 2 system. Also the amplitude of the displacement decreases with time. It is also seen that the output displacement contains more than one frequency. Figure 53 shows the relative displacement of the system. Since the output displacement is almost identical to the input.

Figure 54 shows the acceleration response of the Type 1 active system. The acceleration goes through much more severe transient than in the case of Type 2 active system. The system reaches the steady state only after 7.5 sec. and steady state acceleration is about 10 times less than the input acceleration.

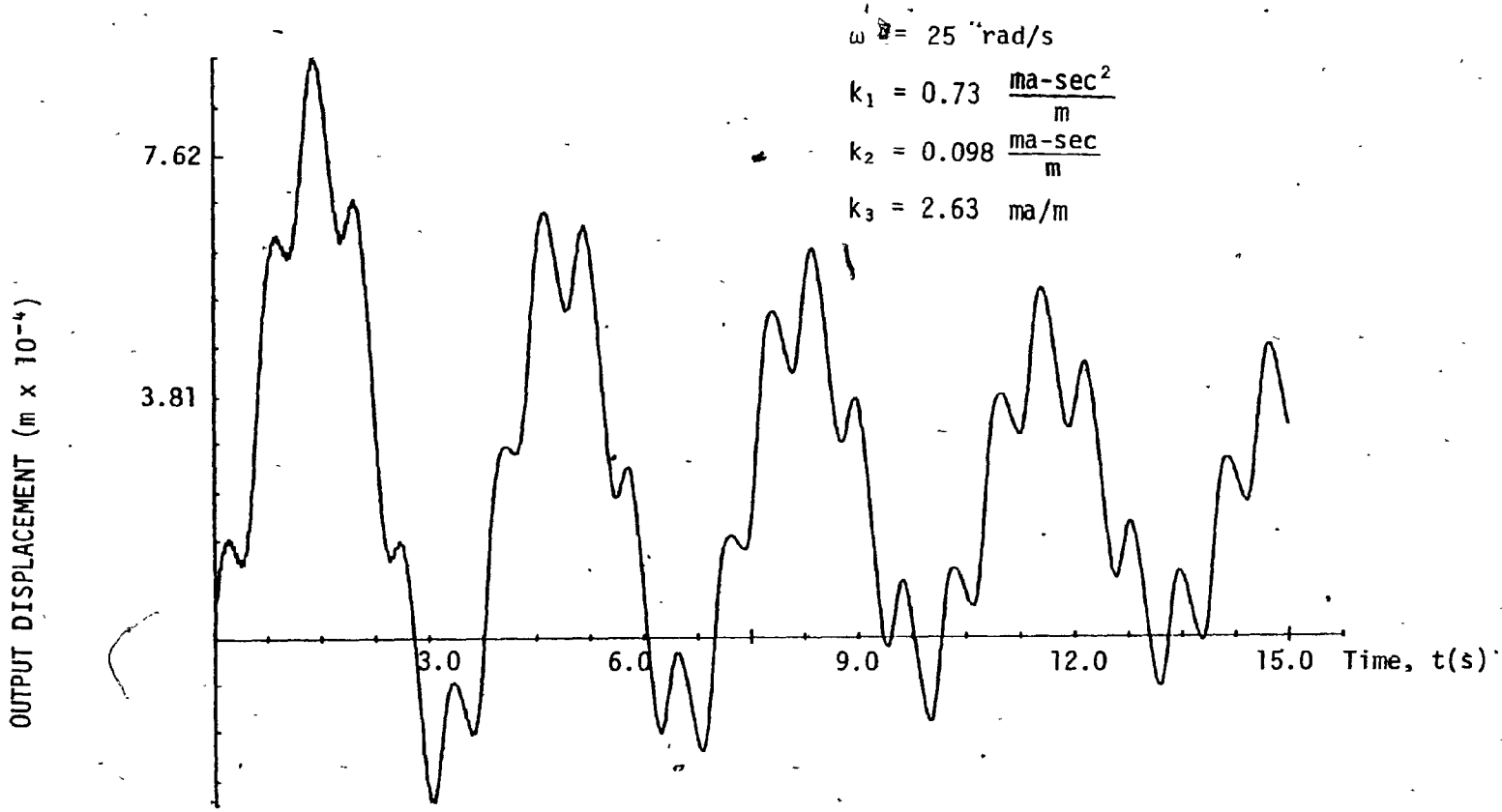

Fig. 52: Displacement Time Response for the Active System Type 1 at 25 rad/s

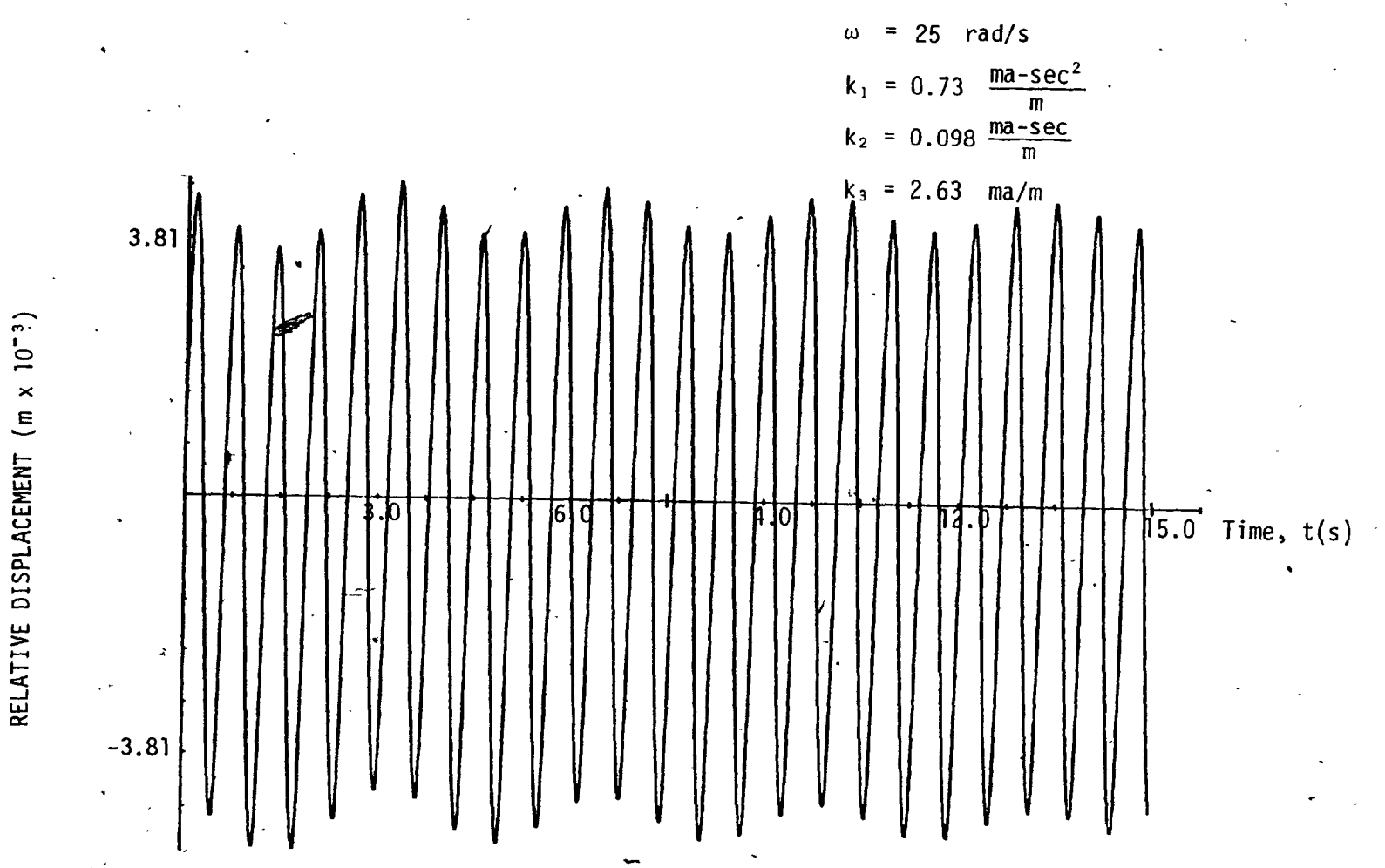

Fig. 53: Relative Displacement Time Response for the Active System Type 1 at 25 rad/s

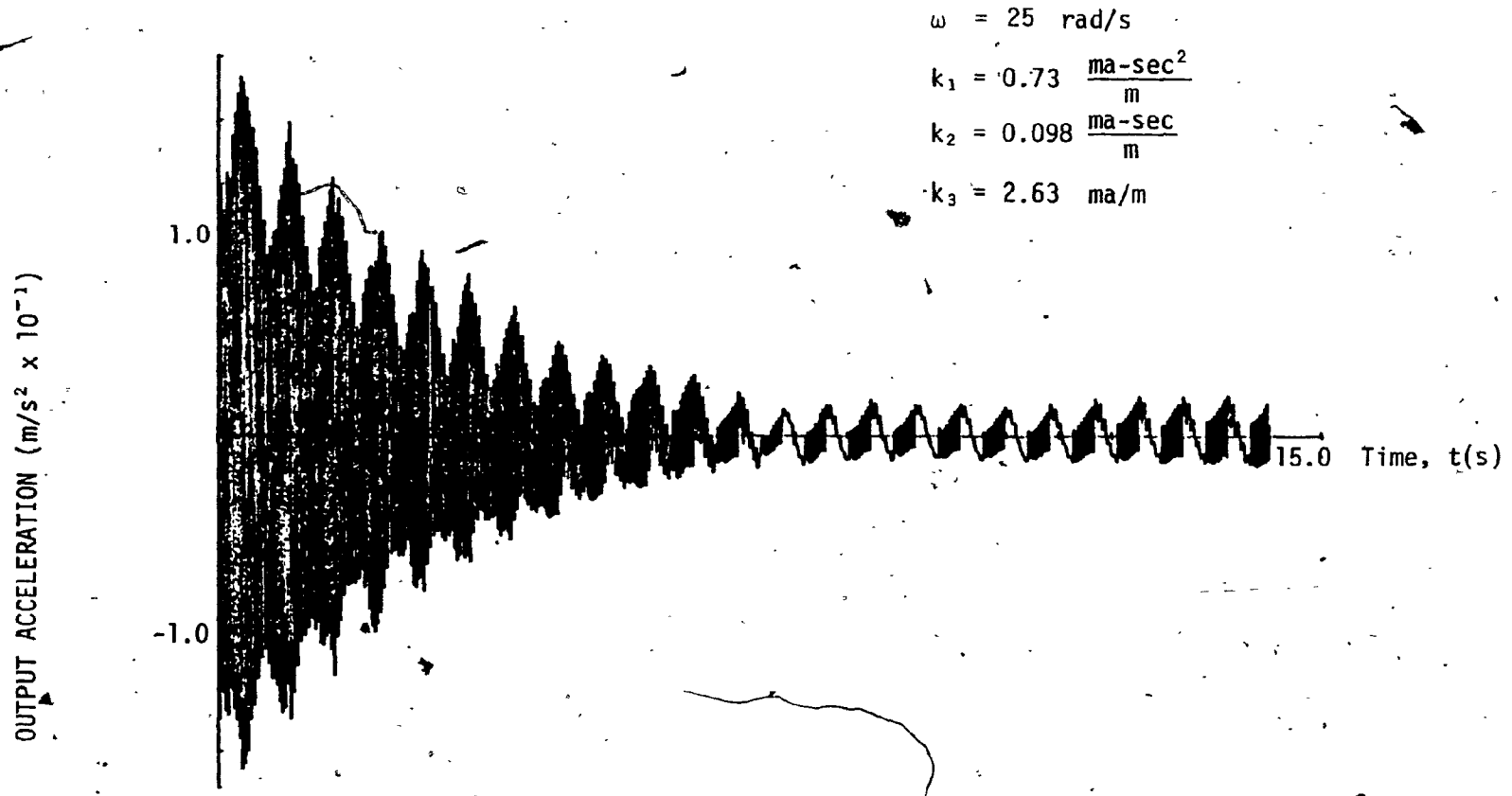

Fig. 54: Acceleration Time Response for the Active System Type 1 at 25 rad/s

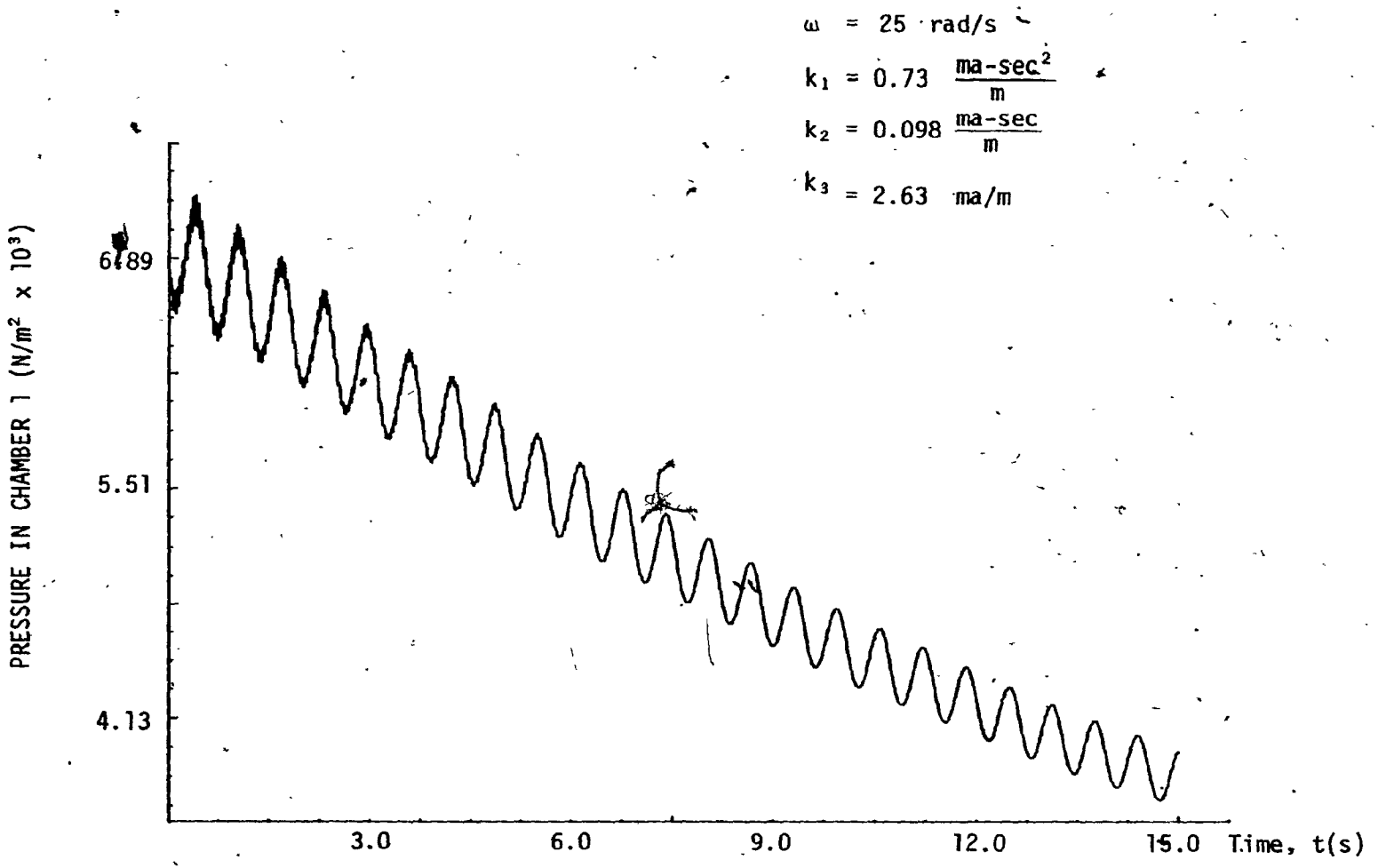

Fig. 55: Pressure Time Response for the Active System Type 1 at 25 rad/s

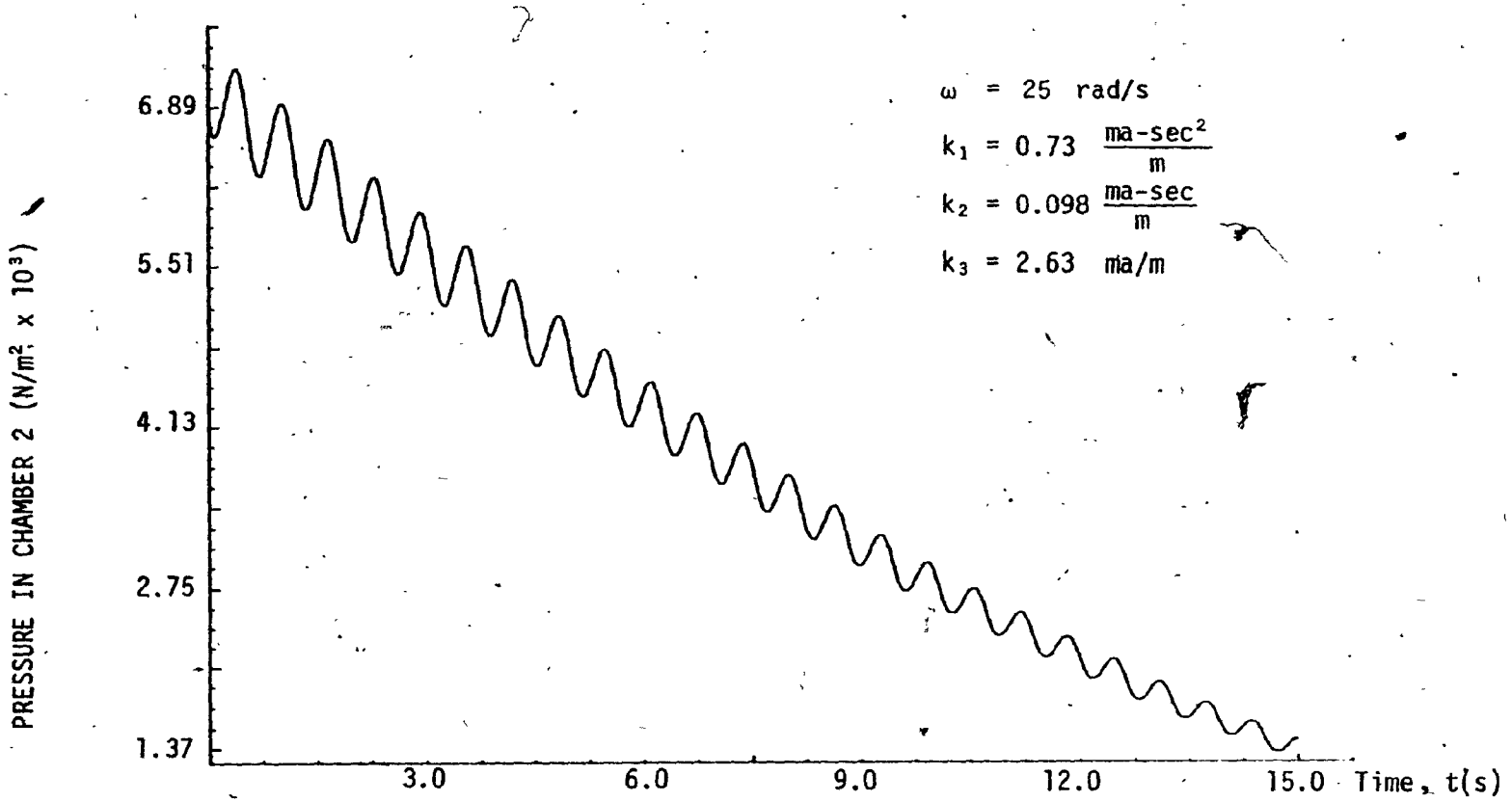

Fig. 56: Pressure Time Response for the Active System Type 1 at 25 rad/s

Figures 55 and 56 show the pressure in chamber 1 and chamber 2 respectively. As it can be seen from these figures, both the chamber pressures reduce as the time increases. This phenomenon makes the system to be impractical since the system will not come to the initial state when the input becomes zero after some time. Moreover, since this system uses two servo-valves, the cost of the system increases considerably.

3.8.3 Response of Type 2 Active Isolation System to Pulse Like Input

The pulse like inputs are shown in Section 2.5. These inputs are used to evaluate the performance of the Type 2 active system.

Figure 57 shows that the output displacement of the active system for the rounded pulse input. Time response shows that the amplitude of displacement reduces as the time increases. The shock severity parameter γ used for this case is 10. For this value of $\gamma = 10$, the input displacement, velocity and acceleration are zero for time greater than 0.4 sec. But Figure 54 shows that the output displacement has a finite amplitude even after 15 sec. The peak output displacement is about 1.5 times less than the peak input displacement. Figure 58 shows the relative displacement plotted against time. The peak relative displacement takes place in less than 0.4 sec. and has a magnitude of 3.56×10^{-3} m.

Figure 59 gives the velocity of the mass. The velocity plot shows that the system goes through initial transient for approximately

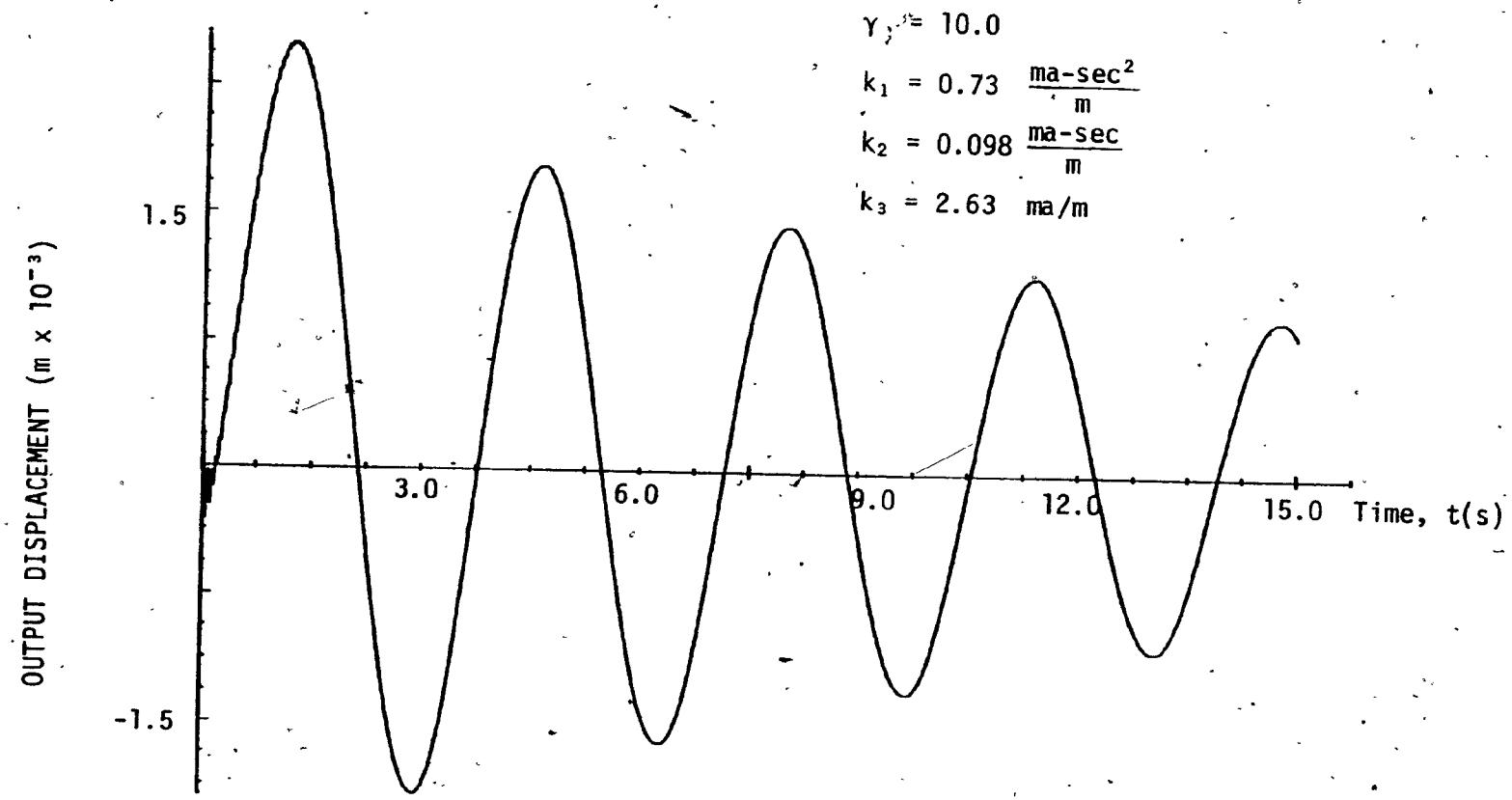

Fig. 57: Displacement Time Response for Pulse Like Input.

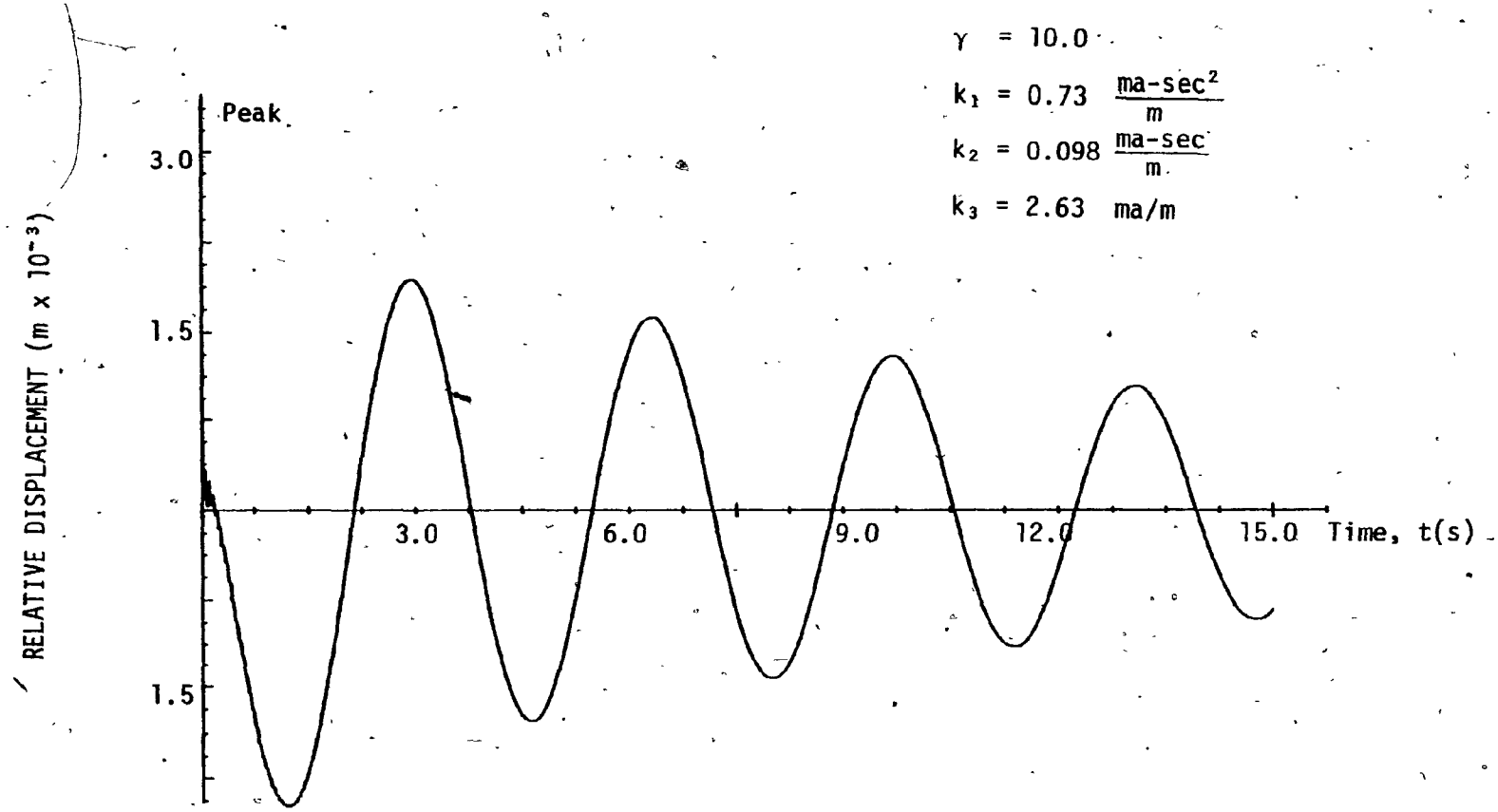

Fig. 58: Relative Displacement Response for Pulse Like Input.

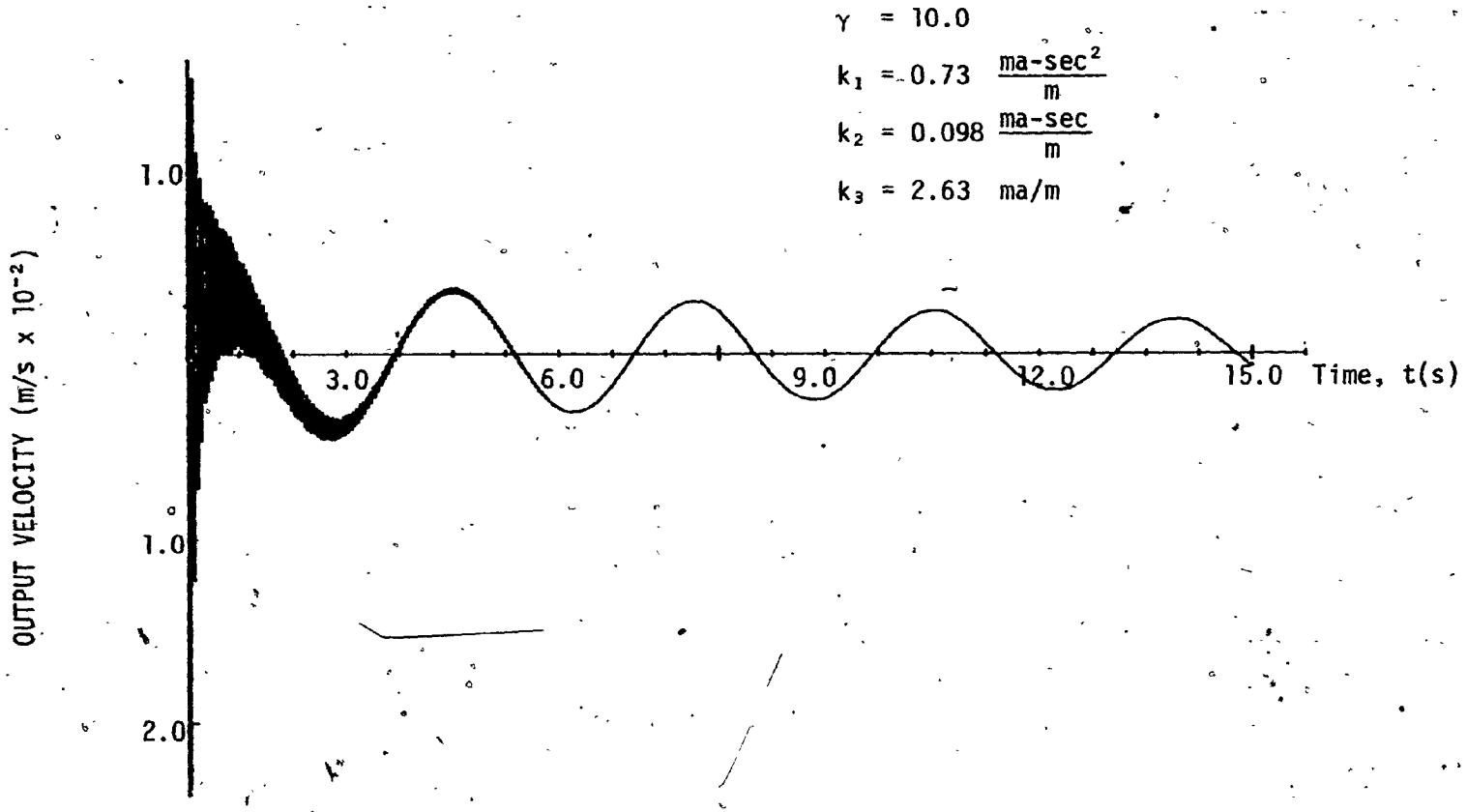

Fig. 59: Velocity Response for Pulse Like Input.

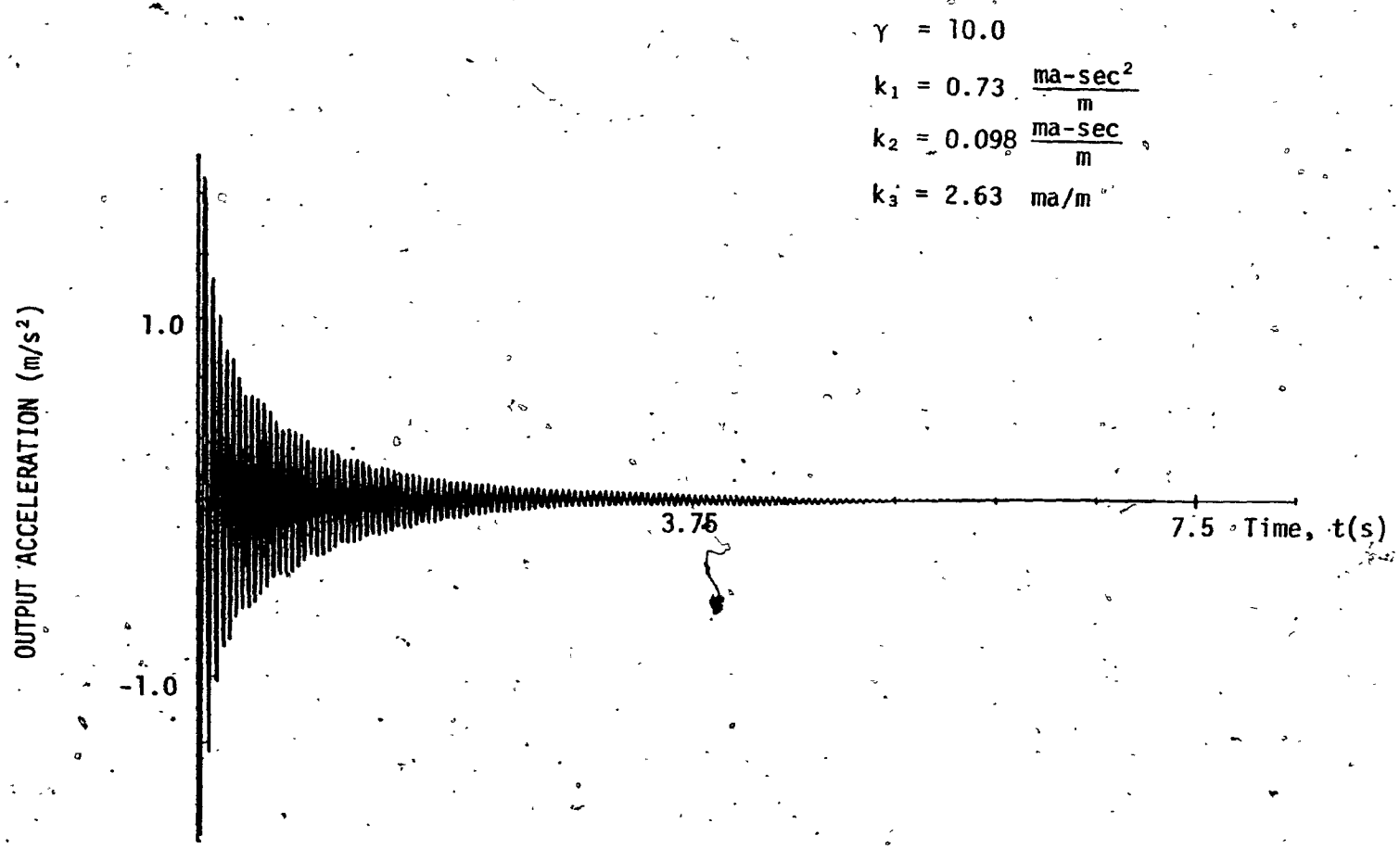

Fig. 60: Acceleration Response for Pulse Like Input.

5 sec. and then exponentially decays. Figure 60 shows the output acceleration with the peak output acceleration about 800 times lower than the input acceleration. It can be seen that the output acceleration also goes through an exponential decay.

Figure 61 shows the acceleration ratio between the output and the input plotted against the severity parameter γ_0. The Figure 61 clearly shows that as the shock parameter increases, the transmitted acceleration (force) to the mass decreases. Even for small values of γ_0 like $\gamma_0 = 1$ the acceleration transmitted to the mass is about 50 times smaller. Figure 62 gives the plot between the shock severity parameter and the ratio between the peak relative displacement and the peak input displacement. Since the output displacement is small, this ratio is close to 1.0 (less than - 3 db).

3.8.4 Response of Type 2 Active Isolation System to Input Excitation of the Form $x=x_0(1-\cos \omega t)$

The third input excitation considered in this thesis is of the form $x = x_0(1-\cos \omega t)$. Similar to the passive system, the excitation frequency is considered to be 1 rad/sec. with the maximum displacement amplitude of 5×10^{-2} m. The input displacement, velocity and acceleration plots are shown in Section 2.5 .

The output displacement of the Type 2 active system for the above mentioned input excitation is plotted in Figure 63. The output displacement goes through a transient for about 3 sec. and then goes through both positive and negative cycles. The maximum output displace-

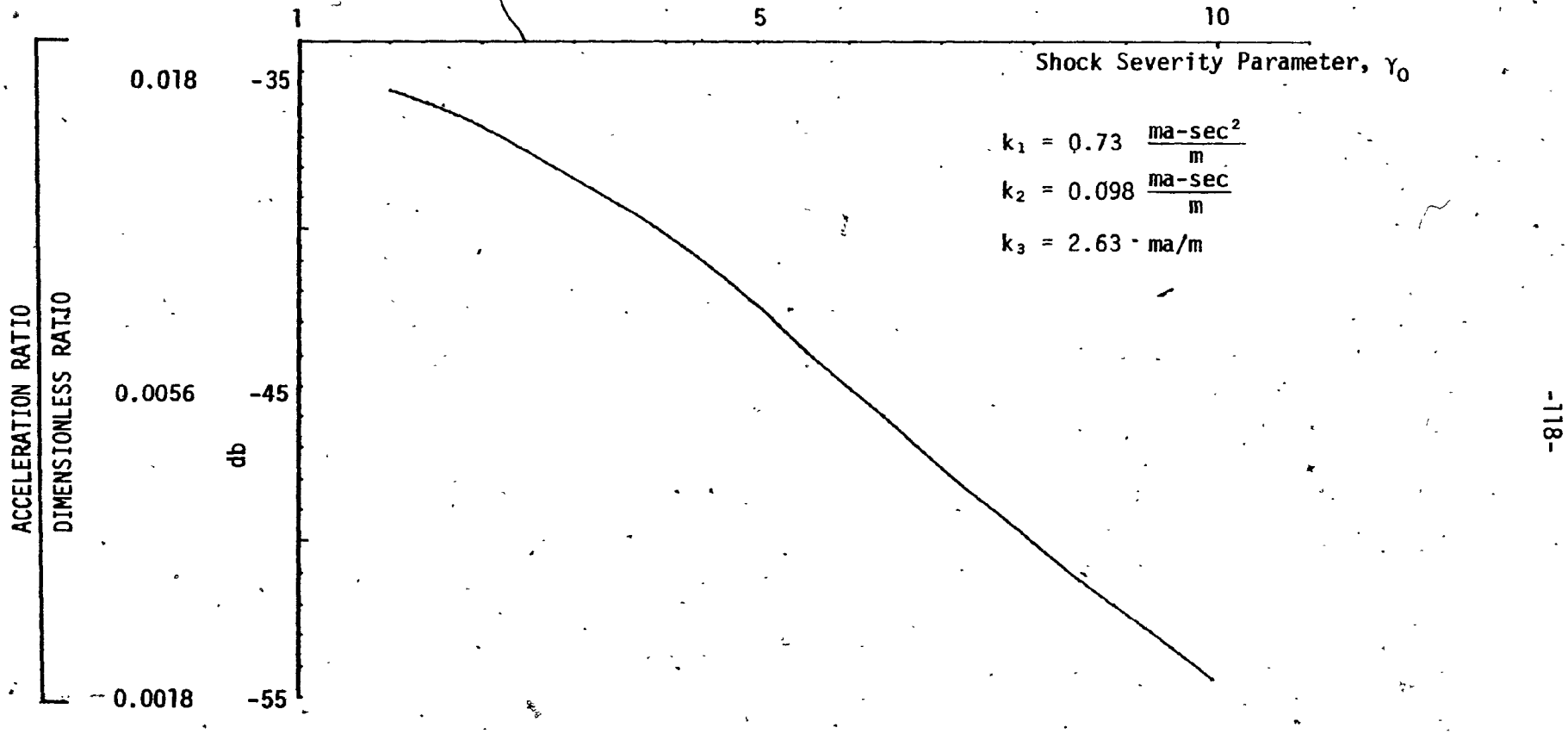

Fig. 61: Acceleration Ratio Plot for Different Values of γ_0

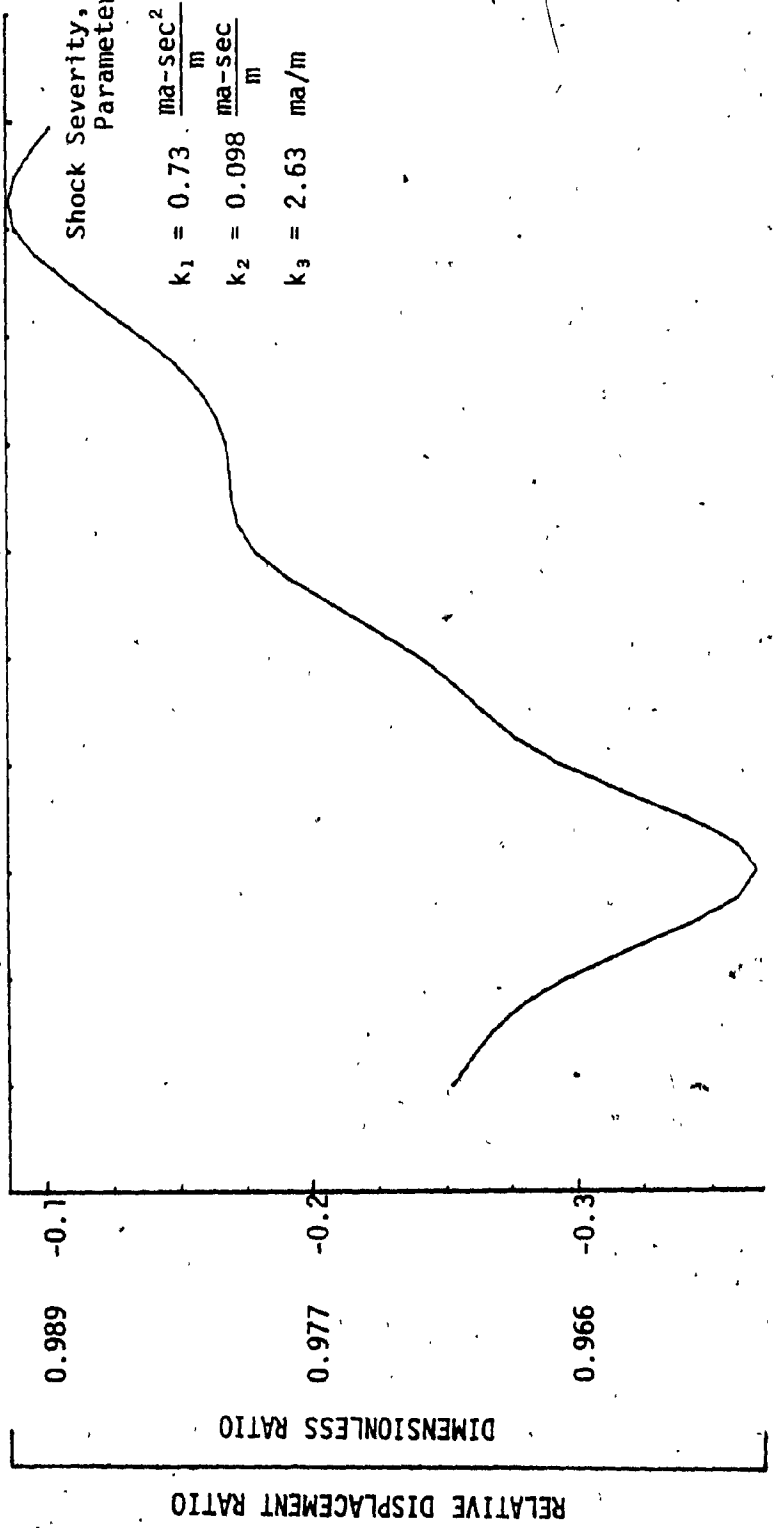

Fig. 62: Relative Displacement Ratio Plot for Different Values of γ_o

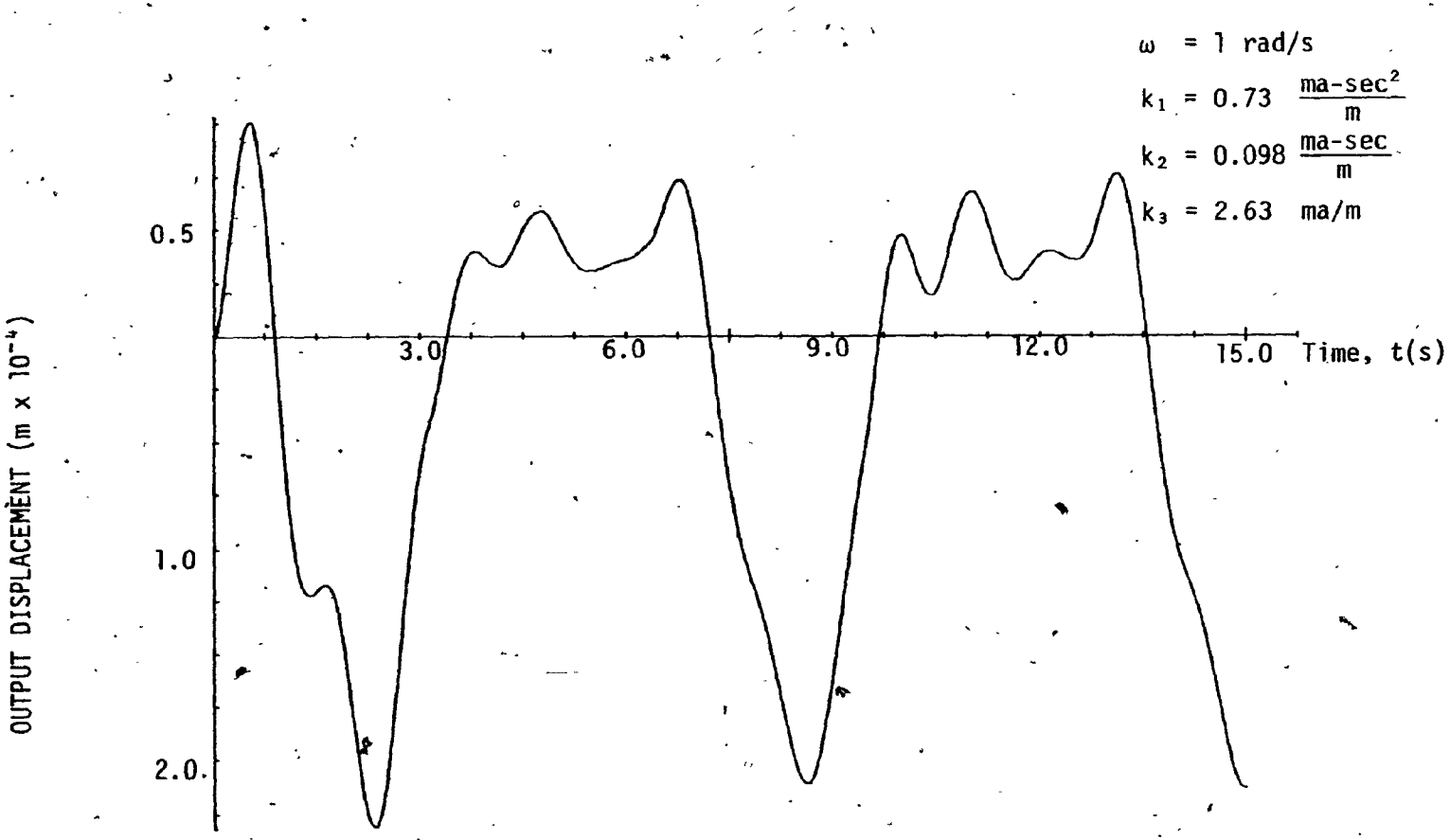

Fig. 63: Displacement Time Response for Input of the Form $X = X_0 (1-\cos\omega t)$

ment is about 200 times less than that of the input displacement plotted against time. Since the output displacement is about 200 times less than the input, the relative displacement is almost identical to that of the input. (Figure 64)

Figure 65 shows the output velocity plotted against time. The output velocity contains more than one frequency. Figure 66 shows the output acceleration of the system. The output acceleration is very oscillatory during the initial transient period with the highest transmitted acceleration occurring during this period. However, the peak output acceleration is only 20% of the maximum input acceleration.

3.9 THE EFFECT OF VARIATION OF THE FEEDBACK GAINS IN THE SYSTEM PERFORMANCE

Acceleration, velocity and displacement feedback gains k_1, k_2 and k_3 respectively are varied in order to study their effect on the system performance. The input excitation considered in this parametric study is sinusoidal. The input frequency was varied from 2.5 rad/sec. to 50 rad/sec. with an amplitude of 4.57×10^{-3} m. One parameter at a time is varied with the rest of the parameters having a constant value as used in Section 3.8. Acceleration and relative displacement transmissibility for different gains are plotted and also the time response of output displacement and acceleration is given.

3.9.1 The Effect of Variation of the Acceleration Feedback Gain k_1

Figures 67 and 68 show the output displacement and accelera-

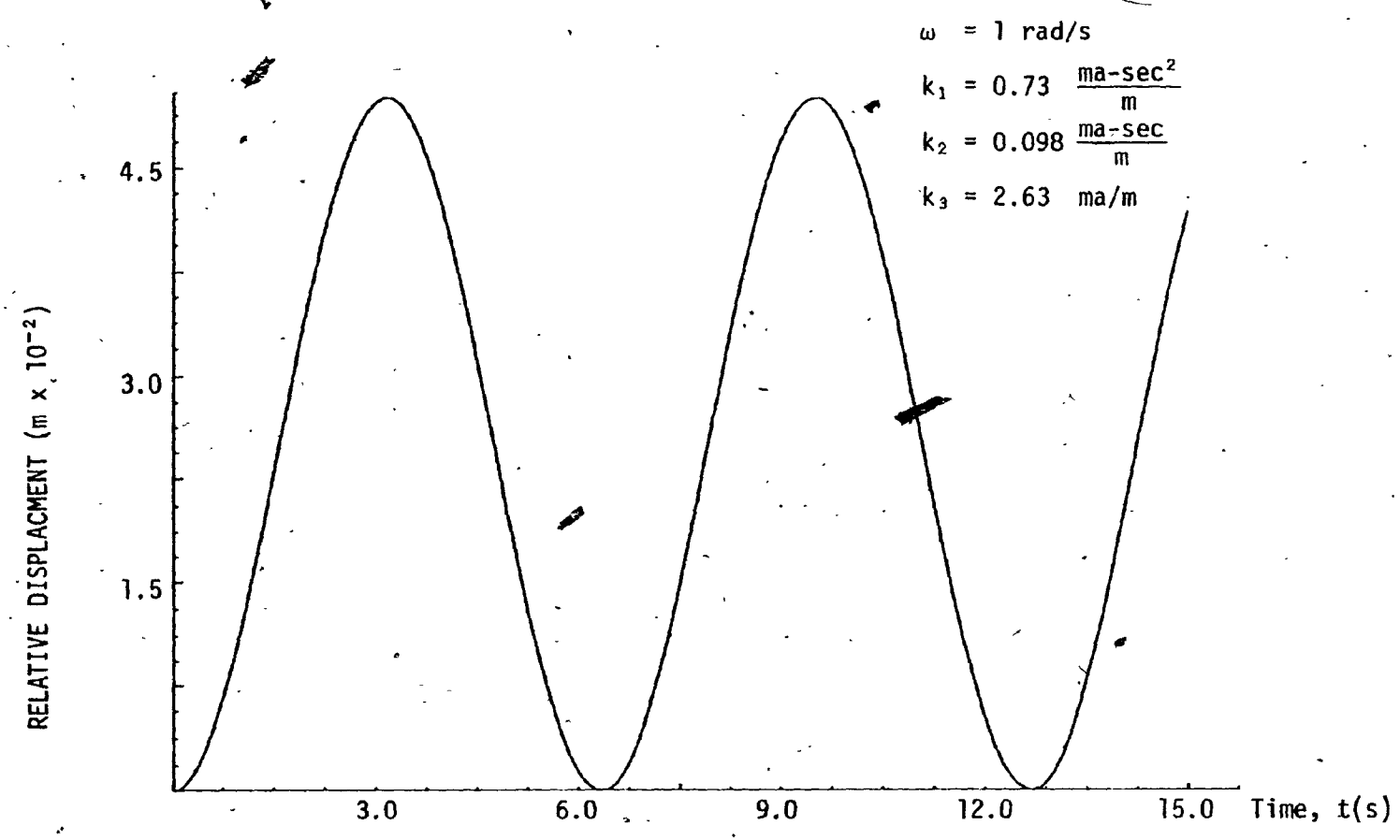

Fig. 64: Relative Displacement Time Response for Input of the Form $X = X_o (1-\cos\omega t)$

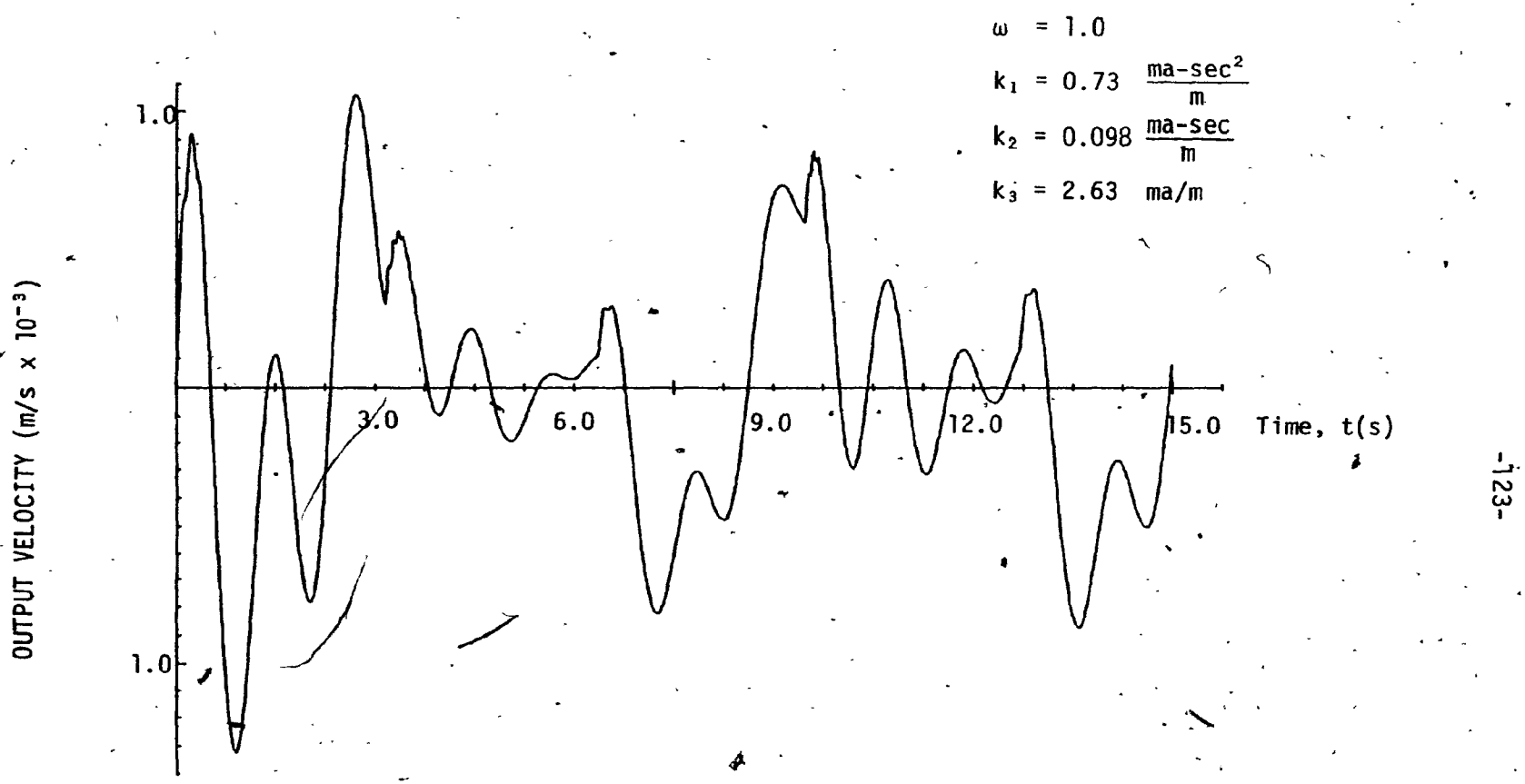

Fig. 65: Velocity Time Response for Input of the Form $X = X_o (1-\cos\omega t)$

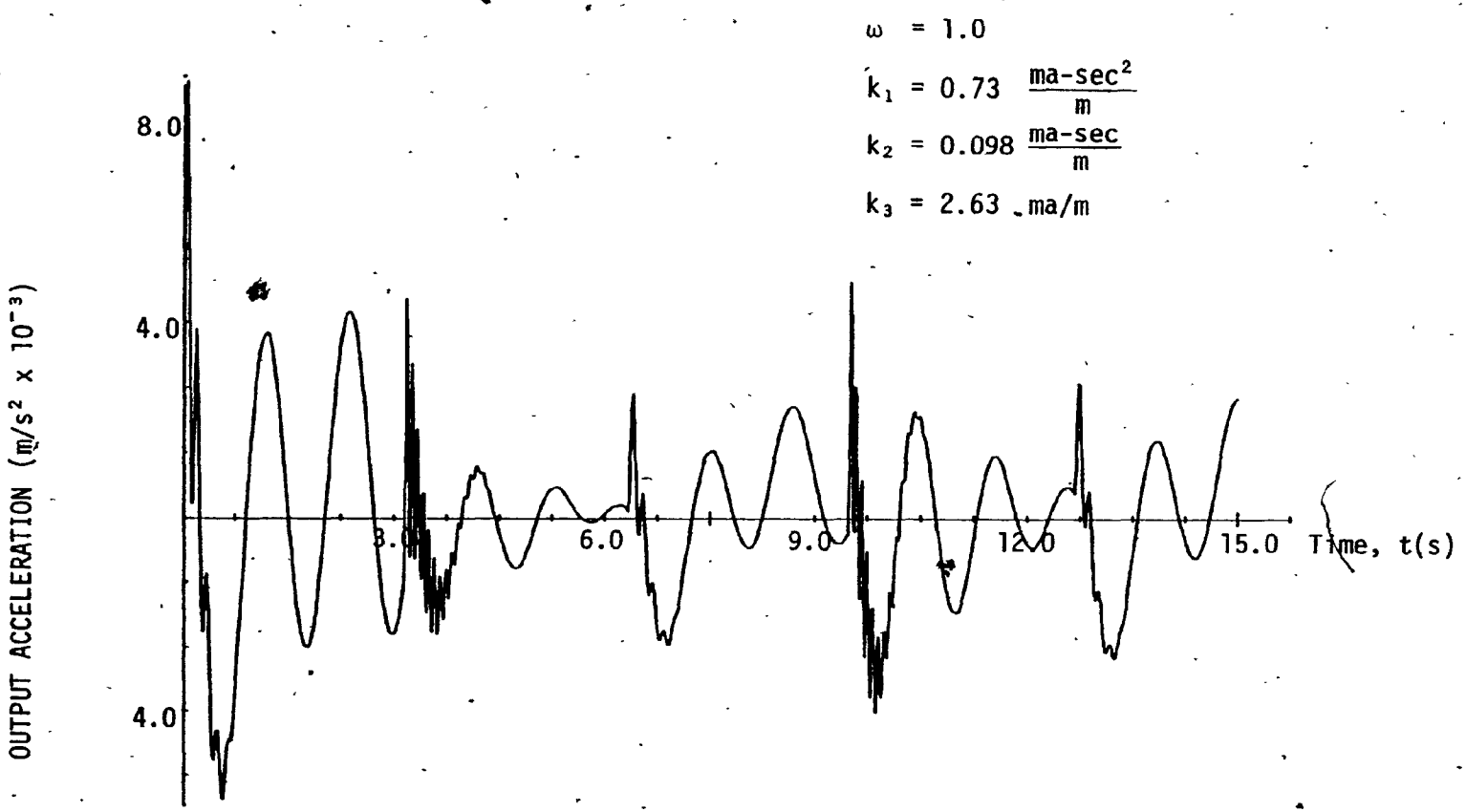

Fig. 66: Acceleration Time Response for the Input of the Form $X = X_o (1-\cos\omega t)$

tion plotted against time for the excitation frequency of 2.5 rad/sec. for a zero acceleration feedback gain. From the output displacement plot it is evident that the output oscillates at much higher frequency than the input and the peak output displacement is about 10 times higher than that of the peak input displacement.

The output acceleration is also oscillatory with the steady state acceleration about 9 times greater than the input acceleration of 2.8575×10^{-2} m/s^2. A similar behaviour is observed when the input excitation frequency is increased and for ω = 20 rad/s, the system becomes unstable.

Figures 69 and 70 give the output displacement and acceleration plots for the acceleration feedback gain of 0.073 ma-sec^2/m. The output displacement is less oscillatory and its peak value is about 10 times less than that of peak input displacement. From the acceleration plot it can be seen that the system reaches steady state in about 0.75 sec. and the transmitted acceleration is reduced by about 4 times.

For the rest of the frequencies, the output response is very much similar and stable.

Figures 71 and 72 show the output displacement and acceleration of the active system for k_1=1.46 ma-sec^2/m. It can be seen that the active system is oscillatory for ω=2.5 rad/s. However, at higher input excitation frequencies, the system has less oscillations.

Figure 73 shows the acceleration transmissibility plots for various values of the acceleration feedback gains. The acceleration

transmissibility for the feedback gain of k_1=0 is not shown since the system is unstable. By comparing the performance of the system for the different gains, it is evident that the system has good isolation performance for the feedback gain of k_1 = 0.73 ma-sec^2/m. Figure 74 shows the relative displacement transmissibility plots for the variation in the acceleration feedback gains. When the acceleration feeback gain is increased from 0.073 to 0.73 ma-sec^2/m the performance of the system becomes better. But when the feedback gain is further increased to 1.46 ma-sec.^{2}/m the performance becomes worse.

3.9.2 The Effect of Variation of the Velocity Feedback Gain k_2

Figure 75 shows the output displacement of the active system plotted against time. The velocity feedback gain used in this case is k_2 = 0.0. Figure 76 shows the output acceleration of the system. Both the output displacement and acceleration are very similar to that of the case when k_2 = 0.098 ma-sec./m, as shown in Section 3.5. The peak output displacement is about 10 times less than the peak input displacement and the steady state output acceleration is about 1.5 times less than the input acceleration. The system is found to be stable for all the frequencies considered.

Figure 77 shows the output displacement for the velocity feedback gain of 0.98 ma-sec/m. By increasing the velocity feedback gain the output displacement seems to contain only one frequency. But the output displacement is about 1.11 times greater than the input displacement. Figure 78 shows the output acceleration of the active system. The output accel-

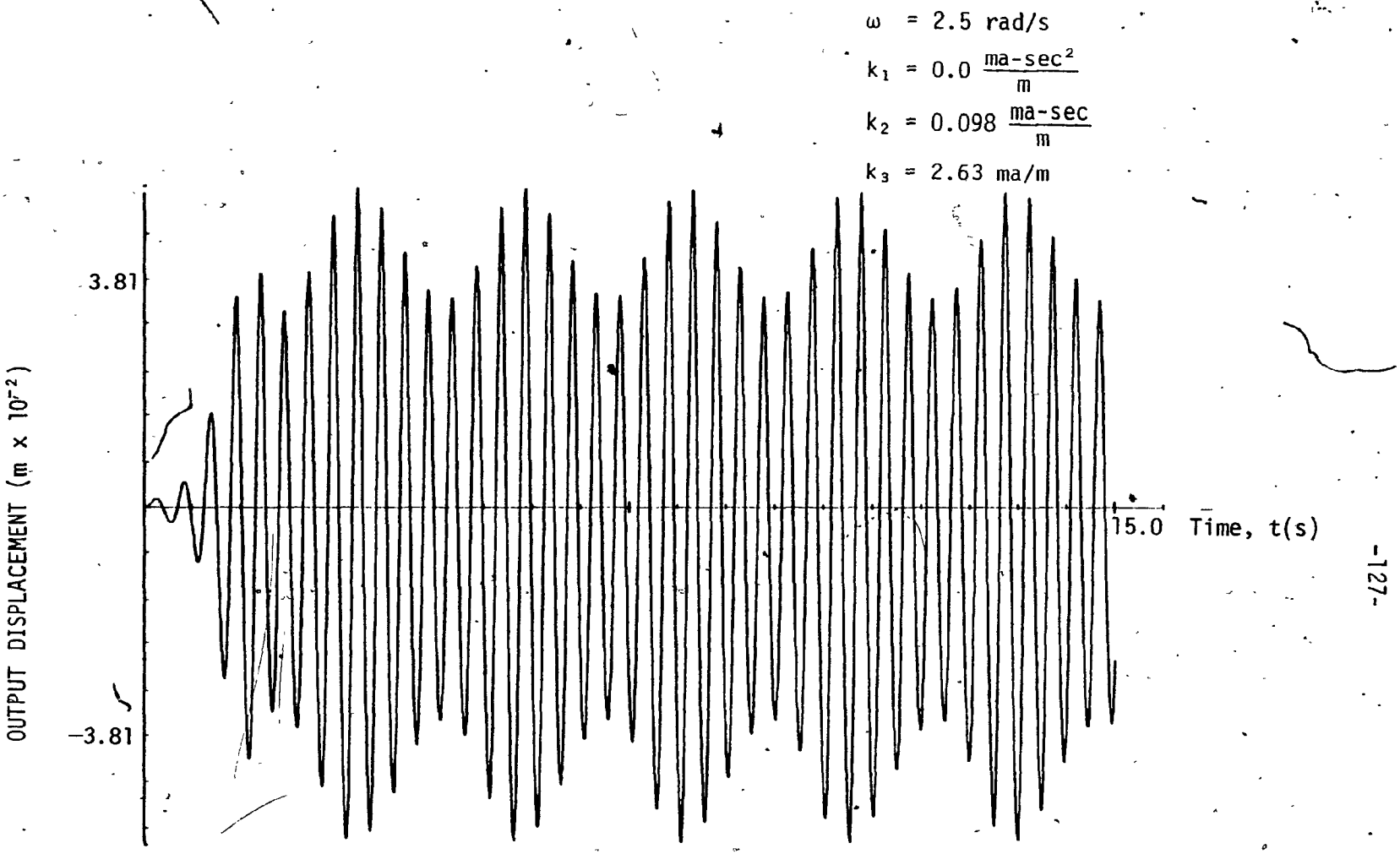

Fig. 67: Output Displacement Time Response for $\omega = 2.5$ rad/s and $k_1 = 0$.

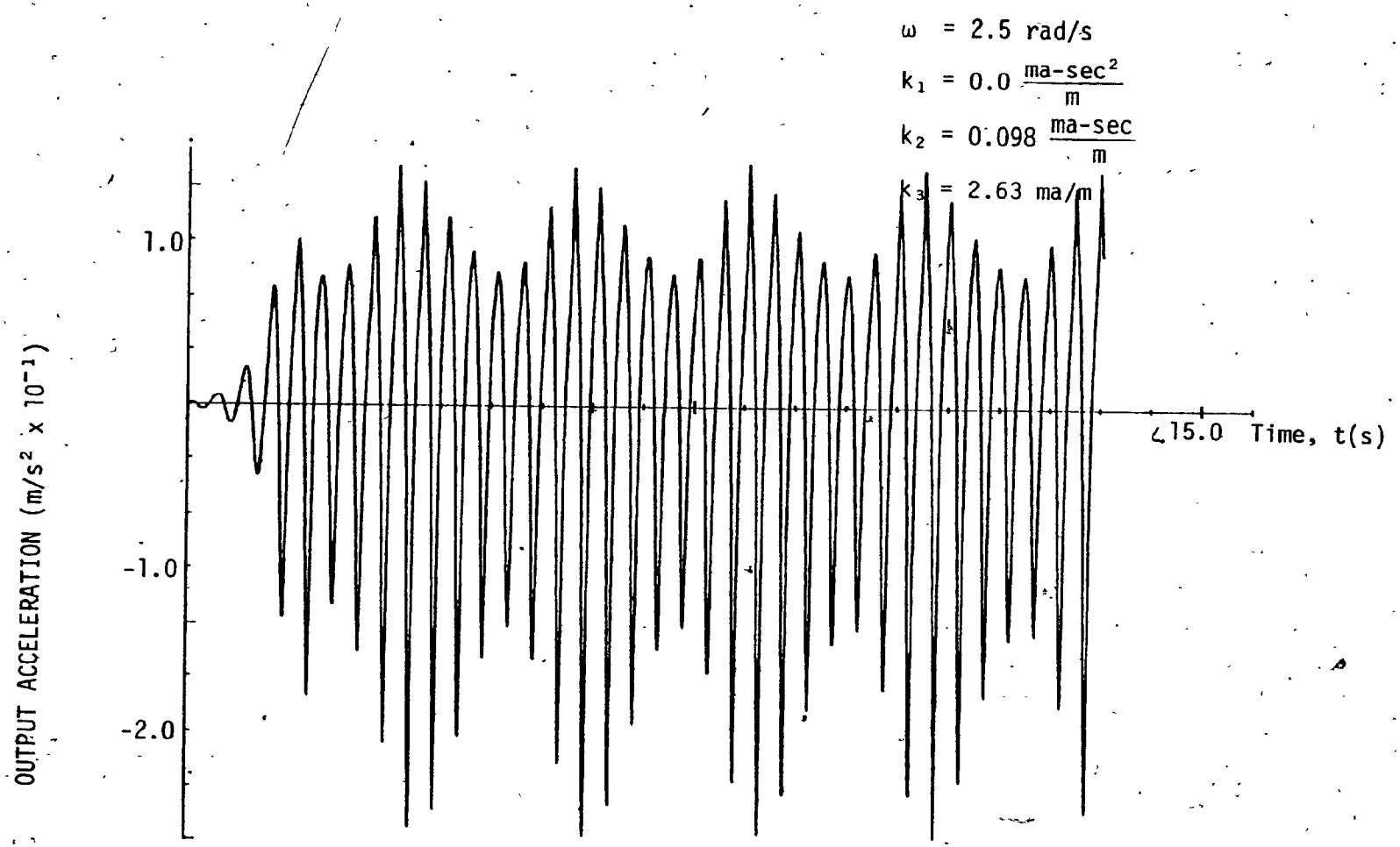

Fig. 68: Output Acceleration Time Response for ω = 2.5 rad/s and k_1 = 0

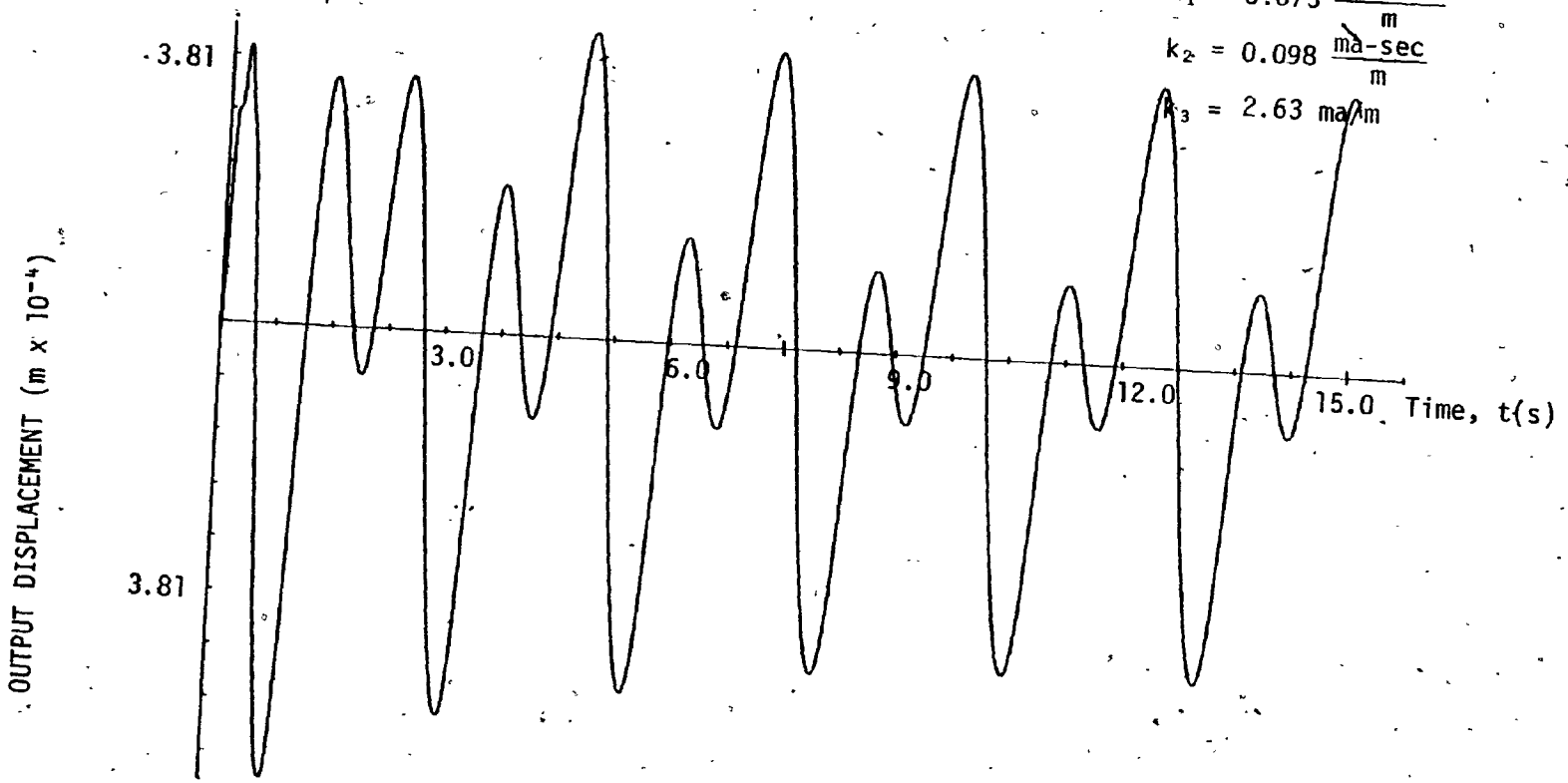

Fig. 69: Output Displacement Time Response for $\omega = 2.5$ rad/s and $k_1 = 0.073$ ma-sec^2/m

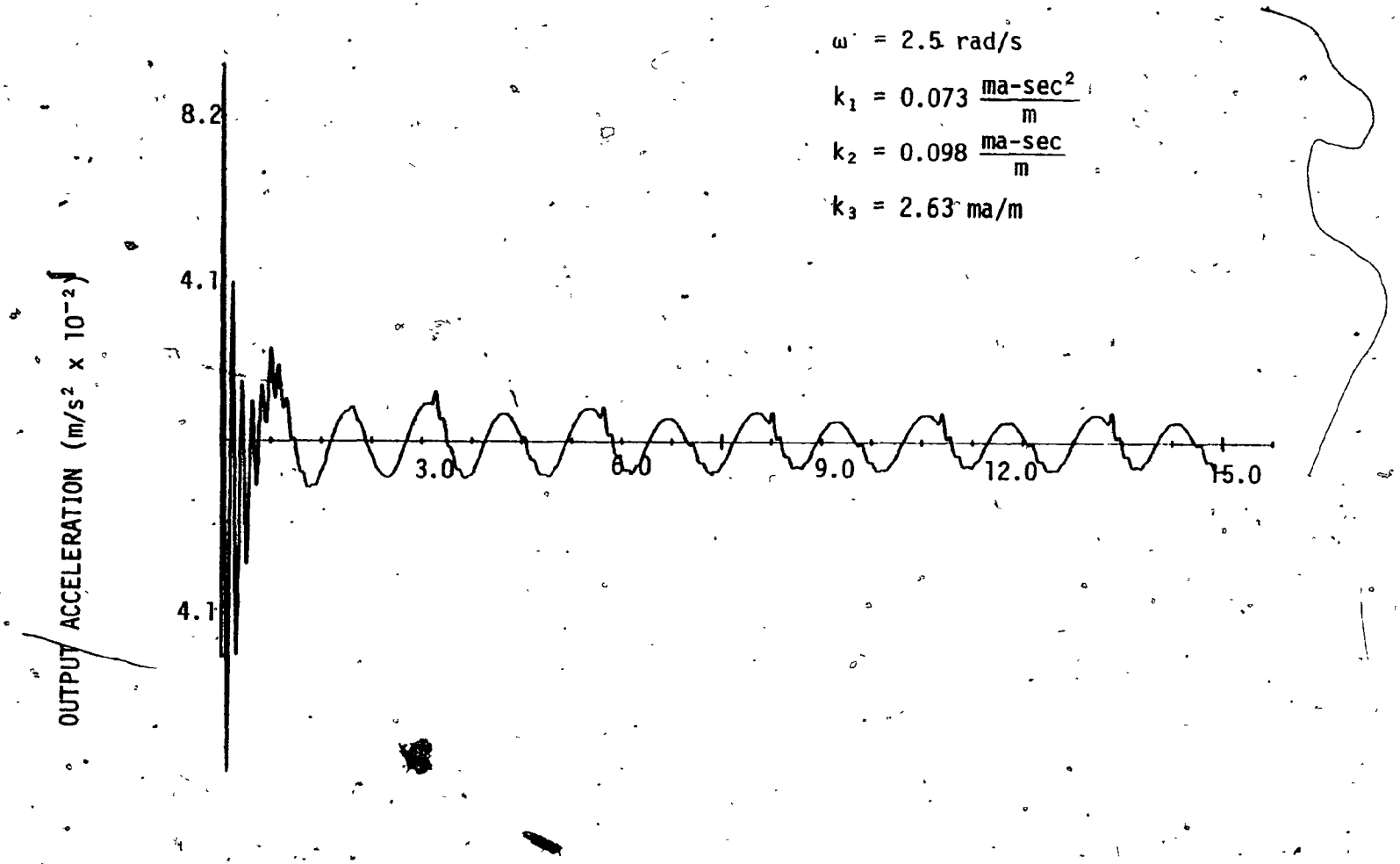

Fig. 70: Output Acceleration Time Response for $\omega = 2.5$ rad/s and $k_1 = 0.073$ ma-sec^2/m

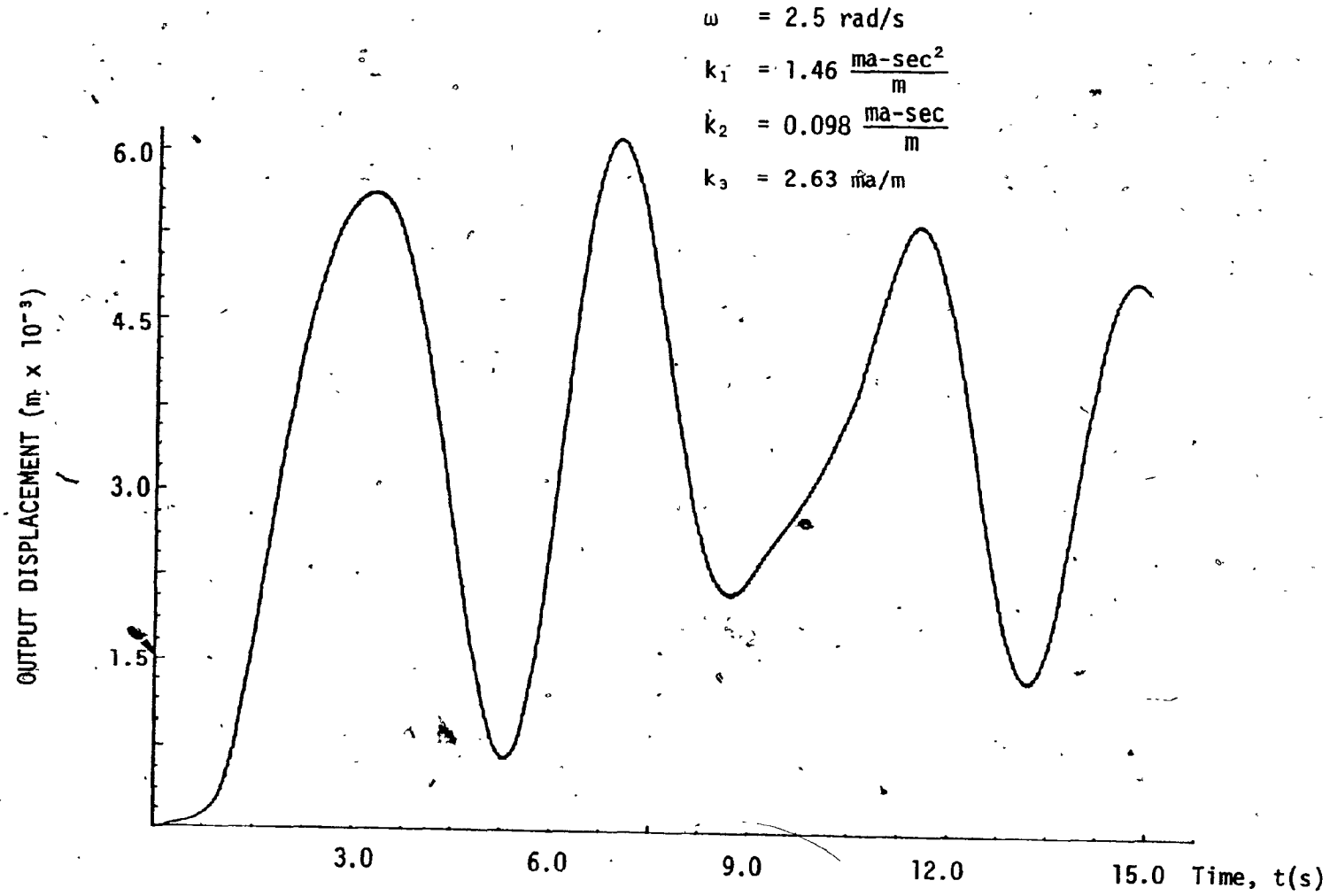

Fig. 71: Output Displacement Time Response for $\omega = 2.5$ rad/s and $k_1 = 1.45$ ma-sec^2/m

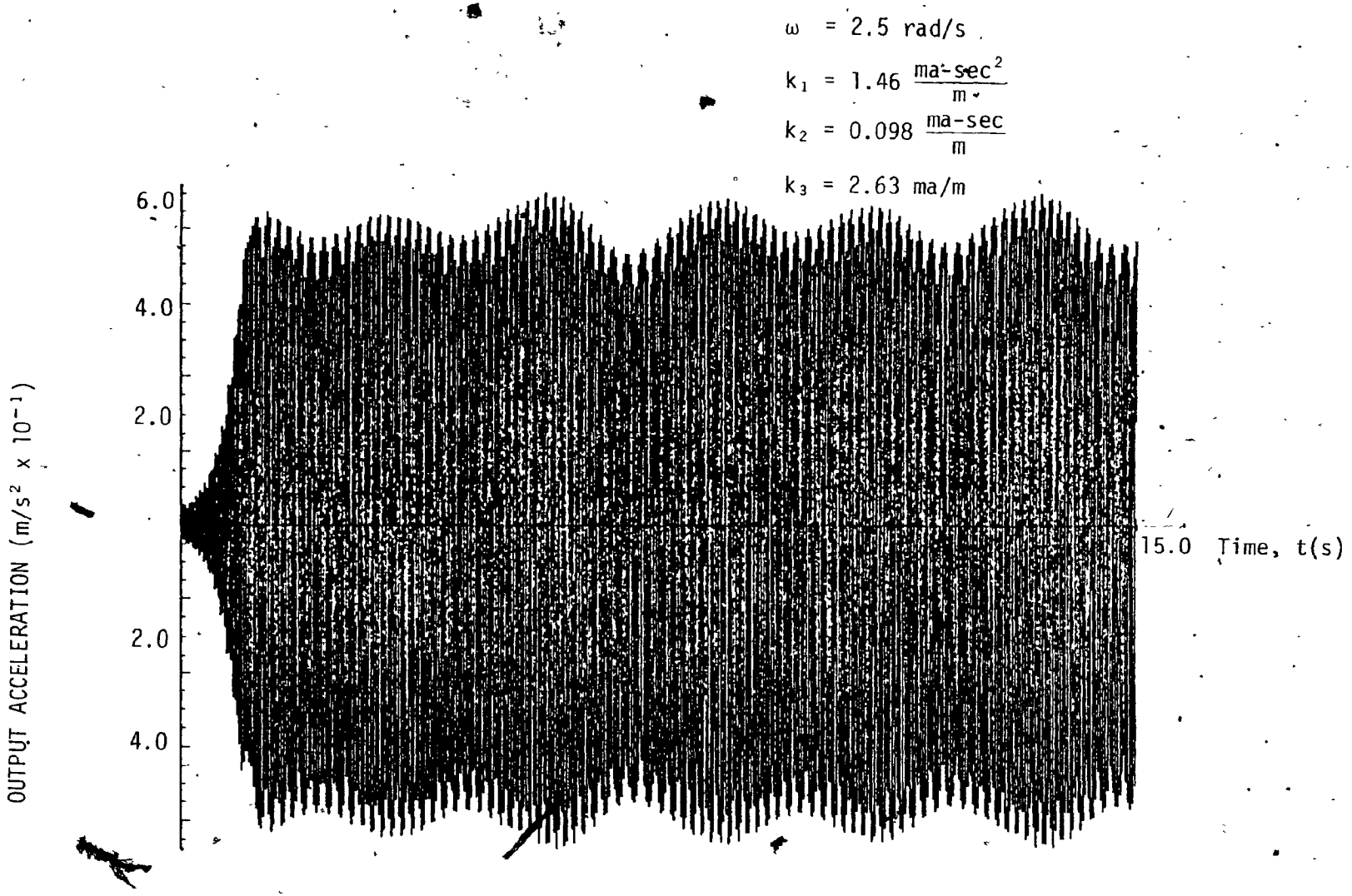

Fig. 72: Output Acceleration Time Response for ω = 2.5 rad/s and k_1 = 1.46 ma-sec/m.

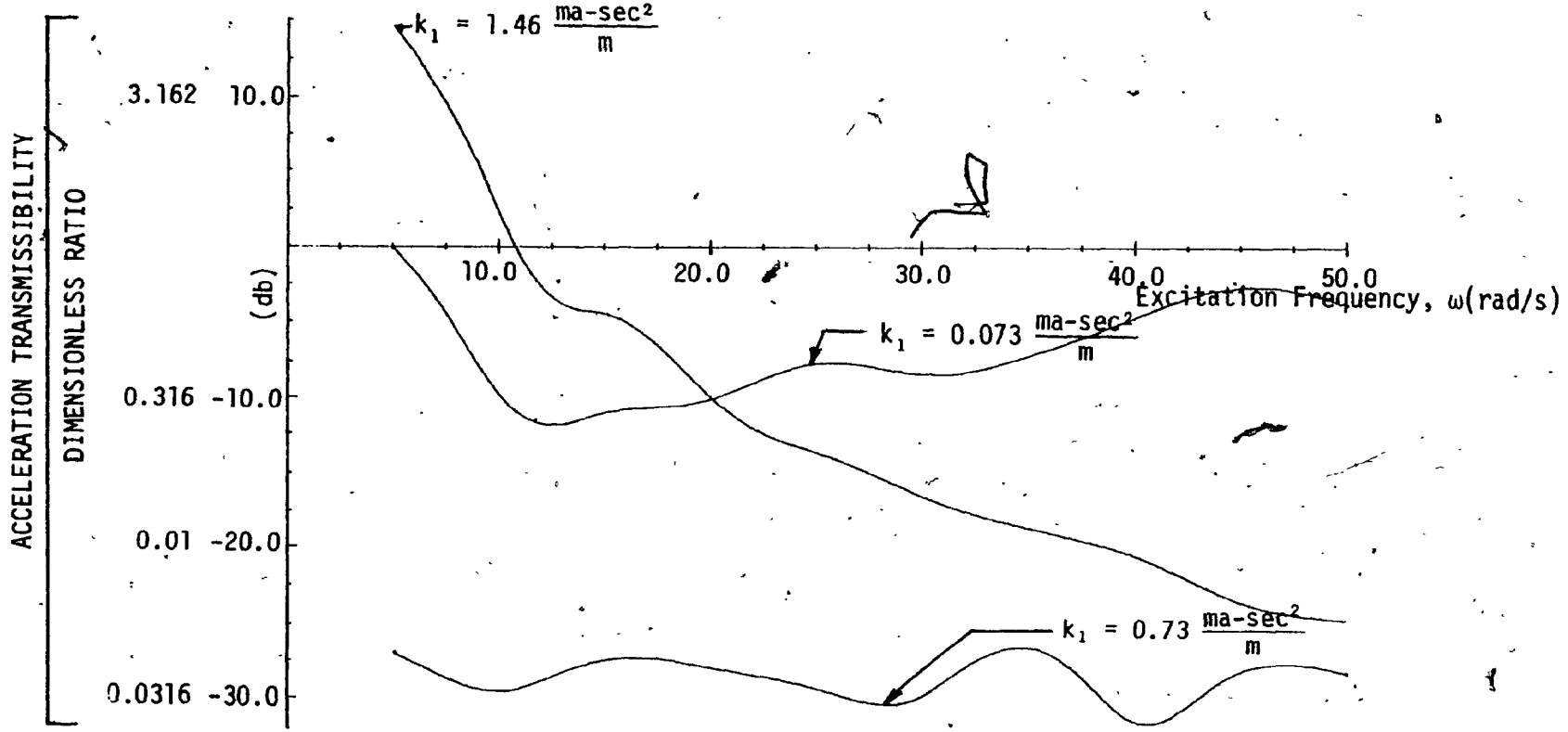

Fig. 73: Acceleration Transmissibility Plots for Variation in Gain k_1

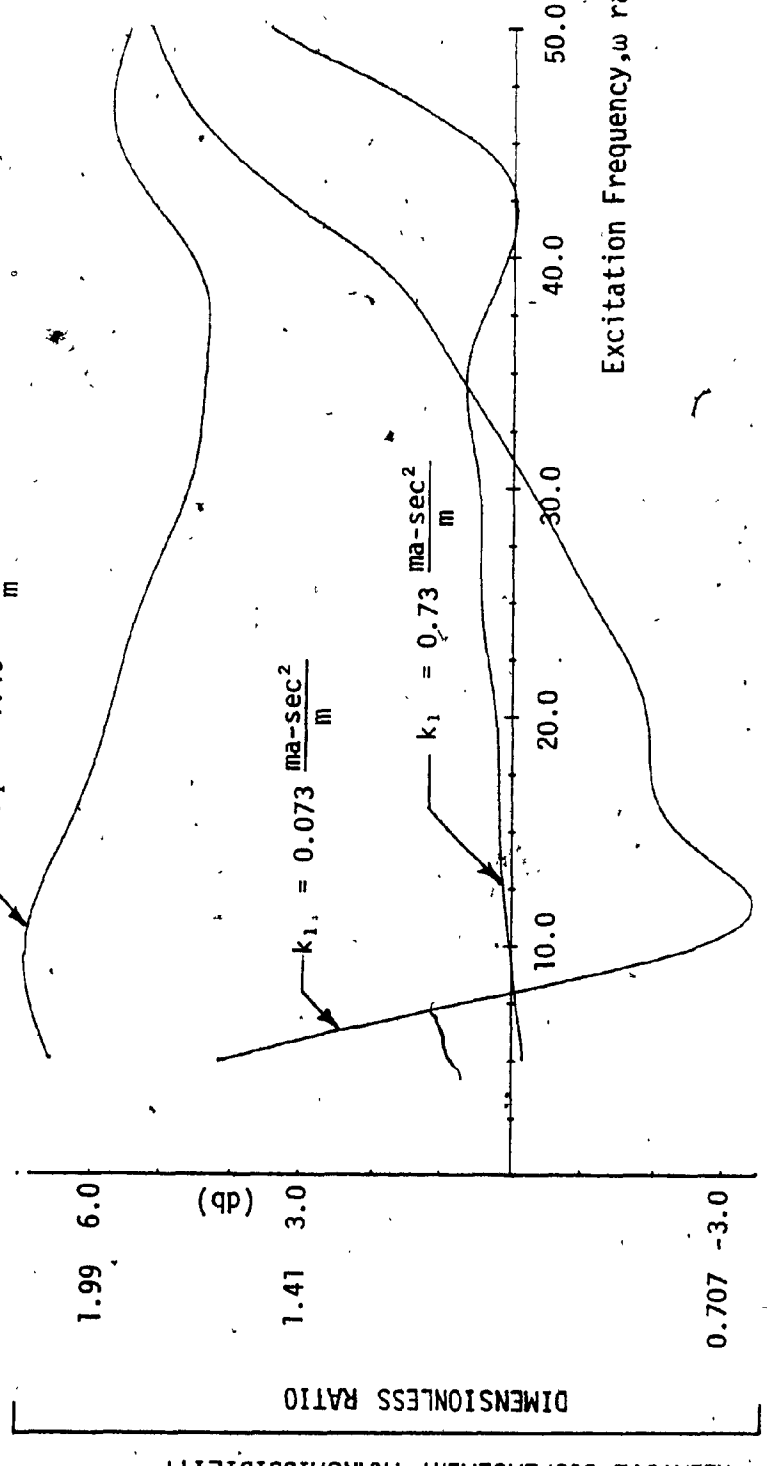

Fig. 74: Relative Displacement Transmissibility Plots for Variation in Gain k_1

eration goes through an exponential decay. However, the maximum acceleration transmitted is about twice the input acceleration.

Figures 79 and 80 show the output displacement and acceleration for a velocity feedback gain of k_2 = 1.90 ma-sec./m. As it can be seen the system becomes unstable. However, the system is stable for input excitation frequencies higher than 2.5 rad/s.

Figure 81 shows the acceleration transmissibility of the system for different velocity feedback gains. It can be seen that at high frequencies higher than 25 rad/s the system has very similar transmissibility characteristics for all four values of k_2. At low frequencies less than 20 rad/sec., the transmissibility characteristic is similar for k_2 = 0.0 and 0.098 ma-sec/m, and the system has relatively high transmissibility for k_2 = 0.98 and 1.96 ma.s/m.

Figure 82 gives the relative displacement transmissibility for the active system for four different velocity feedback gains. From the figure it is seen that the transmissibility plots are very close to 0 db (1) for the middle range of frequencies and increases sharply at higher frequencies. In order to have a stable system for all the frequencies considered, the velocity feedback gain of k = 0.098 ma-sec/m can be used.

3.9.3 The Effect of Variation of the Displacement Feedback Gain k_3

The output displacement of the active system for the displacement feedback gain of k_3 = 0.0 ma/m is plotted against time in Figure 83. The output displacement shows an oscillatory behaviour and becomes unstable.

Figure 84 shows the output acceleration of the system which goes

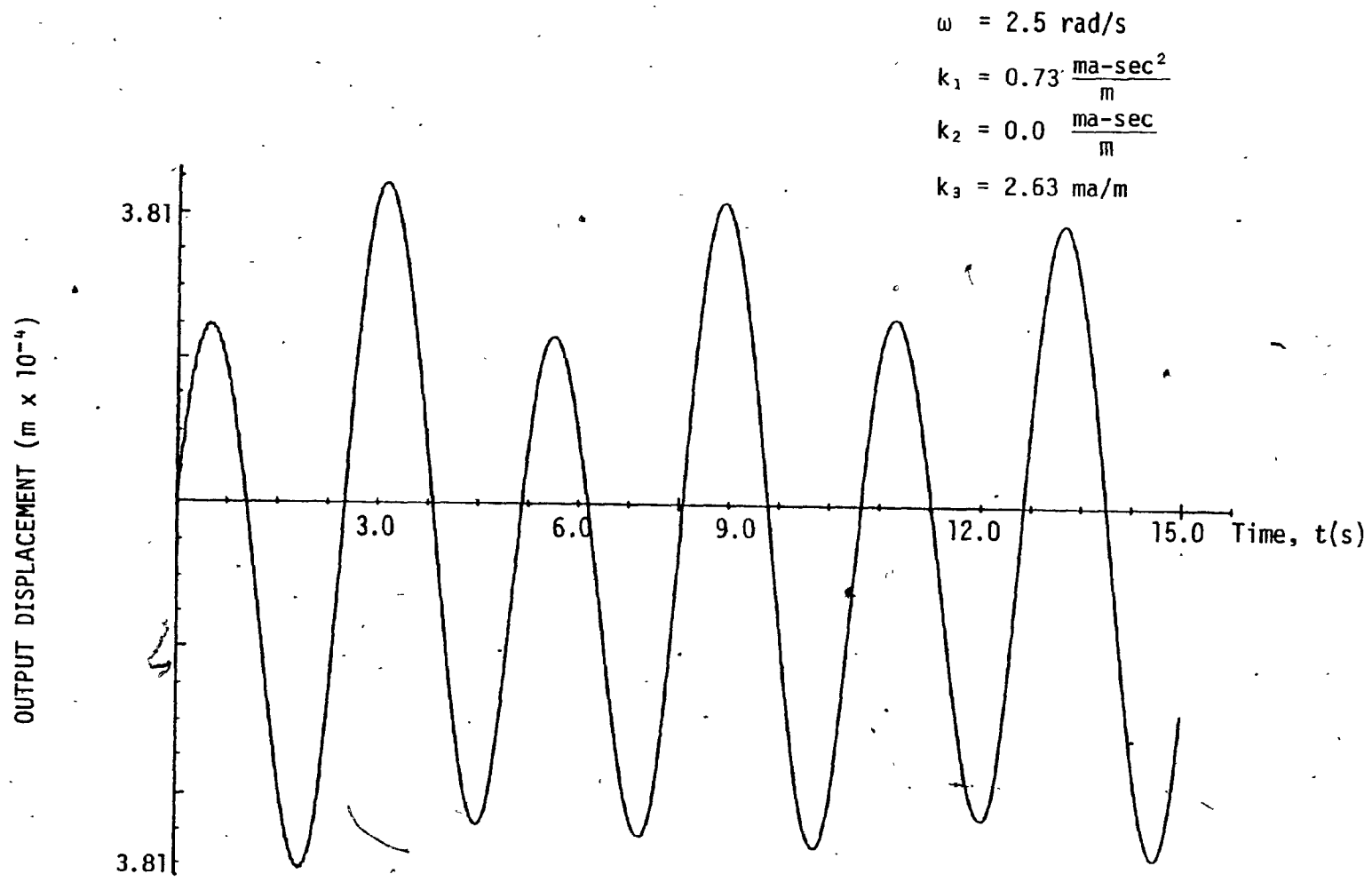

Fig. 75: Output Displacement Time Response for ω = 2.5 rad/s and k_2 = 0.0 ma-sec/m

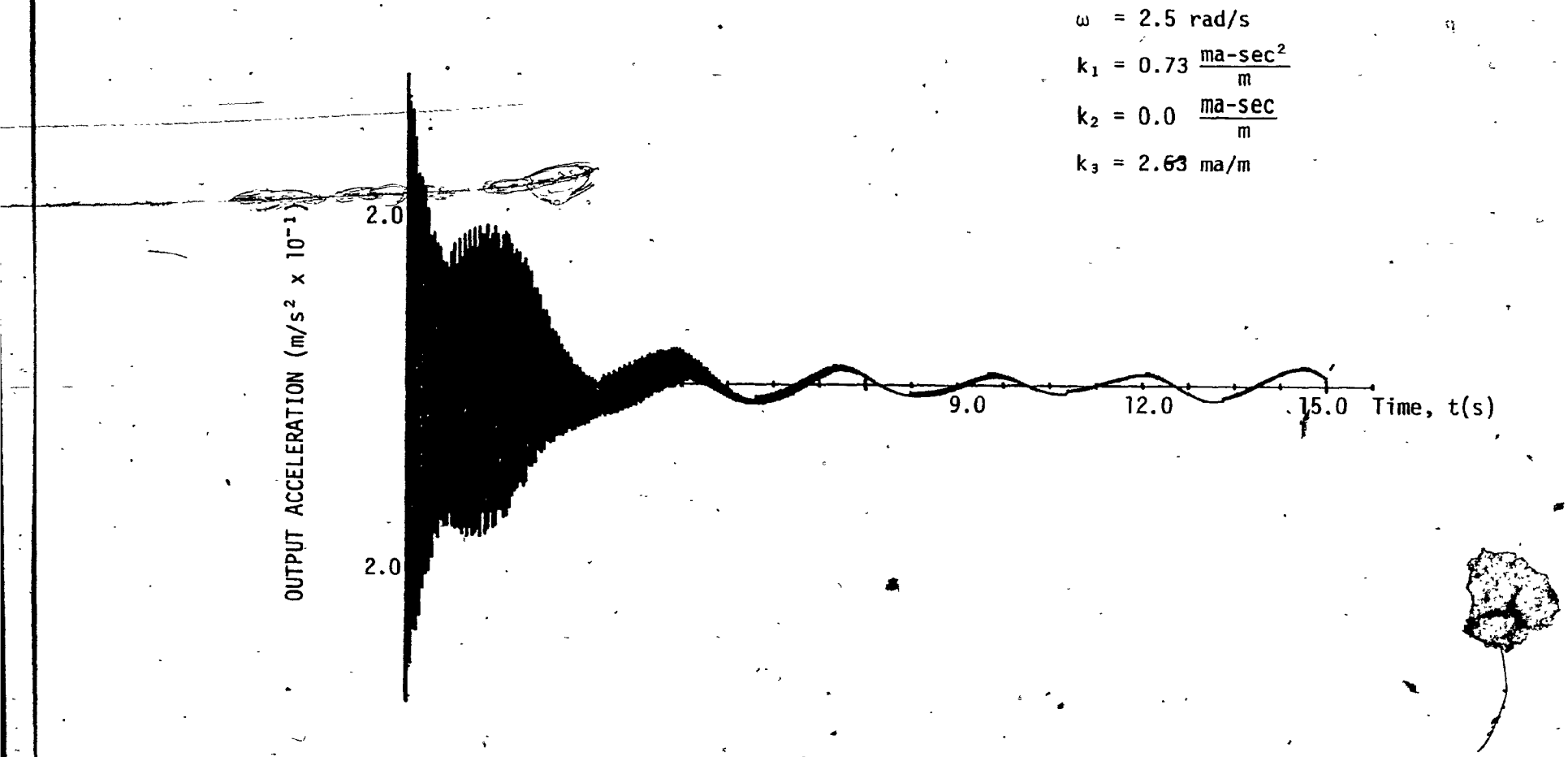

Fig. 76: Output Acceleration Time Response for ω = 2.5 rad/s and k_2 = 0.0 ma-sec/m

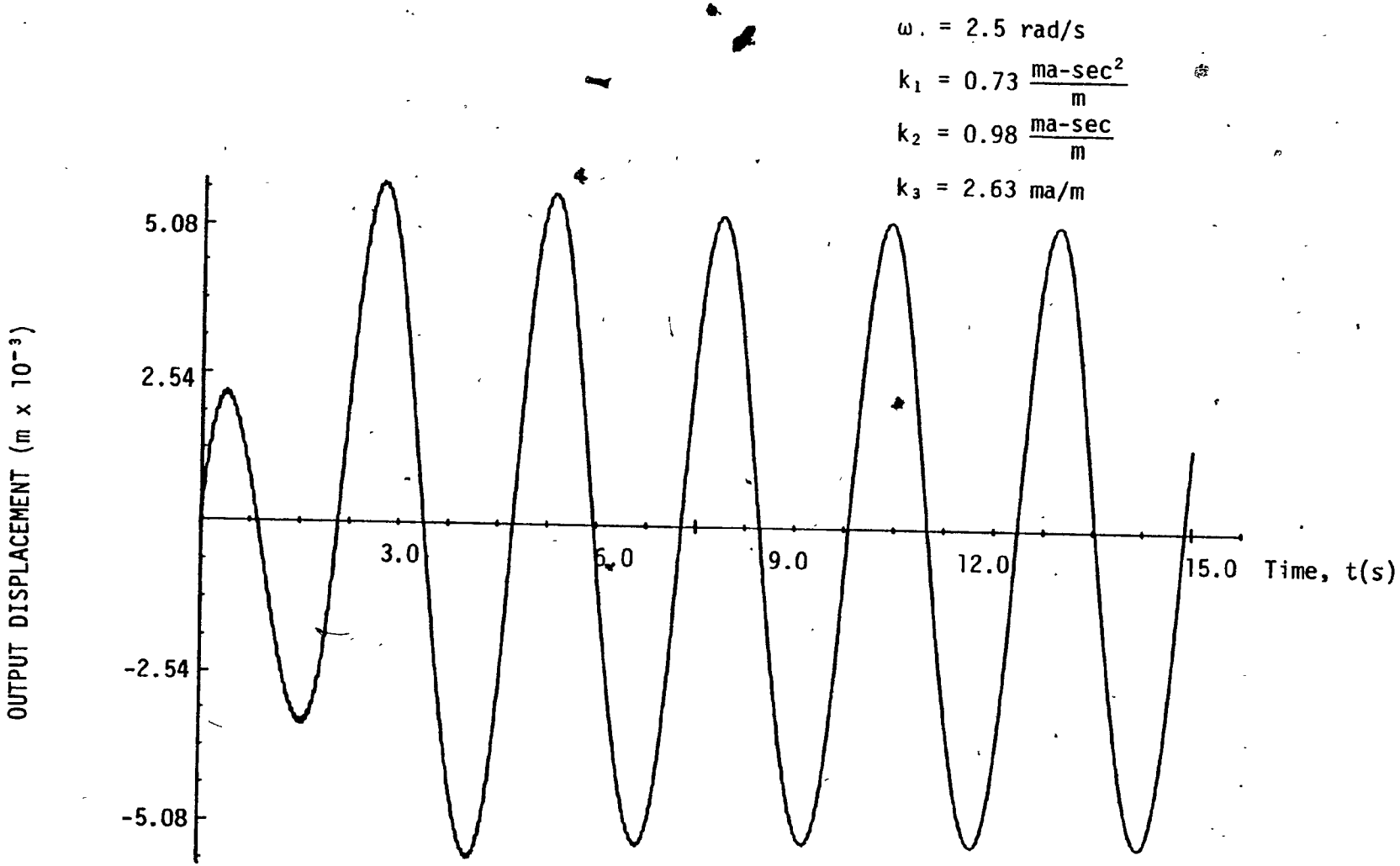

Fig. 77: Output Displacement Time Response for ω = 2.5 rad/s and k_2 = 0.98 ma-sec/m

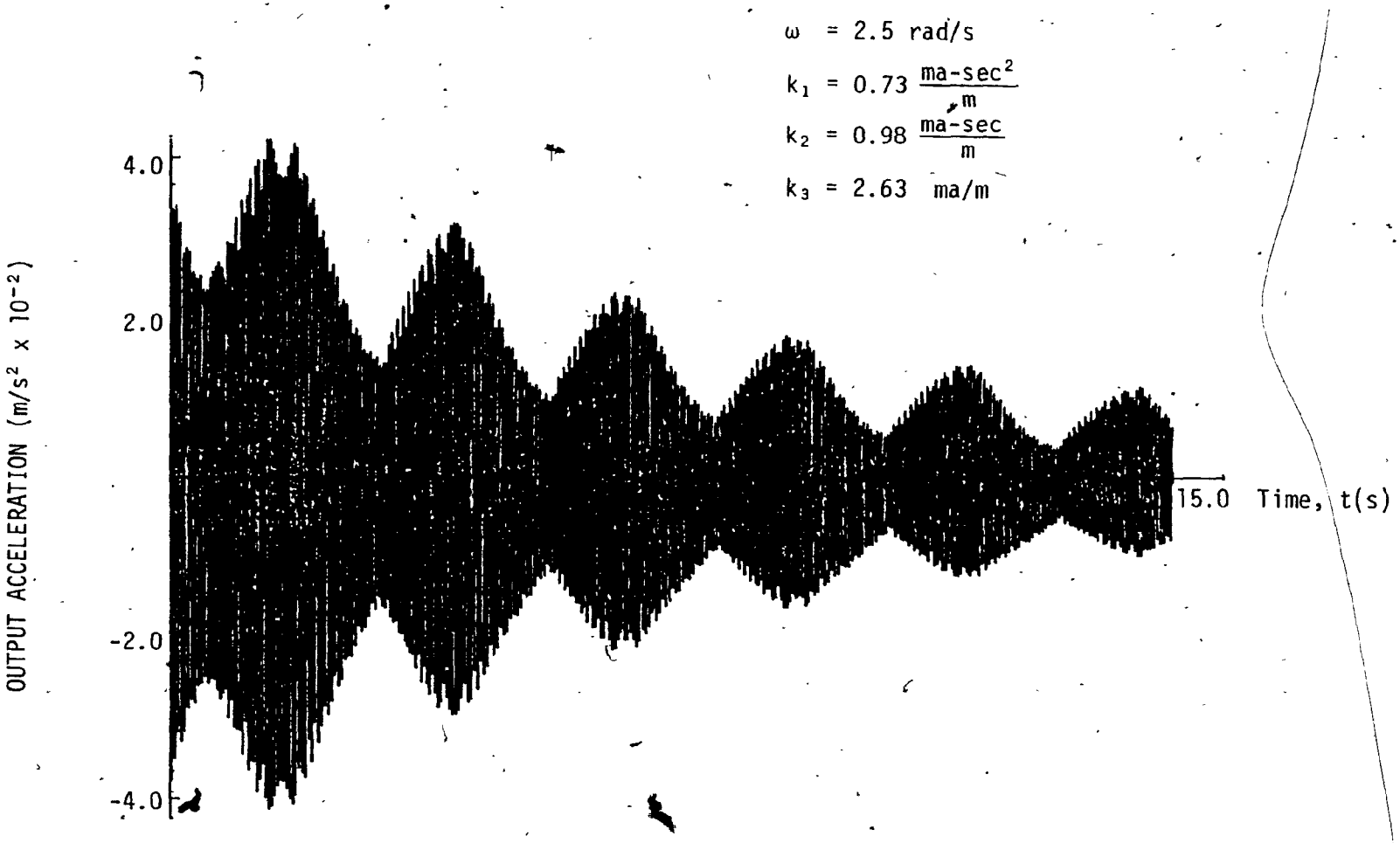

Fig. 78: Output Acceleration Time Response for ω = 2.5 rad/s and k_2 = 0.98 ma-s/m

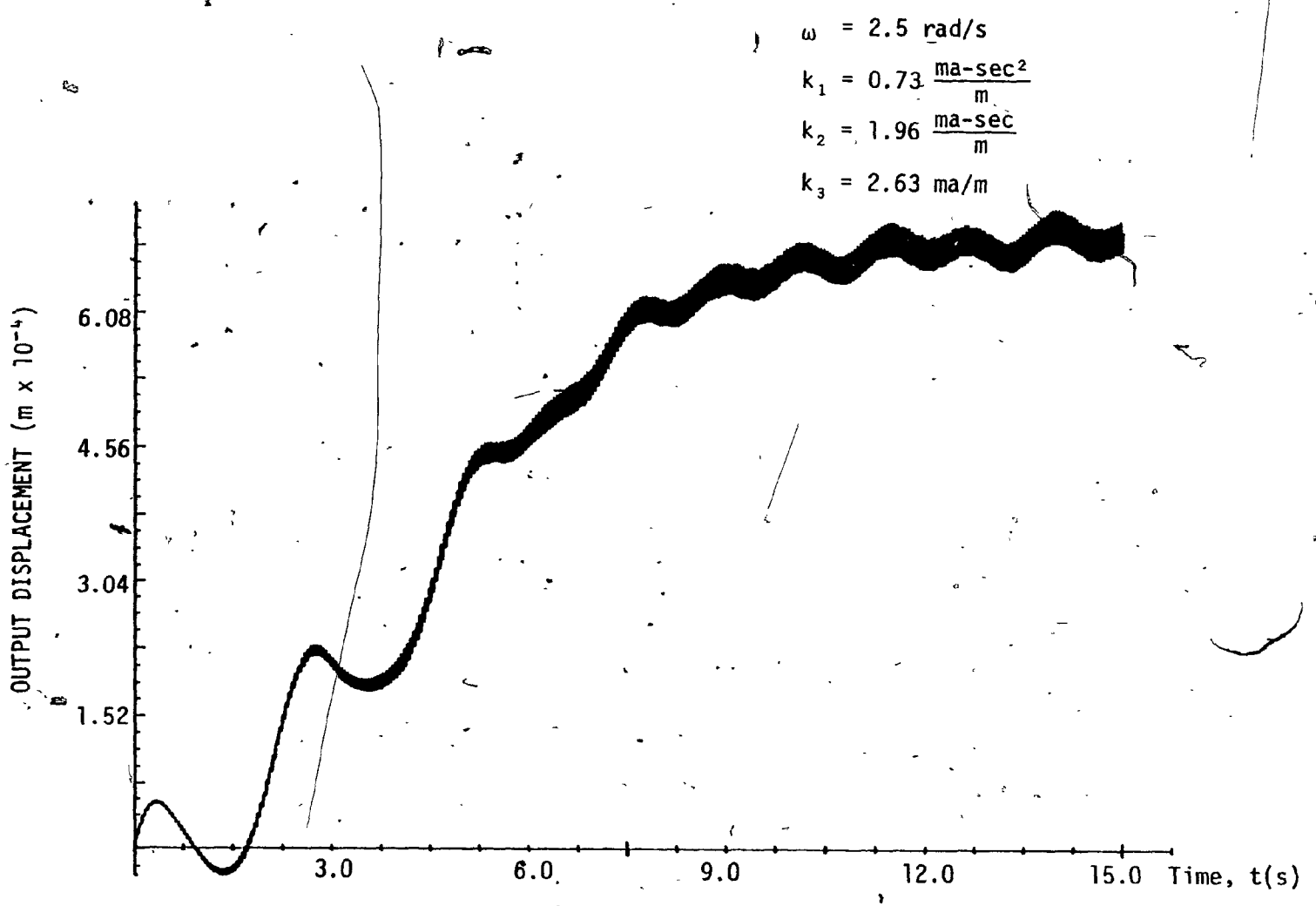

Fig. 79: Output Displacement Time Response for ω = 2.5 rad/s and k_2 = 1.96 ma-s/m

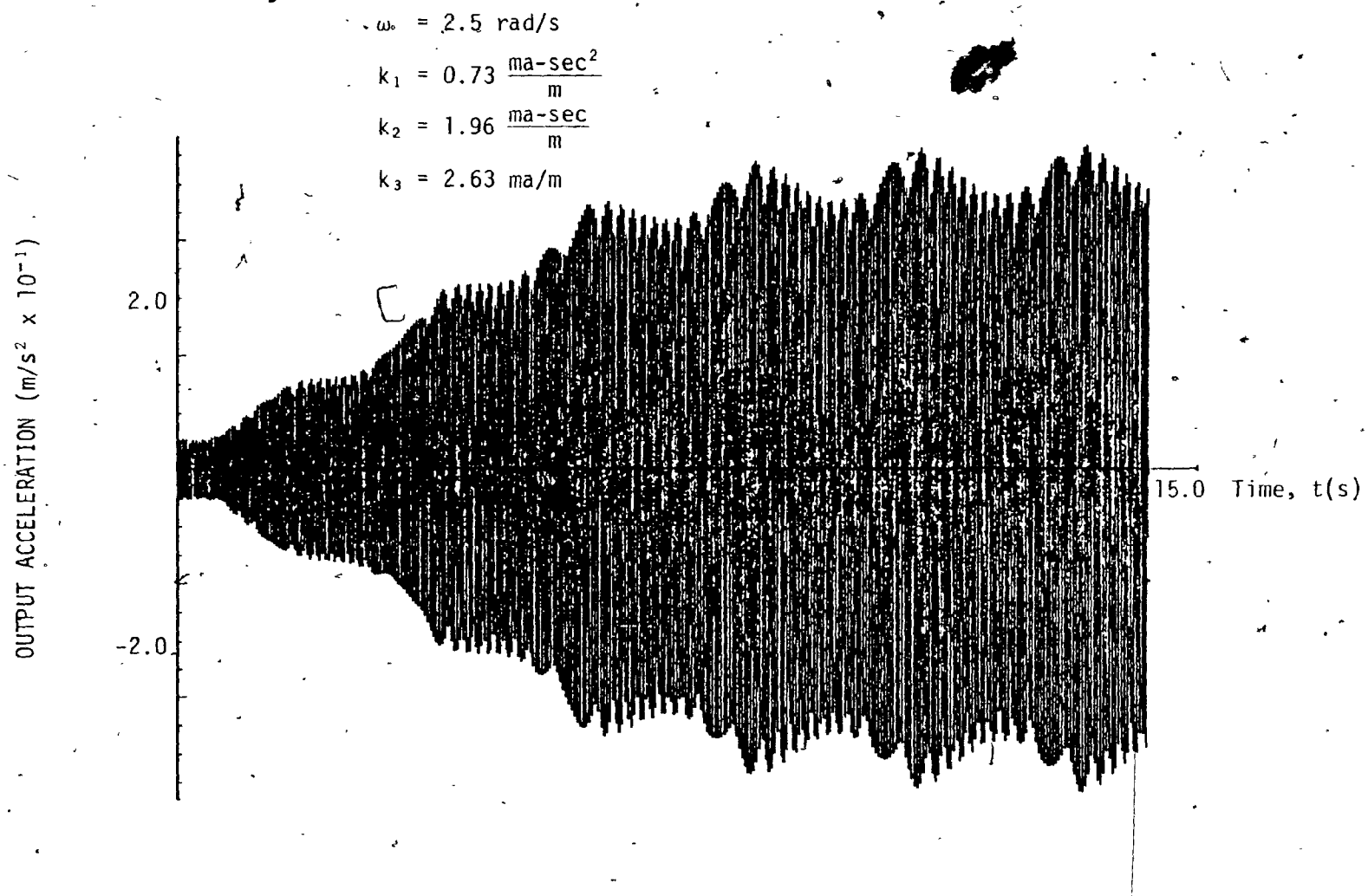

Fig. 80: Output Acceleration Time Response for ω = 2.5 rad/s and k_2 = 1.96 ma-s/m

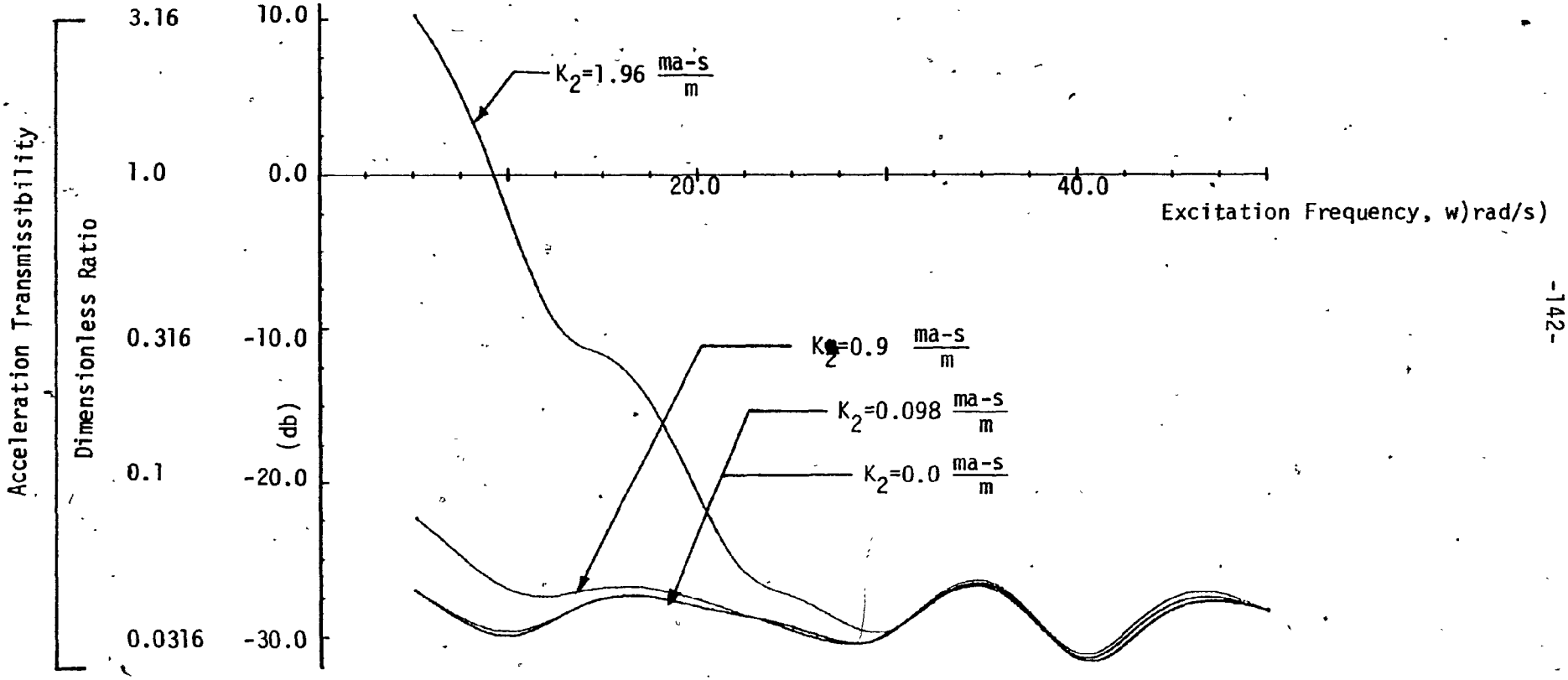

FIGURE 81. Acceleration Transmissibility Plot for Variation in Velocity Feedback Gain

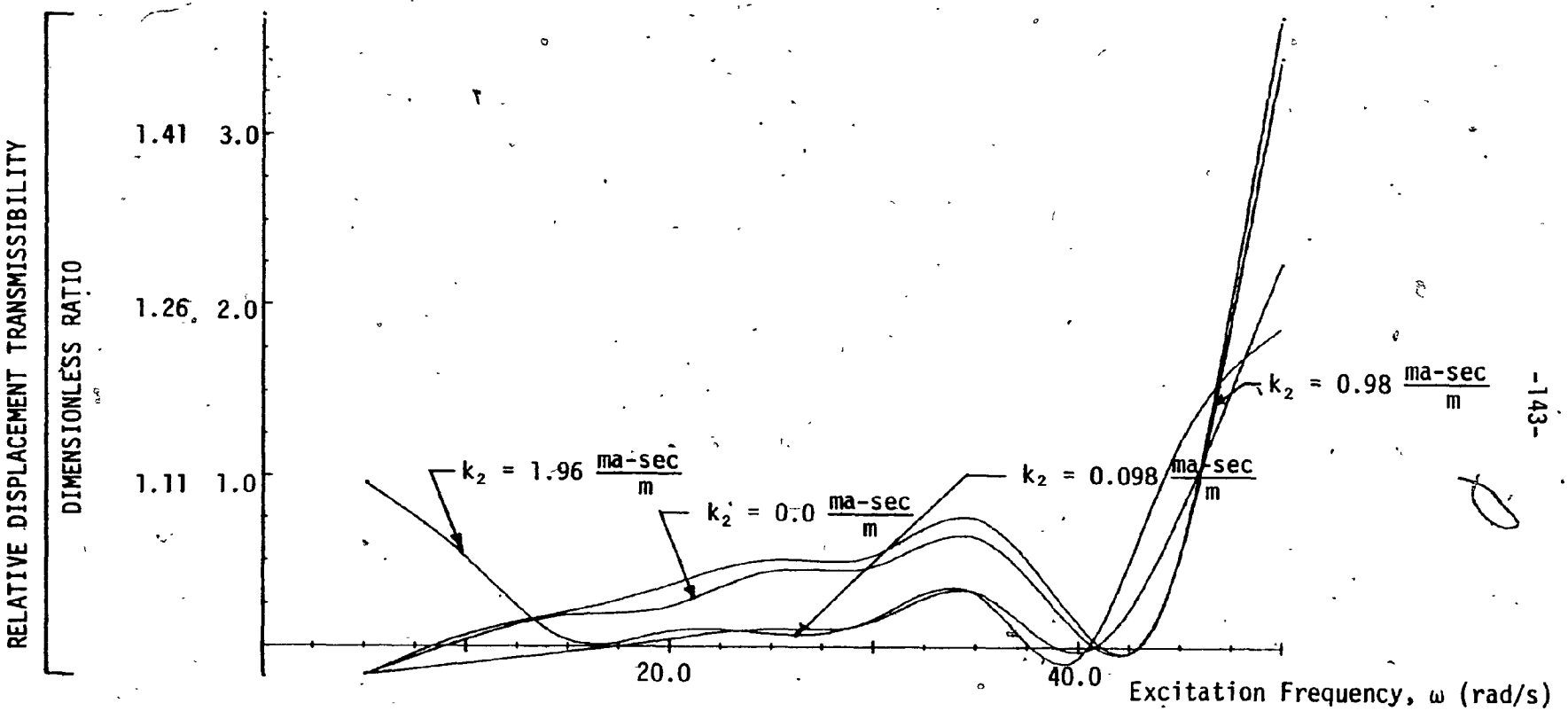

Fig. 82: Relative Displacement Transmissibility for Variation in Velocity Feedback Gain.

through initial oscillation. The oscillations exponentially decay and settle to a value of 1.67×10^{-3} m/sec.^{2} which is about 17 times less than the input acceleration.

Figures 85 and 86 show the output displacement and acceleration for the displacement feedback gain of $k_3 = 0.1315$ ma/m. With a small increase in the displacement feedback, the system becomes stable. It is seen that the increase in the displacement feedback gain does not have any influence on the output acceleration.

Figure 87 shows that by further increasing the displacement feedback gain to 1.135 ma/m, the output displacement is very much stable. The steady state displacement is about 30 times less than the peak input displacement. Figure 88 shows the output acceleration which has very similar behaviour as in the case of other values of k_3.

Figure 89 shows the acceleration transmissibility for different displacement feedback gains. As has been mentioned previously, the displacement feedback gain has very little effect on the acceleration transmissibility. Since the system is unstable for the displacement feedback gain of $k_3 = 0$, an acceleration transmissibility plot for $k_3 = 0$ is not shown.

The relative displacement plot is shown in Figure 90 and it is seen that as the gain k_3 is increased, the relative displacement of the system reduces.

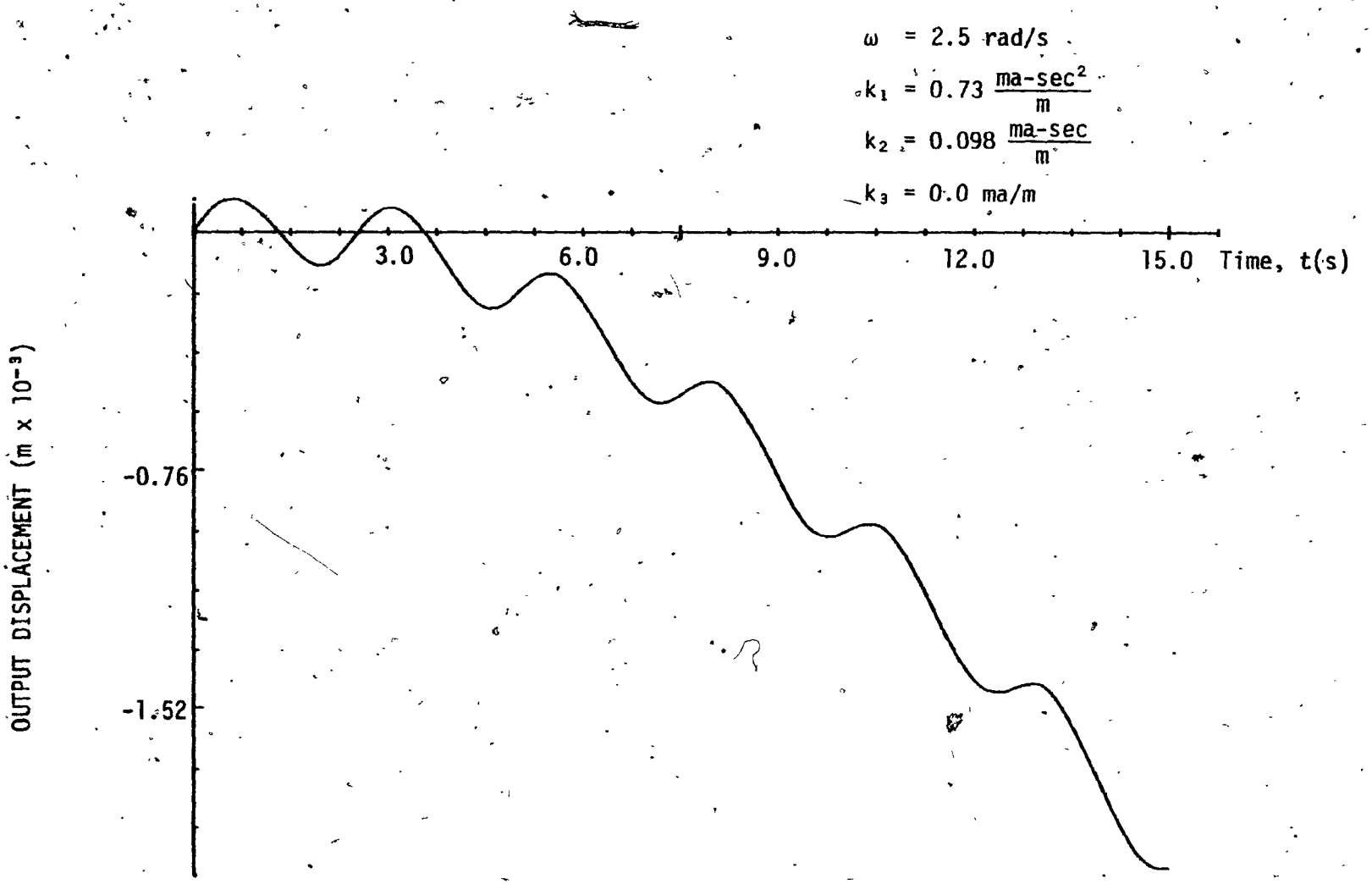

Fig. 83: Output Displacement Time Response for ω = 2.5 rad/s and k_3 = 0.0 ma/m

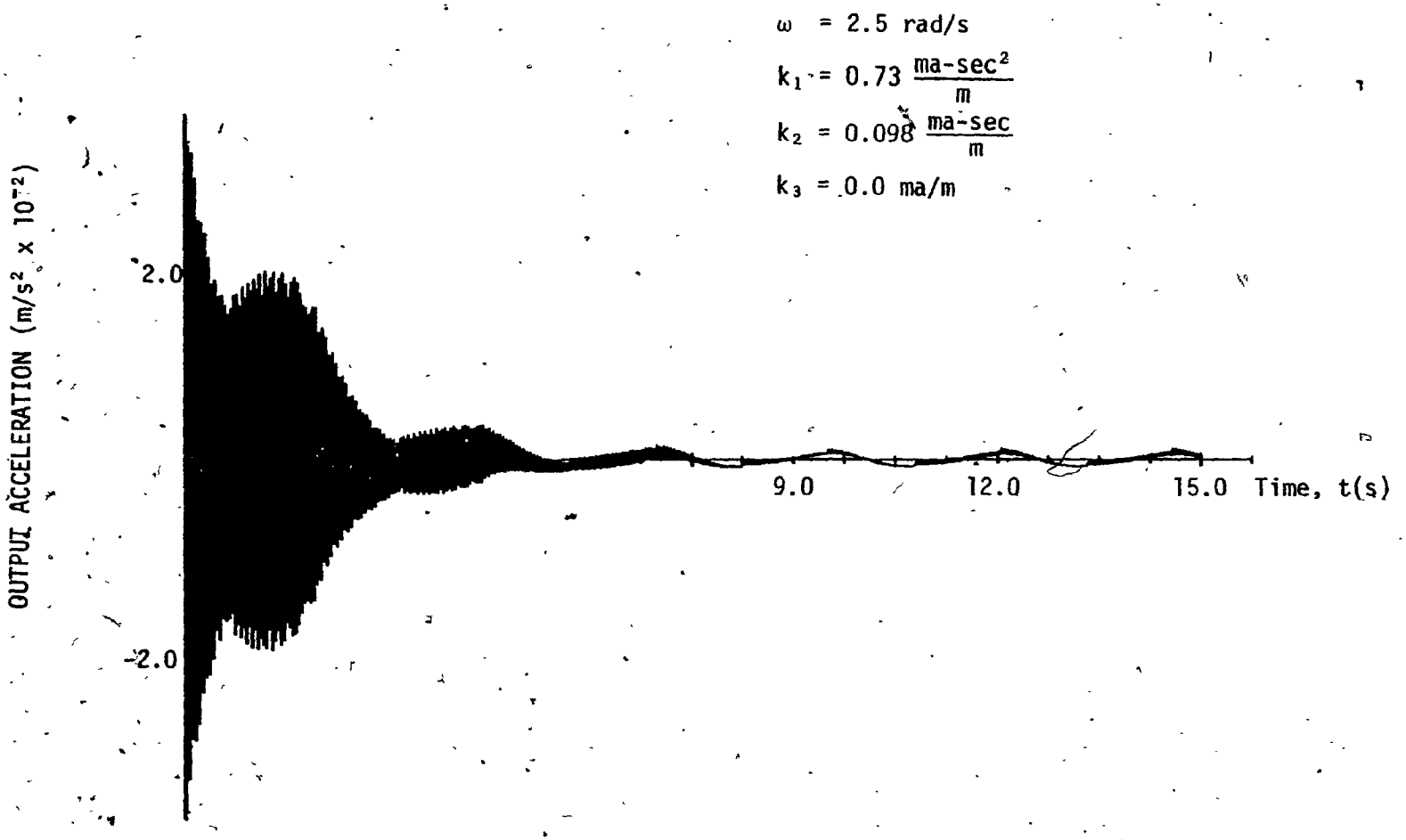

Fig. 84: Output Acceleration Time Response for ω = 2.5 rad/s and k_3 = 0.0 ma/s.

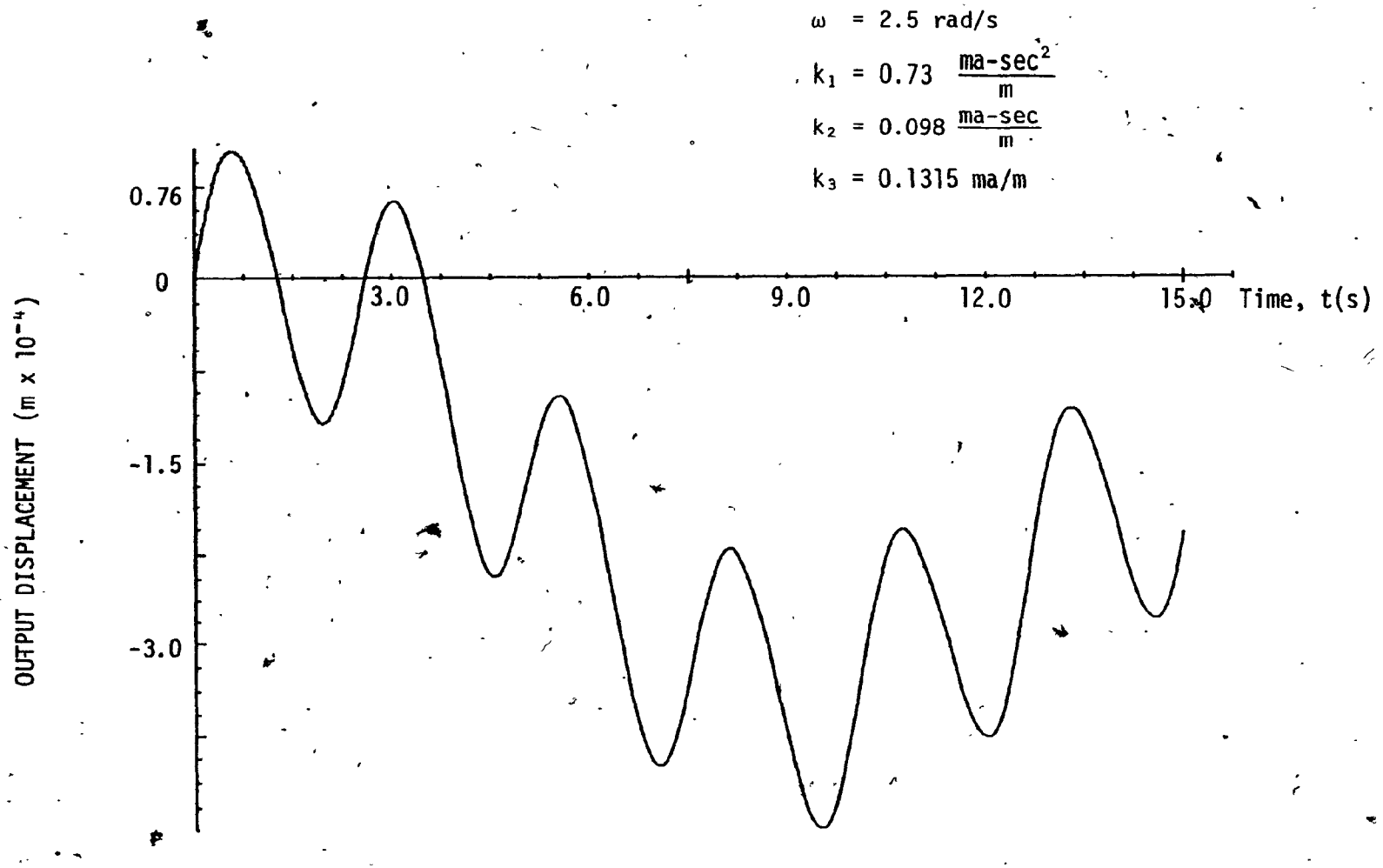

Fig. 85: Output Displacement Time Response for ω = 2.5 rad/s and k_3 = 0.1315 ma/m.

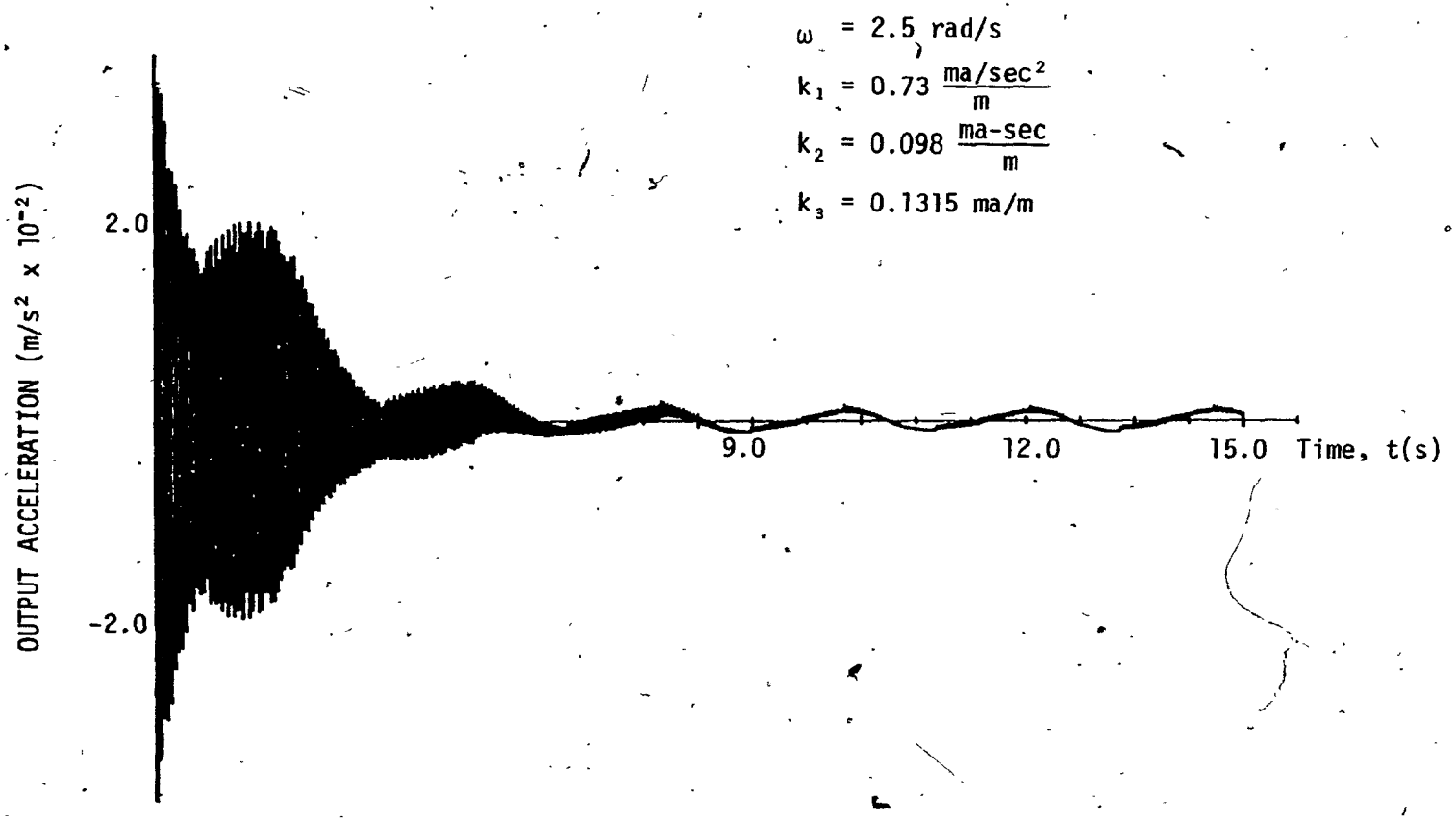

Fig. 86: Output Acceleration Time Response for ω = 2.5 rad/s and k_3 = 0.1315 ma/m.

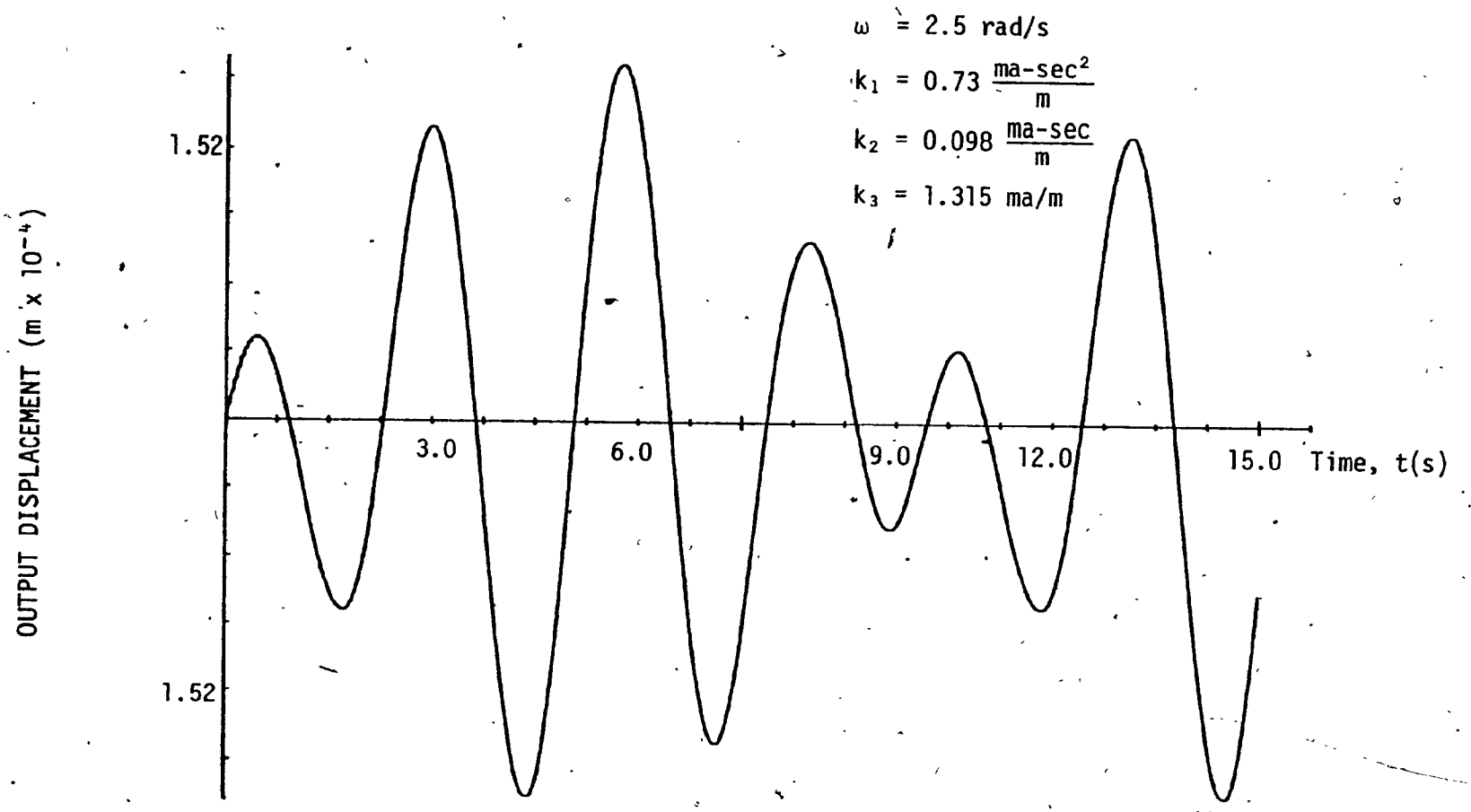

Fig. 87: Output Displacement Time Response for ω = 2.5 rad/s and k_3 = 1.315 ma/m.

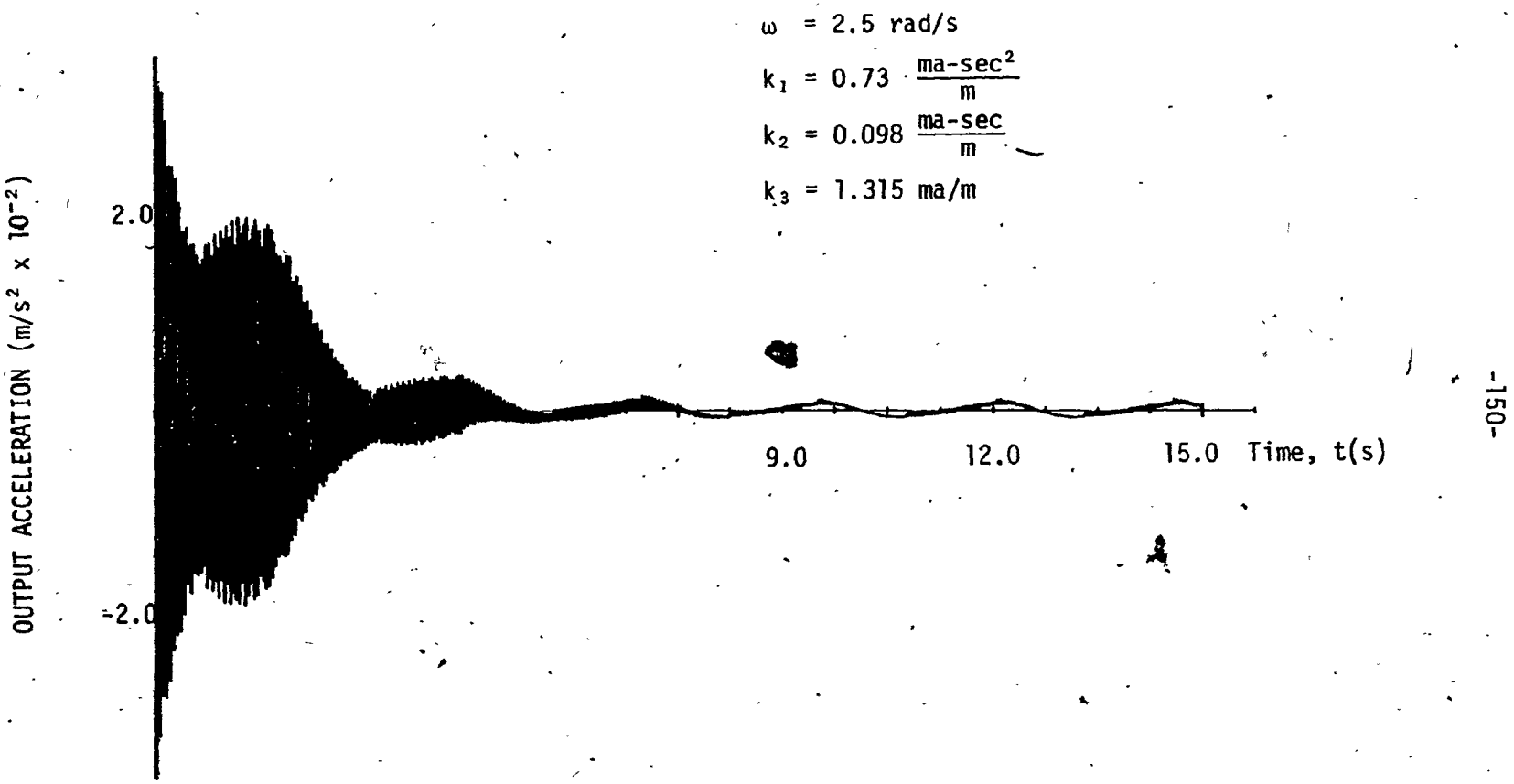

Fig. 88: Output Acceleration Time Response for ω = 2.5 rad/s and k_3 = 1.315 ma/m.

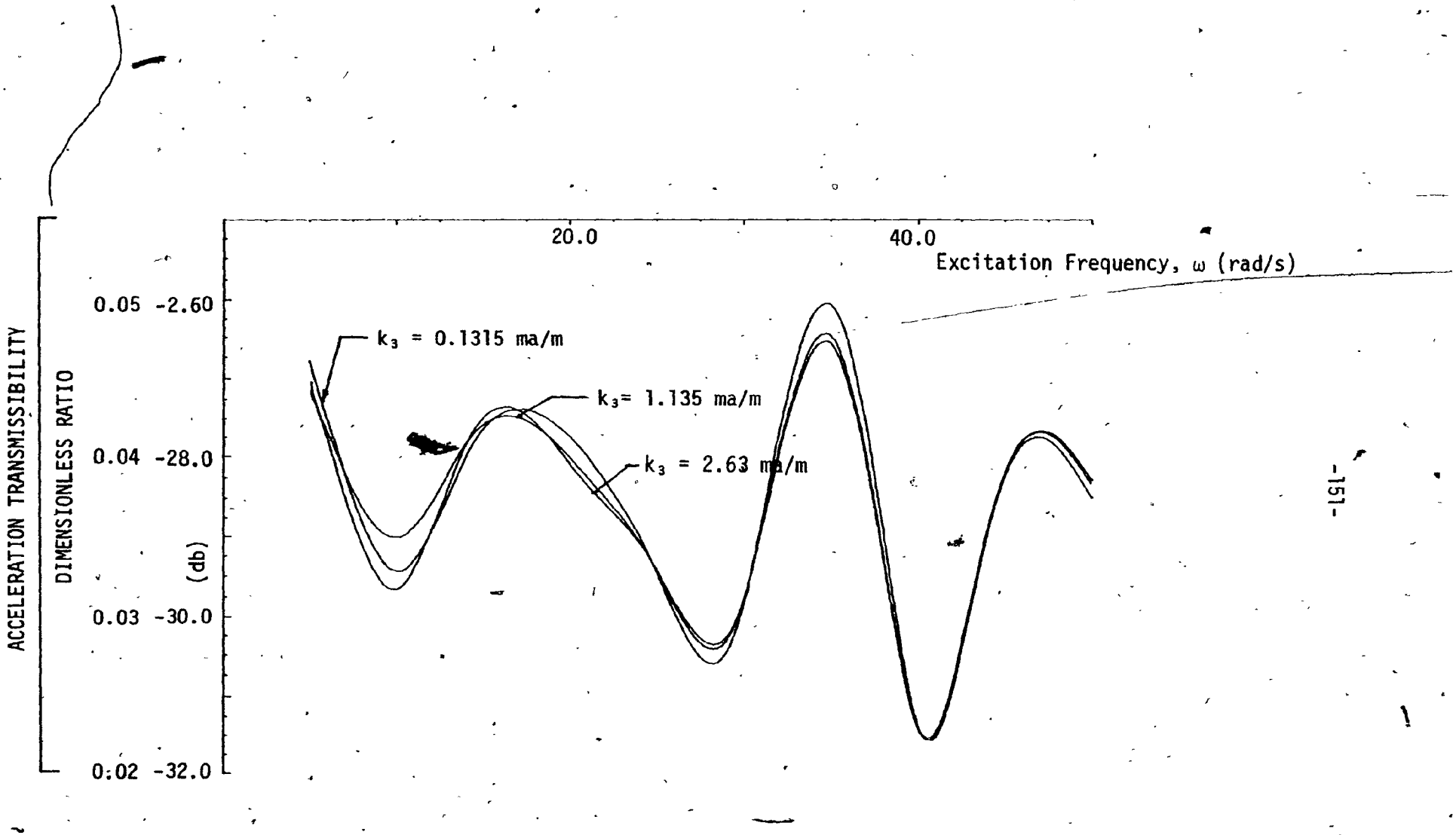

Fig. 89: Acceleration Transmissibility Plot For Variation in k_3

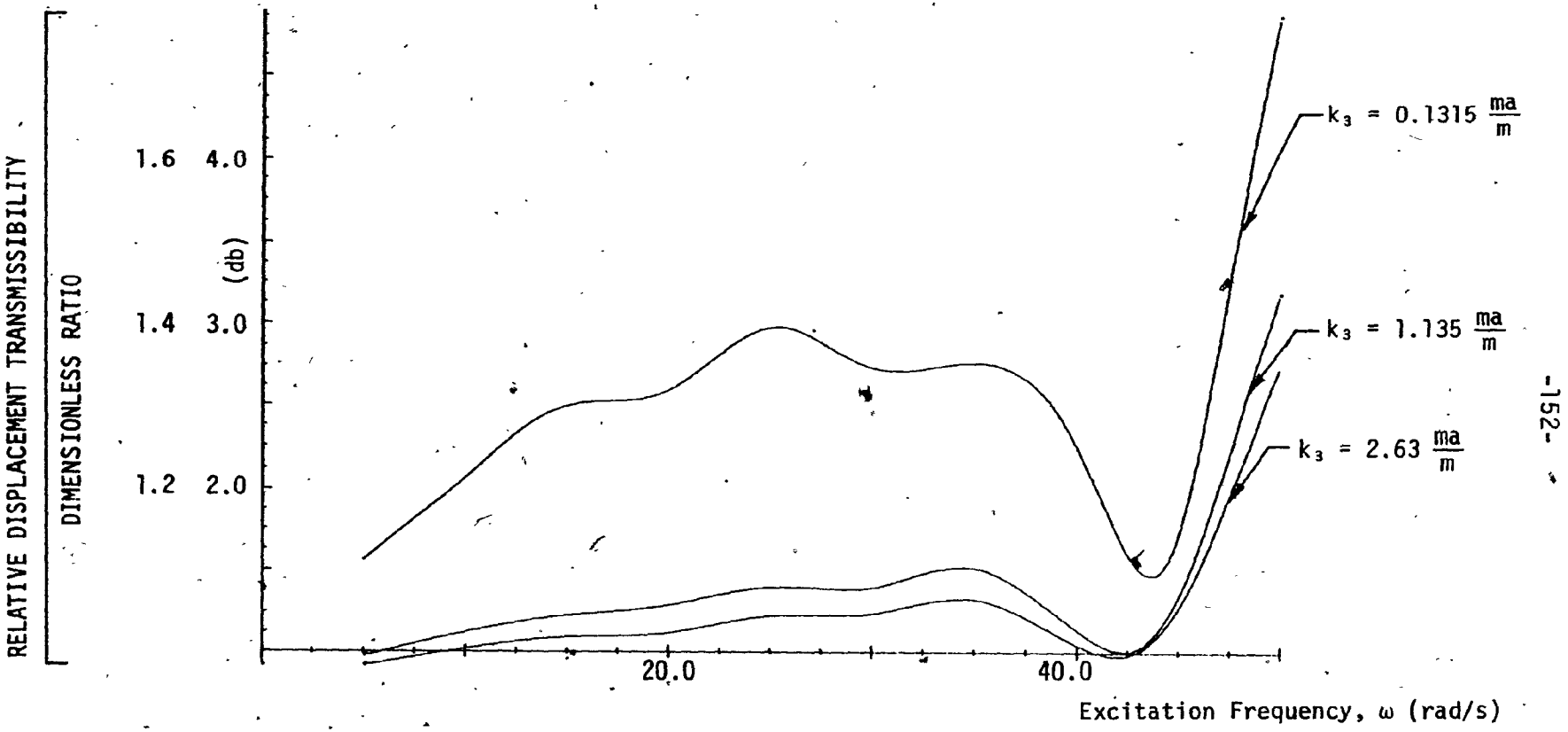

Fig. 90: Relative Displacement Transmissibility Plot for Variation in k_3

3.10 The Effect of Variation of the Input Amplitude on the System Performance

In general, non-linear systems have different output response characteristics for different magnitudes of input. Therefore in order to study the effect of the input amplitude on this non-linear active system, the amplitude of the sinusoidal excitation is kept at different values and the frequency is swept from 5 rad/s to 50 rad/s. The acceleration and relative displacement plots are shown.

Figure 91 shows the acceleration transmissibility plot for different input amplitudes. It can be seen that as the input amplitude increases, the maximum transmitted acceleration also increases. Figure 92 shows the relative displacement transmissibility of the system for different input amplitudes. Similar to that of the acceleration transmissibility, the relative displacement transmissibility increases with increases in the input amplitude. It is interesting to note that the frequency at which the peak acceleration and relative displacement occur increases as the input amplitude decreases.

For higher input amplitudes, the energy required by the active system increases. In order to achieve better performance for higher amplitude inputs, the energy level in the active system should be increased. The energy required in an active system depends on the supply pressure and the pre-charged initial chamber pressures. Hence the supply pressure and the initial chamber pressures are increased individually to see the effect on the system performance.

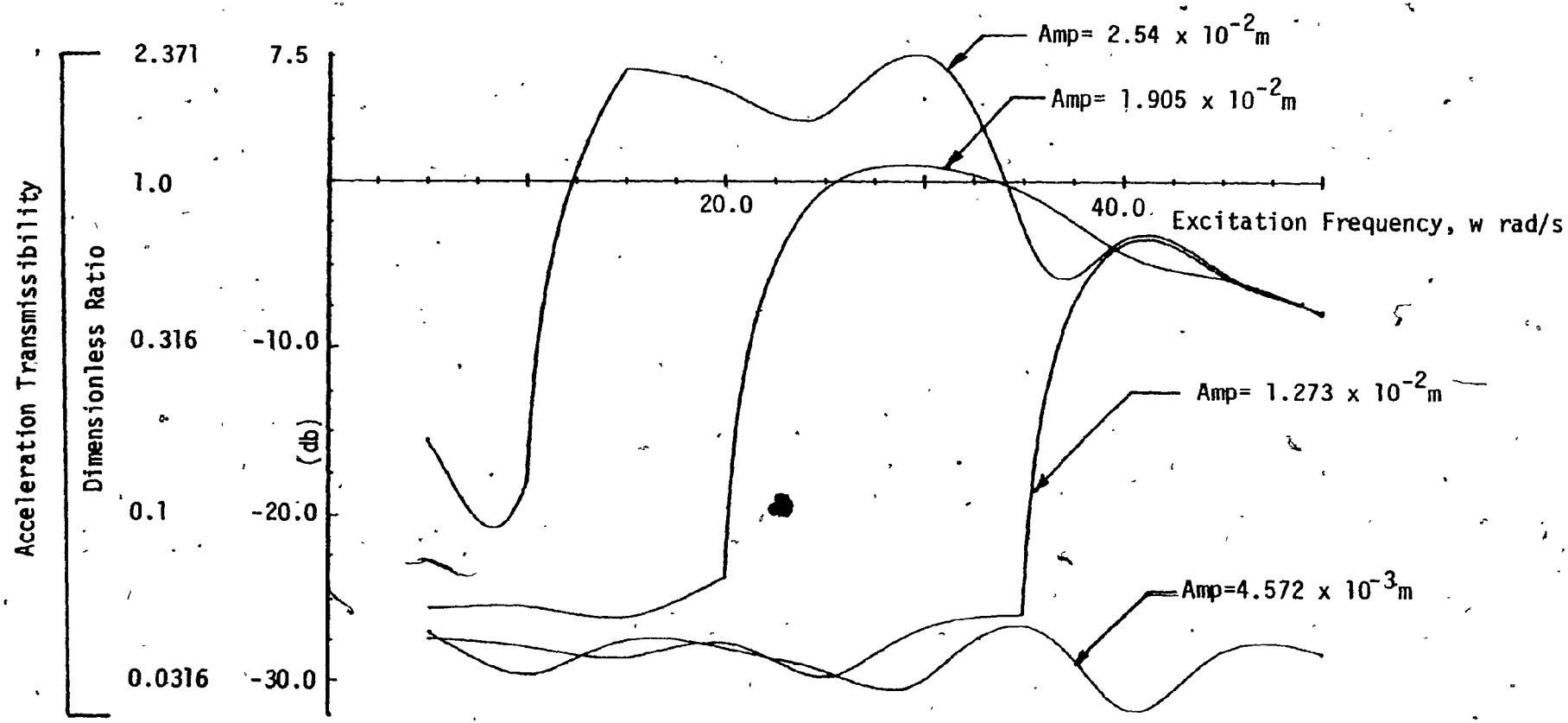

FIGURE 91. Acceleration Transmissibility Plot for Variation in Input Amplitude

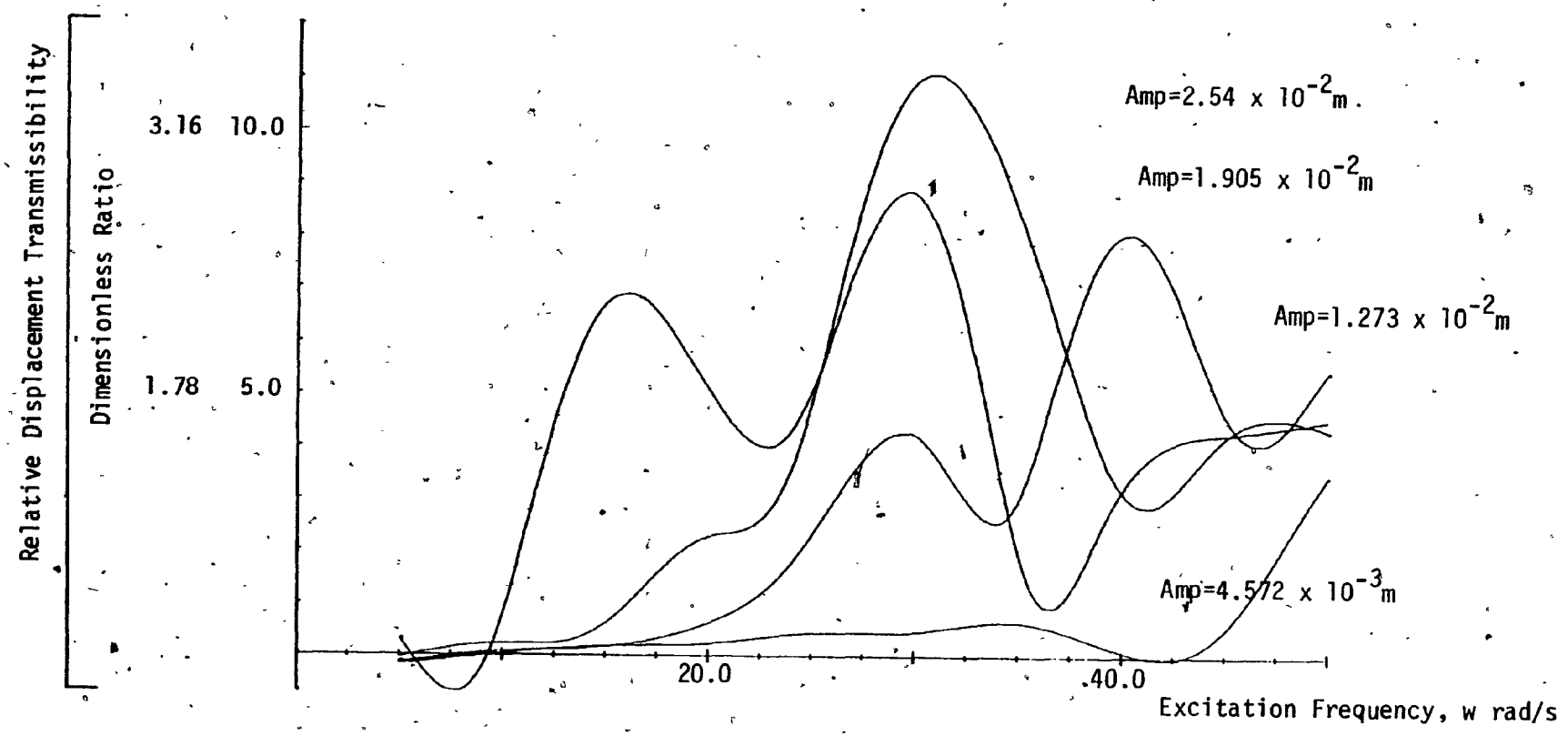

Fig. 92: Relative Displacement Transmissibility Plot for Variation in Input Amplitude

Figure 93 shows the acceleration transmissibility plot for an input amplitude of 0.0254 m. It can be seen from the figure that the peak acceleration transmitted to the isolated mass decreases only by a very small amount by increasing either the supply pressure or the initial chamber pressures. However, it is important to note that by increasing the supply pressure, the system has good isolation characteristics up to 30 rad/s and only after which it increases sharply to a peak value of 5 db (1.8) at 35 rad/s. It is also seen that at higher excitation frequencies, the acceleration transmissibility displayed a monotonically decreasing behavior. By increasing only the chamber pressures it can be noted that the system has good performance up to 20 rad/s and then it sharply increases to a peak value at 25 rad/s and decreases as the excitation frequency increases. Figure 94 shows the relative displacement transmissibility plot for increase in supply and chamber pressures. The relative displacement has a similar characteristic to that of the acceleration transmissibility.

3.11 The Effect of Mass Variation on the System Performance

The inertial mass to be isolated is kept constant so far in this thesis. However, it will be interesting to know the sensitivity of the system for variations in the mass. For this purpose the mass of the system is increased or decreased by 20% and the computer simulation was carried out for the Type 2 active system.

Figure 95 shows the acceleration transmissibility plot for different values of mass. It is seen that the magnitude of acceleration trans-

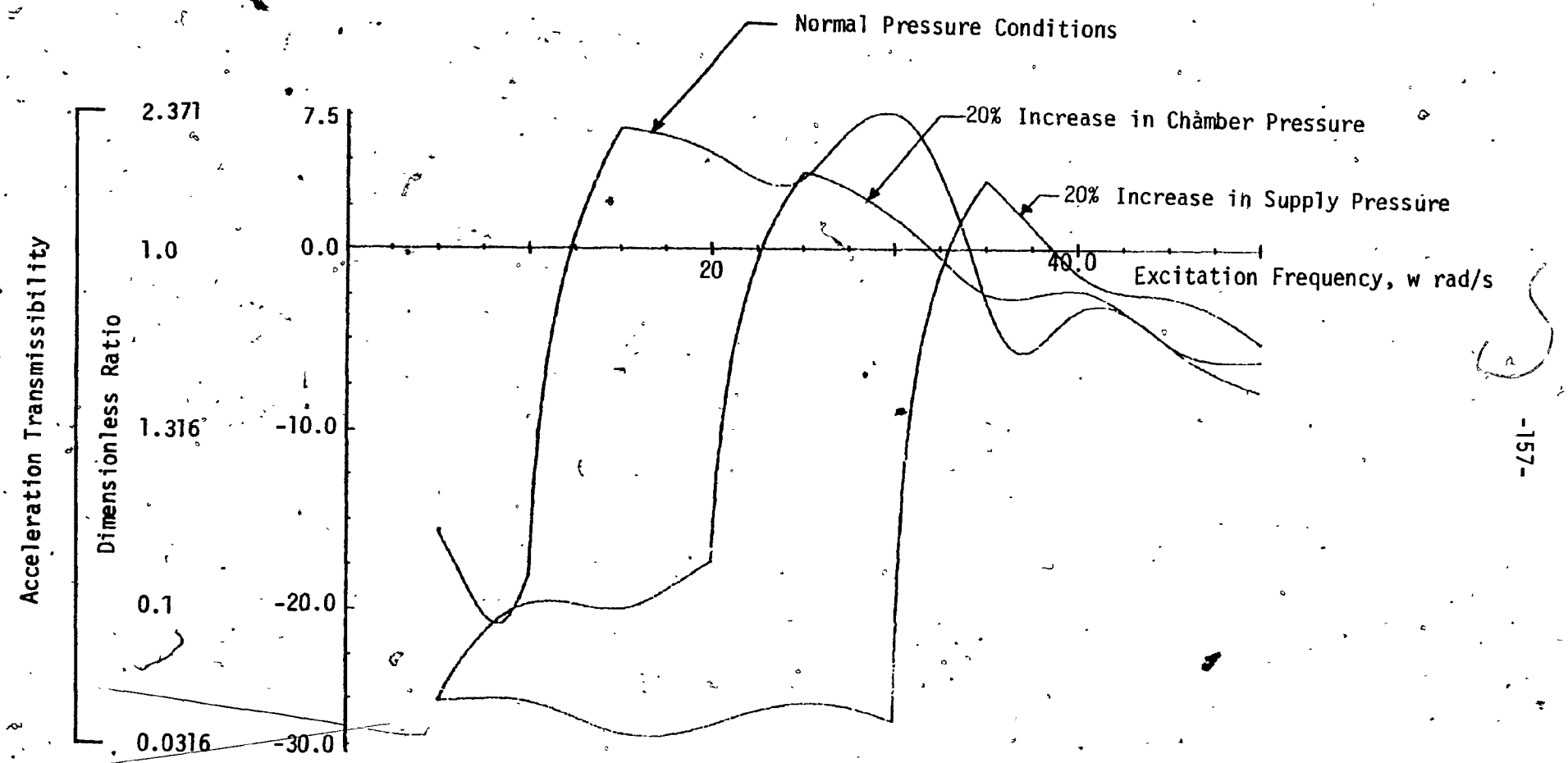

Fig. 93: Acceleration Transmissibility Plot for Increase in Supply and Chamber Pressures

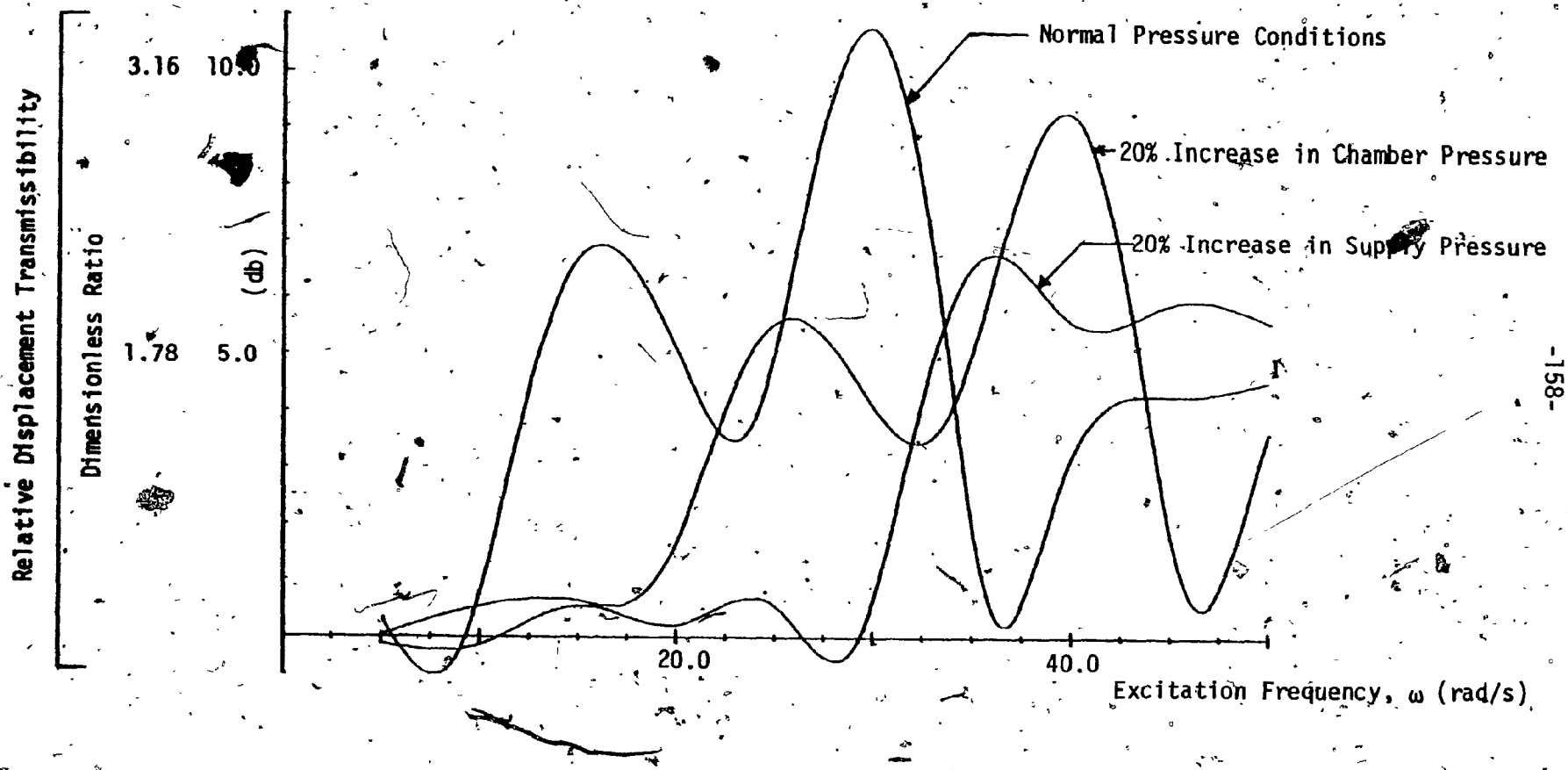

Fig. 94: Relative Displacement Plot for Increase in Supply and Chamber Pressures

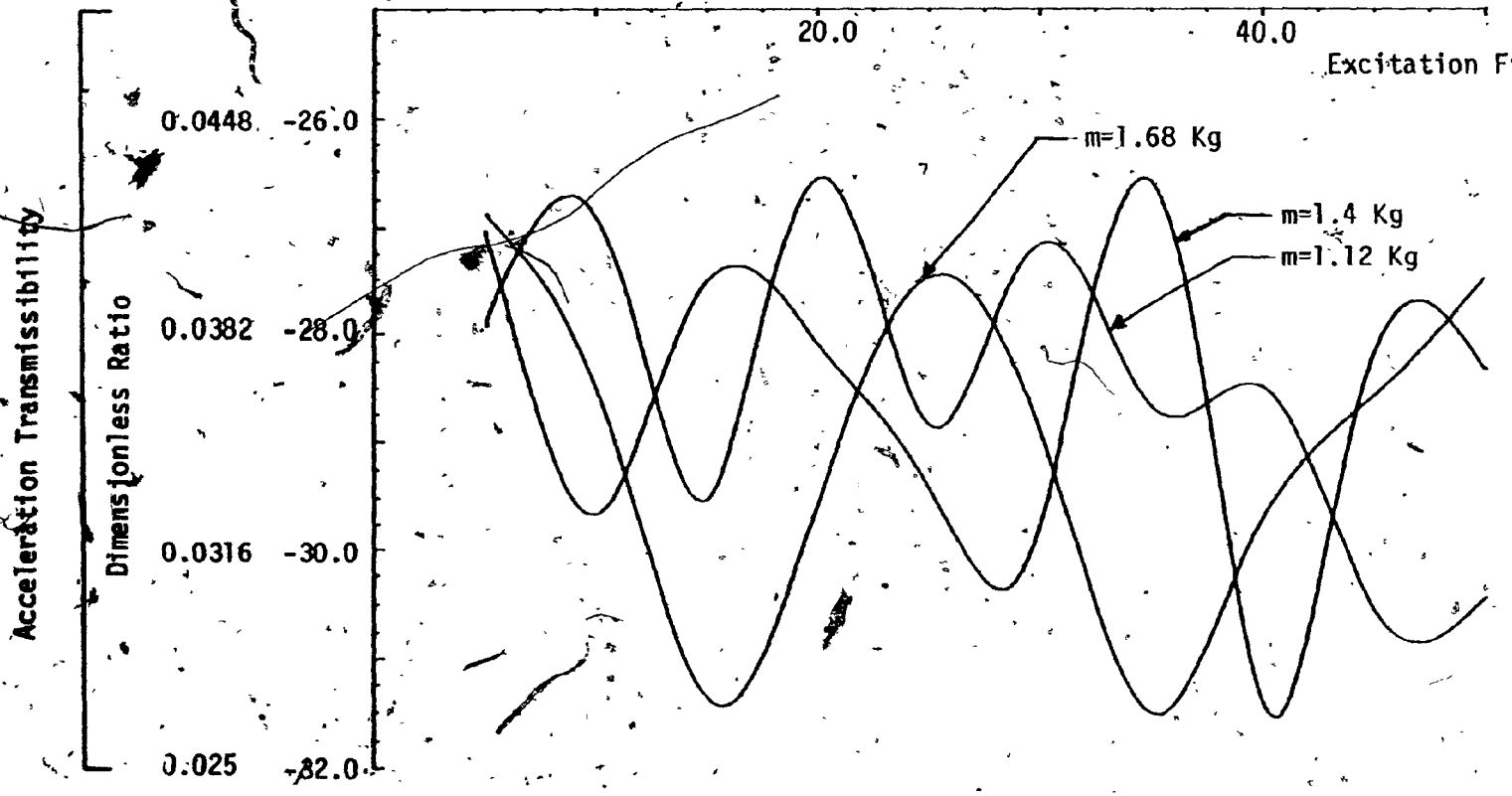

FIGURE 95. Acceleration Transmissibility Plot for Variation in the Isolated Mass

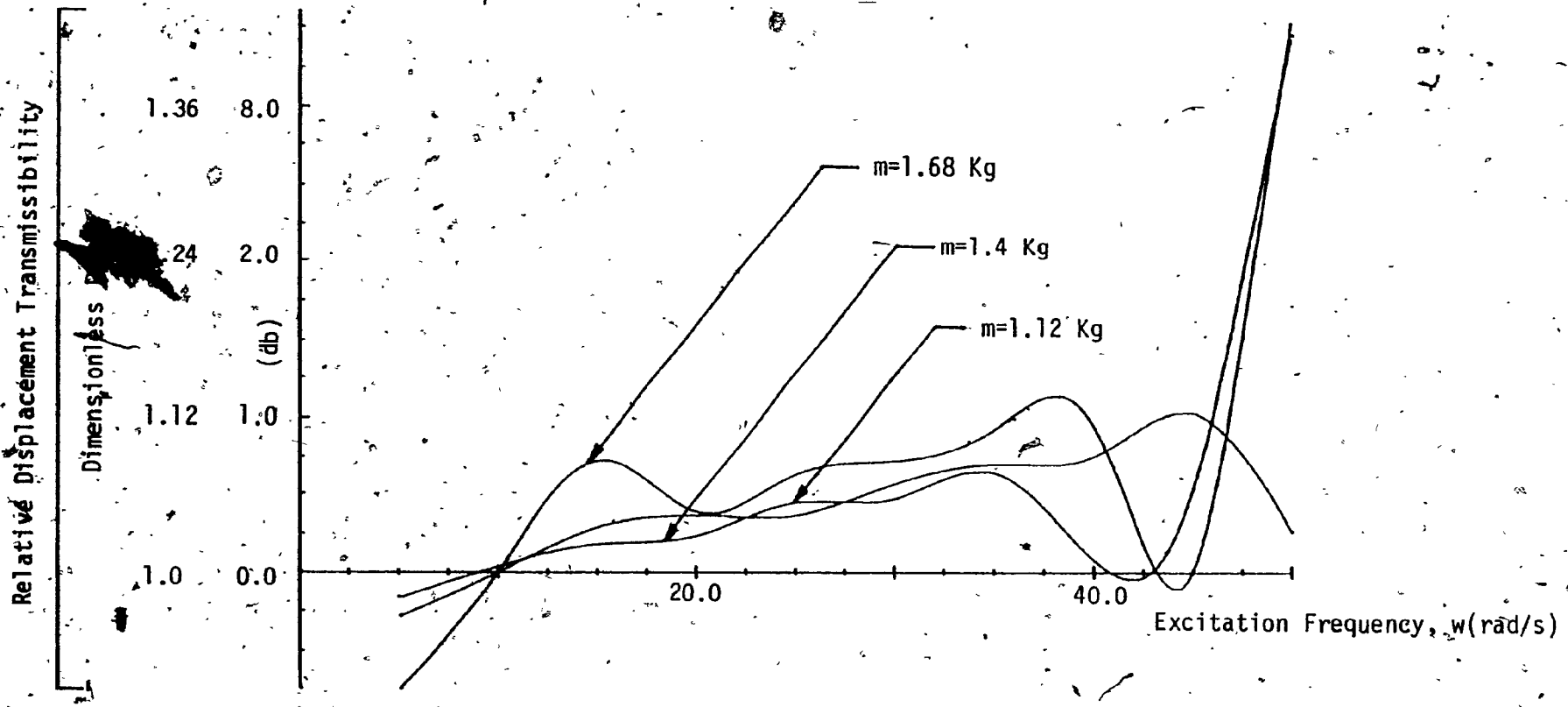

Fig. 96: Relative Displacement Plot for Variation in the Isolated Mass

mitted to the isolated mass does not change considerably by changing the system mass.

Figure 96 shows the relative displacement transmissibility for different values of the isolated mass. From the figure it is seen that for low frequencies there is no significant change in the relative displacement transmissibility by increasing the mass. However, by decreasing the mass by 20%, the relative displacement transmissibility reduces considerably at higher frequencies.

3.12 Performance Comparison of Passive and Active Isolation Systems

A direct comparison between the active and passive isolation systems is possible for sinusoidal input of amplitude 4.6×10^{-3}m, pulse-like input and input of the form of $x = x_0 (1-\cos \omega t)$.

Comparison of relative displacement or acceleration time response for the sinusoidal input between the active and passive systems shows that the active system goes through a more severe transient in the initial period than the passive system. The settling time is much shorter for passive system than for active system. For passive system both the output acceleration and displacement oscillate with the excitation frequency and have a constant amplitude. However, in the case of an active system both the output acceleration and displacement time response contain more than one frequency with amplitudes that settle to a steady state after an initial transient period.

Figures 18 and 49 show the absolute displacement transmissibility

plots for both passive and active systems. The active system shows a very small output displacement for the frequency ranges considered as compared to that of the passive system. But the relative displacement transmissibility shows that the passive system (figure 14) has a small value for low frequencies below the resonance and has a constant value which is more than unity for higher frequencies after the resonance. In the case of the active system, the relative displacement transmissibility is approximately unity until 42 rad/s and gradually increases to a value of 1.5 (3.5 des) at 50 rad/s.

The acceleration transmissibility plot of the passive and active systems are shown in Figures 17 and 51 respectively. The acceleration transmissibility for the active system displayed alternate increasing and decreasing characteristics with three peaks at 18 rad/s, 35 rad/s and at 48 rad/s. However, the peak transmissibility is observed to be less than 0.05 (-26 db). This indicates that the acceleration transmitted to the mass is about 20 times less than the input acceleration. The passive system has higher transmitted acceleration levels at frequencies below the natural frequency, while there is a considerable reduction in the amount of acceleration (force) transmitted to the mass at higher frequencies.

For pulse-like input, the displacement and acceleration time response shows very similar characteristics for both active and passive systems. The maximum output displacement for the passive system is almost the same as that of input displacement, while for the active system, the maximum output displacement is 1.5 times less than the peak input dis-

placement. Also the peak transmitted acceleration is much smaller for the active system than for the passive system.

For the input of the form $x = x_o (1-\cos \omega t)$, the passive system has a very small relative displacement and the absolute output displacement follows the input. In the case of active system the output displacement is about 200 times less than the input displacement. The acceleration transmitted to the mass is about the same as that of the input for the passive system but the active system transmits only about 20% of the maximum input acceleration.

Based on the comparison between the active and passive systems, it can be concluded that the active system has better acceleration and displacement isolation characteristics than the passive system.

CHAPTER 4

CHAPTER 4

EXPERIMENTAL PROCEDURE

4.1 GENERAL

The theoretical prediction of the active isolation system shows that the system isolates the input acceleration level considerably and also minimizes the displacement of the mass. In order to verify the theoretical predictions, an experimental investigation is needed. In this chapter an experimental procedure is outlined that includes the description and sizing of components. However no experiments were conducted and will be a subject of future work.

4.2 EXPERIMENTAL SET-UP

The complete schematic of the experimental set-up for Type 2 Active Isolation System is given in Figure 97. The active isolator is mounted on the platform of a hydraulic shaker and supports the inertial mass. The isolator consists of a pneumatic cylinder arranged in parallel with a mechanical spring. The shaker is used to generate the vibrational inputs and is capable of producing sinusoidal displacements up to 7.62×10^{-2} m in the frequency range of 0 to 200 Hz.

The Chamber 2 is sealed so that no flow in and out of Chamber 2 is allowed. The Chamber 1 is connected to the electro-pneumatic servo-valve. For a positive relative displacement the fluid will be exhausted to atmosphere through the servo-valve. When the relative displacement is negative, the Chamber 1 is charged from a pressure source through the servo-valve. The movement of the spool in the servo-valve is controlled by a command signal (input current). By sensing system

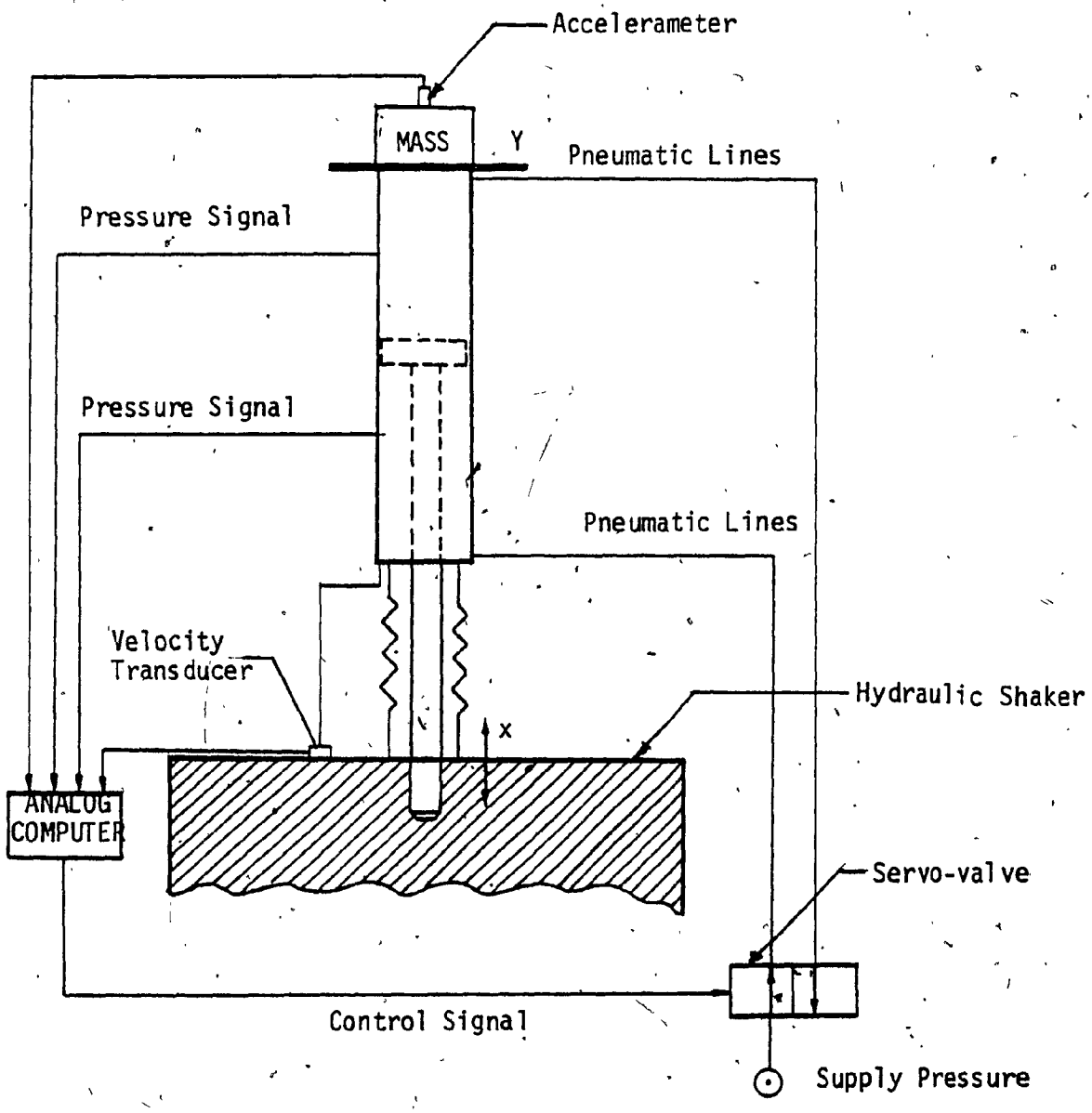

Fig. 97: Schematic of the Experimental Setup for Type 2 Active System

variables such as acceleration, relative velocity and pressures and appropriately combining them, the command signal is generated to drive the servo-valve.

4.3 SELECTION OF COMPONENTS

4.3.1 Pneumatic Cylinder

The size of the cylinder is selected from the mass, spring rate, initial compressed length of the spring and from the initial pressure in the cylinder chambers. For the values of the above parameters used in the simulation, the cylinder bore area is determined to be 9.6774×10^{-4} m^2 and the piston rod diameter is found to be 8.89×10^{-3} m. The cylinder stroke length used is 0.1524 m.

Since the values used in the simulation are not optimum values, the size of the cylinder can be changed depending on the values of the mass, spring rate and the initial pressure in the cylinder chambers.

4.3.2 Servo-Valve:- An electro-pneumatic servo-valve provides an output flow proportional to an electrical input current. This electro-pneumatic servo-valve is characterized by the operating pressure and the operating flow rates. For the active system studied, the chamber pressure is selected as 5.52×10^5 N/m^2 and the supply pressure as 8.27×10^5 N/m^2. The maximum flow rate is selected to be 0.84 SCMM for an input frequency of 50 rad/sec. For the system pressures selected an electro-pneumatic servo-valve with a rated flow of 1.49 SCMM and a maximum valve pressure drop of 6.9×10^5 N/m^2 can be used. For this operating pressure and flow rate, the rated current is 200 m.A. and the coil resistance is 22 ohms. The sectional view of the servo-valve

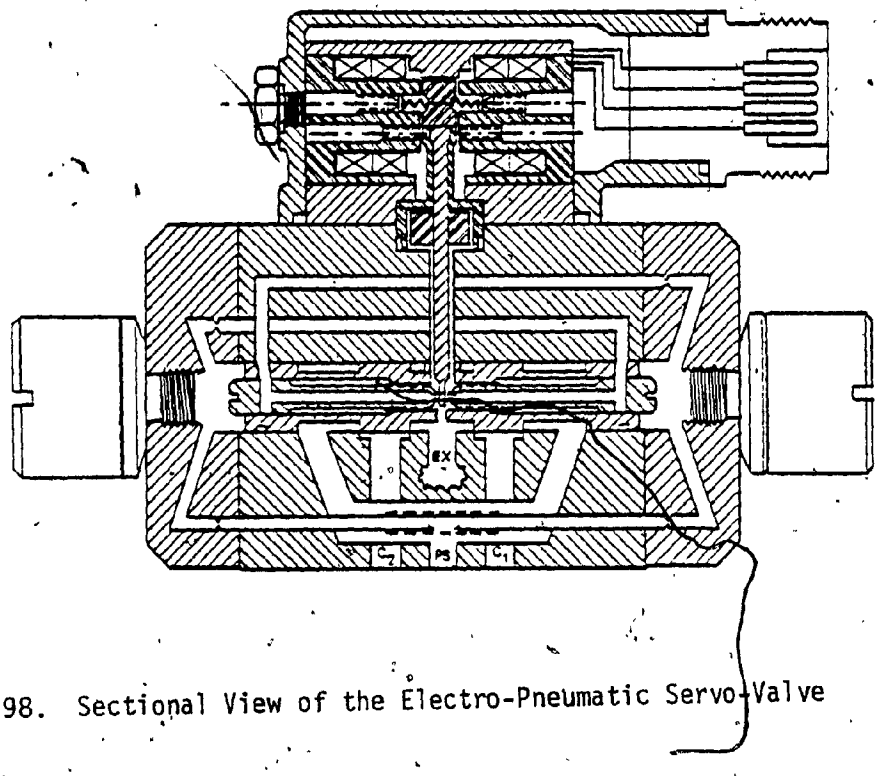

FIGURE 98. Sectional View of the Electro-Pneumatic Servo-Valve

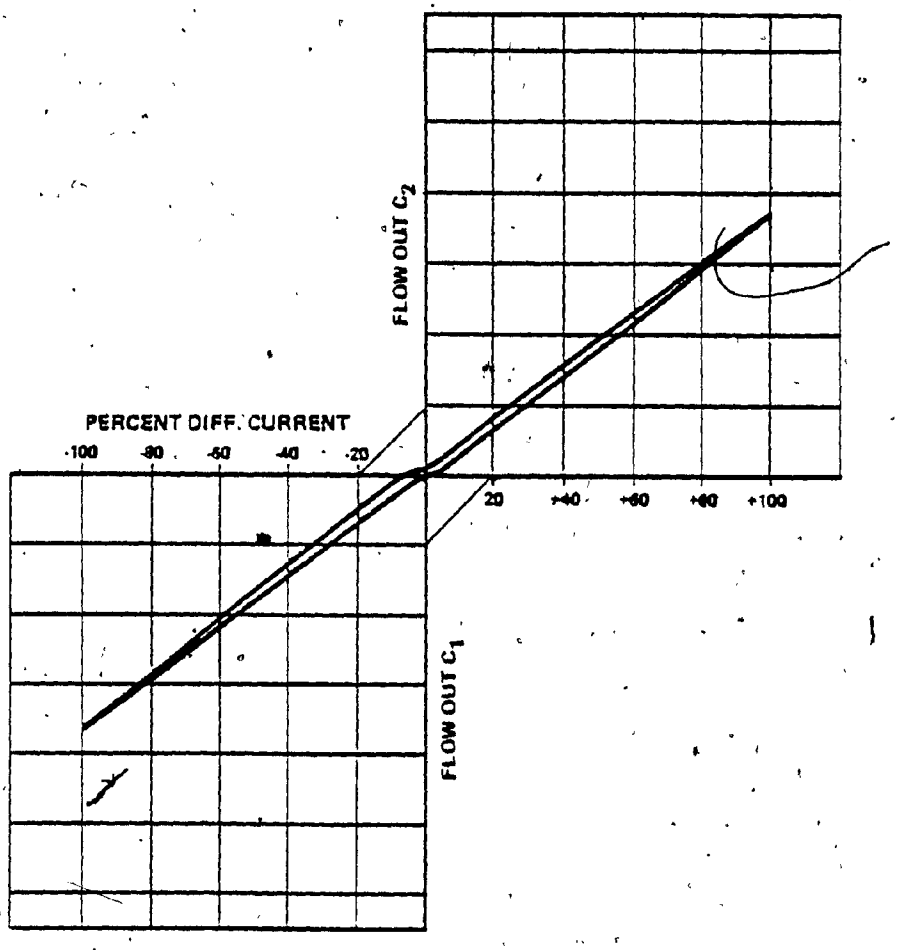

FIGURE 99. Performance Characteristic of the Electro-Pneumatic Servo-Valve

is shown in Figure 98 and the performance characteristic of the servo-valve is shown in Figure 99.

4.4. GENERATION OF CONTROL SIGNAL

The control signal is achieved from the mathematical manipulation of the measured values of absolute acceleration, velocity, displacement, pressures and relative velocity. The mathematical manipulation can be achieved either by a micro-processor or by a portable analog computer such as EAI 180. Since the experiment will be carried out in the laboratory and also to have flexibility in changing the feedback gains, as analog computer can be used. The non-dimensionalized equation of the control signal given by equations (3.76) and (3.77) can be patched on the analog computer.

The equations (3.76) and (3.77) should be amplitude scaled. The time scaling is not needed since the control should be carried out in real time. By using the maximum values for the variables as given in Table 4.1, the non-dimensionalized control signal i_c^* can be written as

$$i_c^* = \left[a_1 \cdot p_2^* + a_2 + a_3 \cdot p_1^*\right] \cdot \frac{(\dot{x}-\dot{y})^*}{p_1^*} + a_4\ddot{y}^* + a_5\dot{y}^* + a_6 y^* \quad (4.1)$$

where

$$a_1 = \frac{A_o \cdot c_2\, p_2\,(max)}{L \cdot Ag \cdot \beta \cdot c_1 \cdot i_c\,(max)} \cdot \frac{(\dot{x}-\dot{y})(max)}{p_1\,(max)}$$

$$a_2 = \frac{A_o\ c_3}{1.2 \cdot L \cdot Ag \cdot \beta \cdot c_1 \cdot i_c\,(max)} \cdot \frac{(\dot{x}-\dot{y})(max)}{p_1\,(max)}$$

$$a_3 = \frac{A_o\ p_1\,(max)}{L \cdot Ag \cdot \beta \cdot i_c\,(max)} \cdot \frac{(\dot{x}-\dot{y})(max)}{p\ (max)}$$

$$a_4 = \frac{k_1 \cdot A_0 \cdot \ddot{y}\,(max)}{L \cdot Ag \cdot \beta \cdot i_c\,(max)}$$

$$a_5 = \frac{k_2 \cdot A_0 \cdot \dot{y}\,(max)}{L \cdot Ag \cdot \beta \cdot i_c\,(max)}$$

$$a_6 = \frac{k_3 \cdot A_0 \cdot y\,(max)}{L \cdot AG \cdot \beta \cdot i_c\,(max)}$$

where i_c^*, p_1^*, p_2^*, $(n-y)^*$, $\ddot{y}^*$, $\dot{y}^*$ and y^* are all normalized variables. The analog computer circuit diagram of the equation 4.1 is shown in Figure 100. The potentiometer values for the analog computer circuit is given in Table 4.2.

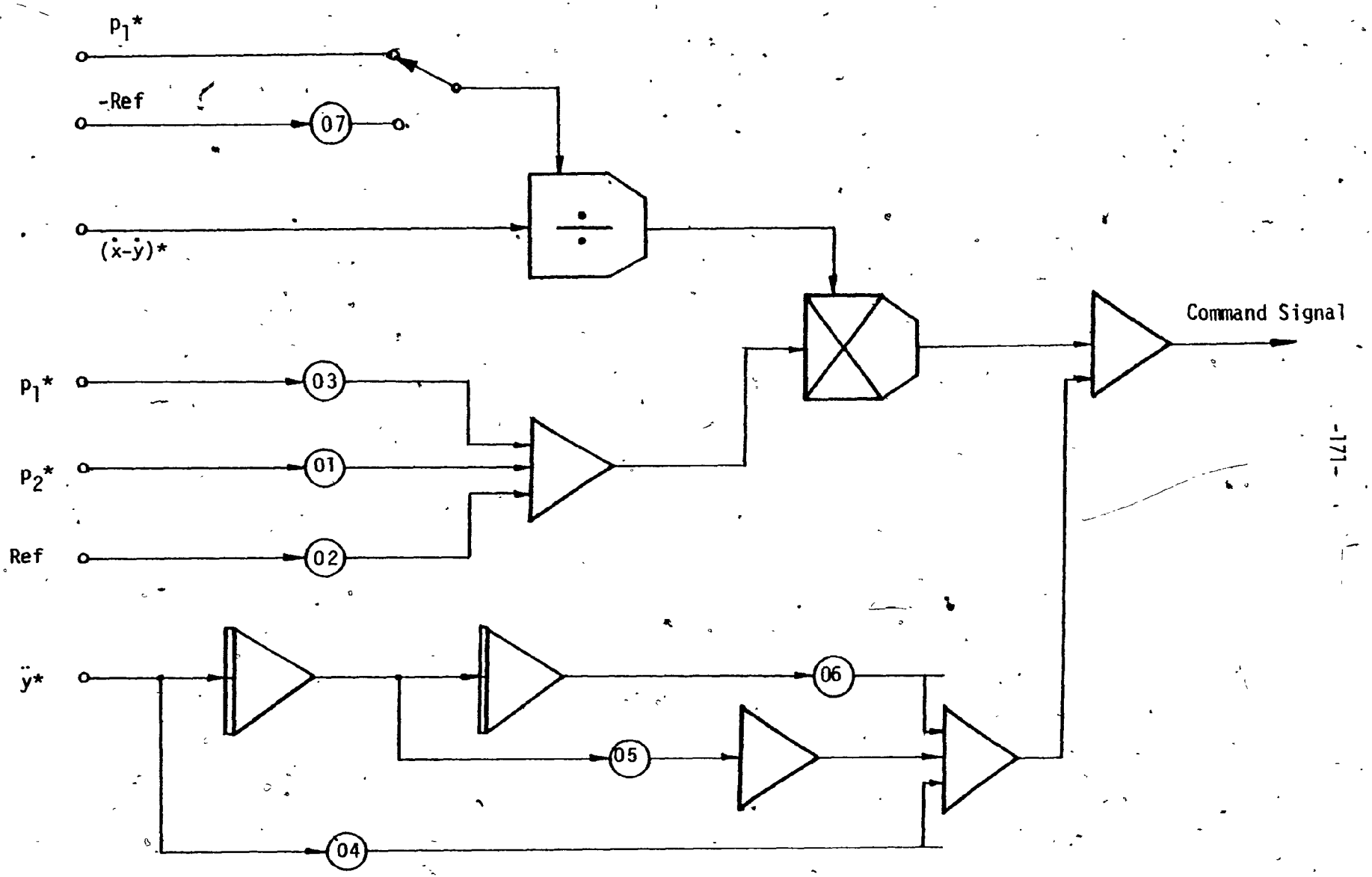

Fig. 100: Analog Computer Circuit Diagram for Control Logic 2

TABLE 4.1

VARIABLES	MAXIMUM VALUES
Pressure (1) p_1	1.25
Pressure (2) p_2	1.25
Relative Velocity $(\dot{x}-\dot{y})$	3.0
Acceleration $(\ddot{y})$	8.0
Velocity $(\dot{y})$	3.0
Displacement (y)	0.03

Maximum Values for the Analog Computer Variables

TABLE 4.2

POT NO.	FORMULA AND CALCULATION	RESULTS
01	a_1	0.214
02	a_2	0.073
03	a_3	0.381
04	a_4	0.01
05	a_5	0.076
06	a_6	0.00076

Potentiometer Values for Analog Computer

CHAPTER 5

CHAPTER 5

CONCLUSIONS AND RECOMMENDATIONS FOR FUTURE WORK

The purpose of this thesis is to study the performance of passive and active pneumatic isolation systems. In the first part of this thesis, a passive pneumatic system with an orifice damping is simulated for sinusoidal, pulse like and input of the form $X = X_0 (1-\cos\omega t)$ excitations. In the second part of the thesis, an active isolation system is studied for the aforementioned input excitations. In the active system, the flow in and out of a cylinder chamber is controlled by a control logic so that the jerk of the inertial mass is zero.

Based on the simulation results of the passive isolation system, the following conclusions can be drawn:

- The peak absolute displacement of the isolated mass decreases with increase in the orifice area until a critical value.

- The acceleration transmitted to the isolated mass decreases with increase in the orifice area until a critical value.

- Frequencies higher than the resonance produce low acceleration transmissibility and a monotomically decreasing absolute output displacement transmissibility.

- The relative displacement transmissibility is small for low frequency below the resonance and has a constant value after the resonance.

- Damping in the passive system is provided by the orifice area between the two cylinder chambers.

- Increasing the orifice area until a critical value increases the damping factor. Further increasing of orifice area beyond the critical value produces oscillations.

- For pulse like input the maximum output displacement has the same amplitude as the input displacement and has an oscilatory response that decays exponentially to zero. As the severity parameter γ of the pulse input increases, the output acceleration decreases while the relative displacement increases.

- For input excitation of the form $X = X_0 (1-\cos\omega t)$, both the output displacement and acceleration follows the input very closely.

- The magnitude of input velocity is limited by the initial pressures in the two chambers and also by the piston stroke.

Based on the simulation results for the Type 2 active isolation system, the following are the conclusions:

- Absolute displacement transmissibility has a very low value for low frequencies and as the frequency increases the transmissibility fluctuates.

- The relative displacement transmissibility remains a constant (approximately unity) for lower frequencies however for frequencies higher than 42 rad/s the transmissibility increases sharply with the excitation frequency.

- Acceleration transmissibility has a characteristic that increases and decreases as the frequency is varied. Three peaks at approximately 15, 35 and 45 rad/s are observed. The maximum peak transmissibility is

found to be less than -26 db.

- For low frequency (ω = 2.5 rad/s) sinusoidal inputs, the output displacement time response has no high frequency components and is oscillatory with variable amplitude. In the case of high frequency, (ω = 25 rad/s) excitation, the output displacement is a decreasing sine function with high frequency oscilations superposed on it.

- For both low and high frequency sinusoidal excitation, acceleration time response has initial high amplitude oscilation which decays and settles to a steady state sinusoidal function with low amplitude. The settling time in the case of high frequency inputs is small compared to the low frequency excitation.

- The stability of the system is mainly controlled by feedback gains.

- For zero acceleration feedback gain the system becomes unstable. Selecting the value of the feedback gain k_1 in the neighborhood of $0.73 \frac{ma\text{-}s^2}{m}$, the system performs at its best. When the gain k_1 is increased to a higher value the system performance deterioted considerably.

- For low values of velocity feedback gain k_2, the system remains stable at all excitation frequencies (0 to 50 rad/s). At high values of k_2 ($1.9 \frac{ma\text{-}s}{m}$), the system becomes unstable at excitation frequency less than 2.5 rad/s. The relative displacement transmissibility plots are almost similar for various values of k_2 with a constant value of approximately unity at low frequencies and sharply increasing at high frequencies. The variation of k_2 has negligible influence on the acceleration trans-

missibility.

- The variation of k_3 has no effect on the acceleration transmissibility for higher values of k_3 (k_3 greater than 1.135 ma/m) any increase of k_3 has no influence on the relative displacement transmissibility. For a value of $k_3 = 0$ the system is found to be unstable.

- Variation in the input amplitude indicates that as the input amplitude increases the performance of the system deteriorates.

- For higher amplitude inputs the acceleration transmissibility can be maintained to be a small value up to 30 rad/s by appropriately increasing the supply pressure. However, for input frequencies higher than 30 rad/s the transmissibility sharply increases. By increasing the supply pressure the relative displacement transmissibility has a value of unity up to 30 rad/s and increases for higher frequencies.

- For higher input amplitudes, increasing the chamber pressures the acceleration transmissibility increases for the increasing excitation frequency up to 20 rad/s and then decreases. The peak acceleration transmissibility has a value of 1.5. In this case, the relative displacement has a similar behaviour as that of acceleration transmissibilty.

- By increasing the system mass by 20% the performance of the system has negligible change. However, the decrease of the mass by 20% results in a lower acceleration and relative displacement transmissibility.

- For pulse like input with $\gamma = 10$ the maximum output displacement is about 1.5 times less than the peak input displacement. As the severity parameter γ of the pulse input increases, the output acceleration ratio

decreases. The relative displacement ratio stays close to unity for all values of γ considered.

- For input of the form $X = X_0 (1-\cos\omega t)$ the output displacement is about 200 times less than the input displacement. The relative velocity is very close to the input. The peak acceleration is about 20% less than the input acceleration.

In the following, some suggestions for future work are summarized.

- Optimal values of the feedback gains k_1, k_2, and k_3 should be calculated by choosing an objective function such as minimizing the peak transmitted acceleration with a constraint on the relative displacement.

- Investigation on the influence of lag, lead network function instead of proportional feedback gains should be carried out. It is anticipated that such a feedback control will eliminate the high frequency fluctuation in the transmitted acceleration and displacement.

- A study should be carried out to find the performance characteristic of the active system for the random inputs.

- An explicit stability analysis should be carried out on a linearized model of the active system to better understand the behaviour of the active system.

- For the active system investigated in this thesis, the flow from Chamber 1 is discharged to atmosphere whenever the relative velocity is positive. It is recommended that future work be carried out in making it as a closed loop system so that no energy is wasted by venting flow to atmosphere.

- An experimental work should be initiated in order to assess the validity of the theoretical results and also to study the reliability of the hardware.

REFERENCES

REFERENCES

1. Caton, A.T. and R. Holmes, "Design and Performance of a Coulomb Shock Isolator", Journal Mechanical Science, Vol. 15, No. 4, (1973).
2. Cornelius, K.T., "A Study of the Performance of an Optimum Shock Mount", Shock and Vibration Bulletin, Bulletin 38, Part 3, No. V., (1968).
3. Snowdon, J.C., "Isolation from Mechanical Shock with a Mounting System Having Non-Linear Dual-Phase Damping", The Shock and Vibration Bulletin, Bulletin 41, Part 2, December (1970).
4. Venkatesan, C. and R. Krishnan, "Harmonic Response of a Shock Mount Employing Dual-Phase Damping", Journal of Sound and Vibration, Vol. 40(3), (1975).
5. Mercer, C.A. and P.L. Rees, "An Optimum Shock Isolator", Journal of Sound and Vibration, Vol. 18(4), (1971).
6. Ruzicka, J.E. and T.F. Derby, "Vibration Isolation with Non-linear Damping", Journal of Engineering for Industry, Vol. 93, Series B, May (1971).
7. Hundal, M.S., "Design of Impact Absorber with Quadratic Damping", ASME Paper No. 76-WA/DE-12, (1976).
8. Soliman, J.I. and E. Ismailyadeh, "Optimization of Unidirectional Viscous Damped Vibration Isolation System", Journal of Sound and Vibration, Vol. 36(4), (1974).
9. Mayne, R.W., "The Effect of Fluid and Mechanical Compliance on the Performance of Hydraulic Shock Absorbers", ASME Paper No. 73-DET-1, (1973).

10. Karnopp, D.C., "Are Active Suspensions Really Necessary", ASME Paper No. 78-WA/DE-12, (1978).

11. Wolkovitch, J., "Techniques for Optimizing the Response of Mechanical Systems to Shock and Vibration", SAE Transaction, Vol: 77, (1969).

12. Karnopp, D.C., "Active and Passive Isolation of Random Vibration", Published in ASME Monograph AMD, Vol. 1, (1973).

13. Hendrick, J.K., "Some Optimal Control Techniques Applicable to Suspension System Design", ASME Paper No. 73-ICT-55, (1973).

14. Bender, E.K., "Optimum Linear Preview Control with Application to Vehicle Suspension", Journal of Basic Engineering, Vol. 90, No. 2, (1968).

15. Karnopp, D.C. and A.K. Trikha, "Comparative Study of Optimization Techniques for Shock and Vibration Isolation", Journal of Engineering for Industry, Vol. 91, Series B, No. 4, November (1969).

16. Hullender, D.A., D.N. Wormley and H.H. Richardson, "Active Control of Vehicle Air Cushion Suspensions", Journal of Dynamic Systems, Measurements and Control, Vol. 93, No.1, (1972).

17. Young, J.W. and D.N. Wormley, "Optimization of Linear Vehicle Suspensions Subjected to Simultaneous Guideway and External Force Disturbances", Journal of Dynamic Systems, Measurement and Control, Series G, Vol. 95, No. 2, (1975).

18. Hendrick, J.K., G.F. Billington and D.A. Dreesbach, "Analysis Design and Optimization of High Speed Vehicle Suspensions using State Variable Techniques", Journal of Dynamic Systems, Measurement, and Control, Vol. 96, No. 2, (1974).

19. Crosby, M.J. and D.C. Karnopp, "The Active Damper - A New Concept for Shock and Vibration Control", The Shock and Vibration Bulletin, No. 43, (1973).

20. Karnopp, D.C., M.J. Crosby and R.A. Harwood, "Vibration Control using Semi-Active Force Generators", Journal of Engineering for Industry, Vol. 96, Series B, No. 2, May (1974).

21. Hanna, C.R. and W.O. Osbon, "Vehicle Ride Stabilization by Inertia Control", Proceedings of the National Conference on Industrial Hydraulics, Volume XV, October 19-20, (1961).

22. Osbon, W.O., L.R. Allen, and A.R. Wilhelm, "Active Suspensions for Automotive Military Vehicle", Westinghouse Research Laboratories, Scientific Paper 65-1D1-Hydra-p , June (1973).

23. Rinehart, R.E., R.E. Roach, J.A. Bain, and P.F. Croshaw, "Transit Car Ride Quality : Prediction, Test and Improvement", ASME Paper No. 73-ICT-76, (1973).

24. Klinger, D.L. and A.J. Calyado, "A Pneumatic On-Off Vehicle Suspension System", Journal of Dynamic Systems, Measurement, and Control, Vol. 99, Series G, (1977).

25. Andersen, B.W., The Analysis and Design of Pneumatic Systems, John Wiley & Sons Inc., New York, (1967).

26. Hornbeck, R.W., Numerical Methods, Quantum Publishers, Inc., New York, (1975).

APPENDIX A

APPENDIX A

The general form of equations 2-2 and 2-3 can be written as

$$\frac{dP}{dt} = -\frac{dV}{dt} \cdot \frac{P}{V} + \frac{dM}{dt} \frac{RT}{V} + \frac{M \cdot R}{V} \cdot \frac{dT}{dt} \qquad (A.1)$$

with temperature assumed to be related to pressure by a polytropic gas constant 'n', the equation relating pressure and temperature can be written as

$$\frac{T}{T_o} = \left(\frac{P}{P_o}\right)^{\frac{n-1}{n}} \qquad (A.2)$$

Differentiating equation (A.2) with respect to time, the rate of change of temperature is given as

$$\frac{dT}{dt} = \frac{T_o}{\left(P_o\right)^{\frac{n-1}{n}}} \quad \frac{n-1}{n} (P)^{-\frac{1}{n}} \quad \frac{dP}{dt} \qquad (A.3)$$

multiplying both sides by $\frac{MR}{V}$, we have

$$\frac{M \cdot R \cdot}{V} \cdot \frac{dT}{dt} = \frac{M \cdot R}{V} \cdot \frac{T_o}{\left(P_o\right)^{\frac{n-1}{n}}} \quad \frac{n-1}{n} \quad (P)^{-\frac{1}{n}} \quad \frac{dP}{dt} \qquad (A.4)$$

From equation of state (PV = MRT), we have

$$MR = \frac{PV}{T} \qquad (A.5)$$

Substituting equation (A.5) in (A.4) gives:

$$\frac{M \cdot R}{V} \quad \frac{dT}{dt} = \frac{P}{T \cdot} \cdot \frac{T_o}{\left(P_o\right)^{\frac{n-1}{n}}} \cdot \frac{n-1}{n} \quad (P)^{-\frac{1}{n}} \cdot \frac{dP}{dt}$$

$$= \frac{T_o}{T} \cdot \left(\frac{P}{P_o}\right)^{\frac{n-1}{n}} \cdot \frac{n-1}{n} \cdot \frac{dP}{dt} \qquad (A.6)$$

Substituting equation (A.2) in (A.6) gives

$$\frac{M \cdot R}{V} \cdot \frac{dT}{dt} = \frac{T_o}{T} \frac{T}{T_o} \cdot \frac{n-1}{n} \frac{dP}{dt} = \frac{n-1}{n} \cdot \frac{dP}{dt} \qquad (A.7)$$

Now combining equations (A.6) and (A.1), and rearranging the rate of change of pressure is given by

$$\frac{dP}{dt} = n \left[-\frac{dV}{dt} \frac{P}{V} + \frac{dM}{dt} \frac{RT}{V} \right] \qquad (A.8)$$

APPENDIX B

APPENDIX B

Defining once again the reference quantities mentioned in Section (2.3)

Reference Length	L
Reference Area	A_1
Reference Pressure	P_0
Reference Temperature	T_0
Reference Volume	$V_0 = A_1 \cdot L$
Reference Mass	$M_0 = P_0 V_0 / RT_0$
Reference Time	α

Take reference time α is defined as

$$\alpha = \frac{\beta \cdot V_0}{A_1 \cdot k \cdot R \cdot \sqrt{T_0}}$$

Define the following non-dimensional quantities:

$$x = \frac{X}{L} \; ; \quad y = \frac{Y}{L} \; ; \quad t_1 = \frac{T_1}{T_0} \; ; \quad t_2 = \frac{T_2}{T_0}$$

$$p_1 = \frac{P_1}{P_0} \; ; \quad p_2 = \frac{P_2}{P_0} \; ; \quad M^* = \frac{M}{M_0} \; ; \quad a = \frac{A}{A_1}$$

$$a_1 = \frac{A_1}{A_1} = 1 \; ; \quad a_2 = \frac{A_2}{A_1} = AR$$

$$\tau = \frac{t}{\alpha}$$

were τ is the non-dimensionalized time AR is the area ratio.

Now the time deviative $\frac{d(\cdot)}{dt}$ can be written as

$$\frac{d(\cdot)}{dt} = \frac{d(\cdot)}{d\tau} \quad \frac{d\tau}{dt}$$

$$= \frac{d(\cdot)}{d\tau} \quad \frac{1}{\alpha}$$

and the second time derivative becomes

$$\frac{d^2(\cdot)}{dt} = \frac{d(\cdot)}{d\tau} \cdot \frac{d\tau}{dt} \cdot \frac{d(\cdot)}{d\tau} \cdot \frac{d\tau}{dt}$$

$$= \frac{d^2(\cdot)}{d\tau^2} \cdot \frac{1}{\alpha^2}$$

Pressure Equations

To non-dimensionalize the pressure equation, divide throughout the equation (2.21) by the reference pressure P_0 and by using the dimensionless parameters as described above, equation (2.21) becomes

$$\frac{d}{d\tau}\left(\frac{P_1}{P_0}\right) = n\left[\frac{\alpha}{P_0} \cdot \frac{R \cdot T_0}{LA_1} \cdot \frac{t_1}{(1-x+y)} \cdot \frac{dM^*}{d\tau} - \frac{\alpha}{P_0} \cdot \frac{P_0}{L} \cdot \frac{L}{\alpha} \cdot \frac{p_1}{1-x+y}\left(\frac{dx}{d\tau} + \frac{dy}{d\tau}\right)\right]$$

By further simplification, the rate of change of pressure in Chamber 2 is given by

$$\frac{dP_1}{d\tau} = n\left[\frac{t_1}{1-x+y} \cdot \frac{dM^*}{d\tau} - \frac{p_1}{1-x+y}\left(-\frac{dx}{d\tau} + \frac{dy}{d\tau}\right)\right] \qquad (B.1)$$

Similarly the rate of change of pressure in Chamber 2 is given by

$$\frac{d}{d\tau}\left(\frac{P_2}{P_0}\right) = n\left[\frac{\alpha}{P_0} \cdot \frac{R \cdot T_0}{L \cdot A} \cdot \frac{M_0}{\alpha} \cdot \frac{t_2}{1+x-y} \cdot \frac{dM}{d\tau} - \frac{\alpha}{P_0} \cdot \frac{P_0}{L} \cdot \frac{L}{\alpha} \cdot \frac{p_2}{1+x-y}\left(\frac{dx}{d\tau} - \frac{dy}{d\tau}\right)\right]$$

which further can be reduced to

$$\frac{dP_2}{d\tau} = n\left[-\frac{1}{AR} \cdot \frac{t_2}{1+x-y} \cdot \frac{dM^*}{d\tau} - \frac{p_2}{(1+x-y)} \cdot \left(\frac{dx}{d\tau} - \frac{dy}{d\tau}\right)\right] \qquad (B.2)$$

Flow Characteristic Equation

To non-dimensionalize the flow characteristic equation, divide throughout equation (2.16) by the reference mass M_0. By using the dimensionless parameters the flow equation becomes

$$\frac{d}{d\tau}\left(\frac{M}{M_o}\right) = -\frac{k \cdot P_1 \cdot A \cdot N_{12}}{T_1^{\frac{1}{2}}} \quad \frac{\alpha}{M_o} \quad \text{For} \quad P_1 > P_2$$

$$= -\frac{k \cdot P_1 \cdot A \cdot N_{12}}{T_1^{\frac{1}{2}}} \quad \frac{\beta \cdot V_o}{A_1 \cdot k \cdot R \cdot T_o} \quad \frac{R \cdot T_o}{P_o \cdot V_o^{\frac{1}{2}}}$$

which can be simplified as

$$\frac{dM^*}{d\tau} = -\frac{p_1 \cdot a \cdot \beta}{t_1^{\frac{1}{2}}} \quad N_{12} \quad \text{for } p_1 > p_2 \tag{B.3}$$

The factor N_{12} is already non-dimensionalized. Similarly the flow characteristic equation for $p_1 < p_2$ can be written as

$$\frac{dM^*}{d\tau} = \frac{p_2 \cdot a \cdot \beta}{t_2^{\frac{1}{2}}} \quad N_{12} \quad \text{for } p_1 < p_2 \tag{B.4}$$

The non-dimensional temperatures t_1 and t_2 can be obtained from the dimensionless parameters as

$$\frac{T_1}{T_o} = \left(\frac{P_1}{P_o}\right)^{n-1/n}$$

$$t_1 = \left(p_1\right)^{n-1/n} \tag{B.5}$$

and

$$\frac{T_2}{T_o} = \left(\frac{P_2}{P_o}\right)^{n-1/n}$$

$$t_2 = \left(p_2\right)^{n-1/n} \tag{B.6}$$

Load Equation

By dividing the load equation (2.23) by L-m and using the dimensionless parameters the load equation becomes

$$\frac{d^2}{d\tau^2}\frac{Y}{L} = \frac{P_1 A_1}{\alpha m}\alpha^2 - \frac{P_2 A_2}{Lm}\alpha^2 + \frac{k\alpha^2}{m\,L}(\delta + X - Y)$$

$$- \frac{g\alpha^2}{L} - \frac{A_1 \cdot 14 \cdot 7 \cdot \alpha^2}{L \cdot m} + \frac{14 \cdot 7 \cdot \alpha^2 \cdot A_2}{L \cdot m}$$

Let $c_1 = \dfrac{A_1\,\alpha^2\,p_0}{L \cdot m}$

$c_2 = \dfrac{A_1\,\alpha^2\,p_0}{L \cdot m}$

$c_3 = k\alpha^2/m$

$c_4 = g\alpha^2/L + \dfrac{101{,}325\,\alpha^2}{L \cdot m}(A_1 - A_2)$

With these non-dimensionalized constants, the load equation can be written as

$$\frac{d^2y}{d\tau^2} = c_1 p_1 - c_2 p_2 + c_3(\delta^* + x - y) - c_4 \qquad (B.7)$$

APPENDIX C

APPENDIX C

RUNGE-KUTTA METHOD

The differential equations which describes the behaviour of the system can be solved using a Runge-Kutta integration method. The general procedure involved is outlined as follows.

Let $dy/dx = F(x,y)$

Then using the Runge-Kutta method (26), the discrete solution of equation is given as,

$$y(n + 1) = y(n) + \frac{1}{6} (k_1 + 2k_2 + 2k_3 + k_4)$$

where

$$k_1 = h.F\ (x,y)$$

$$k_2 = h.F\ \left[x + \frac{h}{2}, \left[y + \frac{k_1}{2}\right]\right]$$

$$k_3 = h.F\ \left[x + \frac{h}{2}, \left[y + \frac{k_2}{2}\right]\right]$$

$$k_4 = h.F\ (x + h,\ y + k_3)$$

h is the step size equal to $\{x(n + 1) - x(n)\}$.

This procedure is programmed and used to solve the system equations.

APPENDIX D

```
      PROGRAM PASSIVE (INPUT,OUTPUT,TAPE11,TAPE12,TAPE13,TAPE14,TAPE
     *15,TAPE16,TAPE17)
      DIMENSION DEP(20),RSLT(20)
      REAL LIMIT
      COMMON/ CON/C1,C2,C3,C4,W,ALP,AL,PE,TL
      COMMON/CON1/AK,A12
      READ *,C1,C2,C3,C4
      READ *,ALP,AK,A12
      PRINT 50,A12
   50 . FORMAT (20X,*ORI. AREA=*,G18.6)
      AL=1.0
      PE=1.4
   10   CONTINUE
      READ *,W,TL,LIMIT
      PRINT 100,W
  100 FORMAT (20X,* EXITING FREQUENCY=*,G18.6)
      IF (W.GT.90.0) STOP
      DEP(1)=1.0
      DEP(2)=1.0
      DEP(3)=0.0
      DEP(4)=0.0
      T=0.0
      H=0.0025
      N=4
      RSLT(1)=0.0
      RSLT(2)=0.0
      RSLT(3)=0.0
      RSLT(4)=0.0
      CALL DIFEQS (DEP,T,RSLT,H,N,LIMIT)
      GO TO 10
      END
```

```
      SUBROUTINE EVF(DEP,T,RSLT)
      DIMENSION DEP(20),RSLT(20)
      COMMON/ACC/X,DX1,DX2
      COMMON/CON/C1,C2,C3,C4,W,ALP,AL,PE,TLI
       COMMON /FLOW/ DM2
       COMMON /TEP/ T1,T2
      X=0.06*SIN(T*W*ALP)
     DX1=0.06*ALP*W*COS(W*ALP*T)
      DX2=-0.06*W*W*ALP*ALP*SIN(W*ALP*T)
150    CONTINUE
       P1=DEP(1)
      P2=DEP(2)
      CO1=1.0-X+DEP(4)
      CO2=0.5525*(1.0+X-DEP(4))
      T1=P1**((PE-1.0)/PE)
      T2=P2**((PE-1.0)/PE)
      CALL CFLOW (DEP)
      RSLT(1)=(PE/CO1)*(-DEP(1)*(DEP(3)-DX1)-DM2*T1)
      RSLT(2)=(PE/CO2)*(-DEP(2)*0.5625*(DX1-DEP(3))+DM2*T2)
      RSLT(3)=C1*DEP(1)-C2*DEP(2)+C3*(AL+X-DEP(4))-C4
      RSLT(4)=DEP(3)
      RETURN
      END


      SUBROUTINE CFLOW(DEP)
      DIMENSION DEP(20)
      COMMON/CON/C1,C2,C3,C4,W,ALP,AL,PE,TLI
      COMMON/CON1/AK,A12
       COMMON /FLOW/  DM2
       COMMON /TEP/ T1,T2
      DATA GAM/1.4/
      P1=DEP(2)
      PU=DEP(1)
      PL=DEP(2)
      P2=DEP(1)
       TE1=T2
      IF(P2.GT.P1) GO TO 15
      GO TO 20
15    CONTINUE
      P=P2
      P2=P1
      P1=P
       TE1=T1
20    IF((P2/P1).LE.0.5283) GO TO 25
      ANU=(P2/P1)**(2.0/GAM)-(P2/P1)**((GAM+1.0)/GAM)
      AN12=SQRT((ANU*14.92992))
      GO TO 30
25    AN12=1.0
30    DM2=SGN(PU-PL)*P1*A12*AK*AN12/SQRT(TE1)
      RETURN
      END


      FUNCTION SGN(X)
      IF(X) 1,2,3
1     SGN=-1.0
     RETURN
2     SGN=0.0
      RETURN
3     SGN=1.0
      RETURN
      END
```

```
      SUBROUTINE DIFEQS (DEP,T,RSLT,H,N,LIMIT)
      DIMENSION DEP(20),RSLT(20),DEPT(20)
       REAL LIMIT
      REAL K1(20),K2(20),K3(20),K4(20)
      COMMON/ACC/X,DX1,DX2
      COMMON/CON/C1,C2,C3,C4,W,ALP,AL,PE,TL
       COMMON /FLOW/ DM2
      COMMON /TEP/ T1,T2
       AA=4.0
      WRITE (11,9) T,DEP(4)
     WRITE (12,9) T,DEP(1)
       AM=0.0
       AAM=0.0
       BB=AA*H
       RD=X-DEP(4)
      RV=DX1-DEP(3)
       FG=C1*DEP(1)-C2*DEP(2)
5      CONTINUE
      CALL EVF(DEP,T,RSLT)
      DO 10 I=1,N
      K1(I)=H*RSLT(I)
      DEPT(I)=DEP(I)+0.5*K1(I)
10    CONTINUE
      TT=T+0.5*H
      CALL EVF(DEPT,TT,RSLT)
      DO 15 I=1,N
      K2(I)=H*RSLT(I)
      DEPT(I)=DEP(I)+0.5*K2(I)
15    CONTINUE
      CALL EVF(DEPT,TT,RSLT)
      DO 20 I=1,N
      K3(I)=H*RSLT(I)
      DEPT(I)=DEP(I)+K3(I)
20    CONTINUE
      TT=T+H
      CALL EVF(DEPT,TT,RSLT)
      DO 25 I=1,N
      K4(I)=H*RSLT(I)
      DEP(I)=DEP(I)+0.16666666*(K1(I)+2.0*K2(I)+2.0*K3(I)+K4(I))
25    CONTINUE
      T=T+H
      IF(ABS(T-BB).LE.0.0001) GO TO 29
      GO TO 38
29     CONTINUE
     WRITE (12,9) T,DEP(1)
      WRITE (11,9) T,DEP(4)
       AA=AA+4.0
       BB=AA*H
38     CONTINUE
9          FORMAT (5X,2(G18.6,3X))
      IF (T.GT.LIMIT) GO TO 80
      GO TO 5
80    CONTINUE
      RETURN
      END
```

APPENDIX E

```
      PROGRAM FINAL1 (INPUT,OUTPUT,TAPE11,TAPE12,TAPE13,TAPE14
     *,TAPE5,TAPE16,TAPE17)
      REAL LIMIT,K1,K2,K3 .
      DIMENSION DEP(20),RSLT(20)
      COMMON/GAIN/K1,K2,K3,SLFBS
          COMMON/FREQ/ AMPL
      COMMON/CON/ C1,C2,C3,C4,W,ALP,AL,PS,PE,AK
      AL=1.0
          PS=2.0
          C1=98.56
          C2=55.44
          C3=28.18
          C4=71.3
          ALP=0.744
          AK=2000.0
          SLFBS=0.8
          PE=1.4
1           CONTINUE
100       FORMAT (1H1,20X,*EXITING FREQUNCY=*,F8.2)
        READ *,W
       PRINT 100,W
       K1=0.1
       K2=0.01
         K3=0.2
        H=0.002
         PRINT 110,K1,K2,K3
110      FORMAT (///,20X,*THE FEED BACK GAINS ARE *,//,
     *28X,*K1=*,F8.4,//,28X,*K2=*,F8.4,//,28X,*K3=*,F8.4)
      DEP(1)=0.0
      DEP(2)=1.0
      DEP(3)=1.0
      DEP(4)=0.0
        DEP(5)=0.0
      N=5
          RSLT(1)=0.0
         RSLT(2)=0.0
          RSLT(3)=0.0
          RSLT(4)=0.0
         RSLT(5)=0.0
          LIMIT=10.0
      T=0.0
     CALL DIFEQS (DEP,T,RSLT,H,N,LIMIT)
2         STOP
      END
```

```
      SUBROUTINE DIFEQS (DEP,T,RSLT,H,N,LIMIT)
      COMMON/CONV/ C1,C2,C3,C4,W,ALP,AL,PS,PE,AK
          REAL LIMIT,DEP(20),RSLT(20),DEPT(20),K1(20)
          REAL K2(20),K3(20),K4(20)
      COMMON /INPUT/ X,DX1,DX2
          AA=4.0
          BB=AA*H
       WRITE (5,19)
       WRITE (12,19)
   19    FORMAT (*   1251    *,     *    1     *)
         WRITE (5,9) T,RSLT(4)
       WRITE (13,19)
       WRITE (13,9) T,RD
    5  CONTINUE
       CALL EVF(DEP,T,RSLT)
       DO 10 I=1,N
       K1(I)=H*RSLT(I)
       DEPT(I)=DEP(I)+0.5*K1(I)
   10  CONTINUE
       TT=T+0.5*H
       CALL EVF(DEPT,TT,RSLT)
       DO 15 I=1,N
       K2(I)=H*RSLT(I)
       DEPT(I)=DEP(I)+0.5*K2(I)
   15  CONTINUE
       CALL EVF (DEPT,TT,RSLT)
       DO 20 I=1,N
       K3(I)=H*RSLT(I)
       DEPT(I)=DEP(I)+K3(I)
   20  CONTINUE
       TT=T+H
       CALL EVF(DEPT,TT,RSLT)
       DO 25 I=1,N
       K4(I)=H*RSLT(I)
       DEP(I)=DEP(I)+0.16666666*(K1(I)+2.0*K2(I)+2.0*K3(I)+K4(I))
   25  CONTINUE
           T=T+H
       IF(T.GE.LIMIT) GO TO 50
       GO TO 5
   50     RETURN
       END


      SUBROUTINE EVF (DEP,T,RSLT)
      COMMON/CONV/ C1,C2,C3,C4,W,ALP,AL,PS,PE,AK
      DIMENSION DEP(20),RSLT(20)
      COMMON /INPUT/X,DX1,DX2
          DATA TAU/0.1/
        X=0.33*SIN(T*ALP*W)
        DX1=0.33*W*ALP*COS(W*ALP*T)
         DX2=-0.33*W*W*ALP*ALP*SIN(T*ALP*W)
  150     CONTINUE
      A1=1.0-X+DEP(5)
      A2=1.0+X-DEP(5)
      DV=DX1-DEP(4)
          T1=(DEP(2))**((PE-1.0)/PE)
        CALL SIGNAL (DEP,RSLT,XV,DM,AN12,T1)
        RSLT(1)=((XV-DEP(1))*ALP)/TAU
      RSLT(2)=(PE/A1)*(DM*T1+DV*DEP(2))
      RSLT(3)=-(PE/A2)*(DEP(3)*DV)
      RSLT(4)=C1*DEP(2)-C2*DEP(3)+C3*(AL+X-DEP(5))-C4
      RSLT(5)=DEP(4)
      RETURN
      END
```

```
      SUBROUTINE SIGNAL (DEP,RSLT,XV,DM,AN12,T1)
      DIMENSION DEP(20),RSLT(20)
      REAL L,K1,K2,K3
    COMMON/CON/ C1,C2,C3,C4,W,ALP,AL,PS,PE,AK
    COMMON /INPUT/ X,DX1,DX2
      COMMON /GAIN/ K1,K2,K3,SLFBS
     DATA L,A0,A3/0.25,0.012,0.007/
    RV=DX1-DEP(4)
    P1=DEP(2)
    P2=DEP(3)
     RD=1-X-DEP(5)
        A1=(A0)/(AK*L*AG)
        A2=C2/C1
        A3=C3/(C1*1.2)
       A4=K1*RSLT(4)+K2*DEP(4)+K3*DEP(5)
       IF(ABS(A4).GT.SLFBS) GO TO 5
        GO TO 15
5       CONTINUE
       IF(A4.GT.0.0) GO TO 10
       A4=-SLFBS
       GO TO 15
10        CONTINUE
       A4=SLFBS
15        CONTINUE
        IF(RV.GT.0.0) GO TO 20
         FS=-A4/(AG*AK*L)
         XV=(A1/PS)*(P1+A2*P2+A3)*ABS(RV)+FS
        GO TO 25
20      CONTINUE
         FS=-A4/(AG*AK*L)
         XV=-(A1/PS)*(P1+A2*P2+A3)*RV+FS
25      CONTINUE
         CALL FLOW (DEP,DM,AN12,T1)
         RETURN
         END


      SUBROUTINE FLOW (DEP,DM,AN12,T1)
      DIMENSION DEP(20)
     REAL L
     COMMON /CON/ C1,C2,C3,C4,W,ALP,AL,PS,PE,AK
      DATA L,A0,AG,GAM/0.25,0.012,0.007,1.4/
      PU=PS
      PL=DEP(2)
      IF(DEP(1).GT.0.0) GO TO 5
      AREA=L*AG*DEP(1)/A0
     AN12=1.0
      DM=AREA*AK*DEP(2)/SQRT(T1)
     RETURN
5       CONTINUE
      P1=DEP(2)
      P=PS
      IF(P1.GT.PS) GO TO 10
      GO TO 15
10      CONTINUE
     P=P1
     P1=PS
15      CONTINUE
     IF((P1/P).LE.0.5283) GO TO 20
      ANU=(P1/P)**(2.0/GAM)-(P1/P)**((GAM+1.0)/GAM)
      AN12=SQRT(ANU*14.92992)
     GO TO 25
20      CONTINUE
      AN12=1.0
25      CONTINUE
     AREA=L*AG*DEP(1)/A0
     DM=(SGN(PU-PL)*P*AREA*AK*AN12)/SQRT(T1)
      RETURN
     END


     FUNCTION SGN(X)
     SGN=ABS(X)/X
    RETURN
    END
```

APPENDIX F

```
      PROGRAM PNUEMAT (INPUT,OUTPUT,TAPE11,TAPE12,TAPE13,TAPE14,TAPE
     *15,TAPE16,TAPE17)
      DIMENSION DEP(20),RSLT(20)
      REAL LIMIT,K1,K2,K3
      COMMON/CON/C1,C2,C3,C4,W,ALP,AL,PS,PE,AK
      COMMON/GAIN/K1,K2,K3,SLFBS
    5  CONTINUE
       AL=1.0
       PS=2.0
       C1=98.56
       C2=55.44
       C3=28.18
       C4=71.3
       ALP=0.744
        AK=2000.0
       K1=0.1
       K2=0.01
       K3=0.2
       SLFBS=0.5
      PE=1.4
       READ *,W
       LIMIT=20.0
      DEP(1)=0.0
      DEP(2)=0.0
      DEP(3)=1.0
      DEP(4)=1.0
      DEP(5)=0.0
      DEP(6)=0.0
      INDEP=6.0
      H=0.0025
      N=6
       IF( W.EQ.0.0) STOP
      CALL DIFEQS (DEP,T,RSLT,H,N,LIMIT)
      STOP
      END
```

```
      SUBROUTINE DIFEQS (DEP,T,RSLT,H,N,LIMIT)
      DIMENSION DEP(20),RSLT(20),DEPT(20)
      REAL LIMIT
      REAL K1(20),K2(20),K3(20),K4(20)
      COMMON/INPUT/X,DX1,DX2
      COMMON/CON/C1,C2,C3,C4,W,ALP,AL,PS,PE,AK
      COMMON/ENERGY/EN,EN1
      X=0.0
       F0=43.12
      DX1=0.06
      DX2=0.0
  600   FORMAT (2X,*MAX DIS=*,G18.6,5X,*TIME=*,G18.6)
      BB=4.0
       WRITE (11,9) T,RD
       WRITE (12,9) T,RSLT(5)
      WRITE (13,9) T,DEP(3)
      WRITE (14,9) T,DEP(4)
      WRITE (15,9) T,DEP(6)
       AA=H*B3
    5 CONTINUE
      CALL EVF(DEP,T,RSLT)
      DO 10 I=1,N
      K1(I)=H*RSLT(I)
      DEPT(I)=DEP(I)+0.5*K1(I)
   10 CONTINUE
      TT=T+0.5*H
      CALL EVF(DEPT,TT,RSLT)
      DO 15 I=1,N
      K2(I)=H*RSLT(I)
      DEPT(I)=DEP(I)+0.5*K2(I)
   15 CONTINUE
      CALL EVF(DEPT,TT,RSLT)
      DO 20 I=1,N
      K3(I)=H*RSLT(I)
      DEPT(I)=DEP(I)+K3(I)
   20 CONTINUE
      TT=T+H
      CALL EVF(DEPT,TT,RSLT)
      DO 25 I=1,N
      K4(I)=H*RSLT(I)
      DEP(I)=DEP(I)+0.16666666*(K1(I)+2.0*K2(I)+2.0*K3(I)+K4(I))
   25 CONTINUE
       T=T+H
      IF((AA-T).LE.0.00001) GO TO 60
      GO TO 63
   60 CONTINUE
       IF (ABS(DEP(6)).GE.DD) GO TO 100
       GO TO 200
  100  CONTINUE
       DD=ABS(DEP(6))
       DIS=DEP(6)
       TIME=T
  200  CONTINUE
      RD=X-DEP(5)
       WRITE (11,9) T,RD
      WRITE (12,9) T,RSLT(5)
    9 FORMAT (5X,2(G16.8,2X))
      WRITE (13,9) T,DEP(3)
       WRITE (14,9) T,DEP(4)
       WRITE (15,9) T,DEP(6)
       BB=BB+4.0
       AA=H*BB
   65   CONTINUE
       IF (T.GT.LIMIT)  GO TO 70
       GO TO 5
   70   CONTINUE
       PRINT 600,DIS,TIME
       RETURN
       END
```

```
      SUBROUTINE EVF(DEP,T,RSLT)
      DIMENSION DEP(20),RSLT(20)
      COMMON/INPUT/X,DX1,DX2
      COMMON/CON/C1,C2,C3,C4,W,ALP,AL,PS,PE,AK
      DATA TAU/0.1/
      X=0.06*SIN(ALP*W*T)
      DX1=0.06*ALP*W*COS(ALP*W*T)
      DX2=-0.06*ALP*ALP*W*W*SIN(ALP*W*T)
      CO1=1.0-X-DEP(6)
      CO2=0.5625*(1.0+X-DEP(6))
      T1=DEP(3)**((PE-1.0)/PE)
      T2=DEP(4)**((PE-1.0)/PE)
      CALL SIGNAL (DEP,S1,S2,RSLT,CO1,T1,T2)
      RSLT(1)=((S1-DEP(1))*ALP)/TAU
      RSLT(2)=((S2-DEP(2))*ALP)/TAU
      CALL FLOW (DEP,DM,DM1,T1,T2,EN)
      RSLT(3)=(PE/CO1)*(DM*T1-DEP(3)*(DEP(5)-DX1))
      RSLT(4)=(PE/CO2)*(DM1*T2-DEP(4)*0.5625*(DX1-DEP(5)))
      RSLT(5)=C1*DEP(3)-C2*DEP(4)+C3*(AL+X-DEP(6))-C4
      RSLT(6)=DEP(5)
      RETURN
      END

      SUBROUTINE SIGNAL (DEP,S1,S2,RSLT,CO1,T1,T2)
      DIMENSION DEP(20),RSLT(20)
      REAL L,K1,K2,K3
      COMMON/INPUT/X,DX1,DX2
      COMMON/CON/C1,C2,C3,C4,W,ALP,AL,PS,PE,AK
      COMMON/GAIN/K1,K2,K3,SLFBS
      DATA L,A0,AG/0.25,0.012,0.007/
      P1=DEP(3)
      P2=DEP(4)
       RV=DX1-DEP(5)
      A5=K1*RSLT(5)+K2*DEP(5)+K3*DEP(6)
      IF (ABS(A5).GT.SLFBS) GO TO 5
      GO TO 15
    5 IF(A5.GT.0.0) GO TO 10
      A5=-SLFBS
      GO TO 15
   10 A5=SLFBS
   15 CONTINUE
      IF(RV.GT.0.0) GO TO 20
      A1=(-CO1*RV*A0)/(AK*PS*L*AG)
      A13=A1*((C3/C1)*(1.0/1.4)+(P1/CO1))
      F6=A5/(AK*AG*L)
      S1=(A13-F5)
       S2=(0.5625*RV*A0)/(AK*AG*L)
       RETURN
   20 CONTINUE
      A1=(CO1*RV*A0)/(AK*AG*L*P1)
      A13=A1*((C3/C1)*(1.0/1.4)+(P1/CO1))
      F5=A5/(AK*AG*L)
       S1=-A13-F5
       S2=(P2/PS)*(A0/(AK*L*AG))*0.5625*RV
    RETURN
      END
```

```
      SUBROUTINE FLOW (DEP,DM,DM1,T1,T2,EN)
      DIMENSION DEP(20)
       REAL L
      COMMON/CON/C1,C2,C3,C4,W,ALP,AL,PS,PE,AK
      DATA L,A0,AG/0.25,0.012,0.007/
      IF (DEP(1).GT.0.0) GO TO 5
       AREA=L*AG*DEP(1)/A0
       DM=AREA*AK*DEP(3)/SQRT(T1)
       GO TO 15
    5  CONTINUE
       PL=DEP(3)
      XV=DEP(1)
       T=T1
       CALL CHECK (PL,XV,DM,T)
       IF (DM.LT.0.0) GO TO 10
       EN=DM*PS
       GO TO 15
   10  EN=0.0
   15  CONTINUE
      IF (DEP(2).GT.0.0) GO TO 20
       AREA=L*AG*DEP(2)/A0
       DM1=AREA*AK*DEP(4)/SQRT(T2)
       RETURN
   20  CONTINUE
       PL=DEP(4)
       T=T2
       XV=DEP(2)
       CALL CHECK (PL,XV,DM1,T)
       IF (DM1.LT.0.0) GO TO  25
       EN=DM1*PS
       RETURN
   25  CONTINUE
       EN=0.0
       RETURN
       END


       SUBROUTINE CHECK (PL,XV,DM,T)
      REAL L
       COMMON /CON/ C1,C2,C3,C4,W,ALP,AL,PS,PE,AK
       DATA L,A0,AG,GAM/0.25,0.012,0.007,1.4/
       PU=PS
       P1=PL
       P=PS
       IF (P1.GT.PS) GO TO 10
       GO TO 15
   10  CONTINUE
       P=P1
       P1=PS
   15  CONTINUE
       IF ((P1/P).LE.0.5283) GO TO 20
      ANU=(P1/P)**(2.0/GAM)-(P1/P)**((GAM+1.0)/GAM)
       AN12=SQRT(ANU*14.92992)
       GO TO 25
   20  CONTINUE
      AN12=1.0
   25  CONTINUE
      AREA=L*AG*XV/A0
       AN12=1.0
      DM=(SGN(PU-PL)*P*AREA*AK*AN12)/SQRT(T)
       RETURN
      END


      FUNCTION SGN(X)
      IF (X) 5,10,15
    5 SGN=-1.0
      RETURN
   10 SGN=0.0
      RETURN
   15 SGN=1.0
      RETURN
      END
```